KUNGL. TEKNISKA HÖGSKOLANS HANDLINGAR

TRANSACTIONS OF THE ROYAL INSTITUTE OF TECHNOLOGY
STOCKHOLM, SWEDEN

Nr 242 1965

Civil Engineering 13

UDC 666.94.015.42

THE MICROSTRUCTURES OF CEMENT GEL PHASES

BY

ÅKE GRUDEMO

STOCKHOLM
AB HENRIK LINDSTÅHLS BOKHANDEL I DISTRIBUTION

Förteckning över

KUNGL. TEKNISKA HÖGSKOLANS HANDLINGAR

Fullständig förteckning finns i häften nr 1—145 och för häften fr.o.m. nr 101 i nr 146—209.

For complete lists see issues No. 1—145 and for issues from No. 101 in No. 146—209.

151. BJERHAMMAR, ARNE, *Electro Optical Distance Measuring.* (Math. & Phys. 4) 101 s. 1960. Kr. 10: 50.
152. SCHLYTER, KURT, *Treatment of Data from Enthalpy Titrations.* (Chem. 5) 18 s. 1960. Kr. 2: 50.
153. BORG, GÖRAN, *A Condition for the Existence of Orbitally Stable Solutions of Dynamical Systems.* (Math. & Phys. 5) 12 s. 1960. Kr. 2: —.
154. BRUNDELL, PER-OLOF, *Current and Potential Distribution on a Circular Loop Antenna.* (El. Engng. 4) 34 s. 1960. Kr. 4: 50.
155. BOHLIN, TORSTEN, *On the Drag on a Rigid Sphere Moving in a Viscous Liquid Inside a Cylindrical Tube.* (Math. & Phys. 6) 64 s. 1960 Kr. 7: 50.
156. SIMON, HEINRICH, *Comparative Investigations of Image and Insertion Parameter Filters.* (El. Engng. 5) 60 s. 1960. Kr. 7: —.
157. NAGEL, BENGT, *Some Topics in Coulomb Scattering.* (Math. & Phys. 7) 30 s. 1930. Kr. 4: 50.
158. KINNUNEN, S., and NYLANDER, H., *Punching of Concrete Slabs without Shear Reinforcement.* (Civil. Engng. 3) 112 s. 1960. Kr. 11: —.
159. ROSÉN, ERIK, *Data and Calculations for the Gasification of Spent Cooking Liquors from the Pulp Industry. Part I: Fundamental Thermodynamic Quantities.* (Chem. 6) 27 s. 1960. Kr. 3: 50.
160. ROSÉN, ERIK, *Data and Calculations for the Gasification of Spent Cooking Liquors from the Pulp Industry. Part II: The Behavior of the Elements Carbon, Hydrogen and Oxygen.* (Chem. 7) 37 s. 1960. Kr. 4: 50.
161. ROSÉN, ERIK, *Data and Calculations for the Gasification of Spent Cooking Liquors from the Pulp Industry. Part III: The Behavior of the Elements Sulfur and Calcium.* (Chem. 8) 32 s. 1960. Kr. 4: —.
162. HALLERT, B., *Investigations into the Accuracy of Various Methods of Photogrammetric Triangulation.* (Math. & Phys. 8) 118 s. 1960. Kr. 11: 50.
163. LUNDBORG, N., *Initiation of Liquid Explosives in Steel Tubes Exposed to Impact.* (Math. & Phys. 9) 22 s. 1960. Kr. 3:.
164. SANDSTRÖM, BENGT, *A Note on Deceleration Processes.* (Math. & Phys. 10) 11 s. 1960. Kr. 1: 50.
165. THEDÉEN, TORBJÖRN, *Electrodiffusion Treated as a Random Walk Problem.* (Math. & Phys. 11) 55 s. 1960. Kr. 7: —.
166. KREISS, HEINZ-OTTO, *Über die Lösung von Anfangsrandwertaufgaben für partielle Differentialgleichungen mit Hilfe von Differenzergleichungen.* (Math. & Phys. 12) 62 s. 1960. Kr. 7: 50.
167. ALFVÉN, H., BERNERYD, S., HANAAS, T., LINDBERG, L. and ÅSTRÖM, E., *On the Oscillation of Electrons in Hyperbolic Magnetic Fields and its Application to Microwave Generation.* (Math. & Phys. 13) 92 s. 1960. Kr. 10: —.
168. REINIUS, ERLING, *The Stability of the Downstream Part of Earth Dams.* (Civil Engng. 4) 44 s. 1961. Kr. 5: 50.
169. TEDER, ANTS, *Carbonation of Sodium Sulphide Melts.* (Chem. 9) 29 s. 1961. Kr. 4:—.
170. BJERHAMMAR, ARNE, *On the Principal Geometrical Problems of Geodesy.* (Math. & Phys. 14) 19 s. 1961. Kr. 2: 50.
171. BJERHAMMAR, ARNE, *A General Formula for an Unbiased Estimate of the Standard Deviation of a Triangulation Network.* (Math. & Phys. 15) 21 s. 1961. Kr. 2: 50.
172. LJUNGGREN, STIG, *Comments on the Theories of Isothermal Multi-Component Diffusion.* (Chem. 10) 31 s. 1961. Kr. 4: —.
173. WIDLUND, OLOF, *On the Expansion of Generalized Functions in Series of Hermite Functions.* (Math. & Phys. 16) 12 s. 1961. Kr. 2: —.
174. NYSÄTER, HANS, *Dynamic measurement of Low Magnetic Fields with special Reference to the Strong Focusing 1.2* GeV *Electron Synchrotron at Lund.* (Math. & Phys. 17) 30 s. 1961. Kr 4:—
175. SCHLYTER, KURT, and MARTIN, DAVID L., *Thermochemical Studies of Reactions between Acetate and Hydrogen Ions.* (Chem. 11) 21 s. 1961. Kr. 3: —.
176. ANIANSSON, GUNNAR, *Thin CsI(Tl) Scintillating Layers Produced by Vacuum Deposition.* (Chem. 12) 22 s. 1961. Kr. 3: —.
177. ANIANSSON, GUNNAR, *Apparatus for Mesauring α-Particle Ranges in Liquids.* (Chem. 13) 44 s. 1961. Kr. 5: —.
178. ANIANSSON, GUNNAR, *The Integral Stopping Power of Liquid Hydrocarbons for 5.3 MeV α-Particles.* (Chem. 14) 35 s. 1961. Kr. 4:50.
179. REINIUS, ERLING, *Steady Uniform Flow in Open Channels.* (Civil Engng. 5) 47 s. 1961. Kr. 5: 50.
180. BOMAN, JAN, *On the Stability of Differential Equations with Periodic Coefficients.* (Math. & Phys. 18) 21 s. 1961. Kr. 3: —.
181. SJÖSTRÖM, SVERKER, *On Random Load Analysis.* (Math. & Phys. 19) 41 s. 1961. Kr. 5: —.
182. SCHLYTER, KURT, *Thermochemical Studies on the Hydrolysis of the Indium (III) Ion.* (Chem. 15) 42 s. 1961. Kr. 5: —.

Forts. å omsl. 3:dje sida

KUNGL. TEKNISKA HÖGSKOLANS HANDLINGAR

TRANSACTIONS OF THE ROYAL INSTITUTE OF TECHNOLOGY
STOCKHOLM, SWEDEN

Nr 242 1965

Civil Engineering 13

UDC 666.94.015.42

THE MICROSTRUCTURES OF CEMENT GEL PHASES

BY

ÅKE GRUDEMO

GÖTEBORG 1965
ELANDERS BOKTRYCKERI AKTIEBOLAG

Synopsis

In the introductory section, a review is given of the general character of cement hydration systems, and of the use of electron-optical methods for examining their structures. The principal part of the paper is a collection of pictures with descriptive text, arranged in the form of a review of electron micrographs and diffraction diagrams given by the various gel phases occurring in the hydration of pure compounds and mixtures of cements of ordinary types.

Errata

Switched figures: 3a and 3c (p. 47), 65a and 65c (p. 91).

Omitted references: (quoted on p. 171):

ASSARSSON G., 1962, Discussion of Taylor 1962, 190-194.

FUNK H., 1961, Über Calciumsilicathydrate mit der Zusammensetzung $CaO \cdot 2SiO_2 \cdot 0.5\text{-}2H_2O$ und die Synthese des Reyerit (= Truscottit) ($CaO \cdot 2SiO_2 \cdot 0.5H_2O$); Zeitschr. anorg. allg. Chemie, 313, 1-13.

I. INTRODUCTORY SECTION

1. Preface

For a period of about one year in 1957–58, the author worked as a guest scientist with the Portland Cement Association (PCA) Research and Development Laboratories in Skokie, Illinois, USA. Most of the time was devoted to electron-optical studies of cement hydration products and related materials by means of the electron microscope then installed at the PCA Basic Research Section. This experimental work resulted in a considerable amount of microfilm records which have later been analysed, evaluated, and reproduced in various ways, and part of the data reported in a few papers and review articles, as referred to in the following.

The original purpose of the present report was to give a complete account of those parts of the experimental material collected at PCA, which were considered to be of general interest or relevance. It was found, however, that important sections of the cement hydration field were not represented in the first set of micrographs selected for this account. Therefore, in order to obtain a reasonably coherent and comprehensive collection of electron-optical data for different types of cement hydration constituents, some results from later work have also been included in this report. For this work, the electron microscope of the Institution of Chemical Technology, KTH, was used, as in earlier studies by the present author. Most of the later data are samples from the studies on hydrothermally-prepared calcium silicate hydrates and on artificial cement paste mixtures, carried out by Dr. *S. Chatterji* of Calcutta, India, during his stay with CBI as guest scientist in 1959–61.

The main results of these later studies were accounted for by Dr. *Chatterji* in two preliminary internal reports, and were also referred to in recent works (*Chatterji* and *Jeffery* 1962, 1963 a, b) as material "to be published". However, the material has been partly duplicated and superseded by data reported in the above papers. For this reason, selected parts of the experimental material have provisionally been re-examined and arranged for insertion in proper connections in the present report, for the purpose of making the data more complete on certain points. Thus, about 80 percent of the micrographs have been taken from the photographic films recorded at PCA, about 5 percent obtained in earlier and later work carried out at CBI by the author, and about 15 percent selected from the studies made by Dr. *Chatterji*.

There are only a few important hydrated phases formed in cement paste hydration at ordinary temperatures. In Portland cement systems, the predominant phase is a calcium silicate hydrate, formed from the calcium silicate anhydrides. Another phase is lime, calcium hydroxide, crystallized from the lime solution formed in the hydrolysis of the calcium silicates. A third phase, or class of phases, is formed as the product of hydration of the aluminate and ferrite components. From this point of view, therefore, the cement hydration system does not appear very complex. However, a characteristic feature of the system is that even within the same general phase, or range of phases, the microstructural elements can show great variations in morphologic habits and electron diffraction patterns, depending on conditions, such as time and temperature of mixing and curing, water content, mechanical treatment, etc. In certain circumstances, a number of new compounds may appear, essentially different from those formed in normal cases.

In compiling the set of electron micrographs selected for reproduction in the present paper, it was found necessary, therefore, to include a very large number of pictures, judged by normal standards, in order to cover all the structures and structural phenomena observed in various samples. Thus, by far the greater number of micrographs have been reproduced with a view to illustrate something essentially new, either the structural elements representative or characteristic of various samples, or some extraordinary and remarkable features observed. In rare cases, one or two micrographs have been included, mainly to fill out the space of a certain page without actually showing any new structures. In some cases, e.g. in the section of micrographs from hardened pastes, a comparatively large number of micrographs from different samples have been reproduced for the sake of reference and in order to make the collection balanced and representative, disregarding the fact that many of the structures shown are almost identical, as well as being nearly void of distinctive features.

In view of the large number of micrographs, some measures have been taken to make it easier for the reader to survey the micrograph section. The micrographs have been arranged in groups of six, and the corresponding sample notation and description can be found on the opposite page. In the list of samples preceding the micrograph section, the specimens studied are arranged alphabetically according to a simple code describing the essential character of the sample. Under each specimen, references to corresponding micrographs are given for certain compounds or structures observed in it. However, it is emphasized that the collection of samples is not systematically selected from one large investigation, but rather brought together from a number of smaller studies, made on various occasions.

2. List of special symbols and abbreviations

As is common in the literature on cement, the following oxide symbols are used:

$C = CaO$, $S = SiO_2$, $A = Al_2O_3$, $F = Fe_2O_3$, $H = H_2O$,
$\overline{S} = SO_3$, $\overline{C} = CO_2$ (also $M = MgO$, $N = Na_2O$, $K = K_2O$)

When no misinterpretation is possible, these symbols are used also for simple compounds such as CH = calcium hydroxide (solid), SH = silica gel, AH_3 = aluminium hydroxide (gibbsite), $C\overline{S}H_2$ = gypsum, $C\overline{C}$ = calcium carbonate (usually calcite), etc. C-S-H is used to denote a calcium silicate hydrate phase of unknown or unspecified composition. The calcium silicate hydrates (I) and (II), as originally denominated by *Taylor* 1950, and with compositions variable within certain ranges, are abbreviated C-S-H(I) and C-S-H(II). C-(A,F)-H denotes a calcium alumino-ferrite hydrate of unknown or unspecified composition. If the composition and crystal structure is partly known, this is indicated in some way in the formula, e.g. $C_4A \cdot aq$(hex.) is a tetracalcium aluminate hydrate of hexagonal symmetry, and with an unknown water content.

w/c = weight ratio water/(anhydrous phase), specifically water/cement ratio.
EM = electron microscopy or micrograph,
ED = electron diffraction or diffractogram.

3. Introduction and general literature references

The formation of crystalline and colloidal solid hydrates in the hydration of portland cement and similar hydraulic binding materials, and the development and intergrowth of various phases to form a hardened hydrogel, are processes governed by the reaction chemistry of the system of minerals and water that constitutes a cement mix. The hydration chemistry of cement and of its pure constituents has been treated in several handbooks and review articles, for example those presented at the latest Symposium on the Chemistry of Cement (Washington, D.C., 1960), to which the reader is referred for exhaustive data and further references on the subject (*Brunauer* and *Greenberg* 1962, *Taylor* 1962, *Jones* 1962, *Greene* 1962, *Hansen* 1962, *Copeland, Kantro*, and *Verbeck* 1962, *Powers* 1962, *Grudemo* 1962). With special regard to the use of electron microscopy in cement research, reference is made to review articles on experimental techniques (*Gard* 1964) and on paste studies (*Grudemo* 1964 a)

in the just-completed textbook on the chemistry of cements, edited by *H. F. W. Taylor*.

As an introduction to the present collection of electron micrographs, it may suffice, therefore, to give only a brief summary of the essential characteristics of the cement-water reaction system.

Some parts of the illustrative material of this paper have been presented in the review articles referred to above, and other data have been published in earlier papers (*Grudemo* 1955, 1959, *Danielsson* 1959).

4. General character of cement hydration structures

In general, the reaction with water of the various cement constituents in a paste mix leads to their ultimate decomposition, and to the formation of a hydrogel causing the mass to stiffen and set within a few hours, and subsequently to harden slowly for almost infinite time.

In a portland cement mix of normal composition, this hydrogel is, physicochemically, an intimate but still heterogeneous mixture of several phases. The predominant phase which is also considered to be mainly responsible for the hydraulic properties of the material, is a colloidal calcium silicate hydrate of indefinite or variable composition. It should be emphasized that this phase which, for the sake of simplicity, can be called C-S-H gel, is neither pure nor easily and unambiguously characterized or identified. This C-S-H gel phase shows distinct points of similarity with the natural mineral tobermorite, or rather with the two calcium silicate hydrate compounds commonly denominated hydrates (I) and (II) (or C-S-H(I) and C-S-H(II), see list of special symbols and abbreviations), which are structurally related to tobermorite but less well crystallized. However, the C-S-H phase resulting from the hydration of cement may well contain small amounts of aluminium or ferric ions, probably replacing silicon ions in the lattice, and can thus be expected to deviate from the pure phases in morphological and microstructural respects. The detection of such deviations and the description of their character are important problems in current studies of paste microstructures. This ill-defined C-S-H gel phase seems to be the only C-S-H compound of any significance in pastes cured at normal temperatures, but steam-cured pastes may contain considerable quantities of other phases in the C-S-H system, which influence the physical properties of the paste.

The second major constituent of cement gel is hydrated lime (CH), dissolved and reprecipitated or otherwise separated, in the process of hydration of the anhydrous calcium silicates. Most of the CH phase occurs in the gel in its

normal, well-crystallized state, with crystals of hexagonal symmetry, but certain data indicate that some part of it may be nearly amorphous. The possible presence of more than one modification of lime must be kept in mind in an analysis of the structural composition of paste samples.

The third gel phase of importance is the group of compounds formed as products of hydration of the aluminate- and ferrite-bearing clinker constituents in a solution containing excessive amounts of calcium and sulfate ions, and also reactive silica complexes. This phase can simply be denominated C-A-H gel phase but seems in reality to be of a complex nature, differing in crystal structure, morphologic habit, oxide composition, and mineralogical identity, with the relative local concentration of the various ions incorporated in it, with curing conditions, and with time. This range of phases includes the more well-defined members $C_4A \cdot aq$(hex.) and $C_4A\overline{S} \cdot aq$(hex.) ("monosulfate"), with solid solutions or lattice substitutions by F, $\overline{C}$, and possibly S, further $C_6A\overline{S}_3 \cdot aq$(hex.) ("trisulfate" or ettringite), also with possible ionic replacements of various types. As indicated, the symmetry of the crystal structure elements of this series of compounds is best described as hexagonal, but deviations from an exactly hexagonal symmetry are common. The relationship between the proposed hexagonal symmetry of the mineral ettringite, and the fibrous habits of supposedly ettringite-type formations observed in EM studies, is obscure. Further, the probable occurrence of phases in the hydrogarnet series, $C_3(A,F)\ (S,H_2)_3$ (cub.), must not be overlooked in the examination and analysis of paste structures. Generally, the detection and characterization of the C-A-H gel phase presents a complicated part-problem in structural studies of cement paste.

From this brief review, it is evident that a hydrating cement paste is a physico-chemical system of great complexity. Thus there is a tendency toward the formation of binary or ternary CH, C-S-H, and C-A-H gel phases, but in the course of hydration, various types of interactions between ions and ionic groups originating from different anhydride constituents, or from admixtures and impurities, can be expected to occur frequently. These effects cause disturbances in the regular formation of the pure-phase crystal lattices of solid hydrates, resulting in lattice restrictions and distortions of various types. This seems to be especially the case in the C-S-H phase developing in cement pastes. On the other hand, the C-S-H compounds formed in the pure ternary system at room temperature are poorly crystallized substances in themselves, even under conditions of crystallization less restricted than those of paste hydration. Thus a further decrease in size or degree of crystallinity of the structural elements is in most cases difficult to recognize by any method of investigation. In other phases, such as the hexagonal-plate C-A-H gel phase, a limited degree of lattice substitutions or solid solution may stabilize a certain structure.

5. Influence of the water-to-solid ratio

The type and course of the reactions between the crystals of the cement minerals and water depend on a number of factors, among which, of course, are the mineral composition of the cement and, in particular, the water/cement ratio (w/c).

In the extreme case of a very large excess of water, the cement compounds will ultimately become completely hydrolysed, the equilibrium products being silica, alumina, and ferric hydroxide gels in a very dilute solution containing, among other ions, all the lime originally present in the cement.

With a smaller w/c ratio, of the order of a few hundred, the equilibrium concentration of lime in solution will approach saturation, and the major final product of hydration at ordinary temperatures will be colloidal calcium silicate hydrate (C-S-H), structurally related to the mineral tobermorite or its colloidal analogue C-S-H(I), which is regarded as essentially a tobermorite monolayer phase. This C-S-H phase has a C/S ratio in the range 0.8 to 1.5, with possible inclusions or substitutions of aluminium and ferric ions in its more or less irregularly-built crystal lattice. Mixed with this C-S-H phase are calcium aluminate or aluminoferrite hydrate (C-(A,F)-H) compounds of one type or other, with possible inclusions or lattice substitutions of a number of ionic groups such as sulfate, chloride, carbonate, and silica, and including compounds (1) with cubic crystal symmetry and a C/(A+F) ratio of 3 (hydrogarnet), (2) with hexagonal layer-lattice symmetry and different values of the C/(A+F) ratio, ranging from one in monocalcium aluminate hydrate, CAH_{10}, to four in hydrocalumite, C_4AH_{13}, and (3) with hexagonal fiber-lattice symmetry and a C/(A+F) ratio of 6 in the ettringite-type compounds, the prototype of which is C_6AH_{33}.

With a w/c ratio below about 100, the liquid phase will normally become rapidly saturated with lime, the more rapidly the higher the content of simultaneously-dissolved sulfate and alkali ions is. Consequently, lime hydrate will appear in the precipitated solid-hydrate phases. As stated above, this lime will normally be well-crystallized, but certain conditions seem to favour the formation of amorphous high-lime phases. In the C-S-H phase formed simultaneously by dissolution or conversion otherwise of the calcium silicates, the C/S ratio has a lower limit of 1.5, and tends to increase above this value. This increase corresponds to deviations, in morphology and crystal structure, from the prototypes of lower C/S ratios, either the pseudohexagonal plates of well-crystallized tobermorite, or the thin foils of C-S-H(I). In the saturation range of lime concentration in the liquid phase, the C/(A+F) ratio in the hexagonal-plate phases of C-(A,F)-H is generally in the vicinity of 4. These phases are stable at ordinary temperatures, or at least are easily formed and highly persistent. At elevated temperatures, the formation of isometric hydrogarnet phases is promoted.

In concentrated suspensions and paste mixes, corresponding to a w/c ratio of the order of unity or less, the stoichiometric conditions at equilibrium are not essentially different from those which have now been described for more dilute systems. The reactions in the liquid phase, involving dissolution of the anhydrous material and precipitation of hydrates, are the same, even if the relative quantity of material in solution at any moment of the reaction is much smaller. In an ordinary cement paste, only about one-tenth of one percent, at most, of the reactive material can appear in solution at a time. Consequently the w/c ratio has little influence on the stoichiometric relationships, but the degree of crystallinity and the colloidal structure of the hydrated phases can be considerably affected by changes in the relative amount of liquid phase in mixes with w/c ratios so small that the particles are actually in contact with each other. This can be expected to occur approximately at w/c 0.3 to 0.5, corresponding to ordinary paste proportions. It is conceivable, however, that the hydration reactions and the development of certain hydrated structures around any cement particle can be disturbed by adjacent particles involved in similar reactions, even at much higher w/c ratios.

The very general description given above of the influence of variations in concentration of solid phase on the hydration reactions and on the microstructures of solid hydrates developing in the liquid phase, is of course valid only in regions where there is a truly liquid phase present, i.e. where the mobility of the ions and ionic groups liberated from the anhydrous cement crystals is not severely restricted by solid matter in their vicinity. However, it is a common observation that, in the hydration of especially the calcium silicate constituents of cement, at least part of the hydrated products form a layer or coating of steadily increasing thickness on the surface of the undispersed cement particles.

If not broken up by mechanical treatment or disrupted at certain intervals by its own osmotic pressure, as suggested by *Powers* 1961, this layer prevents the direct contact between the unhydrated cement material and the outer liquid phase, causing a retardation of further hydration. The permeability of the surface coating to water molecules diffusing inwards, and to dissolved ions going in the opposite direction, depends on the local porosity of the layer, which may be large in dilute systems, and on the texture and orientation of the particle elements in it, which may vary with the composition of the cement particle on which it is formed. However, in practically any cement-water mix part at least of the hydrate phases forming in later stages of hydration, are actually developed in processes involving a slow penetration of water molecules through the internal regions of the larger cement grains, and a simultaneous rearrangement of the ions of the anhydrous crystal structure into small and distorted crystals, or subcrystalline elements, of some kind of hydrated compound.

6. Influence of increased temperature

Quite naturally, the temperature of reaction has a considerable influence on the character of the hydration products. One effect is, of course, that the rates of reaction increase with temperature. At room temperature, it usually takes many months or years to attain equilibrium or complete hydration in a cement-water mixture. It is not known, and has been questioned, whether the products then obtained are true equilibrium phases, or if they are only metastable, although persisting for practically unlimited times. Even at 100° C, it usually takes weeks and months to reach a steady state, but at 200° C and saturation vapour pressure, the reaction is mostly complete within a few hours' time.

Another effect of a temperature rise is that the hydrated phases described above become unstable with respect to other hydrates. As a rule, there is no fundamental change in the C-S-H gel phase at temperatures of about 100° C or a little higher. Even at higher temperatures, colloidal phases are frequently observed as the primary C-S-H product, probably due to the fact that after mixing the batches cannot be brought rapidly enough to the temperature determined for the synthesis. The equilibrium products in C-S-H systems at temperatures above about 120° C are all relatively well-crystallized minerals, of which there are about twenty species recognized and defined, either as natural minerals or as artificially-prepared products, in many cases as both.

The various types of C-(A,F)-H compounds of hexagonal symmetry are all highly-hydrous materials. As a rough basis of comparison, the equivalent w/c ratios calculated from the chemical formulas given for these compounds can be used. These are e.g. for C_6AH_{33}: 1.35, for C_4AH_{19-13}: 1.05 to 0.70, for CAH_{10}: 1.14, for $C_6A\bar{S}_3H_{30}$ (ettringite): 0.80, for $C_4A\bar{S}H_{10-12}$ ("monosulfate"): 0.44 to 0.53, compared with about 0.3 to 0.4 for solid, air-dry C-S-H gel materials. The C-(A,F)-H hexagonal-symmetry compounds are therefore probably unstable even at room temperature and decompose easily, or are not formed at all, at higher temperatures. In steam-cured cement systems, the alumina and ferric oxide from the cement may be incorporated in a number of hydration products of variable types: (1) in AH_3 (gibbsite) or oxyhydrates of lower water contents, possibly also in amorphous hydrates $(A,F)H_n$, (2) in isometric hydrogarnet phases, or in $C_4A_3H_3$, (3) in increasing amounts of solid solution in the C-S-H gel phase, (4) combined with silica in (A,F)-S-H phases of the general character of clay minerals.

7. Influence of state of subdivision of starting materials

From what has been stated above, on the general course of reaction of cement hydration systems, it follows that one can expect to find mainly three types of particle structures in a completely-reacted system: (1) well-crystallized, com-

paratively large particles formed in processes of regular crystallization from ions dissolved in a saturated solution, or from smaller crystal nuclei growing by accretion of similar crystals in the surroundings, (2) products formed directly on the liquid-solid interfaces, usually developing into a surface coating of some thickness, and consisting of subcrystalline elements with crystal-lattice restrictions and distortions of various types, (3) products formed in the interior of the original cement particles by topochemical conversion of the anhydrous crystal structure, caused by the action of water molecules slowly diffusing through the particle, usually consisting of very badly-crystallized or amorphous material.

A finer dispersion of the anhydrous material, obtained for example by prolonged grinding, can be expected to change the proportions between surface-layer and internal phases in favour of the former. In addition, the rate of reaction expressed as the amount of anhydrous phase decomposing per unit time, is likely to be higher at all times.

It is evident that the mixture of three types of solid hydrate phases represents a steady state rather than final equilibrium of the reacting system of oxides. If an attempt were made to reconstruct a certain cement mix by reacting a mixture of oxides, including water, of a chemical composition identical with that of the cement in question, the products of hydration would certainly be very different from those of the cement mix. Only in the special cases of high dilution, vigorous stirring for long times, or autoclave treatment at high enough temperatures for long enough times would the ultimate results of reaction be identical in phase composition, if not in microstructure. Similarly, two cements can have the same oxide composition, but still give pastes of different structures, due to differences in the distribution of oxides in the clinker minerals, caused for example by variations in the burning procedures. Differences in the mechanical mixing procedures of batches taken from the same cement paste mix would certainly cause differences in early microstructural development, probably also in the structures observed after long times of hardening.

8. Considerations on methods for studying cement hydration structures, with special reference to electron microscopy

Ordinary portland cement, as it comes out of the mill after the final grinding of the clinker nodules from the furnace, together with admixtures such as gypsum, is a fine powder composed of crystals of the various cement clinker constituents, and possibly minor amounts of glass phase. The average size of the crystal particles is of the order of 5 to 10 microns, with a distribution of sizes roughly in the 1 to 50 micron range. The phase composition, the crystal

size distribution, and the crystal structures and lattice substitutions of the various clinker constituents in this mixture are the primary factors influencing the performance of cement when used as a hydraulic binding material. These properties are best studied and analysed by such methods as light microscopy and X-ray diffraction, in combination with standard or special methods of quantitative chemical analysis.

When this composite crystal powder reacts with water, whether in a paste mix or in dilute suspension, the morphological elements in the particles or particle aggregates of the resulting hydration products are generally of a much smaller size. Coherent aggregates of smaller hydrate particles may have roughly the same size and shape as the anhydrous crystals which they have replaced, but even the largest particle dimension of some new products of crystallization rarely exceeds one micron, and even the well-crystallized phases consist of particles with their crystal lattices restricted in one or two directions. The smallest particle dimension is commonly of the order of 100 Å, or even smaller, down to the size of monomolecular units.

Thus most of the particles in a fully-hydrated cement paste are submicrocrystalline or colloidal, so their shapes, sizes, and aggregation properties cannot be studied by means of the light microscope, due to the limited resolving power of this instrument. Similarly, the detection and analysis of the hydrated phases by means of X-ray diffraction is considerably more difficult than the corresponding analysis of the anhydrous compounds, for various reasons. The badly-crystallized phases developing as products of hydration of the silicates give only a few weak and diffuse X-ray reflexions, even if they occur in considerable quantities in a paste sample. The products of hydration of the aluminate or aluminoferrite constituents, although in general better crystallized, and although of some importance because of their probable influence on the setting of the cement paste, are minor constituents from the point of view of over-all composition. Consequently, their X-ray reflexions tend to become lost in the general background, or to be masked by stronger reflexions from other substances, such as remaining anhydrous material.

It is for systems of particles within the colloidal and microcrystalline range of sizes – covering approximately the three decades from 20 Å to 2 microns – that the electron microscope has found its chief application. With the development of three-stage electron microscope constructions, it has also become possible to examine and record simultaneously the electron-optical image and the corresponding electron diffraction pattern given by a number of small, selected areas of the sample.

In cement research, EM methods can be used (1) to study the morphology of particles, texture of particle aggregates, crystal habits and crystal growth phenomena, (2) to characterize different phases by means of their appearance in pure or comparison preparations, and to identify from these observations

similar phases when they appear in cement paste mixtures, and (3) to observe changes in the morphology or crystallization properties of these phases caused by variations in composition, temperature, age of the sample, or preparation methods applied. Selected-area ED techniques, in combination with ordinary EM studies, can give much additional information in studies of cement hydration products where, as stated above, X-ray diffraction analysis may fail to give useful data, on account of the diffuseness or weakness of the X-ray patterns given by certain hydrated phases. The data obtained from ED patterns can be used (1) to identify various phases from their combined EM-ED characteristics, (2) to detect very small amounts of minor phases, (3) to study degree of crystallinity, lattice imperfections, and special diffraction effects in distorted crystal elements or lattices with substitutions, and in certain cases (4) to determine true unit cells and crystal symmetry. Useful data can sometimes be obtained by means of the technique of dehydrating and recrystallizing certain particles using a temporarily and locally increased electron beam intensity for heating the sample, until the ED diagram changes to a recognizable pattern of some anhydrous or lower-hydrate phase.

9. Notes on sample preparation in electron-optical studies

Some consideration should be given to the suitability of various methods of preparing paste samples for EM examination.

Obviously, the chief requirement for cement paste, when used as a construction material, is that of high mechanical strength and dimensional stability. These properties are closely connected with the microstructure and texture of the cement gel, and depend on the strength and resistance to deformation under load of the solid hydrate particles, and in particular on the character of links and bonds developed in the surfaces of contact between adjacent gel particles. It is therefore desirable to use methods of preparation which leave the original gel structure intact. On the other hand, in order to study the minute details of the gel particles directly, it is necessary to break down the paste into a fine powder.

In the experience of some investigators, ordinary methods of crushing and grinding, or alternatively of scraping and lathe-cutting, seem to cause relatively little distortion or disturbance of the finer details of the gel structure. A final step of wet-grinding of the powder, in a little ethyl alcohol or similar liquid, seems to produce a slightly better degree of dispersion of the material for EM examination purposes. In order to obtain a sufficiently high degree of dispersion with especially hard or tough paste samples some investigators have

employed ultrasonic treatment of coarsely-ground material suspended in a suitable organic liquid, apparently without harmful or disturbing effects.

The powdered paste can be placed dry on the EM specimen film, to which at least the smaller particles usually adhere in sufficient quantities. Alternatively, the dispersed material can be immersed in a suitable organic liquid which does not attack the specimen appreciably or cause the particles to coagulate, then a drop of the suspension placed on the specimen film, and the solid material allowed to settle. Ethyl alcohol has been used as immersion liquid in the preparations described later in this paper, other investigators have used butyl alcohol, trichloroethane or similar liquids.

Water can be considered unsuitable as a suspension medium for powdered paste specimens, since it attacks and hydrolyses the hydrate constituents, thus destroying the original microstructure. However, if EM specimens are prepared as quickly as possible after immersing the ground material, the effect of water may be confined to a breaking-up of the larger aggregates into their microstructural elements, the latter being attacked only slightly. In this way, water can be used to reveal the internal microstructure of samples consisting of large aggregates that are difficult to disperse by other means.

Saturated lime solution can be used as a suspension liquid, since if offers an environment with which the hydrated constituents of a powdered paste are in approximate equilibrium. Extreme care must be taken, however, to avoid carbon dioxide attack of the solution and the sample particles.

Many particles in powdered paste or other cement hydration products consist of aggregates of smaller elements, and their surfaces are often rough and irregular. Thus, when an EM specimen is prepared in the usual way by depositing the sample particles on a thin collodion film, they tend to pierce this and cause the whole film to break, especially when heated through absorption of electron beam energy. To avoid this, it has become customary to reinforce the collodion film by evaporating a thin layer of carbon on to it in vacuum. For practical EM examination purposes, such a composite film is nearly structureless, and also gives weak and insignificant ED effects. Upon excessive heating, however, graphitization can occur, causing a few strong, diffuse rings to appear in the ED diagrams. Alternatively, the collodion film can be strengthened by an evaporated layer of some metal, e.g. aluminium, silver, or gold. The ED diagrams of such films contain the powder pattern rings from the corresponding metal. In certain studies, it is useful to have such a pattern on the photographic record, since it provides an internal calibration standard for other patterns present. However, these strong patterns may easily mask and conceal weak reflexions from other substances, and the use of metal backing layers is therefore to be avoided in general EM survey studies, and especially in the detection and analysis of the weak ED effects given by certain important paste constituents.

10. Notes on the calibration of electron diffraction diagrams

The accuracy of lattice spacings obtained from measurements on the ED diagrams is inferior to that reached in X-ray diffraction measurements (*Grudemo* 1955), or in electron diffractometers specially designed for the purpose of ED measurements. However, in careful work, it should be possible to attain an accuracy of about 0.5 percent or even less.

The data on spacings given in connection with various ED diagrams below have usually been obtained by measurements made directly on the original film. The measuring device most commonly used has been a 20 mm micrometer scale, with 0.1 mm divisions, clamped in an adjustable manner directly on to the film, and inspected by a 12x magnifier. With sharp reflexion spots or rings, the accuracy of measurement can be estimated at about 0.01 mm, at least for mean values of a few readings. For a 2 Å reflexion, this corresponds to a accuracy of 0.2 percent.

To a good degree of approximation, the equation $d \cdot D = P$ is valid, where d is a lattice distance (in Å), D is the corresponding diameter, of a ring or pair of opposite spots, measured on the film (in mm), and P is a parameter which is substantially constant. Its variation within a certain diagram can be expressed as $P = P_0(1 + k/d)$. In the film records given by the PCA instrument, the term k/d is almost immeasurably small, at the most about 0.004 at $d = 1$ Å, whereas in the Swedish records, the corresponding value varies between about 0.01 and 0.02.

P_0 represents the actual value of the parameter on a certain occasion, and with certain settings of the controls. Thus, for given positions of the high tension (80 kV has been used throughout) and the prefocusing control at a certain magnification, it can vary with time during the daily run of the instrument, with the position of the ED focusing (magnification) control, and with the degree of defocusing necessary to bring out the proper diagram on the EM screen, possibly also with the character of the specimen. A few checks of the characteristics of the PCA microscope showed that the daily variation was small, less than one percent, and that the accuracy of adjustment could be estimated at about ± 0.3 percent, on the average. For more than one year and about one hundred runs, the variation of the parameter P_0 never seemed to exceed ± 0.5 percent of an average value. The parameter of the Swedish instrument varied within wider limits, and more erratically. In one series of tests, which is probably typical, the parameter increased about 4 percent during the first two hours of equilibration, after starting the electron microscope, then oscillated slowly in an interval of 1 to 2 percent. In other runs, the parameter has shown a slow and unpredictable drift of 1 to 2 percent, and the long-time variations have been still larger.

Several substances have been used as ED calibration standards on various occasions. Vacuum-deposited layers of certain metals, such as pure gold or silver, are very useful for this purpose. One disadvantage with such samples is a certain difficulty in reproducing them in very thin layers of uniform thickness and distribution of crystal orientation. In cement hydration systems, suitable standards can often be provided by compounds within the samples themselves, e.g. by crystalline formations of C, CH, and $C\overline{C}$ which give easily-recognizable interferences from known lattice spacings.

In other cases, ED diagrams from the clay mineral hectorite have been used for calibration purposes. This colloidal substance, which is morphologically very similar to low-lime C-S-H(I), of the crinkly-foil variety, is easily prepared for EM observations, and gives a strong ring diagram containing the cross-grating (*hk*) reflexions from the hexagonal base unit cell of hectorite. It should be noted, however, that the size of this unit cell is not always constant. Thus, for one species of hectorite the value 5.24 Å was measured (by comparison with ED patterns of C and CH), for another species of different origin the value 5.28 Å was obtained (from X-ray diffractometer measurements). The mineral contains hydroxyl water which may be slowly liberated in the dehydrating conditions prevailing in the electron microscope, causing the lattice to shrink. In one test, made with the Swedish microscope, a hectorite specimen was exposed to an electron beam of normal intensity for three intervals of 30 min. each, and during this treatment shrank about 3 percent, before the unit cell attained stable dimensions. When kept overnight in air of normal humidity, the lattice regained its earlier dimensions, but started to shrink at about the same rate, about two percent per hour, when again exposed to the same conditions. In a similar test, made with the PCA microscope, a hectorite specimen was measured every two minutes while being exposed to the electron beam. This exposure gave a total shrinkage of about 0.3 percent over the first 8 two-minute periods.

The figures on dehydration shrinkage of hectorite are of a certain interest in relation to drying processes of a probably similar nature taking place in the hydrated cement compounds of various types, during the time required for the EM examination of a certain sample. This type of shrinkage which manifests itself as a decrease of the lattice spacings in ED patterns, has been observed earlier for C-S-H(I) materials (*Grudemo* 1955), which in addition showed anisotropic shrinkage, i.e. the lattice contracted less in the direction of the supposed silica chains in the structure than perpendicular to the chains. In the micrograph section below, numerous examples are given of similar substances in different indefinite states of dehydration and correspondingly variable degrees of lattice contraction. Only subcrystalline materials, with restricted or distorted lattice growth, and with a high specific surface, seem to react in this way when placed in very dry conditions. A higher degree of

crystallinity, e.g. that of the minerals with cross-grating layer lattices of hexagonal symmetry exemplified by CH and C-A-H (hex.), is probably associated with a more exactly defined water dissociation pressure at a certain temperature. Consequently, when exposed to sufficiently severe conditions of dehydration, these structures give off water suddenly, without much previous contraction of the lattice, and are transformed to other crystalline compounds or to a glass.

In the experience of the author, a convenient method of calibration of ED diagrams is to measure the diameter of a suitable interference ring given by a known lattice spacing, directly on the fluorescent screen and at certain time intervals, as needed. For these measurements, a simple comparator has been constructed, consisting of a long-distance, low-magnification microscope mounted on a traverse slide and stopped in its movement to each side by two oppositely-placed micrometer screws. This device is clamped to the screen of the desk-model electron microscope. For calibration substance, thin evaporated layers of Au or Ag can be used, and a suitable spacing is d_{220} (1.442 and 1.445 Å, respectively, in a ten-degree interval about room temperature).

11. Notes on electron micrographs

The photographic material was prepared by copying cropped areas, selected from the original microfilms, on to 10×10 cm photographic paper prints which were reduced to the 6×6 cm size used in the final reproduction. Paper gradations varying from very hard to very soft were used, depending on the contrast of the negative. The photographic enlargement varied between 4 and 13 times. The final magnification, as indicated by the one-micron mark at the bottom edge of each micrograph, varies between about 3,000 and 60,000 times. Care was taken to use the best methods of reproduction available, so that the unavoidable losses in detail and definition were kept at a minimum.

In preparing prints of most of the ED patterns, it was found necessary to employ special methods. Many materials of cement hydration contain a certain amount of subcolloidal and amorphous substance which, in ED patterns, gives a distribution of diffusely-scattered electrons extending with appreciable intensity to comparatively high scattering angles, equivalent to lattice distances of the order of 2 to 4 Å. The central regions of the corresponding photographic records are therefore frequently very dark, but may still contain many details. There is no normal photographic paper material available that can reproduce satisfactorily a negative with such a large latitude of photographic density. To compensate for this deficiency, a double-exposure method was adopted. The paper was first exposed for a short time with uniform intensity, giving the

correct exposure to the peripheral regions of the ED pattern. These parts were then screened-off by means of a well-centered circular aperture placed between the lens and the printholder stage of the enlargement apparatus, and the paper was given a second exposure, usually two to four times longer than the first one. By choosing the appropriate size and position of the aperture, in combination with the lens aperture, the incident intensity of exposure could be made to fall off from full to zero intensity within a suitable range of radii of the print. Nearly all the ED patterns were reproduced in this way, with two, or in many cases even three, exposures with a variable screening of the incident light. In order to get a high local contrast, photographically-hard paper was used throughout.

The degree of photographic enlargement of the ED patterns has been chosen so that all important diffraction effects, usually within a certain diameter, are included in the print. The scale constant of each diagram is indicated by the marks at the bottom edge, which give the diameter corresponding to 2 Å. Thus an approximate value of the lattice distance corresponding to a certain ring or pair of spots, is obtained simply by dividing twice the distance between the marks by the diameter of the reflexion. Most diagrams are slightly elliptical, owing to an anisotropic dilation of the photographic paper during processing.

Note added in proof: A comparison between the original microfilms, the photographic prints, and the final book-prints shows that each step of reproduction, and especially the last one, is accompanied by a certain loss of contrast and resolution of weak details, in particular in the ED patterns. Several features which are weak but still observable in the originals, and which are sometimes described and discussed in the text, may therefore be invisible, or nearly so, in the figures reproduced in the micrograph section. One example: the weak interstitial reflexions observed in the original microfilm of Fig. 153 b, and used for certain conclusions concerning the structural arrangement in the corresponding crystals, can hardly be detected in the final print.

12. Acknowledgements

The author wishes to express his gratitude towards the following members of the staff of PCA Research and Development Laboratories, Skokie, Illinois, U.S.A., who in various ways, have contributed to, or been connected with, the work reported in this paper:

Dr. *A. Allan Bates*, then Vice President, and Mr. *H. Woods*, Director of Research, sponsored my stay with PCA, and showed their great benevolence and interest in my studies in many ways.

Dr. *T. C. Powers*, then Manager, Basic Research Section, present Research Counselor, PCA, and Dr. *S. Brunauer*, present Manager, Basic Research Section, initiated and arranged for my stay with PCA, followed and guided my work with the greatest interest, and gave me their continual support in a most friendly and generous way.

Dr. *L. E. Copeland*, Basic Research Section, supported me in numerous ways with valuable instruction and advice, as well as helpful discussion.

Several other people at the Basic Research Section, the Analytical Laboratories, the Workshop, and other sections of PCA helped me on many occasions by carrying out certain measurements and analyses, by offering me samples, by constructing various instruments and tools, etc.

The author is much indebted to the CBI Board of Directors for giving their consent and unreserved support to the co-operation between the two institutions, PCA and CBI, as manifested in the author's studies with PCA.

The electron-optical studies have for many years been supported by grants from the Swedish Technical Research Council. A special grant from the Council made it possible for the author to attend the Symposium on the Chemistry of Cement, in Washington and Skokie, 1960. This financial support is hereby gratefully acknowledged.

The studies carried out by Dr. *S. Chatterji*, at present with Birkbeck College, University of London, have been accounted for in the preface. The author wishes to thank Dr. *Chatterji* for his excellent work, and for the most valuable complement to the micrograph collection extracted from his electron-optical microfilm records.

The author is very grateful towards Professor *O. Stelling*, of the Institution of Chemical Technology, KTH, and his staff, for putting the electron microscope and other facilities of the institution at our disposal, and for helpful discussions and suggestions.

Valuable help has been given by Mrs. *D. Danielsson* in correcting and improving the language of the English manuscript.

The author wishes to express his gratitude towards the *Royal Institute of Technology* for permission to publish this paper in their Transactions.

Swedish Cement and Concrete Research Institute,

Stockholm,

June 1964.

13. List of samples

With the general symbol Xy—OA, the following notations are used to characterize the samples:

X refers to starting materials: C=lime, S=silica, T=C_3S (or alite), D=β—C_2S (stabilized, belite), A=C_3A, P=portland cement, H=high-alumina cement. Mixtures are indicated CS, TA, etc.

y refers to type of preparation or state of sample: w=mixed with water to form suspension or slurry, l=mixed with lime solution, s=solution (or non-aqueous suspension), p=paste cured at normal temperatures, wq=aquous suspension cured at elevated temperature and saturated vapour pressure, pq=paste mix, similarly cured.

O is a serial number. A (B, C, etc.) is sometimes introduced to denote various ways of preparing a sample for EM observations, or various times at which a sample is studied.

An asterisk (*) indicates a sample prepared and studied by Dr. *Chatterji*.

Under each sample is a list of compounds or structures observed in it (in certain cases perhaps only a contamination, not the representative structure). The figures refer to the page number and the position on the page (1 to 6).

Al—1

Pure C_3A (prepared at PCA, ground to pass 200 mesh sieve with about 10 percent residue), mixed with supersaturated lime solution, 30.8 millimol per liter, taken directly from ion-exchange column (see Cs—3), in proportion 7.4 millimol C_3A per liter solution, bottle-hydrated on rotating wheel for about 2 months, then stored, examined by EM at about 6 months' age. EM sample preparation: as Aw—1.

17—3 Cubic crystals and plates

Determination of CaO in filtered solution at about 10 months' age gave a ratio C/A about 4.5 in solid in a lime solution of 19.8 millimol per liter, assuming the concentration of A in solution to be negligible.

Al—2

C_3A as in Al—1, mixed with saturated lime solution, 22.2 millimol per liter, in proportion 7.4 millimol C_3A per liter solution, bottle-hydrated for about 2 months on rotating wheel, then stored.

A. Examined a few days after removal from rotating wheel. EM sample preparation: as Aw—1.

12—5/6 CH crystals
17—1 Hydrogarnet crystals
20—3/6 C-A-H (hex.) plates
21—1/6 Similar
22—1/6 Similar
23—1/4 C-A-H (hex.) plates, C$\bar{C}$-contaminated

B. Examined at 6 months' age, otherwise as A.

17—2 Plates and cubic crystals
23—5/6 C-A-H (hex.) plates

Determination of CaO in filtered solution at about 10 months' age gave a ratio C/A about 3.6 in solid, in a lime solution of 18.2 millimol per liter, assuming the concentration of A in solution to be at most 0.1 millimol per liter.

A similar batch (not examined by EM), started with 7.4 millimol C_3A per liter in a lime solution of 11.1 millimol per liter, and ended with a lime concentration of 10.2 millimol per liter.

The concentration of A in solution was not measured, but the composition of the sample is probably near to the invariant point Y of $C_4A \cdot aq - C_{2.4}A \cdot aq$ shown by *Jones* and *Roberts* 1962, Fig. 7, at about 11 millimol C, 1.0 millimol A per liter. Even in this batch, the overall C/A ratio is therefore probably about 3.6.

*Ap—1**

C_3A prepared at CBI (by repeated burning of $C\bar{C}$+A mixture), ground to pass DIN No. 70 sieve, mixed with water, w/c about 0.6, starting temperature 10 to 15° C, to form a thick slurry. Although reaction started immediately, there was no abnormal rise in temperature during mixing. The mixture was cast in plastic capsules. Setting occurred within about 3 hours. Immediately after mixing, and after curing for certain times, paste samples were examined by XD and EM. The EM samples were made by crushing and grinding the paste with ethyl alcohol. A drop of alcohol suspension is placed on an EM specimen screen and allowed to spread and dry.

A. Sampling time: 24 hours

25—5/6 C-A-H (hex.) plate

B. Sampling time: 14 days

103—5/6 Representative particles

*Ap—2**

As Ap—1, but with 1/6 (by weight) of solid C_3A replaced by $C\bar{S}H_2$ (gypsum). The paste mixture was fluid and had not set at 24 hours, but was rather hard after 14 days.

A. Sampling time: 3 hours

44—1/2 Ettringite-type formations

B. Sampling time: 24 hours

44—3/4 Ettringite-type formations

C. Sampling time: 14 days

44—5/6 Plate particles
104—1/2 Representative particles

*Ap—3**

As Ap—1, but with 1/6 (by weight) of solid C_3A replaced by burnt lime, of a highly reactive type. Due to the slaking of lime, this mixture became appreciably warmer during mixing, and after a couple of minutes had an earth-dry consistency. The EM sample shown was taken at 14 days.

104—3/4 Representative particles

*Ap—4**

As Ap—1, but with 1/6 (by weight) of solid C_3A replaced by $C\bar{S}H_2$ (gypsum) and C (burnt lime, highly reactive) in equal amounts. The paste mix was fluid and required more than 24 hours for setting. The EM sample shown was taken at 14 days.

104—5/6 Representative particles

Aw—1

Pure C_3A (prepared at PCA, ground to pass 200 mesh sieve with about 10 percent residue) mixed with water, 7.4 millimol C_3A per liter, bottle-hydrated on a rotating wheel for about 2 months, then stored, examined by EM at about 5 months' age. EM sample prepared by placing a drop of suspension on an EM specimen screen in a stream of dry, CO_2-free air, allowing to settle, sucking away most of the drop, and drying-in the rest.

19—1/6 C-A-H (hex.) crystals
20—1/2 Similar

Determination of CaO in filtered solution at about 10 months' age gave a lime concentration of 7.3 millimol per liter. The concentration of A in solution was not measured but, judging from the diagram, Fig. 7, given by *Jones* and *Roberts* 1962, this value can be estimated to be about 2.5 millimol per liter, giving an overall C/A ratio of about 3.0.

Aw—2

C_3A as in Aw—1, mixed with water in proportion 1:25 (148 millimol per liter), suspension stirred vigorously for 10 min. in a high-speed micro-mixer with sealed lid. The resulting suspension was milky and almost stable, settled very slowly.

A. EM sample prepared immediately, as Aw—1.

17—4 Mainly hydrogarnet phase
24—1/6 Hydrogarnet and C-A-H (hex.) phases, transformations upon heating.

B. EM sample prepared after 40 days' standing of the suspension, otherwise as A.

17—5/6 Mainly hydrogarnet phase
25—1/4 Hydrogarnet and C-A-H (hex.) plates

Cs—1

Saturated CH solution, sprayed in droplets on EM specimen film in air (attack by CO_2 probable), quickly dried by means of heating lamp.

1—1/2 Spherulites

Cs—2

Saturated CH solution, drop placed on EM specimen film in air, kept for a few minutes (formation of carbonate layer probable), then removed by means of filter paper.

1—3/6 Chains of spherulites of different sizes, thermal trans-
2—1/6 formations, formation of $C\bar{C}$ and C.
3—1/6

Cs—3

Saturated CH solution, prepared in ion-exchange column: equal amounts of 0.2-n $CaCl_2$ and 0.044-n CH solutions were passed through anion-exchange resin (IRA-400) saturated with OH^- ions, resulting in an effluent of supersaturated CH solution, about 0.063-n, in which, within a few hours, a precipitate of CH crystals formed and the concentration dropped to saturation, about 0.044-n. EM sample was made by quickly placing small drop of solution on specimen film in a stream of dry, CO_2-free air, and allowing the drop to dry.

4—1/2 Network, CC̄ crystals
6—5/6 Large hexagonal crystals
11—3/4 Striated plate

Cs—4

Saturated CH solution, sprayed in small droplets on to EM specimen film placed in nozzle with stream of dry, CO_2-free air, and allowed to dry.

6—3/4 Hexagonal crystals

Cs—5

CH powder (C.P. reagent $Ca(OH)_2$), dispersed in ethyl alcohol during ultrasonic treatment, suspension sprayed on to EM specimen film placed in nozzle with stream of dry, CO_2-free air, allowed to dry.

6—1/2 CH hexagonal-plate crystals

CSw—1

CH prepared by slaking C from freshly ignited CC̄, mixed with silica (Mallinckrodt's Silicic Acid) and with water, in proportions C/S 2, water/solid 9. Reacted in a steel ball mill at 24° C for 35 days of intermittent grinding, slurry frozen and vacuum-dried at $5 \cdot 10^{-4}$ mm Hg. This is sample F-34 of *Kantro*, *Brunauer*, and *Weise* 1959, and according to their analysis, it consists of afwillite (about 81 percent by weight) and CH (about 17 percent), about 20 percent of the latter constituent being non-crystalline.

EM sample preparation: The concentrated dispersion was diluted ten-fold with saturated lime solution, a drop of the suspension was quickly transferred to an EM specimen screen placed in a stream of dry, CO_2-free air, allowed to settle, and drained away, leaving a thin layer of solid residue on the specimen film.

55—1/6 Representative particles, afwillite

CSw—2

As CSw—1, except for the silicic acid ingredient, which was the highly colloidal silica Cab—O—Sil (cf. Sw—2). This batch was dried after ball-milling.

A. Dry powder dispersed in saturated CH solution, EM sample prepared as for CSw—1.
54—3 Representative particles, C-S-H(I) foils

B. Dry powder deposited as a thin layer on EM specimen screen, excess material shaken away.

54—4/6 Similar

The sample was designated as F-35 by *Kantro et al.* 1959, (not mentioned in the paper). Their X-ray analysis showed no afwillite but, in addition to crystalline CH, the diffuse lines characteristic of either hydrate III or badly-crystallized tobermorite.

CSwq—1

Pure, synthetic, well-crystallized tobermorite, obtained from Professor *H. Funk*, Berlin. EM sample prepared from ethyl alcohol suspension of crystal powder.

45—1/3 Representative crystals

*CSwq—2**

Lime and silica mixed with water to a suspension of thin slurry consistency, C/S 1.0, autoclaved at 200° C and saturation pressure for 1.5 hours. Solid phase washed with acetone and ether, and dried, all in a CO_2-free atmosphere. A small amount of the powder was shaken with ethyl alcohol, and an EM sample made by placing a drop of the ethyl alcohol suspension on an EM specimen screen and allowing to dry.

Specification of starting materials:

Reactive lime was made from $CaCO_3$ (p.a., low in alkali, ignited at about 1000° C for 8 hours, further burnt for some hours immediately before use, silica consisted of Aerosil, 99.9 percent SiO_2, highly colloidal, specific surface area 380 m^2/g.

59—1/2 Xonotlite crystals

*CSwq—3**

Lime and silica in water suspension, C/S 1,5 autoclaved at 200° C and saturation pressure for 48 hours, otherwise as CSwq—2.

60—5/6 Foshagite crystal aggregates
61—1/2 ED patterns

*CSwq—4**

Lime and silica in water suspension, C/S 2, autoclaved at 100° C and saturation pressure for 1.5 hours, otherwise as CSwq—2.

112—3/4 Plate, hexagonal structure, probably contamination

*CSwq—5**

Lime and silica in water suspension, C/S 2, autoclaved at 200° C and saturation pressure for 48 hours, otherwise as CSwq—2.

61—3/6 Hillebrandite crystal aggregates and ED patterns

Dp—1

β—C_2S paste, w/c 0.7, hydrated at 25° C for 17 months, when it was 72.5 percent hydrated, then ground and dried at a vapour pressure of $0.5 \cdot 10^{-3}$ mm. Hg (sample No. C-23, according to *Brunauer* and *Greenberg* 1962).

A. Deposited as dry powder in thin layer directly on specimen screen.

73—3/6 Representative particles
74—1/2 Similar
113—1/2 Floc of nearly amorphous particles, minor constituent

B. Powder dispersed in ethyl alcohol, drop of suspension placed on specimen film, where it spreads and dries quickly.

16—5/6 CH plate, converted to C
73—1/2 Representative fibrous particles
109—1/2 Plate, probably contamination

C. Powder dispersed in water and shaken for a few seconds. It was noticed that the solid phase of this suspension flocculated and settled much more easily than in the alcohol suspension. EM sample made immediately by placing drop of suspension on specimen screen in nozzle with stream of dry, CO_2-free air, removing excess liquid, and allowing to dry.

72—1/4 Representative particles
72—5/6 ED patterns, possibly from anhydrous phase.

*Dpq—1**

β—C_2S mixed with water to a stiff paste, formed into small nodules which were cured in saturated atmosphere over night, and then autoclaved at 100° C and saturation pressure for 72 hours.

The paste was then crushed, washed with acetone and ether, and dried, all in a CO_2-free atmosphere. A small amount of the material was dispersed in ethyl alcohol by means of ultrasonic treatment, and an EM sample made by placing a drop of suspension on the EM specimen screen and allowing to dry.

74—3 Representative particles, fibers.

*Dpq—2**

As Dpq—1, except autoclaving temperature which was 150° C.

74—4 Representative aggregate

*Dpq—3**

As Dpq—1, except autoclaving temperature which was 200° C.

74—5/6 Representative particles

*Dwq—1**

β—C_2S mixed with water to a suspension of thin slurry consistency, autoclaved at 200° C and saturation pressure for 72 hours. Further preparation, see CSwq—2.

46—3/6 Representative crystals, tobermorite.

The β—C_2S used in the Dwq, Dpq, DSwq, and DSpq series of preparations was prepared and given to us some years ago by Dr. *H. F. W. Taylor*, Aberdeen.

*DSpq—1**

β—C_2S and silica (Aerosil, see CSwq—2), in over-all proportion C/S 1.5, mixed with water to a stiff paste, then prepared as Dpq—1, autoclaving temperature 150° C.

46—1/2 Crystal plate, tobermorite

*DSpq—2**

β—C_2S and silica (Aerosil, see CSwq—2), in over-all proportion C/S 1, mixed with water to a stiff paste, then prepared as Dpq—1, autoclaving temperature 200° C.

112—5/6 Plate aggregate, probably contamination

*DSwq—1**

β—C_2S and silica (Aerosil, see CSwq—2), in over-all proportion C/S 1, mixed with water etc., as Dwq—1.

60—2 ED pattern, probably xonotlite
60—3/4 Representative particles

Hp—1

High-alumina (Alcoa, white) cement paste, fully hydrated, ground, EM specimen prepared by depositing a thin layer of dry powder directly on specimen screen placed on a specimen probe, tapping the probe gently to work the powder into the support film, and shaking off the excess material.

102—1/4 Representative particles
111—1/2 Irregular plate, possibly contamination

Hp—2

High-alumina (Lumnite, dark) cement paste, fully hydrated, ground.
EM specimen preparation: As Hp—1.

103—3 Representative gel aggregate

Hpq—1

As Hp—1, but hardened paste was in addition cured at 95° C for 72 hours.

102—5/6 Representative particles
103—1/2 Similar
111—3/4 Thin plate, possibly contamination

Hpq—2

As Hp—2, but hardened paste was in addition cured at 95° C for 72 hours.

103—4 Representative gel aggregate
111—5/6 Thin plate, possibly contamination

The H samples were prepared by Dr. *W. J. Smothers*, Ohio Brass Co. According to his X-ray analysis, the heated samples showed the expected transformation of the hexagonal hydrates into cubic C_3AH_6.

Pp—1

Cement paste, ASTM Type I cement (PCA lot No. 15754, see *Powers* and *Brownyard* 1948), about 1800 cm^2/g, w/c 0.65, cured 5½ years. Ground to pass 200 mesh, dried over dry ice (D-drying) (sample C-49 of *Copeland*, *Kantro*, and *Verbeck* 1962).

A. Small amount of dry powder deposited on specimen screen placed on a glass plate, powder bed allowed to slide back and forth over screen during tapping of the edge of the plate, excess material shaken off.

13—1/2 CH crystal plate
35—1/2 C-A-H (hex.) crystal plate
79—1/4 Representative gel particles

B. Powder dispersed in ethyl alcohol, drop of suspension placed on EM specimen screen where it spreads and dries quickly.

78—1/2 Representative gel particles
107—5/6 Thin plate, probably contamination
109—3/4 Plate aggregate, probably contamination
113—3/4 Floc of small plates, probably contamination

Pp—2

Cement paste, ASTM Type I cement (PCA lot No. 15754, see *Powers* and *Brownyard* 1948), w/c 0.55, vacuum mixed, freshly hardened paste cylinder used 1 day for freezing experiments, then stored in stoppered glass tube for about 5 months.

About 1 mm of surface layer removed by cutting on the lathe, the powder from a few subsequent fine cuts collected and examined.

EM sample preparation: As Pp—1A

34—1/2 C-A-H (hex.) crystal plate
78—3/6 Representative fibrous gel aggregates
106—1/2 Thin plate, probably contamination
113—5/6 Floc of small plates, probably contamination

Pp—3

Cement paste, ASTM Type I cement, w/c 0.70, cast in vial, stoppered and cured at room temperature for about 9½ years then cut on the lathe to produce fine chips which are further dry-ground to pass a 200 mesh sieve.

EM sample preparation: As Pp—1A

34—3/4 C-A-H (hex.) plate
80—1/4 Representative gel aggregates
106—3/4 Plate, probably contamination

Pp—4

Cement paste, w/c 0.35, otherwise as Pp—3. This paste was especially hard and difficult to grind.

80—5/6 Representative gel aggregates

Pp—5

Cement paste, w/c 0.70, prepared from fine fraction (about 8000 cm^2/g) of an ASTM Type I cement (no apparent change in chemical composition in the fine fraction). Cast in glass vial, sealed and kept at room temperature for about 2½ years.

Sample taken from bottom core of the paste cylinder by milling on the lathe. Powder further reduced by grinding with small amount of ethyl alcohol, sample diluted further with ethyl alcohol. Drop of suspension placed on EM specimen screen where it spreads and dries quickly.

34—5/6 C-A-H (hex.) plate
84—1/2 Representative gel particles
106—5/6 Plate, probably contamination (clay mineral)

Pp—6

Cement paste, w/c 1.50, prepared from fine fraction (about 8000 cm^2/g) of an ASTM Type I cement (no apparent change in chemical composition in the fine fraction). Cast in glass vial and sealed. To prevent excessive separation at this very high w/c ratio, the vial was rotated slowly about its axis, placed horisontally, until setting occurred. Kept at room temperature for about 3¼ years.

After this time, the paste was still saturated (moist), and had a soft consistency resembling that of soapstone.

A. Some material was chipped off from the interior by cutting on the lathe, the lathe chips were quickly transferred to a desiccator with ascarite. The dry material was lightly ground and deposited dry on the EM specimen film, as for Pp—1A.

35—3/6 C-A-H (hex.) plates with fibers
36—3/6 Similar
84—3/4 Fibrous gel particles
110—1/2 Plate, probably contamination

B. The lathe chips from A were not dried, but immediately ground with ethyl alcohol and further diluted to a suspension. A drop of this was placed on the EM specimen screen, where it spreads and dries quickly.

36—1/2 C-A-H (hex.) plate
84—5/6 Representative gel particles, fibers
85—1/6 Similar
107—1/4 Mainly plates, probably contamination

Pp—7

Cement paste, ASTM Type I cement (PCA lot No. 15754, see *Powers* and *Brownyard* 1948), w/c 0.45, cured saturated at 5° C for about 7 months, cured isolated at 25° C for about 7 months.

Paste cylinder turned on the lathe, outer layer removed, lathe chips collected from core and ground with ethyl alcohol, further diluted, drop of suspension placed on EM specimen screen and dried in.

14—5/6 CH aggregate
79—5/6 Representative gel particles

Pp—8

Cement paste, ASTM Type II cement (PCA lot No. 15622), about 2200 cm^2/g, w/c 0.60, cured 7½ years at room temperature. Ground to pass 200 mesh sieve, dried over dry ice (sample C-33 of *Copeland, Kantro,* and *Verbeck* 1962).

EM sample preparation: As Pp—1B.

81—1/2 Representative gel particles

Pp—9

Cement paste, ASTM Type III cement (PCA lot No. 15497, see *Powers* and *Brownyard* 1948), about 2500 cm^2/g, w/c 0.6, cured 7½ years at room temperature. Ground to pass 200 mesh sieve, dried over dry ice (sample C-31 of *Copeland, Kantro,* and *Verbeck* 1962).

EM sample preparation: As Pp—1B.

16—3/4 CH plates, converted to C
81—3/4 Representative gel aggregates
110—3/4 Thin plates, probably contamination

Pp—10

Cement paste, ASTM Type IV cement (PCA lot No. 15669, see *Powers* and *Brownyard* 1948), about 2300 cm^2/g, w/c 0.6, cured 7½ years at room temperature. Ground to pass 200 mesh sieve, dried over dry ice (sample C-32 of *Copeland, Kantro,* and *Verbeck* 1962).

A. EM sample preparation: As Pp—1A.

13—3/4 CH crystal
14—1/2 CH crystal
81—5/6 Representative gel aggregates
82—1/3 Similar
108—1/4 Plate aggregates, probably contamination

B. EM sample preparation: As Pp—1B.

82—6 Representative gel particles
110—5/6 Plate particles, probably contamination

C. Dry powder ground with ethyl alcohol, otherwise as B.

16—1/2 CH crystal pattern, compared with mica pattern
82—4/5 Representative gel particles
83—1/6 Various types of gel particles
108—5/6 Plate, probably contamination

Pp—11

Cement paste, Swedish standard cement (Limhamn), Bogue composition (percent by weight) approximately 63—21—5—8—3 for $C_3S—C_2S—C_3A—C_4AF—C\bar{S}$ respectively, according to *Danielsson* (private communication), low in alkali (K_2O 0.1, Na_2O 0.1 percent), w/c 0.30, kept isolated for about 100 days at 20° C, crushed and ground in ethyl alcohol, ultrasonorated in alcohol suspension. Drop of suspension placed on EM specimen screen where it spreads and dries quickly.

87—3/6 Representative gel particles

Pp—12

Cement paste, Swedish standard cement (St. Vika), Bogue composition (percent by weight, computed on 100 percent total weight) approximately 61—18.5—7—8.5—5 for $C_3S—C_2S—C_3A—C_4AF—C\bar{S}$ respectively, according to *Danielsson* 1962, relatively high in alkali (K_2O 0.4, Na_2O 0.4 percent), w/c 0.5, stirred 5 min., which gave a thin slurry of a fluidity much higher than that of the corresponding clinker paste (cf. Pp—13). Cast in small plastic containers with tight-fitting lid, kept in water at room temperature.

A. 2 hours after mixing, the paste was still fluid, some bleeding was observed. A small amount was ground with ethyl alcohol. The alcohol suspension flocculated and settled rapidly in a test tube. A drop of suspension was spread over an EM specimen screen and allowed to dry.

86—1/2 Representative particles

B. 6 hours after mixing, otherwise as A. the paste had started to set, the alcohol suspension of the lightly ground paste flocculated and settled easily.

86—3/4 Representative gel structures

C. After 4 days, paste hard. Ground with ethyl alcohol, suspension did not flocculate as earlier. EM sample prepared as before.

86—5/6 Representative gel structures.
87—1/2 Similar

Pp—13

Clinker paste, Swedish standard cement clinker (St. Vika), with a low natural content of sulfate. Clinker nodules crushed and ground 18 hours in laboratory steel ball mill, paste made with w/c 0.5, stirred 5 min. and cast in small plastic containers with tight-fitting lid, kept in water at room temperature.

A. 2 hours after mixing, the paste was still fluid. A little of the wet paste was stirred with ethyl alcohol and further diluted to give an easily flocculating suspension. EM sample prepared as for Pp—12.

88—1/4 Representative structures

B. 6 hours after mixing, the paste had started to set and was rather dry. Stirred with ethyl alcohol, it formed an easily flocculating suspension. EM sample prepared as before.

88—5/6 Representative structures
89—1/2 Similar

C. 24 hours after mixing, paste hardened, but fragments could be removed by means of a spatula. Ground with ethyl alcohol to form a suspension which did not flocculate appreciably. EM sample prepared as before.

89—3/4 Representative structures

D. After 7 days, the paste was hard as stone. Ground with ethyl alcohol to form a true suspension with very finely-divided material. EM sample prepared as before.

89—5/6 Representative structures

Ppq—1

Cement paste, ASTM Type I cement, w/c 0.46, cured at 98° C, 700 kg/cm² for 24 hours, then kept for some time in water at normal temperature, cut into cubes used in certain tests, then preserved dry in a sealed glass tube for about 7 years. A piece of paste was milled on the lathe and the powder was further ground in a mortar. EM sample prepared by depositing a thin layer of dry powder directly on specimen screen and shaking off excess material.

14—3/4 CH crystal plate
94—1/2 Representative gel aggregates
105—3/6 Plates, probably clay mineral particles

Ppq—2

Cement paste, hydrothermally cured at 177° C, other data equal to Ppq—1. EM sample prepared by dispersing the ground material in ethyl alcohol and placing a drop of suspension on EM specimen screen where it spreads and dries quickly. Another EM sample for which no micrographs are shown, was placed dry on screen, as for Ppq—1. The two samples were essentially identical in appearance.

97—1/6 Representative gel particles
98—1/6 Well-crystallized fibrous material
105—1/2 Plate aggregate, probably clay mineral

Ppq—3

Cement paste, ASTM Type I cement, w/c 0.40, steam-cured at 216° C and saturation pressure for 24 hours, then kept refrigerated for about one year (taken from a series of freezing tests conducted by *G. Verbeck*, PCA). The thawing, moist specimen was cut on the lathe, and lathe chips from the interior immediately immersed in a little ethyl alcohol and ground, then further diluted. EM sample preparation: As Ppq—2.

13—5/6 CH crystal plate
99—1/6 Various gel structures
100—1/6 $C_3S \cdot aq.$ structures
101—1/6 Plate aggregates, clay-type minerals

*Ppq—4**

Standard cement, very similar to that of Pp—11, mixed with water to a stiff paste, further prepared as Dpq—1 (72 hours at 100° C).

94—3/4 Representative gel aggregates
94—5/6 CH crystal plate

*Ppq—5**

As Ppq—4, except for autoclaving temperature which was 200° C (for 72 hours).

95—1/4 Various gel structures.

Pw—1

Portland cement, ASTM Type I (PCA lot No. 15365, see *Powers* and *Brownyard* 1948) mixed with water in proportion w/c 10, boiled and stirred for about one hour (about half the volume evaporated). Liquid phase replaced by ethyl alcohol by repeated sedimentation, decantation, and dilution. EM sample made by placing drop of alcohol suspension on EM specimen film, where it spreads and dries quickly.

A. Freshly prepared alcohol suspension

26—1/2 C-A-H (hex.) plate
67—5/6 Fibrous network

B. Alcohol suspension one day old.

8—3/6 CH crystal plate
26—3/4 C-A-H (hex.) plate

Pw—2

Portland cement, ASTM Type I (PCA lot No. 15365, see *Powers* and *Brownyard* 1948), additionally ground (80 percent passing 400 mesh sieve), mixed with water in proportion w/c 10, stirred 18 hours in a stoppered flask at about 35° C. Small sample taken out, liquid phase quantitatively replaced by ethyl alcohol by repeated dilution, sedimentation, and decantation. EM samples made as for Pw—1.

27—1/6 C-A-H (hex.) structures
37—1/4 Ettringite-type structures

Pw—3

Remainder of Pw—2 boiled in flask with CO_2-protected reflux cooler for 7 hours with continuous stirring, then allowed to cool slowly for 16 hours.

A. Alcohol suspension and EM sample prepared in the same way as for Pw—2.

7—5/6 CH crystal plates
8—1/2 Similar
28—1/2 Various fibrous structures
37—5 Ettringite-type formations
66—5/6 Network of fibers

B. A few hours later, an EM sample was made from the aqueous suspension by spraying on to EM specimen film placed in nozzle with stream of dry, CO_2-free air.

28—3/6 Fibrous network
37—6 Ettringite-type formations
38—1/4 Similar

Pw—4

Portland cement, ASTM Type I (PCA lot No. 15365, see *Powers* and *Brownyard* 1948), mixed with water in proportion w/c 10, stirred vigorously for 10 min. in high-speed micro-mixer, with lid tightened by plastic wax, to prevent CO_2 contamination, then quickly transferred to stoppered bottle.

A. Small sample taken out immediately after mixing, liquid phase quantitatively replaced by ethyl alcohol by repeated dilution, sedimentation, and decantation. EM sample made by placing drop of alcohol suspension on EM specimen film, spreads and dries quickly.

7—1/2 CH crystal plates
68—1/2 Various hydrated structures

B. After 20 hours' standing, an EM sample was made from the remainder of the batch, by spraying the suspension on to an EM specimen film placed in nozzle with stream of dry, CO_2-free air.

7—3/4 CH crystal plates
26—5/6 C-A-H (hex.) crystal plate
68—3/6 Various hydrated structures

Pw—5

Prepared in the same way as Pw—4, but in proportion w/c 4, only 2 min. in high-speed mixer.

42—3/4 Representative structures.

Pw—6

Prepared in the same way as Pw—4, but in proportion w/c 4.

A. EM sample prepared as for Pw—4A.

10—3/4 Thin plate, CH pseuodomorph
29—1/2 Thin plate, unknown identity
42—5/6 Representative structures

B. After mixing, the suspension was stored CO_2-free until next day. After 18 hours, the bleeding water, amounting to 1/3 of total volume, was removed. A sample from the sediment was prepared for EM examination by dispersing in ethyl alcohol, as before.

10—5/6 CH crystal plates
18—1/4 Probably hydrogarnet phase
29—3/6 C-A-H (hex.) crystal plates
43—1/2 Representative structures
69—3/6 Similar

C. Remainder of batch stored for another 50 hours, EM sample from the half-dry paste prepared as before.

18—5/6 Probably hydrogarnet phase
30—1/6 C-A-H (hex.) crystal plates
43—3/6 Representative structures
71—1/6 Similar

Pw–7

Mix of same proportions as Pw–6, but hydrated for one hour in container fixed on a slowly rotating wheel.

A. EM sample prepared as for Pw–4A immediately after one hour's stirring.

9–1/4 Thin plates or foils, phase mixture
39–1/6 Rolled-foil phase, possibly gypsum
40–1/4 Similar
40–5/6 Various hydrated structures

B. Batch agitated on the wheel for 24 hours, EM sample prepared as before.

9–5/6 CH crystal plates
31–1/6 C-A-H (hex.) plates
32–1/4 Similar
41–1/4 Ettringite-type structures
69–1/2 Various hydrated structures

C. After standing for another 24 hours, the bleeding water, amounting to about 1/2 of total volume, was removed, and the sediment stored for another 72 hours. A sample of the half-rigid paste was prepared for EM examination as before.

10–1/2 CH crystal plates
32–5/6 C-A-H (hex.) crystal plates
33–1/6 Same plate, thermal conversions
41–5/6 Ettringite-type structures
42–1/2 Similar
70–1/6 Various hydrated structures

*PSpq–1**

Standard cement, same as in Ppq–4, mixed with silica (Aerosil, see CSwq–2), in over-all proportion C/S 2, and with water to form a stiff paste, further prepared as Dpq–2 (72 hours at 150° C)

95–5/6 Representative gel aggregates
96–1/2 Similar

*PSpq–2**

As PSpq–1, except autoclaving temperature, which was 200° C (for 72 hours).

96–3/6 Representative structures

Sl–1

A few drops of ethyl orthosilicate were pipetted on to the momentarily exposed surface of a saturated CH solution in a weighing bottle with tight-fitting lid, with an over-all C/S ratio for the batch of the order of 10. After a few minutes, a voluminous precipitate started growing out into the solution from the surface. After a few hours, the precipitate had settled on the bottom. A thin, easily cracked film was left on the surface.

After a week, the surface film was wiped off and transferred to a test tube, together with some solution.

A. EM sample made from the flocculated precipitate by placing a drop of suspension on an EM specimen film in a nozzle with stream of dry, CO_2-free air, allowing to settle, and removing the drop by means of filter paper.

47—1/6 Representative structures
48—1/4 Recrystallized structures
109—5/6 Flaky aggregate, probably contamination

B. EM sample from surface film, made similarly.

11—1/2 CH crystal (probably)
48—5/6 C-S-H(I) foils

Sl—2

Ethyl orthosilicate mixed with supersaturated lime solution, 30.8 millimol per liter, taken directly from ion-exchange column (see Cs—3), in proportion 6.3 millimol S per liter solution, bottle-hydrated on rotating wheel for about 2 months, then stored, examined by EM at about 6 months' age. EM sample preparation: As Sl—1A.

53—5/6 Representative structures
54—1/2 Similar

Determination of CaO in filtered solution at about 10 months' age gave a ratio C/S 1.84 in solid, in a lime solution of 19.3 millimol per liter.

Sl—3

Ethyl orthosilicate mixed with saturated lime solution, 22.2 millimol per liter, otherwise as Sl—2.

53—1/4 Representative structures

At 10 months' age: Ratio C/S 1.54 in solid, in a lime solution of 12.5 millimol per liter.

Sl—4

Ethyl orthosilicate mixed with half-saturated lime solution, 11.1 millimol per liter, otherwise as Sl—2.

52—3/6 Representative structures

At 10 months' age: Ratio C/S 1.17 in solid, in a lime solution of 3.75 millimol per liter.

Sl—5

Silica gel, approximate composition SH, C.P. reagent quality, dispersed in half-saturated lime solution, in proportion 5 millimol S and 11.1 millimol C per liter solution, otherwise processed as Sl—2.

52—1/2 Thin C-S-H(I) foils

At 10 months' age: Ratio C/S 1.02 in solid, in a lime solution of 5.9 millimol per liter. Two other batches (not examined by EM) with silica gel (5 millimol S per liter) in saturated (22.2 millimol C per liter) and supersaturated (30.8 millimol C per liter) lime solutions gave at 10 months' age ratios C/S in solid of 1.34 and 2.02, respectively, in lime solution of 15.4 and 20.5 millimol per liter, respectively.

Sw—1

Silica gel, approximate composition SH, C.P. reagent quality, dispersed in water (5 millimol S per liter), shaken for 2 months, standing 4 months.

EM sample preparation: Drop of suspension on EM specimen screen, allowed to settle and drained away, leaving a thin layer of solid on the specimen film.

114—1/4 Representative particles

Sw—2

Colloidal silica, Cab-O-Sil, of very high specific surface area (about 400 m^2/g) dispersed in water. EM sample preparation: As Sw—1.

114—5/6 Representative particles

Tl—1

Pure C_3S (prepared at PCA, Blaine surface area 4500 cm^2/g) mixed with supersaturated lime solution, 30.8 millimol per liter, taken directly from ion exchange column (see Cs—3), in proportion 4.2 millimol C_3S per liter solution, in polyethylene bottle stirred about 2 months on rotating wheel, then stored, examined by EM at about 4 months' age. EM sample prepared by quickly placing a drop of suspension on EM specimen film in nozzle with stream of dry CO_2-free air, allowing to settle, and removing most of the drop by means of a capillary tube.

5—3/4 Hexagonal plate, and $C\bar{C}$ formations
64—5/6 Representative formations
65—1/2 Similar

Determination of CaO in filtered solution at about 10 months' age gave a total solid composition of C/S 4.90 (probably including CH crystallized from the supersaturated solution within the first few hours) in a lime solution of 22.8 millimol per liter.

Tl—2

C_3S as in Tl—1, mixed with saturated lime solution, 22.2 millimol per liter, then treated and examined as Tl—1.

5—5/6 Fibrous network, $C\bar{C}$
11—5/6 Striated plates
38—6 Fibrous structures, similar to ettringite
64—1/4 Various representative structures

After 10 months: C/S 2.69 in solid, 23.5 millimol C per liter in solution.

A similar batch (not examined by EM) started with 7.45 millimol C_3S per liter in a lime solution of 11.1 millimol per liter, and ended (after 10 months) with C/S 2.10 in solid, in a lime solution of 17.8 millimol per liter.

Tp—1

C_3S paste, w/c 0.7, hydrated at 25° C for 17 months, when it was 100 percent hydrated, then ground and dried at a vapour pressure of $0.5 \cdot 10^{-3}$ mm. Hg (D-drying, samples A—D below), or $8 \cdot 10^{-3}$ mm. Hg (P-drying, sample E below) (samples No. C-17 and C-18 according to *Brunauer* and *Greenberg* 1962).

A. Deposited as dry powder in thin layer directly on specimen screen.

15–3/4 CH crystal
76–5/6 Representative aggregate structure

B. Powder dispersed in ethyl alcohol, drop of suspension placed on specimen film where it spreads and dries quickly.

15–1/2 CH crystal plate
76–2/4 Representative gel aggregates
77–1/2 Similar

C. Powder dispersed in water and shaken for a few seconds. It was noticed that the solid phase of this suspension flocculated and settled much more easily than in the alcohol suspension. EM sample made immediately by placing drop of suspension on specimen screen in nozzle with stream of dry, CO_2-free air, allowing to settle, removing excess liquid, and allowing to dry.

49–1/6 Various structures
75–1/6 Representative structures

D. Water suspension from C stored for 80 days, EM sample prepared in the same way as for C.

50–1/6 Representative structures
51–1/3 Fibrous aggregates

E. P-dried sample, deposited dry, equally to A.

15–5/6 CH crystal (probably)
76–1 Representative gel aggregate

*Tp–2**

C_3S-alite, of composition 52 $C_3S \cdot C_6AM$ (material prepared at Basic Research Section, PCA, see *Kantro, Copeland,* and *Brunauer* 1962), mixed with water, w/c 0.60, cast in small plastic vials. Setting occurred between 3 and 24 hours after mixing. Immediately after mixing, and after some times of curing, paste samples were examined by X-ray diffraction and EM. The EM samples were made by crushing and grinding the contents of one vial with ethyl alcohol. A drop of alcohol suspension was placed on an EM specimen screen and allowed to spread and dry.

A. Sampling time 24 hours.

90–1/3 Representative gel structures

B. Sampling time 14 days.

90–4/6 Representative gel structures

*Tp–3**

As Tp–2, but about 8 percent (by weight) of solid C_3S-alite replaced by $C\bar{S}H_2$ (gypsum). Setting properties were about the same as for Tp–2.

A. Sampling time 24 hours.

91–1/3 Representative gel structures

B. Sampling time 14 days.

91–4/6 Representative gel structures

Tw—1

Pure C_3S (prepared at PCA, Blaine surface area 4500 cm^2/g) mixed with water, 14.9 millimol C_3S per liter, in polyethylene bottle stirred about 2 months on rotating wheel, then stored, examined by EM at about 4 months' age. EM sample prepared by quickly placing a drop of suspension on EM specimen film in nozzle with stream of dry, CO_2-free air, allowing to settle, and removing most of the drop by means of filter paper.

4—3/6 Fibrous network, CH, C + $C\bar{C}$
12—3/4 CH crystals
63—1/6 Representative aggregates

Determination of CaO in filtered solution at about 10 months' age gave a total solid composition of C/S 1.69 in a lime solution of 19.5 millimol per liter.

Tw—2

C_3S as in Tw—1, added to boiling water, in proportion about 220 millimol C_3S per liter, boiled and stirred for 5 min., then cooled.

EM sample prepared by spraying suspension on to a specimen screen placed in nozzle with stream of dry, CO_2-free air.

5—1/2 Fibrous network, C + $C\bar{C}$
38—5 Similar
67—1/4 Various representative structures

Tw—3

C_3S as in Tw—1, mixed with water in proportion 1:25 (175 millimol per liter), suspension stirred vigorously for 10 min. in a high-speed micromixer with sealed lid. The resulting suspension settled quickly to a rather dense flocculate.

A. In one sample, taken immediately after mixing, the liquid phase was quantitatively replaced by ethyl alcohol by means of repeated sedimentation, decantation and dilution. A drop of suspension was spread over EM specimen screen and allowed to dry.

65—3/4 Representative aggregates

B. After standing overnight, the original water suspension was shaken up, and an EM specimen was prepared in the same way as for Tw—1.

65—5/6 Representative aggregates

C. After standing 6 weeks, the suspension was again examined as in B.

51—4/6 Fibers and foils
66—1/4 Representative structures

Tw—4

Pure C_3S, mixed with water in proportion w/c 9 (487 millimol C_3S per liter), ground in a steel ball mill at 24° C for 25 days of intermittent grinding, effective grinding time about 59 percent of this, slurry frozen and vacuum-dried at $5 \cdot 10^{-4}$ mm Hg. This is sample D-45 of *Kantro*, *Brunauer*, and *Weise* 1959, and according to their analysis, it consists of a

C_3S_2-hydrate mixture of afwillite and hydrate III, in approximate proportion 87 to 13, together with the theoretical amount of CH, about ten percent of which is non-crystalline.

EM specimen preparation: A thin layer of the dry powder was deposited directly on the specimen screen, and the excess material shaken off.

56—1/3 Conglomerates of plates, afwillite

Tw—5

Pure C_3S, mixed with water in proportion w/c 9 (487 millimol C_3S per liter), ball-milled as Tw—4, with an additional period of 4 weeks agitation following the ball-milling. This is sample D-62 of *Kantro*, *Brunauer*, and *Weise* 1959, and according to their analysis, it consists of apparently pure afwillite ($C_3S_2H_3$) together with the theoretical amount of CH, about ten percent of which is non-crystalline. The specific surface area is 16 m^2/g.

EM specimen preparation: A sample of the slurry was diluted about ten-fold with saturated lime solution, and this suspension was sprayed in small droplets on to an EM specimen screen placed in a stream of dry, CO_2-free air.

57—1/4 Representative particles

Tw—6

Pure C_3S, prepared as Tw—5. The preparation was then used in an attempt to recrystallize the afwillite phase into larger crystals by boiling and refluxing the suspension for some time.

A. Boiled and refluxed for 36 hours. EM specimen preparation: As Tw—5.

56—4/6 Representative particles, afwillite

B. As A, but boiled and refluxed for 7 days.

12—1/2 CH crystal plate
57—5/6 Afwillite crystals
58—1/6 Lath-shaped crystals

*Twq—1**

C_3S mixed with water to a suspension of thin slurry consistency, autoclaved at 100° C and saturation pressure for 72 hours. Further preparation, see CSwq—2.

77—3 Representative aggregate, fibrous

The C_3S used in the Twq and TSwq series of preparations was a batch of pure, triclinic C_3S prepared and given to us some years ago by Dr. *H. F. W. Taylor*, Aberdeen.

*Twq—2**

C_3S-water mixture, autoclaved at 150° C and saturation pressure for 72 hours, otherwise as Twq—1.

77—4/5 Representative structures

*Twq—3**

C_3S mixture, autoclaved at 200° C and saturation pressure for 72 hours, otherwise as Twq—1.

62—1/4 Crystal mixture, blocks and needles
77—6 Similar

*TAp—1**

C_3S-alite (see Tp—2) mixed with C_3A (see Ap—1) in proportion 4:1 (by weight), mixed with water, w/c 0.60, cast in small plastic vials, further prepared and examined as Tp—2.

A. Sampling time 24 hours.

92—1/2 Representative gel aggregates

B. Sampling time 14 days.

92—3/4 Representative gel aggregates
92—5/6 C-A-H (hex.) plate

*TAp—2**

As TAp—1, but about 8 percent (by weight) of solid mixture (alite—C_3A) replaced by $C\bar{S}H_2$ (gypsum).

A. Sampling time 24 hours.

93—1/3 Various gel aggregates

B. Sampling time 14 days.

93—4/6 Various gel aggregates

*TSwq—1**

C_3S and silica (Aerosil, see CSwq—2) in over-all proportion C/S 1, mixed with water, autoclaved at 150° C and saturation pressure for 72 hours, otherwise as Twq—1.

45—4/6 Representative crystals

*TSwq—2**

C_3S and silica (Aerosil), in over-all proportion C/S 1, mixed with water, autoclaved at 200° C and saturation pressure for 144 hours, otherwise as Twq—1.

59—3/6 Various crystals
60—1 ED pattern of xonotlite

*TSwq—3**

C_3S and silica (Aerosil), in over-all proportion C/S 2, mixed with water, autoclaved at 100° C and saturation pressure for 72 hours, otherwise as Twq—1.

112—3/4 Plate aggregate, probably contamination

*TSwq—4**

C_3S and silica (Aerosil), in over-all proportion C/S 2, mixed with water, autoclaved at 200° C and saturation pressure for 72 hours, otherwise as Twq—1.

62—5/6 Various representative structures

II. MICROGRAPH SECTION

1. C-H and C-$\bar{C}$-H

Precipitates from lime solutions, carbon dioxide contamination, spherulitic growth, thermal transformations

Figs. 1 and 2. Sample Cs—1.

EM (1): $\bar{C}$-contaminated lime precipitate, spherulitic formations of between 0.3 and 1μ in diameter.

(*ED:* Particles similar to these gave an original pattern consisting of only one diffuse ring at about 2.9 Å.)

EM (2): Particles similar to those of Fig. 1 heated by means of a temporarily-increased intensity of the electron beam. At a certain intensity, the spherulites of this particular sample were observed to expand suddenly. The expanded spherulites (one of them has burst) show diameters between about 0.5 and 1.5μ.

(*ED:* The sudden explosion of these particles was accompanied by the appearance of spots from calcite crystals in the ED pattern. Upon further irradiation, the pattern changed gradually into a C ring pattern, of cubic symmetry (cf. below, Fig. 3d).

Similar structures and transformations have been described by *Schimmel* 1957 and by *Grudemo* 1955, 1962.

Fig. 3. Sample Cs—2.

EM (3a): Large spherulitic aggregates (diameters 2 to 3μ) consisting of small, gelatinous particle elements (similar to Fig. 27 shown by *Grudemo* 1955). The surfaces of these spherulites are irregular (except for a couple of smaller ones near the upper edge), not smooth as those of the particles in Fig. 1.

ED (3b): Some rather weak arc reflexions from C$\bar{C}$ (calcite). These large aggregates absorb the electron beam power more efficiently than the smaller ones, and are thus heated and partly converted, even in an electron beam of normal intensity.

EM (3c): The same spherulites, after application of an electron beam of higher intensity, are readily converted to C, extremely small crystals of which show up as a fine-grained texture of the interior of the aggregates.

ED (3d): C ring pattern, reflexions at 2.777, 2.405, 1.701, 1.450, 1.389, 1.203, 1.104, 1.076 Å, etc. (values calculated from cubic unit cell, $a_{cub}=4.8105$ Å).

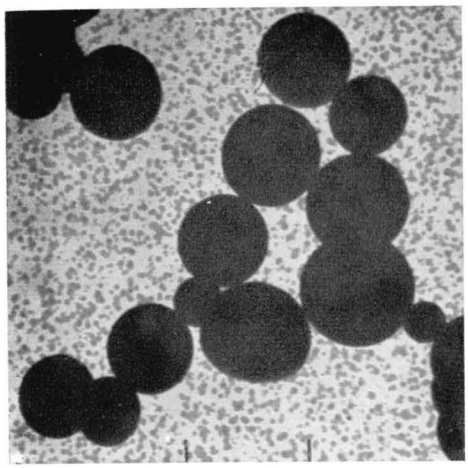

Fig. 1

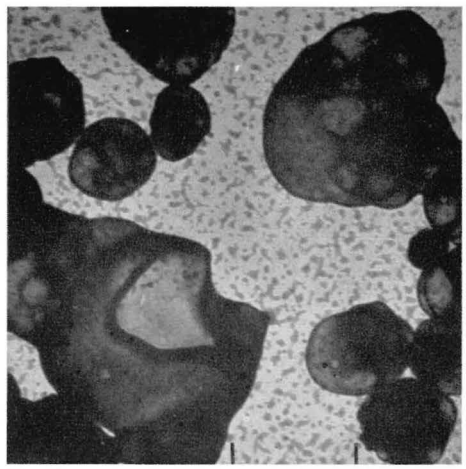

Fig. 2

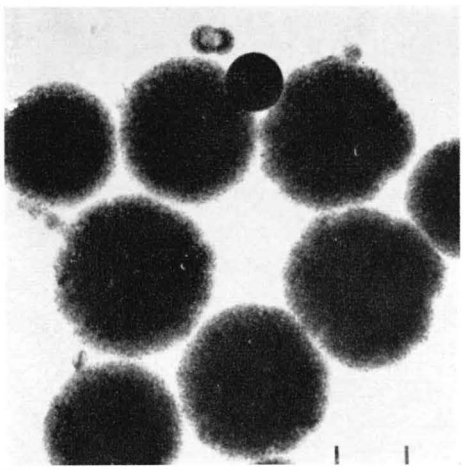

Fig. 3 a

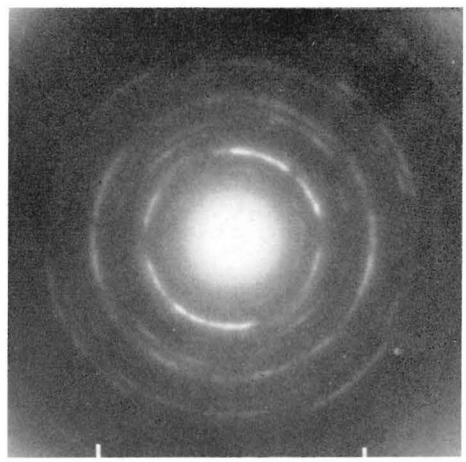

Fig. 3 b

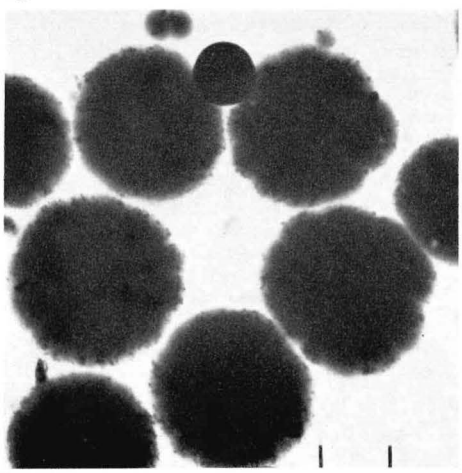

Fig. 3 c

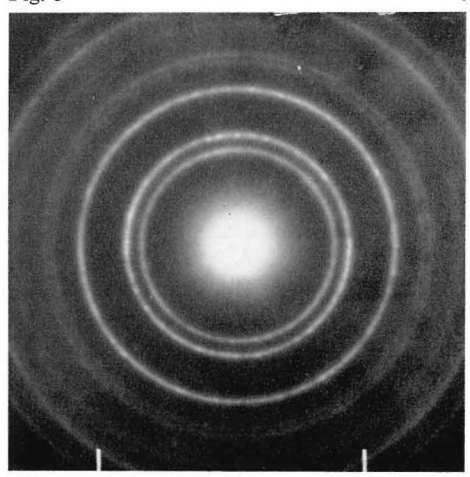

Fig. 3 d

2. C-H and C-$\bar{C}$-H

Precipitates from lime solutions, carbon dioxide contamination, spherulitic growth, thermal transformations (continued)

Fig. 4. Sample Cs—2.

EM (4a): Survey of sample, spherulites of various size classes, large (2 to 3μ), medium (0.3 to 0.5μ), hanging together in chains, and small (less than 0.1μ), also forming chains or clusters.

EM (4b): Central part of Fig. 4a at higher magnification. The larger spherulites are mottled with small C$\bar{C}$ (calcite) crystals, the formation of which is probably caused by the combined effect of vacuum and irradiation by the low-intensity electron beam used in the EM examination. The small spherulites are obviously still in their original, amorphous state, and unaffected by the surrounding conditions.

ED (4c): Spot and arc pattern of calcite, measured reflexions 3.85, 3.12 (spots, CH?), 3.04, 2.495, 2.29, 2.092, 1.932, 1.617, 1.521, 1.439, 1.246, 1.151 Å, etc. It can be observed that some arc reflexions (2.495, 1.439, 1.246) are arranged in hexagonal symmetry. These correspond to prism reflexions (11.0), (30.0), (22.0), respectively), all with $l=0$, using hexagonal-symmetry indexing of the calcite lattice spacings. The most probable explanation for these observations would be that the calcite crystals formed in the amorphous C-$\bar{C}$-H matrix orient themselves in preferential directions, due to some kind of mutual influence between neighbouring crystals.

ED (4d): After annealing for about 30 sec. in a beam of moderately-raised intensity, a C ring pattern (cf. text, Fig. 3d) appears and increases in intensity. This formation of C is accompanied by the decomposition of the first-formed calcite crystals (the C$\bar{C}$ arcs have disappeared). New calcite crystals are formed, but without any pronounced preferential direction of the crystal axes (rings of evenly-distributed spots).

EM (4e): After a short period of stronger irradiation, the internal structure of the larger as well as the smaller spherulites becomes increasingly porous and assumes a sponge-like texture.

ED (4f): After heating for another 30 sec. in a strong-intensity beam, all the calcite spots have disappeared, and only calcium oxide is left. The C crystals seem to increase in size (the reflexion rings are becoming spotty).

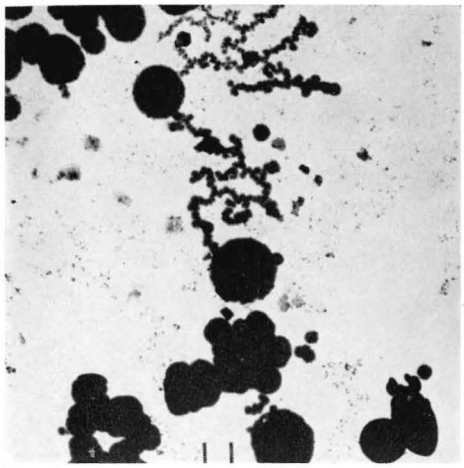

Fig. 4 a

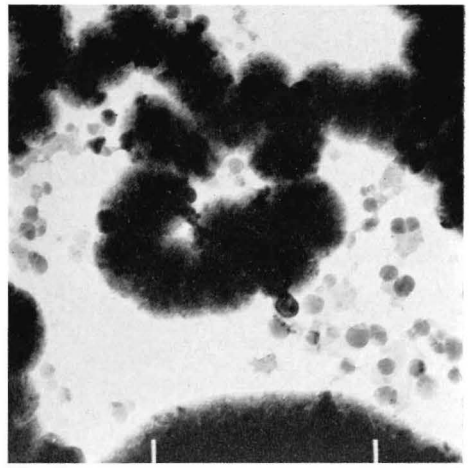

Fig. 4 b

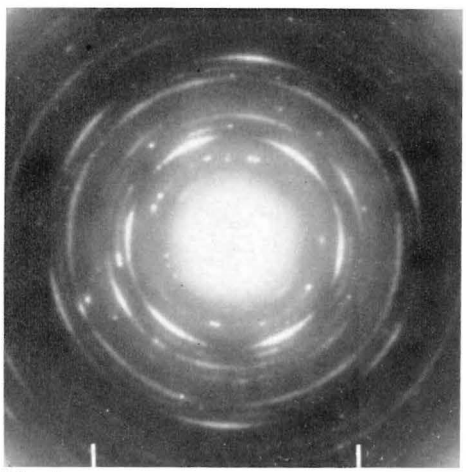

Fig. 4 c

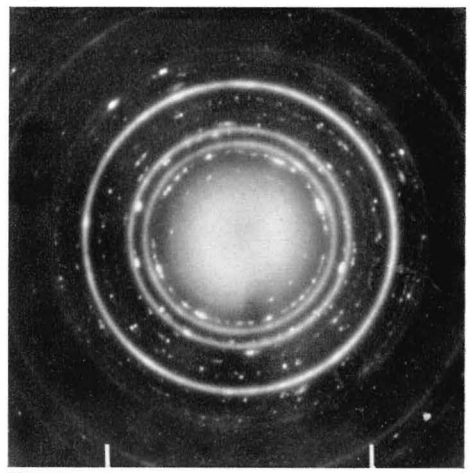

Fig. 4 d

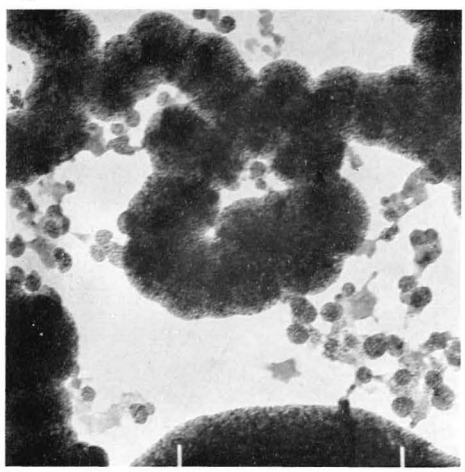

Fig. 4 e

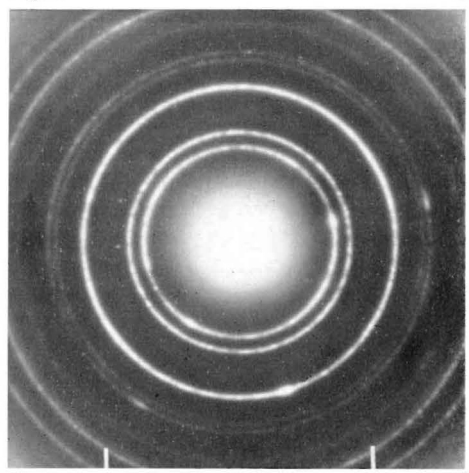

Fig. 4 f

3. C-H and C-$\overline{C}$-H

Precipitates from lime solutions, carbon dioxide contamination, spherulitic growth, thermal transformations (continued)

Figs. 5 and 6. Sample Cs—2.

EM (5a): Field with small spherulites, 0.1μ or less, partly embedded in amorphous mass.

ED (5b): Diffuse halo with maximum about 2.95 Å (weaker, diffuse rings at 2.04, 1.21 Å), indicating an amorphous structure of the solid particles.

ED (5c): After annealing for about 30 sec. in a beam of moderate intensity, a composite diagram has appeared, containing calcite spots and continuous C rings. The change in appearance of the particles at this stage is hardly noticeable.

EM (5d): After annealing for another 30 sec. in a high-intensity beam, the small spherulites as well as the interstitial mass have become spotty and stained with small particles, about 100 Å in size, probably C crystals. The corresponding ED is a C ring pattern, similar to that of Fig. 4f.

EM (6a): Large spherulites (cf. Fig. 3), heated in high-intensity beam, until melting occurred. The mass is then converted to C crystals. A few crystals in the EM show signs of cubic shapes.

ED (6b): Spot-rings, ordinary C pattern, together with a Kikuchi pattern of dark and white streaks. (A Kikuchi pattern can be explained as a combined effect of inelastic scattering and multiple reflexion of electrons on the front and back sides of certain sets of parallel lattice planes. Since the appearance of these effects requires special conditions of crystallinity, crystal size and absorption, they are observed only rarely in routine examinations of cement hydrate samples.)

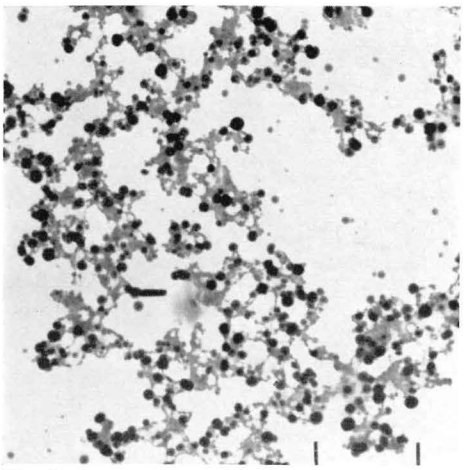

Fig. 5 a

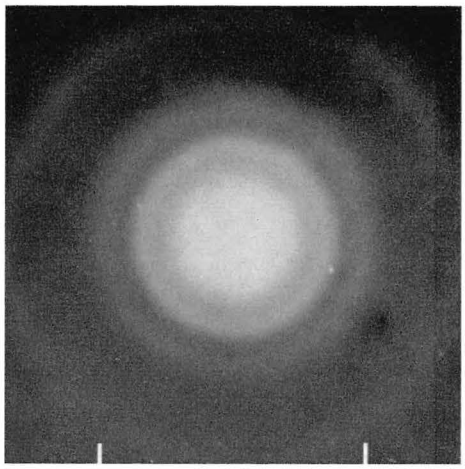

Fig. 5 b

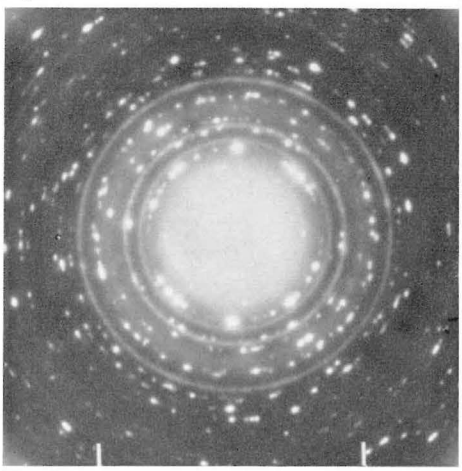

Fig. 5 c

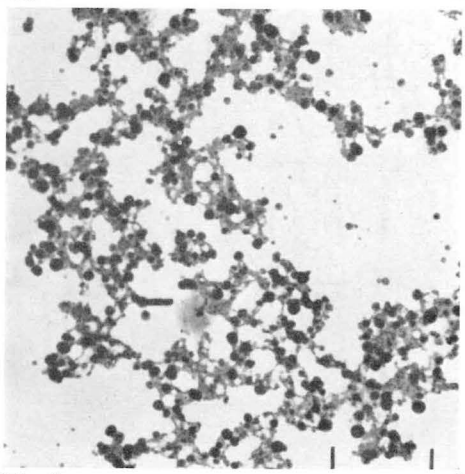

Fig. 5 d

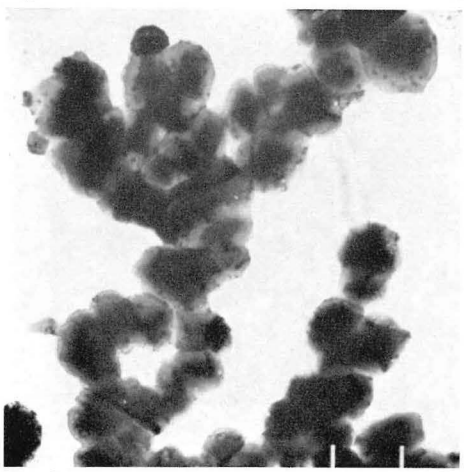

Fig. 6 a

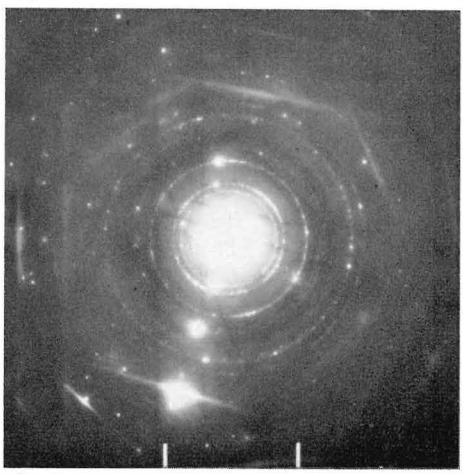

Fig. 6 b

4. C-H and C-$\bar{C}$

Various examples of carbon dioxide contamination

Fig. 7. Sample Cs—3.

EM: Residual product of crystallization in supersaturated lime solution (thin background precipitate seen in Fig. 15), layer of fibrous particles.

ED: Composite pattern, mainly C$\bar{C}$ (calcite) spot-rings, also weak C pattern, with more continuous rings.

Fig. 8. Sample Tw—1.

EM (8a): Network of fibers, formed in small quantities together with more representative hydrated phases (see Figs. 221—224).

ED (8b): Diffuse halo at about 3.0 Å, together with weak spot-rings at about 3.18, 2.23, and 1.84 Å, from unknown substance.

EM (8c): Same particles, after heating in the electron beam. The fibers have become spotted with small crystals.

ED (8d): Composite diagram, consisting of a strong C ring pattern, and a weaker C$\bar{C}$ (calcite) spot-ring pattern.

Judging from the composition of the sample after a long time, C/S 1.69 in a near-saturated lime solution, it seems likely that the formation in Fig. 8 is a high-lime, $\bar{C}$-contaminated, originally amorphous precipitate, formed as a residual phase in the hydration of C_3S, the main phase being a C-S-H(I) gel with C/S about 1.5. The fibrous habits are possibly due to the presence of trace quantities of silica in these particles. It can be noted that CH crystals of regular shapes were also found in the sample (see Fig. 33).

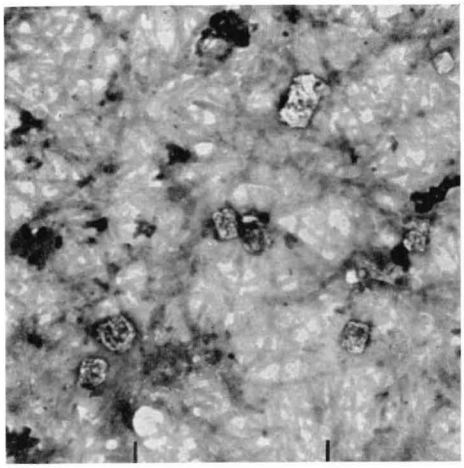

Fig. 7 a

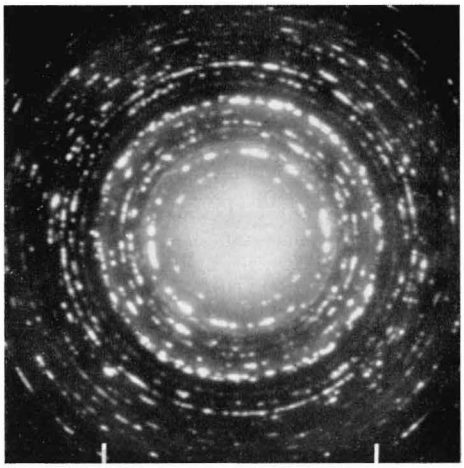

Fig. 7 b

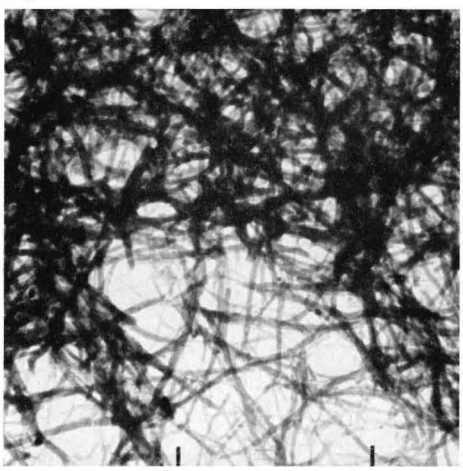

Fig. 8 a

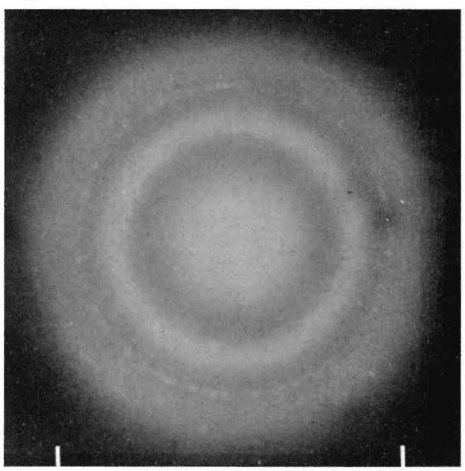

Fig. 8 b

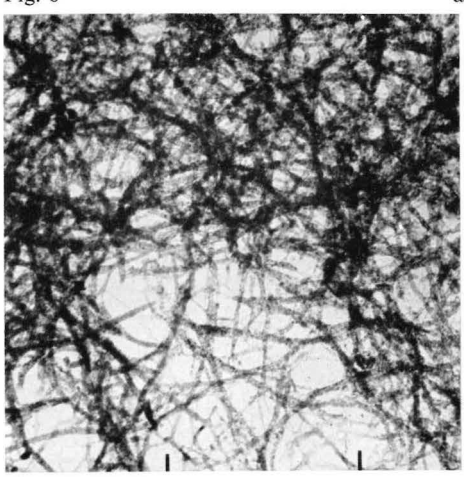

Fig. 8 c

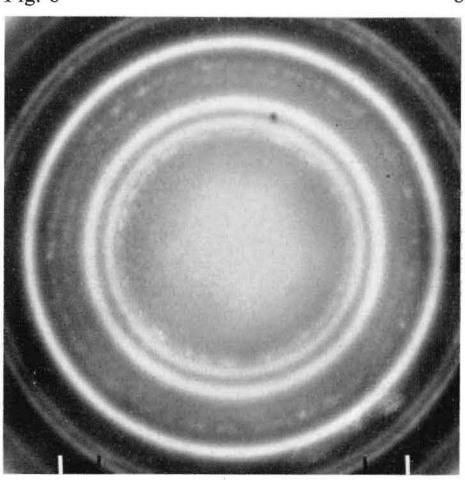

Fig. 8 d

5. C-H and C-$\overline{C}$

Various examples of carbon dioxide contamination (continued)

Fig. 9. Sample Tw—2.

EM: Network of fibers, similar to that of Fig. 8.
ED: Composite diagram, consisting of C$\bar{C}$(calcite) spot-ring pattern, and C ring pattern.

Fig. 10. Sample Tl—1.

EM: Regularly-hexagonal crystal plate, originally CH crystal, but inadvertently transformed to C (cf. ED), also a background precipitate consisting of thin crust-like particles connected by extremely fine threads (cf. Fig. 230).

ED: Composite diagram, consisting of C$\bar{C}$(calcite) spot-rings, from the thin crust particles, and a pseudo-hexagonal diffuse-spot C pattern, with the (220) (1.701 Å) reflexion as the most prominent feature. The latter pattern probably represents the final stage of an oriented transformation CH→C, in which the hexagonal axis of the original CH crystal is turned into one of three possible positions of the cube diagonal of the C crystal lattice. The CH crystal is thus transformed to a mosaic of C crystals, the crystal axes of which assume certain preferred orientations.

Fig. 11. Sample Tl—2.

EM: Network of fibers, phase present in minor quantities in the sample (for representative particles, see Figs. 225—26), similar to those of Figs. 8 and 9.

ED: Similar to the diagram in Fig. 9b.

It can be observed that the calcite patterns given by the precipitates of Figs. 9—11 were recorded without preceding heat treatment. Possibly, the degree of carbon dioxide contamination is higher in these preparations, so that calcite crystallizes more readily from certain high-lime phases originally formed in the hydrolysis of C_3S in these samples than in the phase described in Fig. 8.

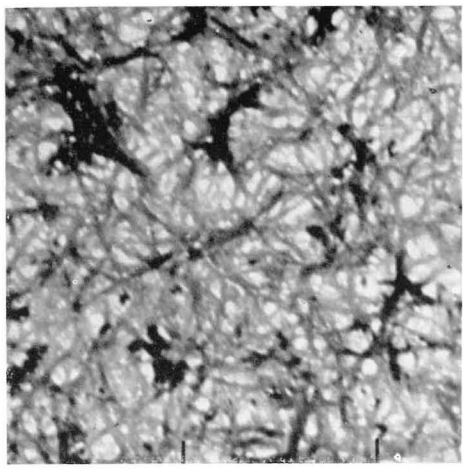

Fig. 9 a

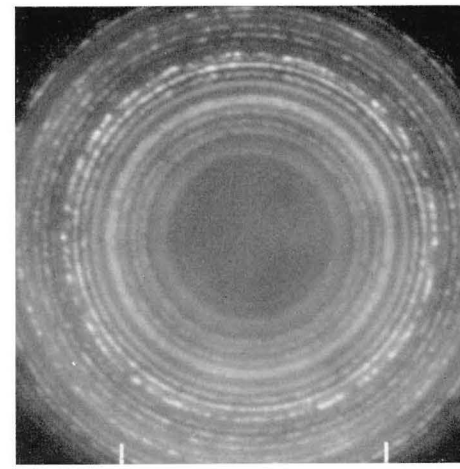

Fig. 9 b

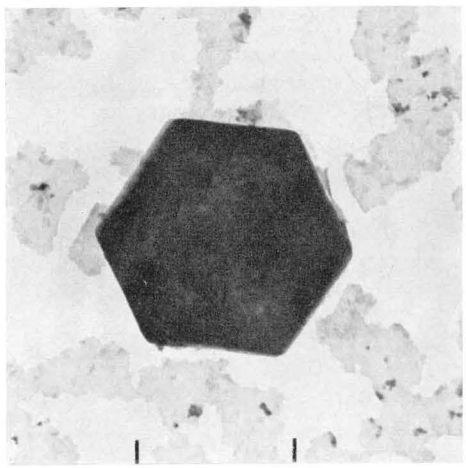

Fig. 10 a

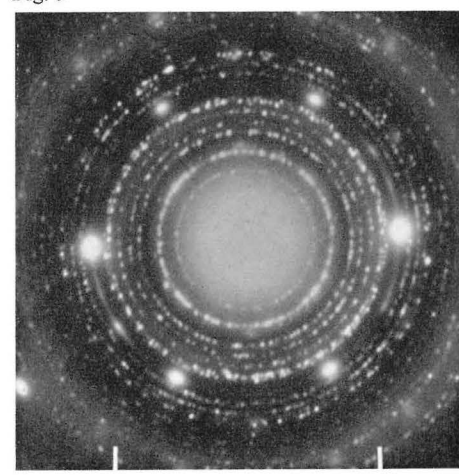

Fig. 10 b

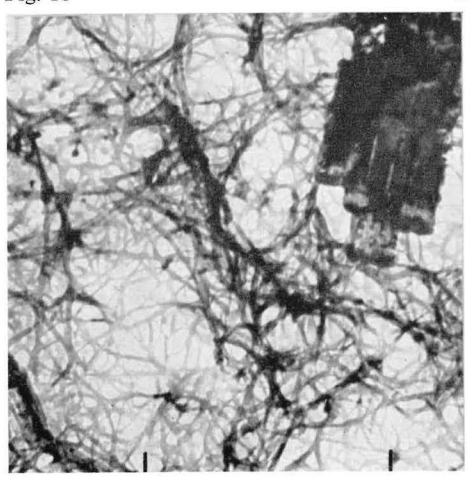

Fig. 11 a

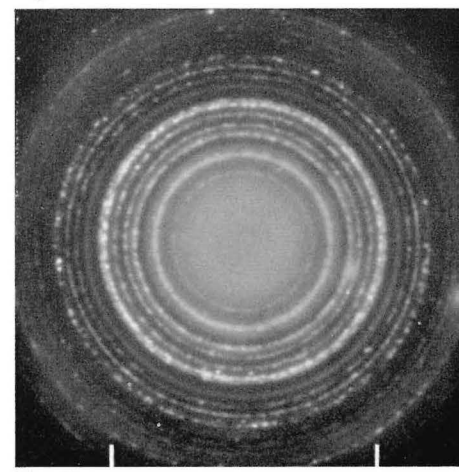

Fig. 11 b

6. C-H

Calcium hydroxide crystals, reference samples

Fig. 12. Sample Cs—5.

EM: CH crystal plates, with many examples of regularly-hexagonal angles. Due to the dispersing effect of the ultrasonic treatment, a considerable number of very thin plates, split-off from thicker crystals, were observed in this sample.

ED: CH spot-ring pattern, reflexions at 3.112 (10.0), 2.628 (10.1), 1.927 (10.2) (only a few spots visible), 1.797 (11.0) (strong), 1.687 (11.1), 1.556 (20.0), 1.483 (20.1) Å, etc. (spacings calculated from CH unit cell, $a_H = 3.593$ Å, $c_H = 4.909$ Å). It is observed that, due to orientation effects, the prism reflexions, with $l=0$, are enhanced with respect to reflexions from oblique planes, with $l=1$ and 2, in comparison with the intensities obtained by X-ray diffraction.

Figs. 13 and 14. Sample Cs—4.

EMs: Examples of CH crystals formed by evaporating a lime solution in carbon-dioxide-free conditions. One common form is the regular trihexagonal plate. The straight-edged crystals in the upper left corner of Fig. 13 have formed at the edge of an evaporated drop.

Figs. 15 and 16. Sample Cs—3.

EMs: Examples of CH crystals formed in carbon-dioxide-free conditions. The regularly-hexagonal plate is the most common habit in this sample. Fig. 16 shows one of the largest crystals observed, about 7μ across.

(*EDs:* The crystal in Figs. 13—16 are too thick to permit any ED effects to be recorded).

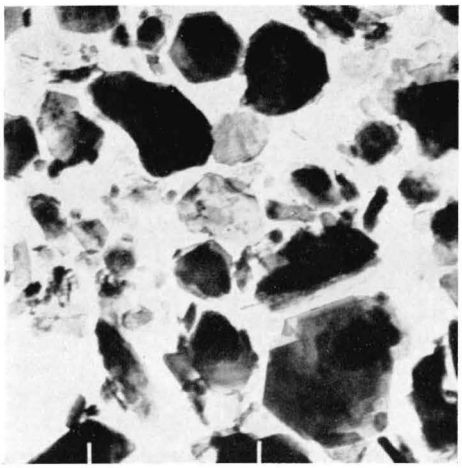

Fig. 12 a

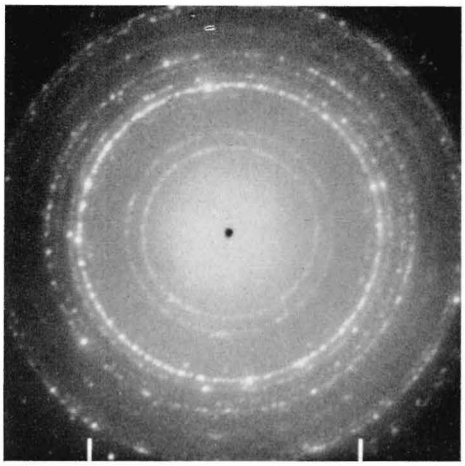

Fig. 12 b

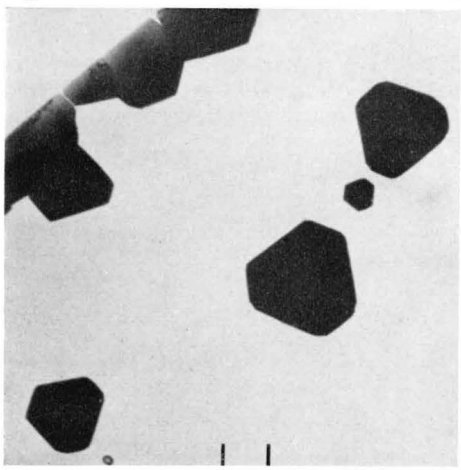

Fig. 13

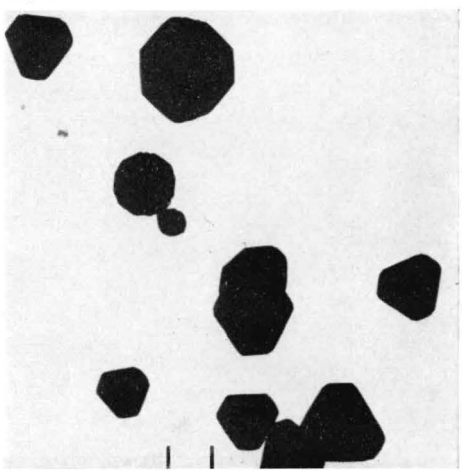

Fig. 14

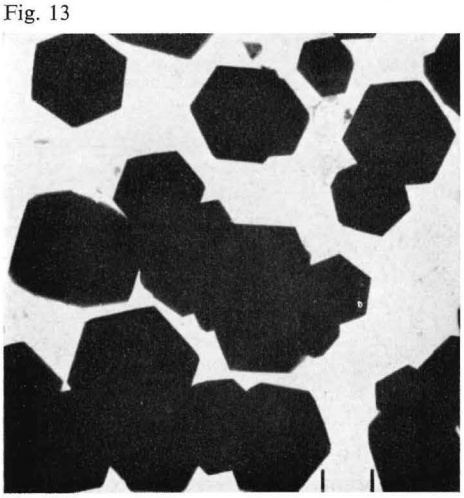

Fig. 15

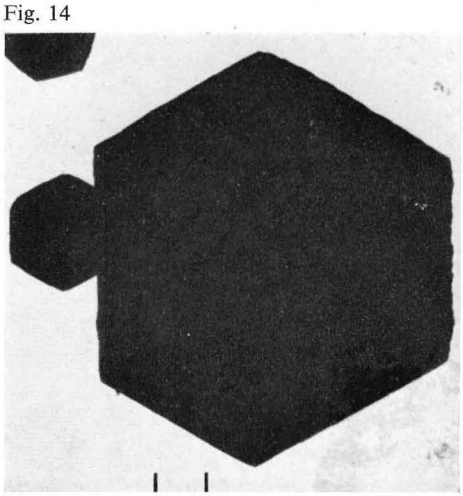

Fig. 16

7. C-H

Calcium hydroxide crystals in portland cement suspensions

Fig. 17. Sample Pw—4A.

EM: Aggregate of thin CH crystal plates, some with regularly-hexagonal angles, others seen to stand on edge, example of crystals in their first stages of formation from the saturated lime solution of a cement suspension.

ED: Nearly complete CH spot-ring pattern (cf. Fig. 12), with (*hk*.0) intensities somewhat enhanced.

Fig. 18. Sample Pw—4B.

EM: CH crystals, after about 1 day's growth in sediment from rapidly-stirred cement suspension, crystals thicker and better crystallized than those in Fig. 17.

ED: CH spot-ring pattern, (*hk*.0) reflexions and a few scattered spots from (*hk*. 1) reflexions.

Fig. 19. Sample Pw—3A.

EM: Example of CH crystals formed in a cement suspension heated to 100° C for some hours, with regularly-hexagonal, as well as irregular, thin plates.

ED: CH spot-ring pattern, with (10.0) and (11.0) reflexions strongly enhanced.

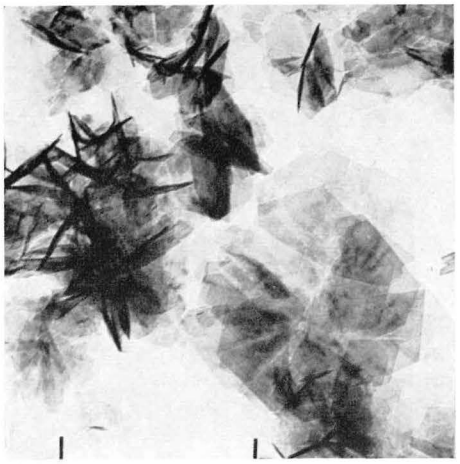

Fig. 17 a

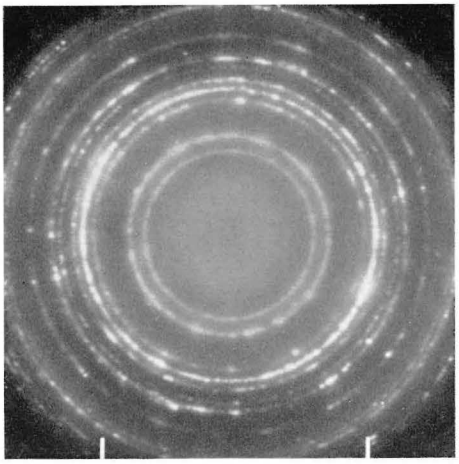

Fig. 17 b

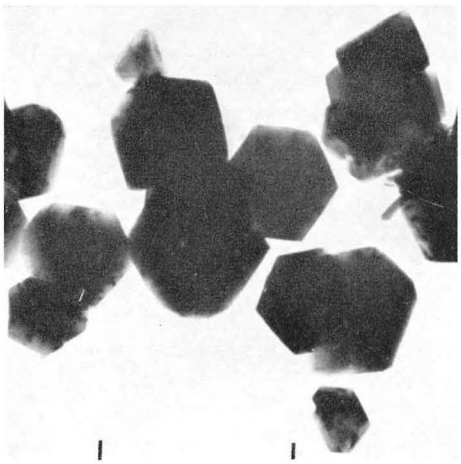

Fig. 18 a

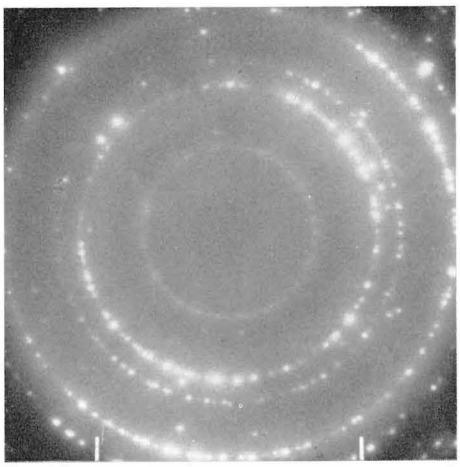

Fig. 18 b

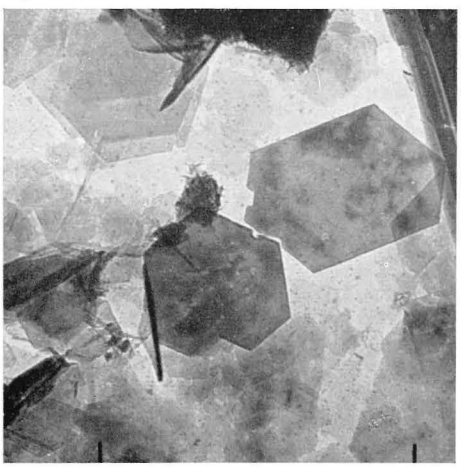

Fig. 19 a

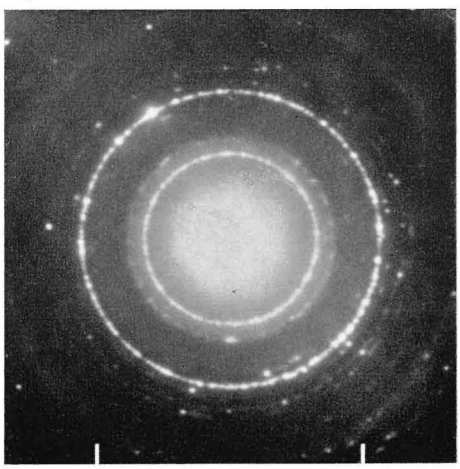

Fig. 19 b

8. C-H

Calcium hydroxide crystals in portland cement suspensions (continued)

Fig. 20. Sample Pw—3A.

EM: Similar to Fig. 19, well-shaped CH crystals and some C-S-H material.

ED: Composite diagram, spots and spot-rings from both CH and C. The crystals of this area are obviously observed in a state of dehydration. With the normal value of the calibration parameter, the following series of spacings has been measured: 3.128 (CH,+0.5), 2.818 (C,+1.6), 2.648 (CH,+0.9), 2.444 (C,+1.8), 1.810 (CH,+0.8), 1.728 (C,+1.6), 1.702 (CH, +0.9), 1.571 (CH,+1.0), 1.493 (CH,+0.7) Å, where the figures within brackets denote the deviations (percent) from the normal values of the spacings. Both lattices seem to be stressed and expanded, possibly due to the fact that there is a conversion going on. In any case, the C lattice is about one percent expanded with reference to the CH lattice from which it is forming.

Fig. 21. Sample Pw—1B.

EM (21a): CH crystal plate of hexagonal shape, with irregular edges. The mottled and striated appearance of the interior indicates the presence of interlamellar inclusions causing slight misalignment of superimposed plate elements.

ED (21b): CH single-crystal spot pattern, mainly (*hk*.0) (cross-grating) reflexions, deviations from hexagonal symmetry very small (about 0.2 percent).

EM (21c): Same plate, after prolonged heating in high-intensity electron beam. The outer contours are unchanged, the interior has assumed a "burnt-out" appearance.

ED (21d): Composite spot pattern of hexagonal symmetry, oriented with respect to original pattern, and irregularly-distributed spots (sharp) from calcite. The heating has caused the spots of the original CH pattern to split up in components: the (10.0) (3.11 Å) reflexions have been replaced by short arcs at 3.56, 3.27, 2.78 and 2.405 Å, the (11.0) (1.797 Å) reflexions (the large spots in Fig. 21b) by arcs at 2.06 and 1.70 Å (the latter reflexions very strong), the (20.0) (1.556 Å) reflexions by arcs at 1.44 and 1.39 Å, etc. The 2.78, 2.405, 1.70, 1.44, and 1.39 Å reflexions can be identified as originating from an oriented aggregate of C crystals. The 3.56 and 2.06 Å reflexions can be indexed as the (10.0) and (11.0) reflexions from a lattice of hexagonal symmetry and unit cell a_H=4.12 Å. The crystallographic identity of the corresponding substance is unknown.

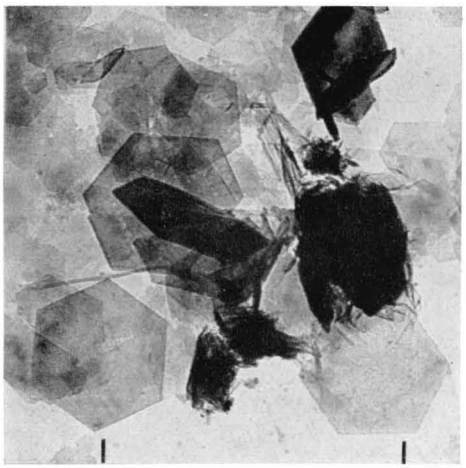

Fig. 20 a

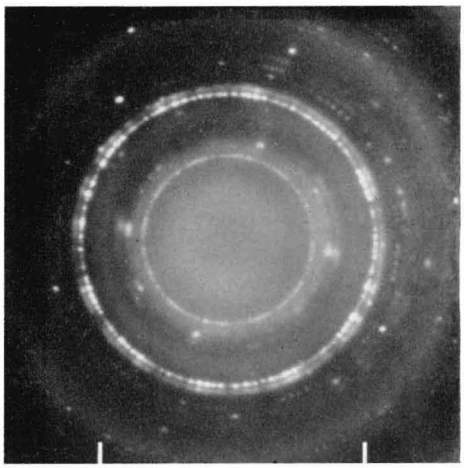

Fig. 20 b

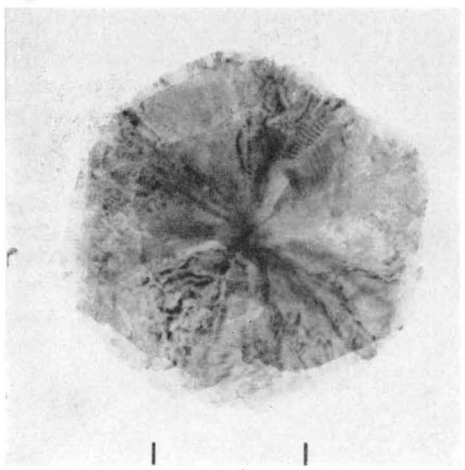

Fig. 21 a

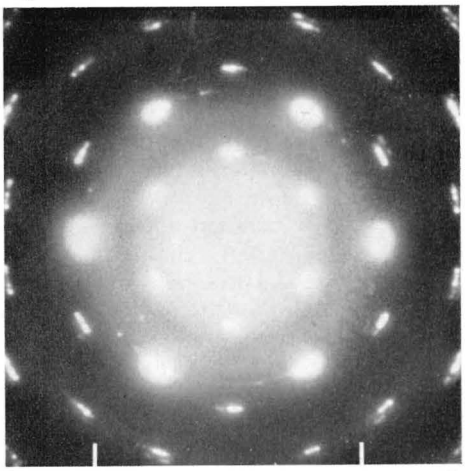

Fig. 21 b

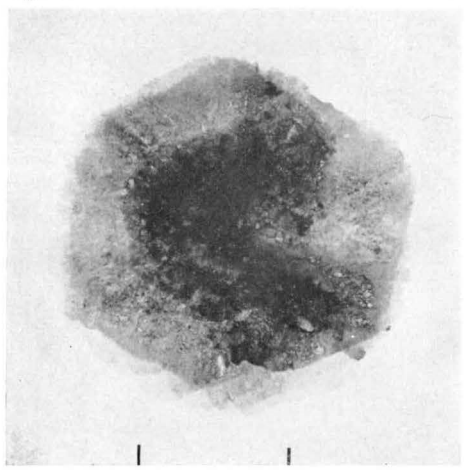

Fig. 21 c

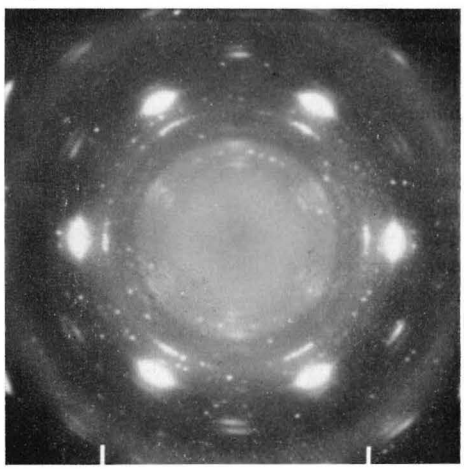

Fig. 21 d

9. C-H

Calcium hydroxide crystals in portland cement suspensions (continued)

Figs. 22 and 23. Sample Pw—7A.

EM (22a): Thin layer of small, irregular plates or foils, representing early, still-disorganized state in the development of the CH phase.

ED (22b): Ring diagram, mainly CH pattern, with (10.0) and (11.0) reflexions strongly enhanced, additional weak reflexions at 2.94 and 1.905 Å (cf. Fig. 23b).

EM (23a): Similar to Fig. 22a, other area of same EM specimen.

ED (23b): Composite ring diagram, reflexions at 6.94, 3.44, 3.11 (strong, CH), 2.92 (strong), 2.64 (CH), 2.32?, 2.25, 1.900 (strong), 1.797 (strong, CH), 1.76?, 1.665 (diffuse, CH?), 1.556 (CH), 1.480 (CH), 1.222, 1.175 (CH), 1.143 (CH), 1.037 (CH), 0.898 (CH). The reflexions not belonging to the CH pattern, including two strong ones at 2.92 and 1.90 Å, are given by some substance of unknown identity, inextricably mixed in variable proportions with the CH phase in its earliest period of development (cf. Figs. 119 and 120). It is suggested that this substance represents a primary phase in the hydration of the aluminate and alumino-ferrite constituents of the cement. It is of a transient nature and cannot be found in later examinations of this sample (cf. samples Pw-7B and C).

Fig. 24. Sample Pw—7B.

EM: CH crystal plates, of well-defined hexagonal habits, obviously resulting from the recrystallization of the disordered CH phase in Figs. 23 and 24.

ED: CH spot-ring pattern, with (10.0) and (11.0) reflexions enhanced.

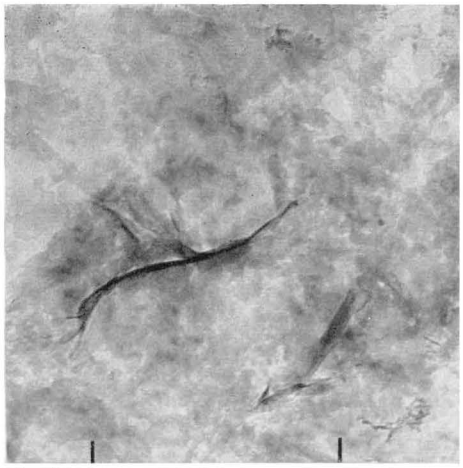

Fig. 22 a

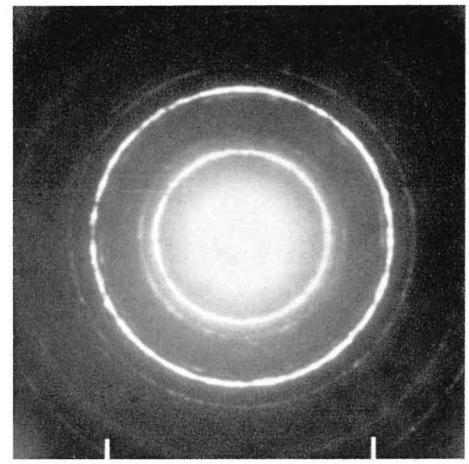

Fig. 22 b

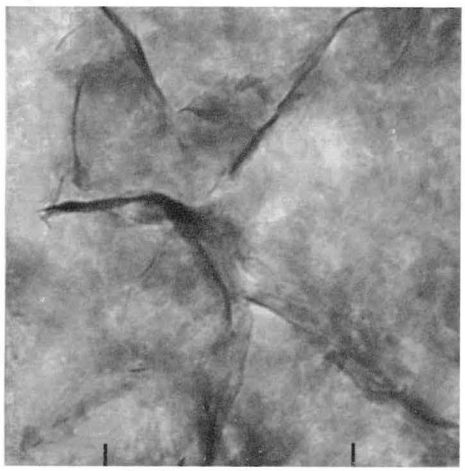

Fig. 23 a

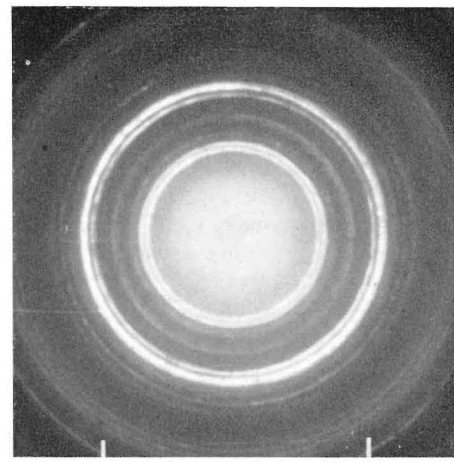

Fig. 23 b

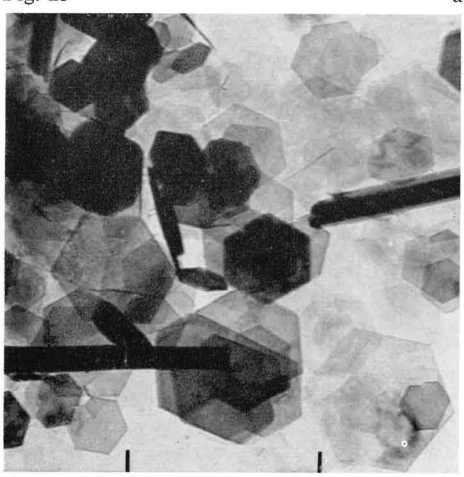

Fig. 24 a

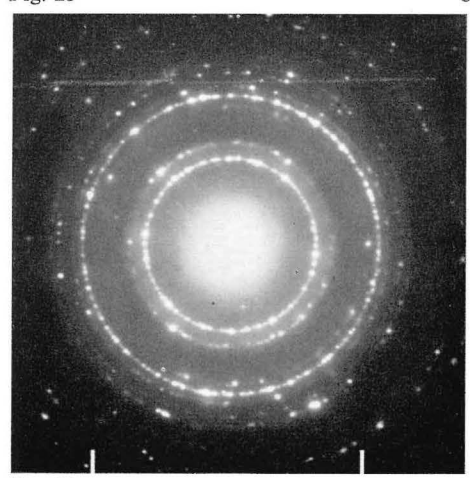

Fig. 24 b

10. C-H

Calcium hydroxide crystals in portland cement suspensions (continued)

Fig. 25. Sample Pw—7C.

EM: CH crystal plates. Some of these are of an appearance similar to those of Fig. 24, other hexagonal forms seem weathered and dissolved, so that only a trace of the edges remains.

ED: CH spot-ring pattern, with the (10.0) and (11.0) reflexions strongly enhanced.

Observations indicate that, in this particular cement suspension, the CH phase is first formed in a rather disorganized state (Figs. 22 and 23), later transformed to a phase with well-shaped, thin crystal plates, of diameters approaching 1μ. (Fig. 24). Further hydration appears to result in a partial dissolution of the CH phase, probably associated with an incorporation of the lime material, thus liberated, in the products of hydration developing at this stage of reaction. (Fig. 25, cf. Figs. 254—258).

Fig. 26. Sample Pw—6A.

EM: Very thin, rounded plate or crust, with semicircular crack, probably a primary form of CH crystallization (cf. Fig. 22).

ED: C spot pattern, from strongly oriented C crystal aggregate formed by dehydration of CH crystal initially present. The hexagonal symmetry of this crystal is retained by the texture of the C crystal aggregate, and reflected in a pseudo-hexagonal arrangement of spots, as shown in the diagram. The series of spacings obtained from measurements show, however, that the true symmetry is cubic, face-centered. In this particular pattern, the spacings given by measurements came out about 2 percent larger than those of the ordinary C crystal structure. This might be a true effect, indicating that the lattices of the oriented aggregate are still in a state of expansion following the oriented dehydration of the CH crystal.

Fig. 27. Sample Pw—6B.

EM: Thin CH plates, well-shaped hexagons.

ED: CH spot-ring pattern, only (*hk*.0) reflexions.

CH crystals were not observed in very large quantities at any stage of hydration of this vigorously-stirred suspension. Especially in the last examination of this sample. (Pw-6C), practically no CH crystals could be found (for one example, see Fig. 262). Possibly, a dissolution process similar to that described under Fig. 25 operates in this sample also.

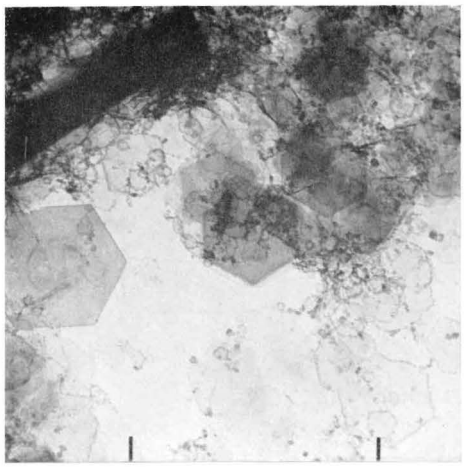

Fig. 25 a

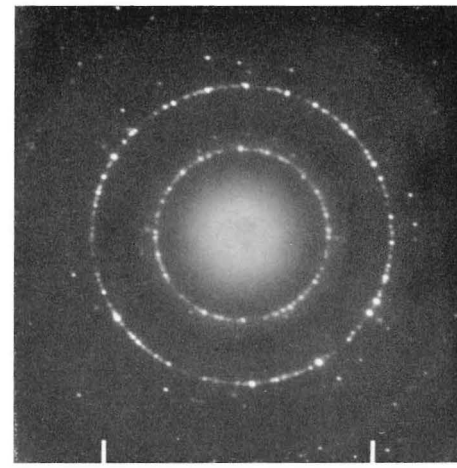

Fig. 25 b

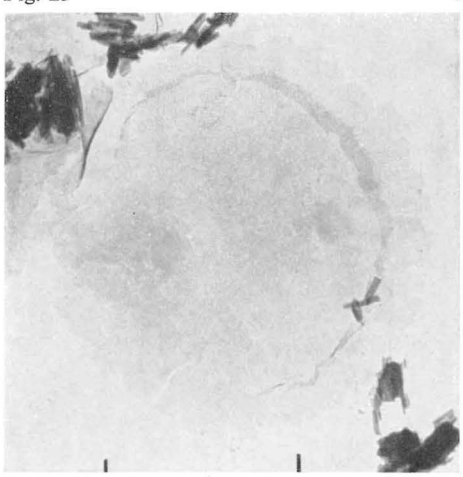

Fig. 26 a

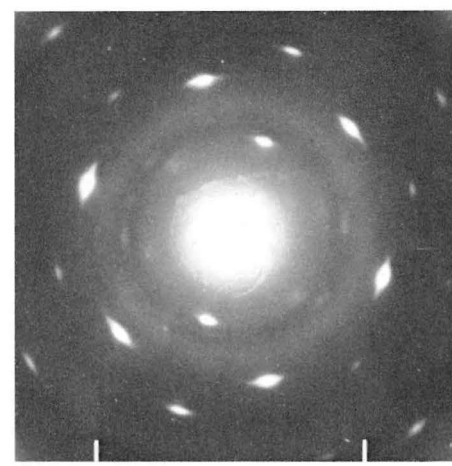

Fig. 26 b

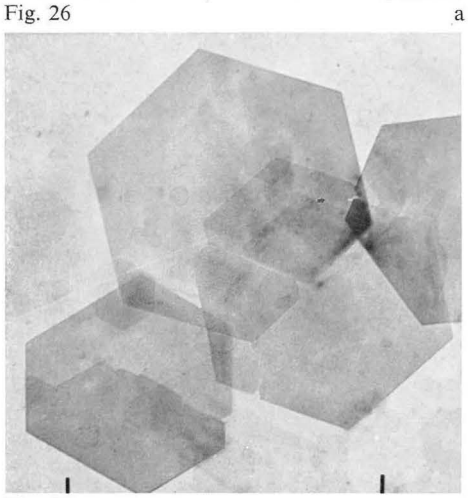

Fig. 27 a

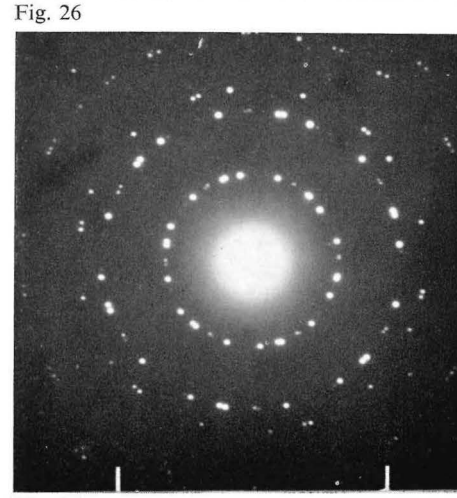

Fig. 27 b

11. C-H

Examples of anomalous growth phenomena

Fig. 28. Sample Sl—1B.

EM: Thin plate with two parallel edges, example of a few particles found in the sample together with C-S-H(I) foils and regularly-crystallized CH (cf. Fig. 160).

ED: Rows of spot reflexions, orders 4, 1, 0, and $\bar{3}$ observed. The distance between spots within the rows corresponds to a unit distance of 4.92 Å, and the distance between rows to various orders of a unit distance of 3.46 Å. These figures can be compared with the unit cell dimensions of CH, c_H=4.91 Å, a_H=3.593 Å, and the equivalent hexagonal unit cell of C (simplest expressed as the nearest distance between identical ions), which is 3.40 Å ($a_C/\sqrt{2}$). These formations are explained, very tentatively, as CH crystals growing in strips of monomolecular layers stacked in the direction of the basal spacing. Due to the anisotropic growth of the layer, the lattice contracts in the direction of the strip (identical with one of the a_H axes). The reason for this one-dimensional growth of the CH layers is unknown. One possibility is that the presence of silica chain elements may have some influence (cf. also Fig. 43).

Fig. 29. Sample Cs—3.

EM: Thin, irregular plate or crust, with parallel striations and cracks.

ED: Composite diagram, $C\bar{C}$ (calcite) spot-ring pattern and C diffuse-spot pattern. The latter pattern resembles the one of Fig. 26b, but has more pronounced two-fold axes of symmetry, even with respect to the (220) spots. It is likely, therefore, that the aggregate of C crystals has been formed by an oriented transformation of a CH crystal, initially formed by crystallization and stacking of CH strip elements, as described in connection with the preceding figure, with the initial c_H direction perpendicular to the cracks.

Figs. 30 and 31. Sample Tl—2.

EMs: Formations similar to those above growing in $\bar{C}$-contaminated surroundings of a C_3S suspension in a saturated lime solution.

It can be noted that the structures in Figs. 28—31 have all been formed in a saturated lime solution obtained by anion exchange techniques using an organic resin. It is possible that minor quantities of organic impurities in this resin, e.g. chain molecules of some kind, have been active in inhibiting the regular growth of CH crystals.

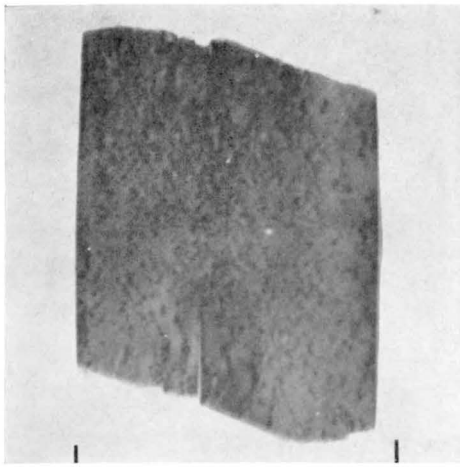

Fig. 28 a

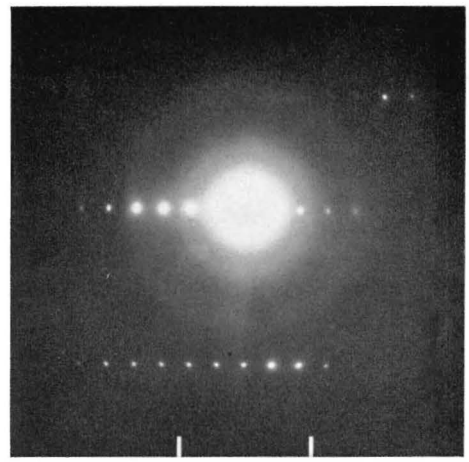

Fig. 28 b

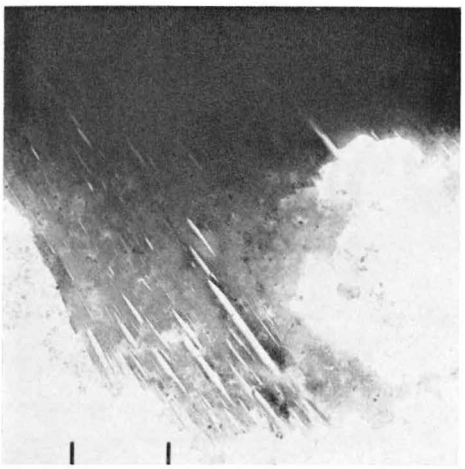

Fig. 29 a

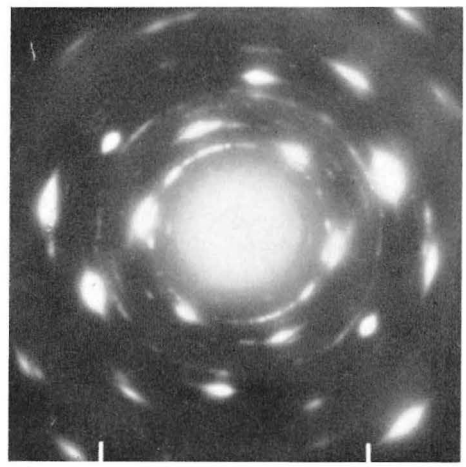

Fig. 29 b

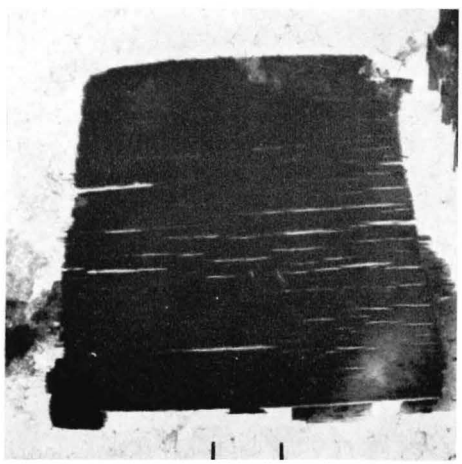

Fig. 30

Fig. 31

12. C-H

Calcium hydroxide crystals in various preparations

Fig. 32. Sample Tw—6B.

EM: Large CH crystal plate, with thinner plates growing irregularly around the edges. To the left, recrystallized afwillite particles, representative of this preparation (cf. Figs. 197 and 198).

ED: CH spot pattern, (*hk*.0) and (*hk*.1) reflexions.

Fig. 33. Sample Tw—1.

EM: CH crystals (with C-S-H(I) foils), hexagonal plates with thinner or hollow central parts.

ED: From one of the crystals, CH single-crystal spot pattern, only cross-grating (*hk*.0) spots.

Fig. 34. Sample Al—2A.

EM: Small CH crystal plates, minor constituent of hydrated C_3A preparation (representative particles, see Figs. 60—64).

ED: CH spot-ring pattern, mainly (*hk*.0) reflexions.

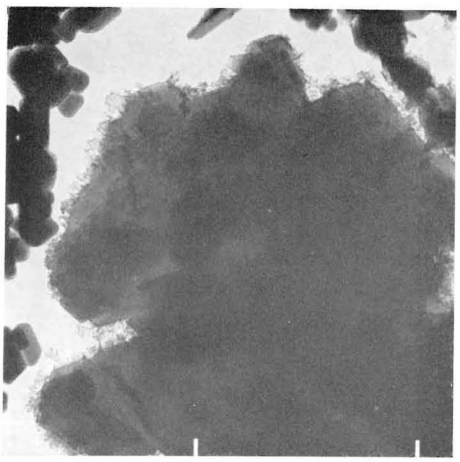

Fig. 32 a

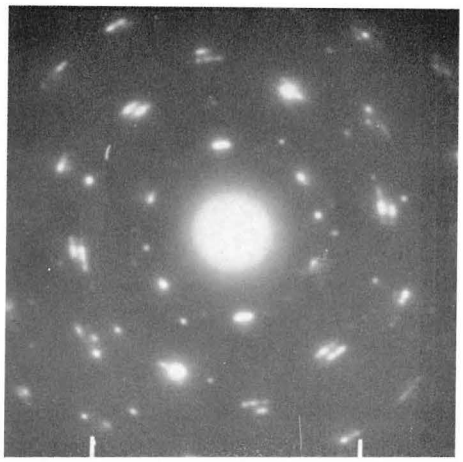

Fig. 32 b

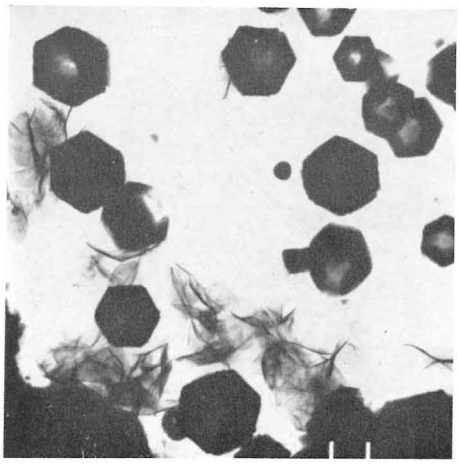

Fig. 33 a

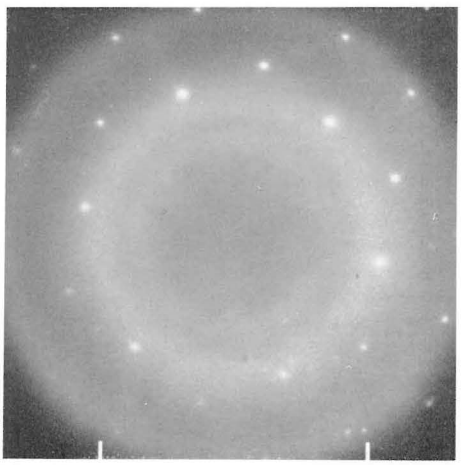

Fig. 33 b

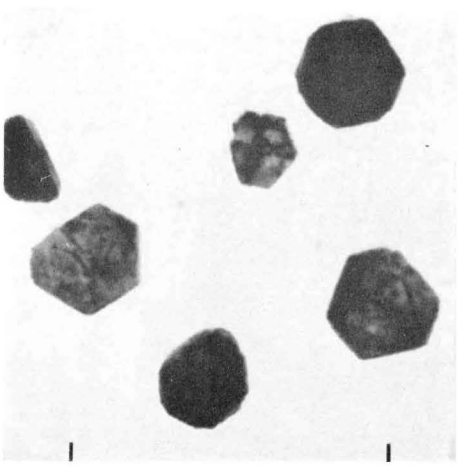

Fig. 34 a

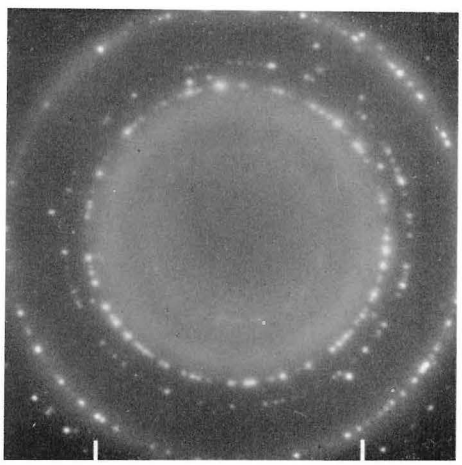

Fig. 34 b

13. **C-H**

Calcium hydroxide crystals in hardened cement pastes

Fig. 35. Sample Pp—1A.

EM: Large, thin CH crystal plate from standard cement paste, part of regular hexagon, with characteristic internal striations, due to slight misalignments caused by interlamellar inclusions.

ED: CH spot pattern, (*hk*.0) spots, nearly exact hexagonal symmetry.

Fig. 36. Sample Pp—10A.

EM: Similar to Fig. 35, from low-heat cement paste.

ED: CH spot pattern, (*hk*.0) and some (*hk*.1) spots, regularly-hexagonal symmetry.

Fig. 37. Sample Ppq—3.

EM: Similar to Fig. 35 from steam-cured standard cement paste.

ED: CH spot pattern, (*hk*.0) spots, very regular and of exactly hexagonal symmetry.

Most CH crystals observed in cement paste specimens appear in the form exemplified above, i.e. rather larger (one μ and more), thin, well-crystallized plates, or fragments of plates.

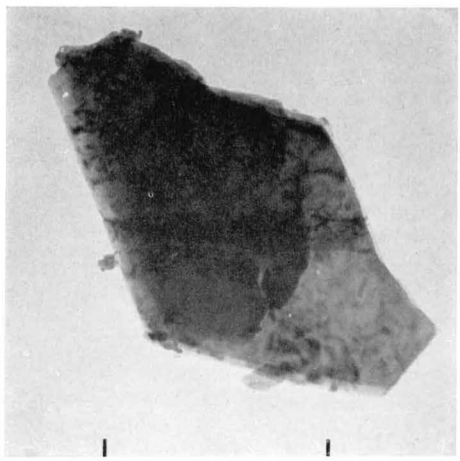

Fig. 35 a

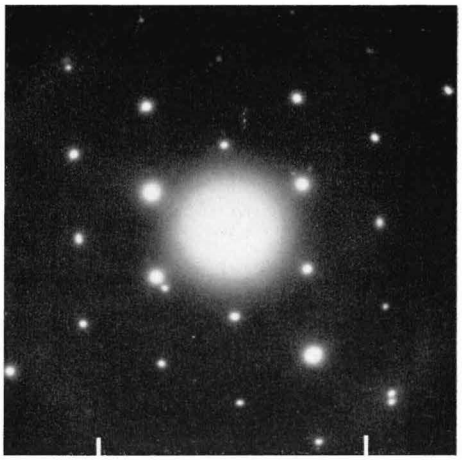

Fig. 35 b

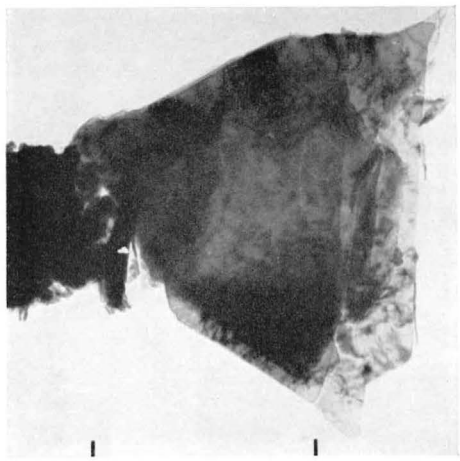

Fig. 36 a

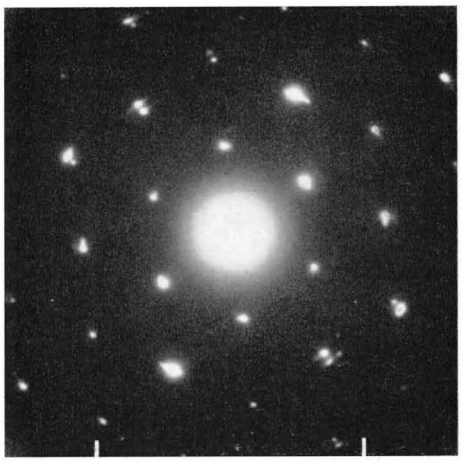

Fig. 36 b

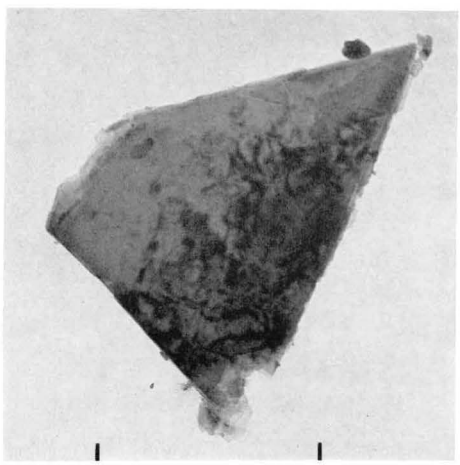

Fig. 37 a

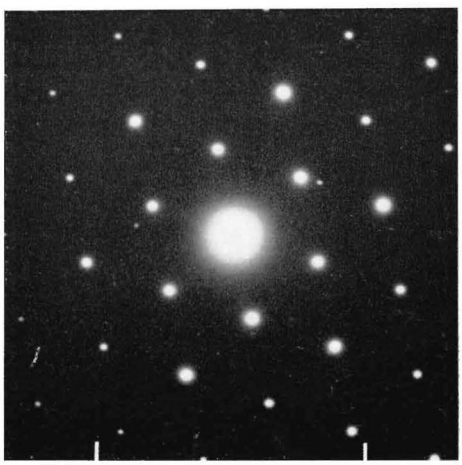

Fig. 37 b

14. C-H

Calcium hydroxide crystals in hardened cement pastes (continued)

Fig. 38. Sample Pp—10A.

EM: Large, thin crystal plate, with hexagonal angles, from low-heat cement paste.

ED: Spot pattern of hexagonal symmetry and irregular intensity distribution. Measurements along different diameters give an equivalent hexagonal cell dimension a_H varying between 3.58 and 3.48 Å. These data indicate that the particle is a CH crystal plate, tilted about 14° out of the plane perpendicular to the line of vision.

Fig. 39. Sample Ppq—1.

EM: Thin plate, protruding at the edge of a larger aggregate, from high-pressure steam-cured paste. The striations are of the type observed in CH plates grown in cement paste mixtures.

ED: Spot pattern of orthorhombic (probably distorted-hexagonal) symmetry. The distances between vertical spot-rows indicate a unit cell of about 3.6 Å, and it is likely that the plate is a CH crystal, tilted so much out of the plane of the paper, that some (*hk*.0) reflexions have been replaced by (*hk*.1) reflexions.

Fig. 40. Sample Pp—7.

EM: Aggregate of small plates, from standard cement paste.

ED: Complete (*hk*.1) spot-ring pattern of CH, including (in the original) even a weak basal (00.1) reflexion. This is a rather rare example of a disordered aggregation of small CH crystals in a paste.

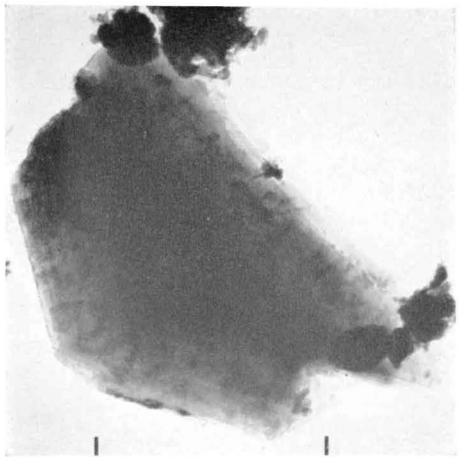

Fig. 38 a

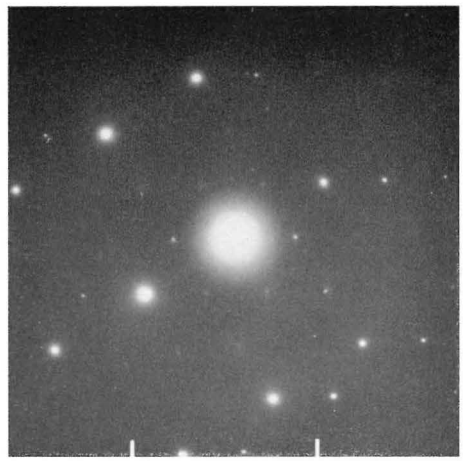

Fig. 38 b

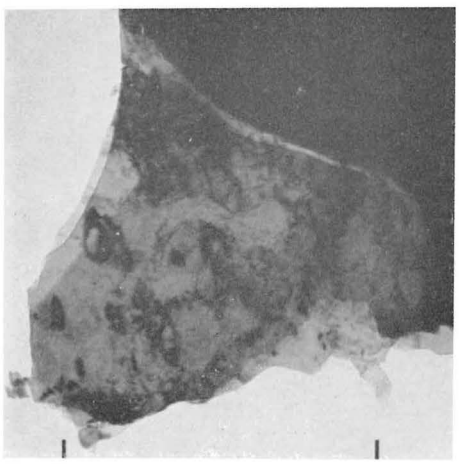

Fig. 39 a

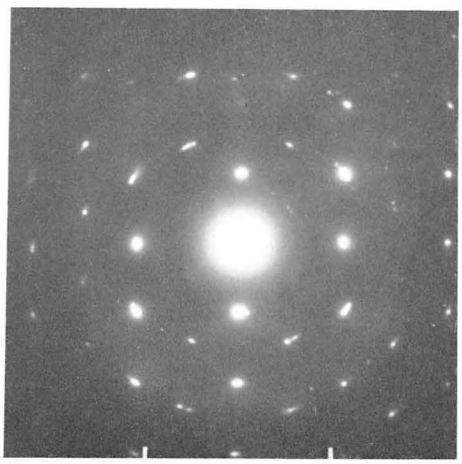

Fig. 39 b

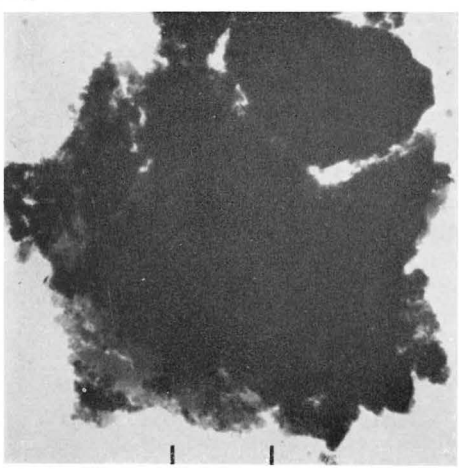

Fig. 40 a

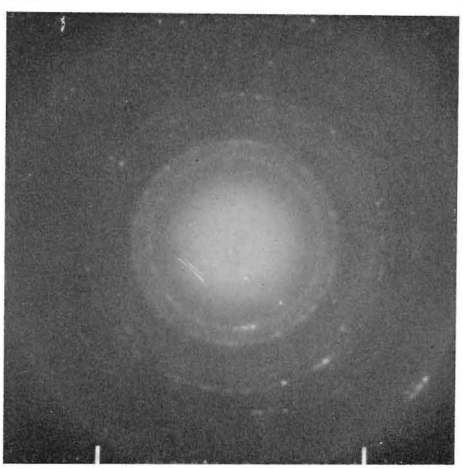

Fig. 40 b

15. C-H

Calcium hydroxide crystals in C_3S pastes

Fig. 41. Sample Tp—1B.

EM: Thin CH crystal plate, with irregular striations, similar to the particles of Figs. 35—37.
ED: CH single-crystal spot pattern, (*hk*.0) and some (*hk*.1) reflexions.

Fig. 42. Sample Tp—1A.

EM: CH crystal plate, of lath-like or elongated type.

ED: Single-crystal spot pattern of hexagonal symmetry, but also resembling a layer-line pattern such as is obtained in X-ray single-crystal rotation diagrams. Certain (*hk*.1) and (*hk*.2) reflexions appear in the layer-line spot-rows outside the corresponding (*hk*.0) spots belonging to the hexagonal-symmetry cross-grating pattern. The layer-line distance corresponds to the hexagonal unit cell $a_H = 3.59$ Å, which indicates that the fiber axis coincides with one hexagonal axis. The lattice layers are possibly creased, or some of them tilted, perpendicular to this direction.

Fig. 43. Sample Tp—1E.

EM: Formations apparently consisting of puckered or wavy layers, or stacked layers seen from the edge.

ED: Incomplete layer-line diagram. The distances in the zero layer-line (row of spots through the center) and between the layer-lines, correspond to lattice distances of 4.91 Å (average of 4 measurements) and 3.54 Å (average of 1st, 2nd, 3rd, and 5th layer-line distances), respectively. These spacings can be identified as the c_H and a_H (somewhat contracted) unit cell distances of the CH lattice (cf. the formations of Figs. 28—31).

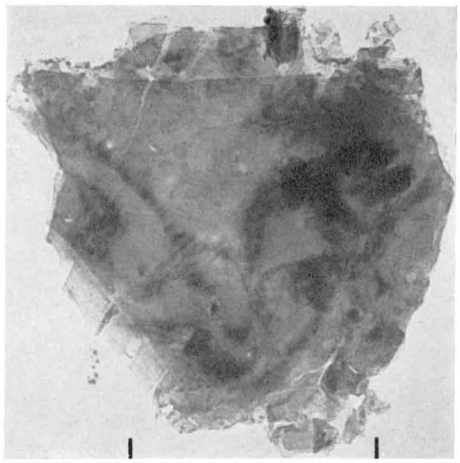

Fig. 41 a

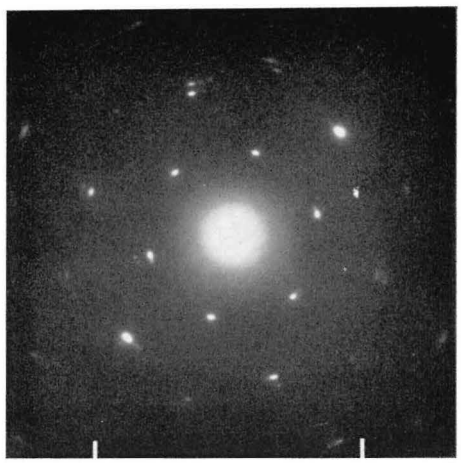

Fig. 41 b

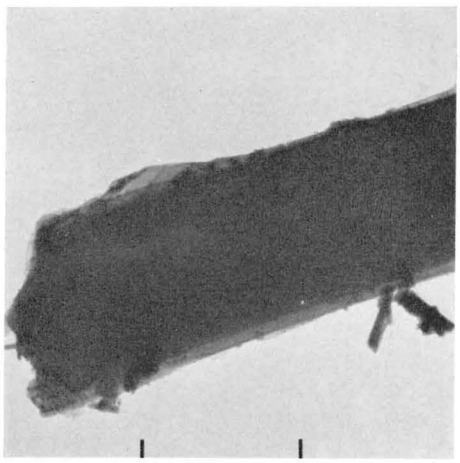

Fig. 42 a

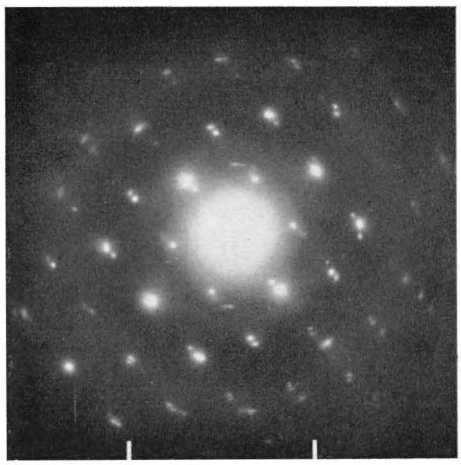

Fig. 42 b

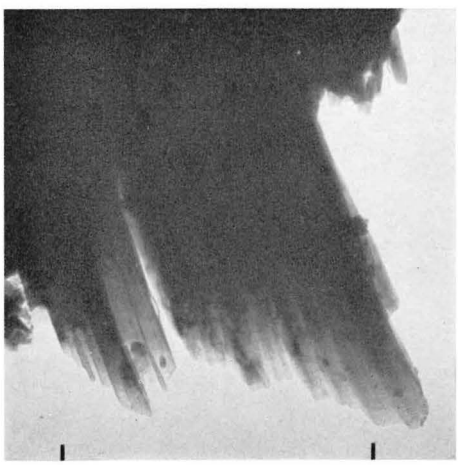

Fig. 43 a

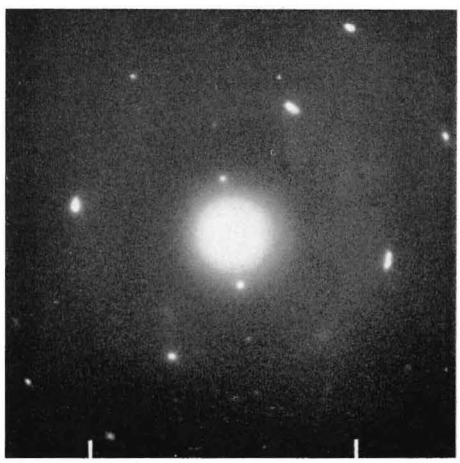

Fig. 43 b

16. C-H

Calcium hydroxide crystals in pastes, extension of single crystal pattern, transformations

Fig. 44. Sample Pp—10C.

ED: CH single-crystal spot pattern given by large plate, strong (*hk*.0) spots and associated (*hk.l*) spots.

Low magnification diagram, showing full extension of pattern, with outer spots corresponding to about 0.5 Å. spacings.

Fig. 45. Sample: muscovite mica.

ED: Cross-grating pattern of hexagonal symmetry, given by thin crystal flake in suspension of wet-ground mica. Low-magnification diagram, as Fig. 44, shown for comparison purposes, to demonstrate the angular extension of spot patterns of this type. The true symmetry of muscovite is monoclinic, but in ED patterns from thin crystals the apparent symmetry is very nearly hexagonal, as is also the case for all layer-lattice clay minerals. Measurements on a series of ED patterns of this type gave an average size of the unit cell $a_H = 5.20 \pm 0.03$ Å. In the handbooks on clay mineralogy, the monoclinic base unit cell of mica is given as $a_0 = 5.2$, $b_0 = 9.0$ Å ($5.2 \cdot \sqrt{3}$), with small variations depending on the actual amounts of various lattice substitutions (Al for Si, Mg or Fe for Al, etc.)

Fig. 46. Sample Pp—9.

EM: Aggregate of large plates in high-early-strength cement paste, with indications of straight crystal edges at regularly-hexagonal angles, interior of granular appearance, only weak indications of striations.

ED: C spot pattern of the oriented-aggregate, pseudohexagonal symmetry type (cf. e.g. Figs. 21 and 26). The particles are probably CH crystal plates unintentionally transformed to C, due to a prolonged exposure to the vacuum of the EM tube.

Fig. 47. Sample Dp—1B.

EM: Dehydrated and recrystallized residue of a plate (probably CH) with apparently hexagonal contours originally. At many places, small spots of the shape of equilateral triangles can be observed. These are probably C crystals, grown pyramidally and viewed along the cube diagonal.

ED: C spot pattern, similar to that of Fig. 46b, from an aggregate formed in a similar way.

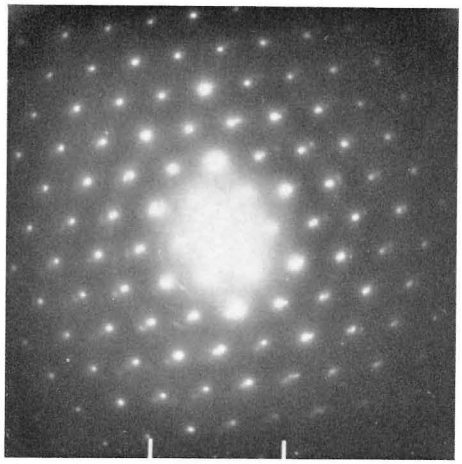

Fig. 44

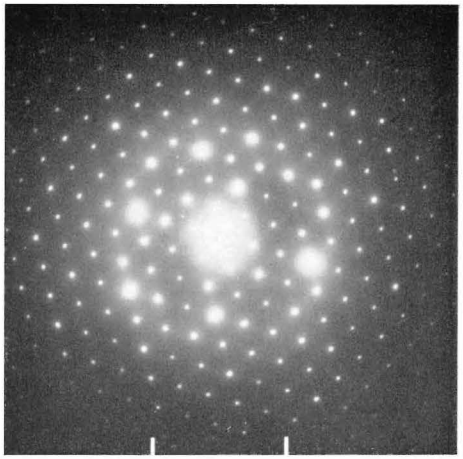

Fig. 45

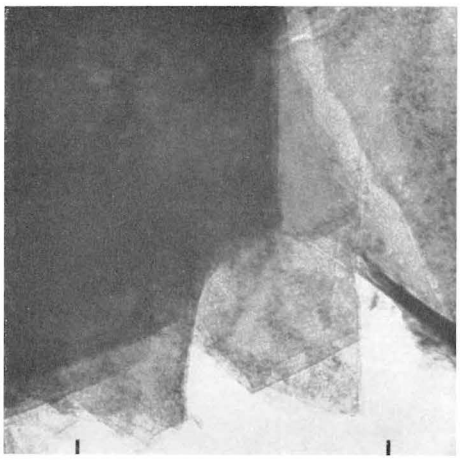

Fig. 46 a

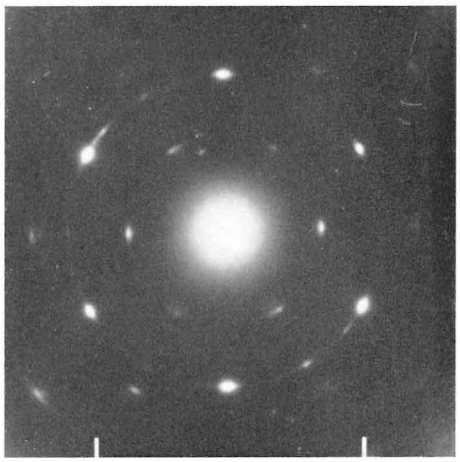

Fig. 46 b

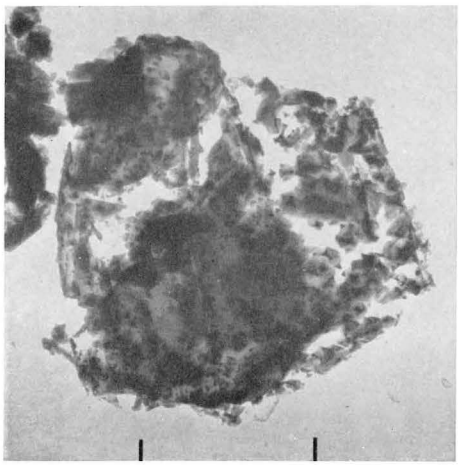

Fig. 47 a

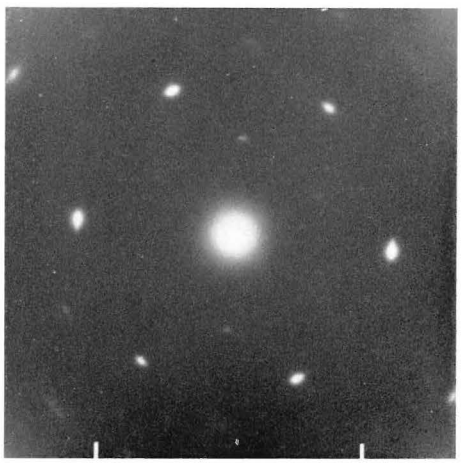

Fig. 47 b

17. C-A-H

Hydrogarnet crystals in C_3A preparations

Fig. 48. Sample Al—2A.

EM: Large C_3AH_6, hydrogarnet, crystals of various isometric forms, probably rhombic dodecahedrons (with hexagonal outlines) and trapezohedrons, together with thin plates of C-A-H(hex.) phase. The latter phase is predominant in this sample (cf. Figs. 60—64), and only a few C_3AH_6 crystals were observed. These are too thick to give any ED effects.

Fig. 49. Sample Al—2B.

EM: The same sample as in Fig. 48, in a later stage of development. The C-A-H(hex.) plate phase is still predominant (cf. Fig. 66), but numerous small crystals, mostly of cubic shapes, are also observed. According to the analysis of the composition after a long time (C/A about 3.6 in solid, in a nearly-saturated solution), the reaction seems to reach a (probably metastable) state of equilibrium where both C_4A aq.(hex.) and C_3AH_6 phases are present in comparable amounts.

Fig. 50. Sample Al—1.

EM: Particles similar to those of Fig. 49. The C_3AH_6 crystals, mostly of cubic habits, seem to be more abundant in this sample, which started with C_3A in a supersaturated lime solution. Assuming that the hydrogarnet phase invariably has a C/A ratio of 3, it follows that the C/A composition of the hexagonal-plate phase must be 5 to 6 rather than 4. However this phase seems to be different from the C_6AH_{33} compound prepared by *Flint* and *Wells* 1944, which shows needle-like habits, similar to ettringite, and probably also different from the C_5AH_{34} compound described by *Assarsson* 1936, which crystallizes as hexagonal prisms or columns. The ED patterns given by the plate particles are similar to that of Fig. 66 b, all of them showing a glass phase mixed with an oriented-aggregate C spot pattern. The plates are most probably a product of dehydration, without change of outer habit, of an initial, highly-unstable hexagonal-plate phase. The crystal structure of this compound could be explained, very tentatively, as a C_4A aq. structure with excess lime, either with some Ca replacing Al ions in the monolayer structure proposed by *Buttler et. al.* 1959, or with some extra Ca ions in the octahedral voids of the clay-type structure proposed by *Grudemo* 1962, 1964b.

Fig. 51. Sample Aw—2A.

EM: Mainly crystals of C_3AH_6, hydrogarnet, with some hexagonal-plate phase. The predominant crystal form seems to be the rhombic dodecahedron, with octagonal and hexagonal cross-sections, but a few crystals may be trapezohedrons. Due to the vigorous stirring, and to the temperature rise caused by it (final temperature about 40° C), the hydration of C_3A seems to be complete after 10 min., and the main product of hydration is the stable isometric phase.

Figs. 52 and 53. Sample Aw—2B.

EMs: Similar to Fig. 51. Hydrogarnet crystals are predominant, but there are still appreci able quantities of thin hexagonal plates (see Figs. 72 and 73). In Fig. 53, there are a few particles of a phase consisting of branched fibers, which can also be observed in Fig. 72.

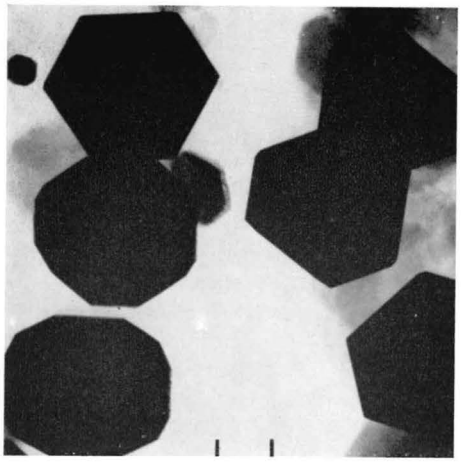

Fig. 48

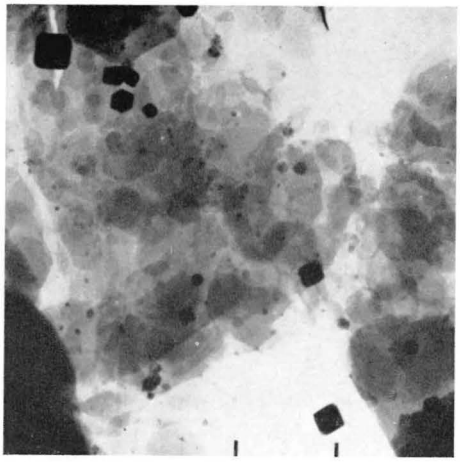

Fig. 49

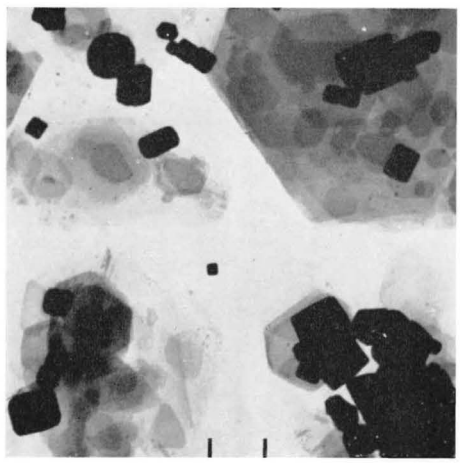

Fig. 50

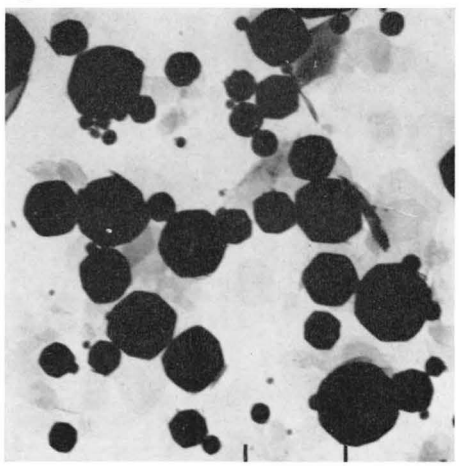

Fig. 51

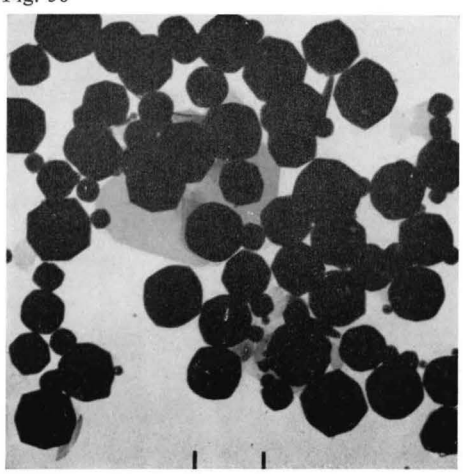

Fig. 52

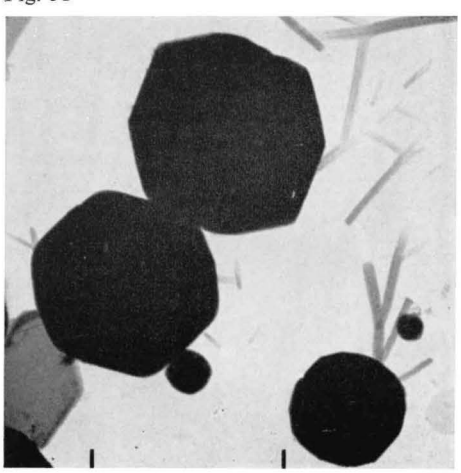

Fig. 53

18. C-A-H

Isometric phases in portland cement suspensions

Figs. 54 and 55. Sample Pw—6B.

EM (54a): Cluster of crystals of various shapes: square, rectangular, elongated-hexagonal, diffusely-rounded.

ED (54b): Spot-ring diagram with spacings *3.18*, 2.86, *2.235*, 2.025, 1.815, 1.585, *1.413*, 1.292 Å (the three most prominent reflexions in italics). These reflexions correspond, within ±0.8 percent, to the (400), (420), (440), (620), (444), (800), (840), and (844) spacings, respectively, from a cubic lattice of unit cell $a_c = 12.68$ *Å*. This value can be compared with the unit cell sizes of C_3AH_6, $a_c = 12.58 \pm 0.01$ Å, and C_3FH_6, $a_c = 12.75 \pm 0.01$ Å, as calculated from data compiled by *Copeland*, *Kantro*, and *Verbeck* 1962. It is possible that the crystals of Fig. 54 represent an intermediate hydrogarnet compound, $C_3(A,F)H_6$. It can be noted that of the ED reflexions observed, only the first two are prominent in X-ray diffraction diagrams. Several of the spacings corresponding to strong X-ray reflexions, such as 5.14 (211), 4.45 (220), 3.36 (321), 2.30 (521), 2.04 (532) (611), 1.745 (640), and 1.680 (642) Å (C_3AH_6 spacings given), are not observed in the ED diagram. It seems that reflexions from spacings for which the crystallographic indices are multiples of four, are enhanced in the ED pattern, whereas especially those with two odd numbers in the index combination are suppressed, in spite of the fact that some of them are among the strongest X-ray reflexions.

EM (55a): Rectangular crystals, found in small quantities in areas adjacent to crystal clusters similar to that of Fig. 54.

ED (55b): (from a single crystal): Simple cubic single-crystal pattern, unit cell $a_c = 3.17 \pm 0.01$ Å (average of three different patterns recorded), which is ¼ of 12.68 Å. The crystals of Figs. 54 and 55 are therefore probably identical or closely-related, with respect to structure, although grown differently.

Fig. 56. Sample Pw—6C.

EM: Clusters of small rounded particles, some with diffusely-crystalline contours.

ED: Spot-ring diagram with spacings 3.3, 3.13, *2.83*, 2.58 (diffuse ring), 2.205, *2.008*, 1.815, 1.704, 1.635, 1.410, *1.268*, 1.153 Å. (the three most prominent reflexions in italics). Excluding the first one at 3.3 Å. which is probably spurious (absent in another, similar diagram), these reflexions correspond, within ±1 percent, to the (400), (420), (422), (440), (620), (444), (642), (553) or (731), (840), (10 00) or (771), and (10 42) spacings, respectively, from a cubic lattice of unit cell $a_c = 12.62$ Å. This figure is indicative of a hydrogarnet phase which, however, differs in certain respects from the one found at an earlier age in the same sample (Figs. 54 and 55). The differences consist of a small (perhaps insignificant) decrease in unit cell size, and a radical change in intensity relationships. This change could possibly be caused by an inclusion of silica in the lattice (substitution of S for 2H), by an increase in the A/F ratio, or by a combination of both.

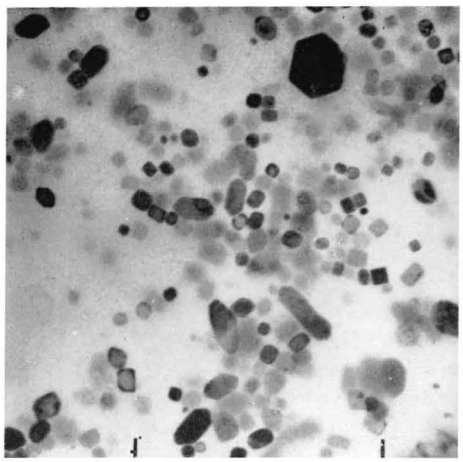

Fig. 54 a

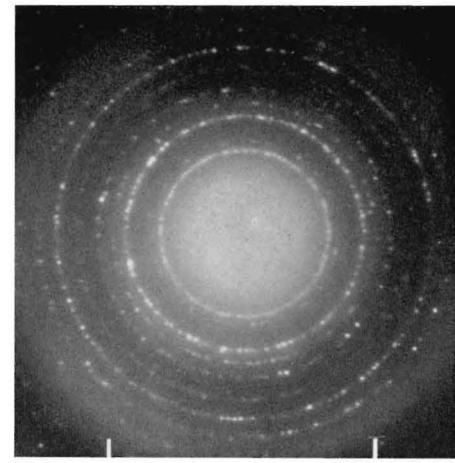

Fig. 54 b

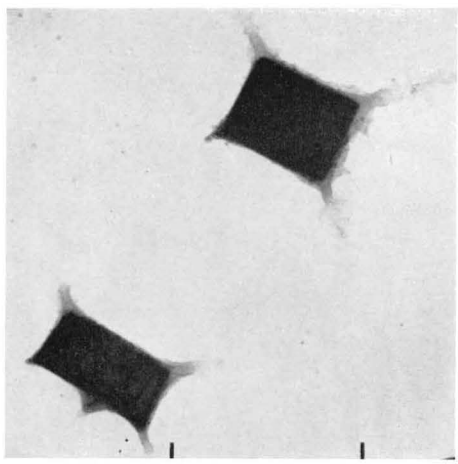

Fig. 55 a

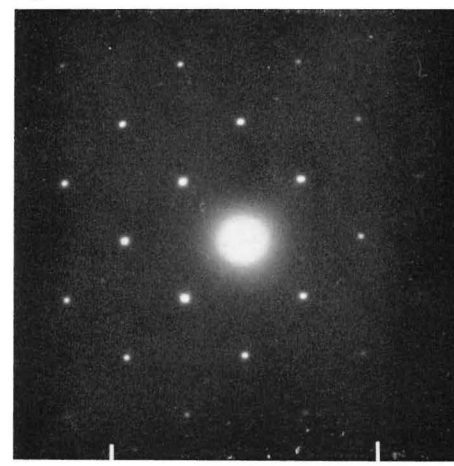

Fig. 55 b

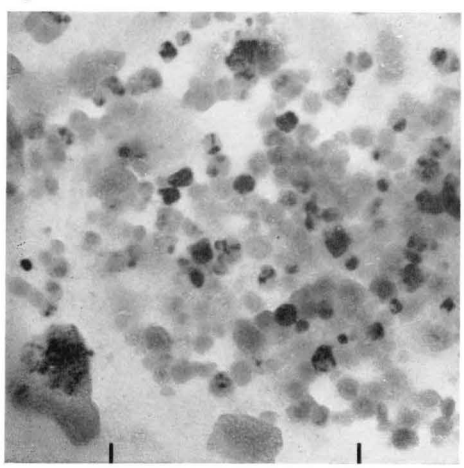

Fig. 56 a

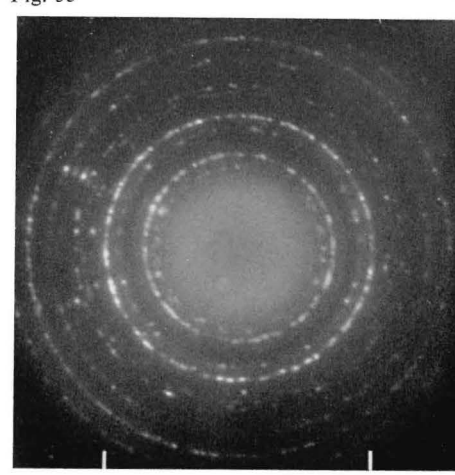

Fig. 56 b

19. C-A-H

Hexagonal-plate hydrates

Figs. 57 and 58. Sample Aw—1.

EMs: (57, 58a): Representative crystals from sample with C_3A hydrated slowly in a large quantity of water. This sample was homogeneous, and no other crystal forms (such as hydrogarnet) were observed. The crystal plates show various hexagonal shapes. They are seldom regular, but elongated, mostly with rounded corners and consisting of aggregated, smaller plates. Their composition is estimated to be about C_3A aq. (cf. list of samples). These data suggest that the plate phase of this sample consists of co-crystallized, thinner plates of C_4A aq. and C_2A aq., for the structures of which various alternatives have been proposed, most recently by *Buttler et. al.* 1959, *Jones* 1962, and *Grudemo* 1962, 1964b.

The basic unit in these structures, as suggested by *Buttler et. al.*, is a close-packed double layer of hydroxyl groups, with two Ca ions and one Al ion in three octahedral cations positions. These layers are interstratified with layers of water molecules, with one or two water layers per basic unit layer in C_4AH_{13} or C_4AH_{19}, respectively. From the latter of these structures. *Jones* derives the C_2AH_8 structure by replacing three protons in the water layers by one Al ion, possibly placed in every third octahedral cation position between the close-packed water layers. The structures proposed by *Grudemo*, on the other hand, are essentially deficient clay-lattice structures, generally with Ca ions in two out of three possible octahedral positions, and Al ions in one out of two possible tetrahedral positions. Thus, C_4AH_{11-13} and C_4AH_{19} are supposed to be structurally similar to the 1:1 clay minerals kaolinite and halloysite, respectively, C_2AH_{7-9} similar to the 2:1 clay minerals, such as montmorillonite. It should be emphasized, that the structures now described are only suggestions, and that the true structures are still to be determined.

ED (58b): Spot patterns of hexagonal symmetry, three slightly rotated patterns of (*hk*.0 spots, $a_H = 5.71$ Å.

ED (58c): Same diagram, after moderate heating in temporarily increased beam intensity. The pattern from 58b is weakened, the measured unit cell is slightly smaller, $a_H = 5.69$ Å. Inside some spots of the strongest C-A-H(hex.) pattern, with indices (*hk*)=(11), (30), (22), (41), etc., there are additional, diffuse spot reflexions, with indices (*hk*)=(10), (11), (20), (21), etc., respectively, from a hexagonal unit cell $a_H = 3.54$ Å, or somewhat smaller than that of CH (3.593 Å). *Buttler et al.* 1959 observed similar phenomena in EM-ED studies of C_4AH_{13} crystals, and gave unit cell distances of 5.7 and 3.6 Å for the two substances. They assume that regular CH layers are formed by successive replacement of Al ions by Ca ions in the octahedral positions, the Al ions and residual O and OH groups segregating into a glass phase. Judging from X-ray diffraction data, these transformations take place already at 100 to 150° C in a normal atmosphere, and most likely at much lower temperatures in the electron microscope. *Grudemo* 1964b suggests another mechanism for the conversion on heating, viz. a collapse of the tetrahedral layers of the postulated clay-type lattice, and an accommodation in the empty octahedral sites of the Al ions thus liberated, forming a layer of composition and structure similar to those of the unheated layer according to *Buttler et al.* This process would cause the pseudo cell of the lattice to expand from 3.3 Å ($5.7/\sqrt{3}$) to a size approaching that of the CH lattice. With an ordered arrangement of the Al ions, as assumed by *Buttler et al.*, the true hexagonal cell dimension would still correspond to the orthohexagonal cell of CH ($a_H = 3.593 \cdot \sqrt{3}$) but all reflexions except those associated with the pseudo cell would be systematically weak, and possibly hard to detect in ED diagrams.

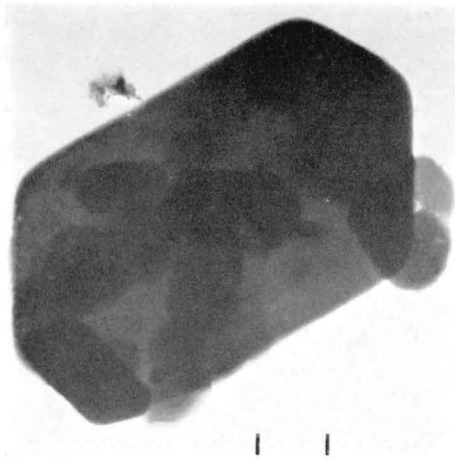

Fig. 57

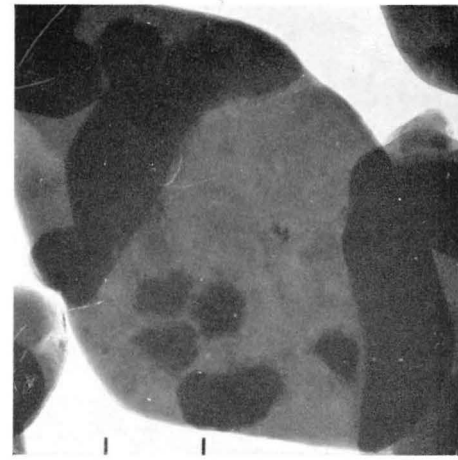

Fig. 58 a

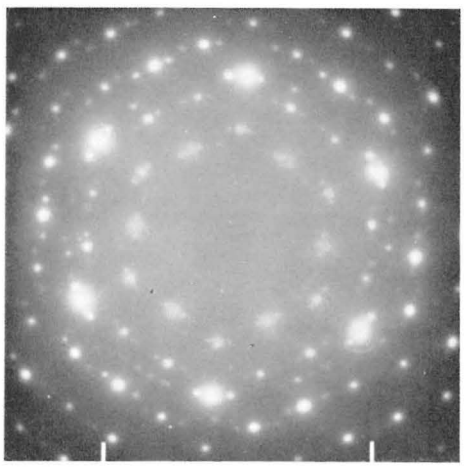

Fig. 58 b

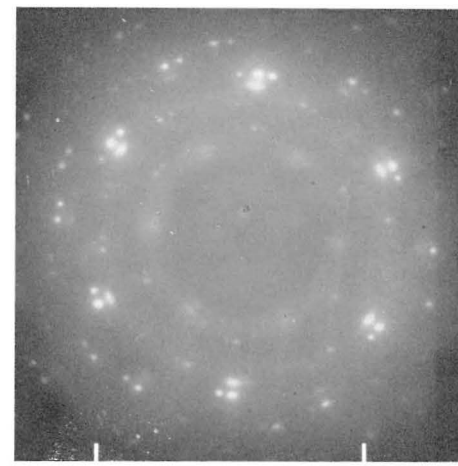

Fig. 58 c

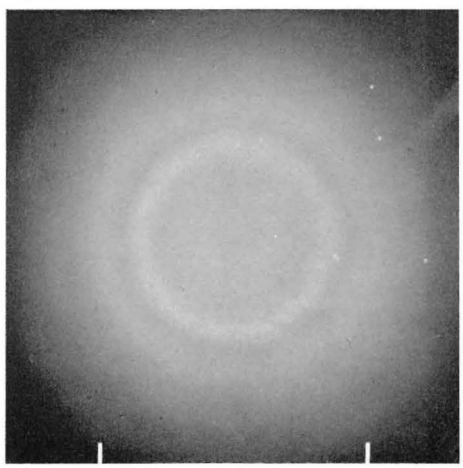

Fig. 58 d

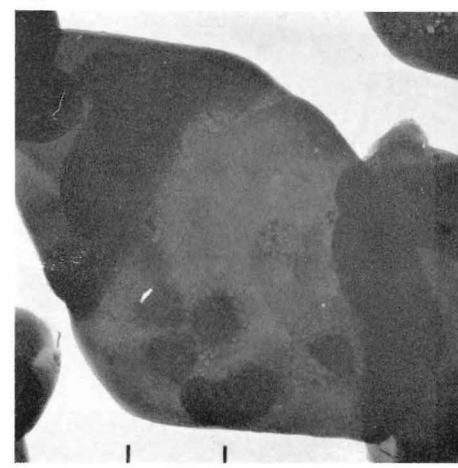

Fig. 58 e

ED (58d): Same region as before, after a longer period of heating. The structure has become converted to a glass, giving only one diffuse ED ring at about 2.9 Å. Another heated crystal gave, in addition to the diffuse ring, an oriented C spot pattern similar to that of Fig. 47b.

EM (58e): The crystal of Fig. 58a, after heating. There are signs of internal recrystallization, but the outer shape of the crystal is essentially unchanged.

---

20. C-A-H

Hexagonal-plate hydrates (continued)

Fig. 59. Sample Aw—1 (cf. preceding page).

EM: Well-crystallized plate aggregate.
ED: Spot pattern of regularly hexagonal symmetry, $a_H = 5.73$ Å.

Fig. 60. Sample Al—2A.

EM (60a): Rounded plate with thin, irregular edges, composition probably about C_4A aq. (hex.), also small, cubic crystal, probably C_3AH_6(cub.).

ED (60b): Regularly-hexagonal spot pattern, $a_H = 5.72$ Å, inner spots ($(hk)=(10)$) clearly visible.

EM (60c): Same particles, after about one minute's heating in temporarily-increased beam intensity.

ED (60d): The corresponding ED pattern shows a diffuse ring from a glass phase, at about 2.9 Å, a hexagonal-symmetry spot pattern corresponding to $a_H = 3.59$ Å, with axes coinciding with the original C_4A aq (hex.) pattern, and some weak spots in a hexagonal-symmetry pattern from a remaining C_4A aq (hex.) crystal, with $a_H = 2.87$ Å (the true cell is probably twice this value, $a_H = 5.74$ Å).

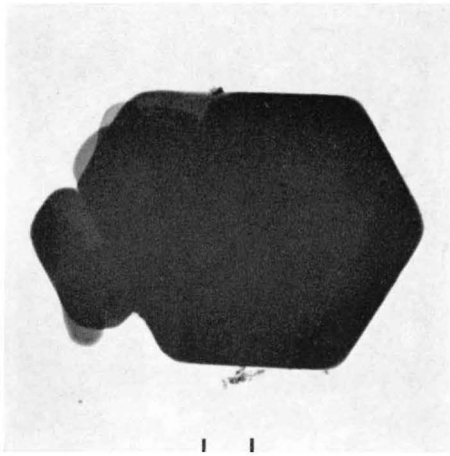

Fig. 59 a

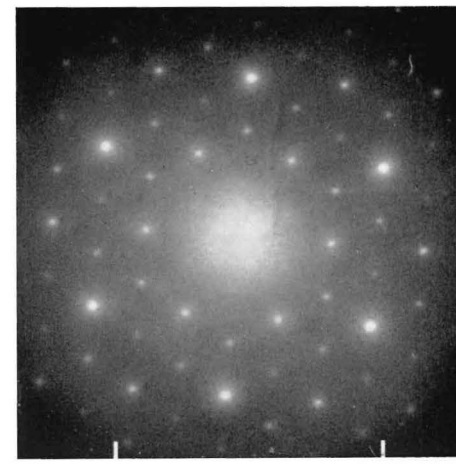

Fig. 59 b

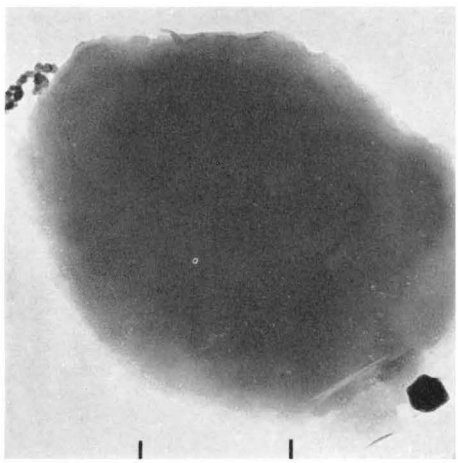

Fig. 60 a

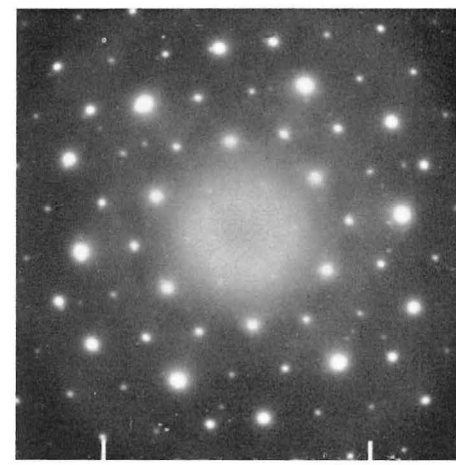

Fig. 60 b

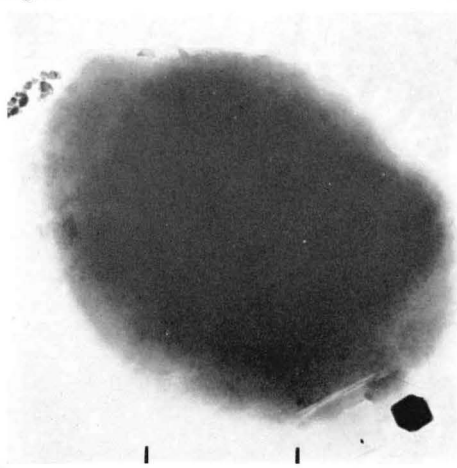

Fig. 60 c

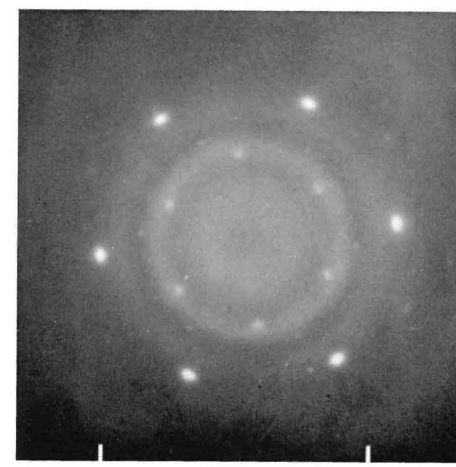

Fig. 60 d

21. C-A-H

Hexagonal-plate hydrates (continued)

Figs. 61 and 62. Sample Al—2A (cf. preceding page).

EM (61a): Thin crystal plate, mainly of uniform thickness and hexagonal angles.

ED (61b): Corresponding ED, spot pattern, regularly-hexagonal symmetry, $a_H = 5.73$ Å, inner spots ($(hk) = (10)$) very weak.

EM (61c): Same plate, after about one minute's heating in temporarily-increased beam intensity, only small changes.

ED (61d): Corresponding ED, diffuse rings at about 2.92, 2.09, 1.18 Å, the crystal has transformed into a glassy phase.

EM (62a): Cluster of superimposed, thin plates, probably C_4A aq (hex.) crystals, and a few cubic crystals, probably C_3AH_6(cub.)

ED (62b): Hexagonal-symmetry spot patterns, $a_H = 5.71$ Å, with sharp spots, and $a_H = 3.55$ Å, with diffuse spots, located inside some spots of the principal pattern. These crystals have not been deliberately exposed to a higher beam intensity than is necessary for observation, but nevertheless, some conversion to a CH-type phase has taken place. The a_H value is lower than that of CH, and it is possible that the crystal phase, from which this pattern originates, is in reality a solid-solution phase (C,A)H (cf. discussion of Figs. 57 and 58).

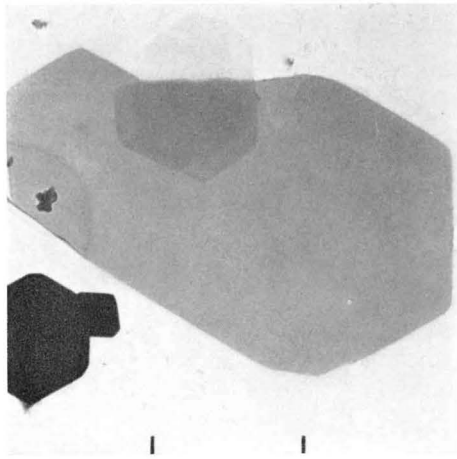

Fig. 61 a

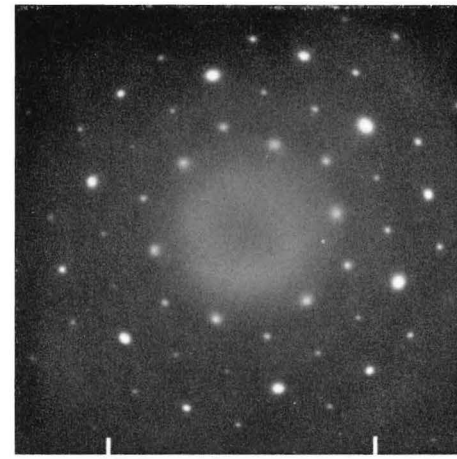

Fig. 61 b

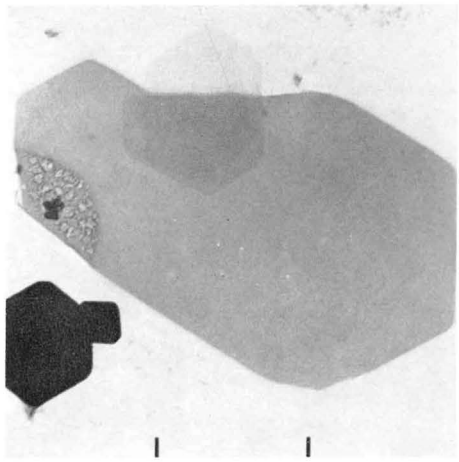

Fig. 61 c

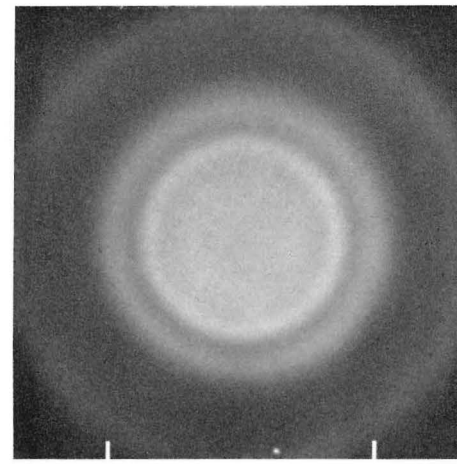

Fig. 61 d

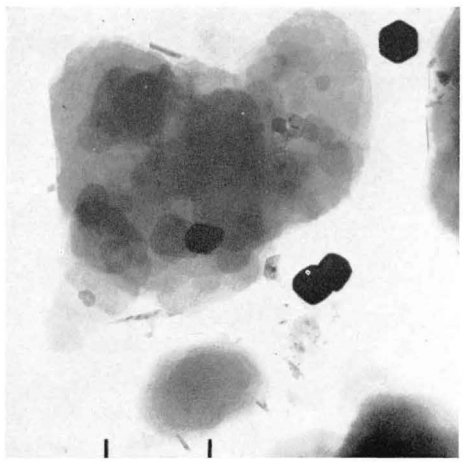

Fig. 62 a

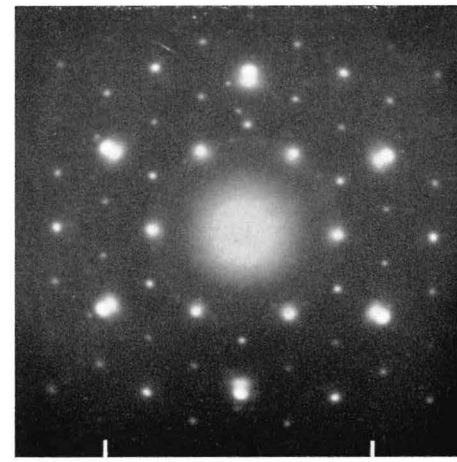

Fig. 62 b

22. C-A-H

Hexagonal-plate hydrates (continued)

Figs. 63 and 64. Sample Al—2A (cf. preceding pages).

EM (63a): Thin plates with hexagonal angles and superimposed, smaller plates.

ED (63b): Corresponding ED, very similar to that of Fig. 62b, measured spacings $a_H = 5.73$ Å for principal diagram, $a_H = 3.57$ Å for diagram of CH-type conversion phase.

EM (63c): Same plates, after about one minute's heating in high-intensity beam. These plates seem completely burnt out internally, but the original outlines are still retained.

ED (63d): Corresponding ED, C ring diagram with enhancements in directions corresponding to the original $C_4A.aq$ (hex.) pattern, and diffuse ring from glass phase at about 2.9 Å.

EM (64a): Thin plate with rounded, irregular outlines.

ED (64b): Regularly-hexagonal spot pattern, C_4A aq (hex.), measured lattice distance $a_H = 5.66$ Å. comparatively strong inner reflexions ($(hk) = (10)$).

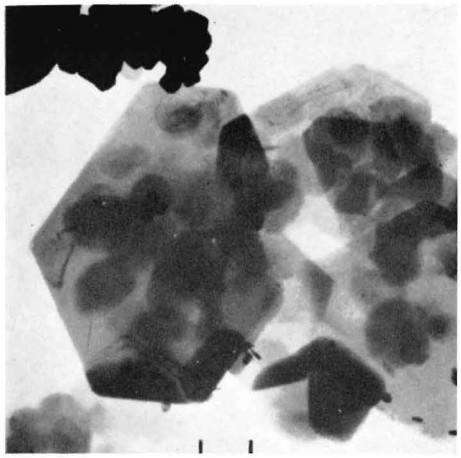

Fig. 63 a

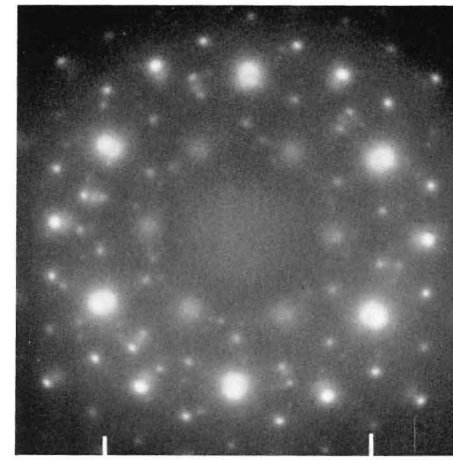

Fig. 63 b

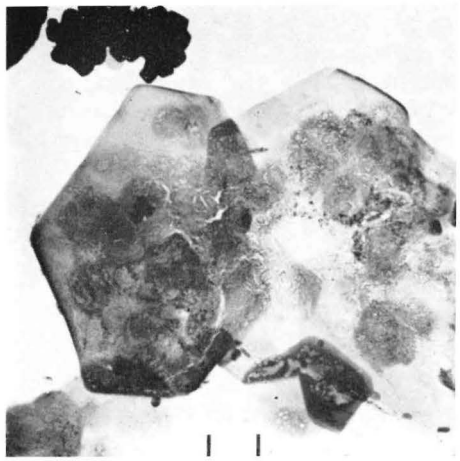

Fig. 63 c

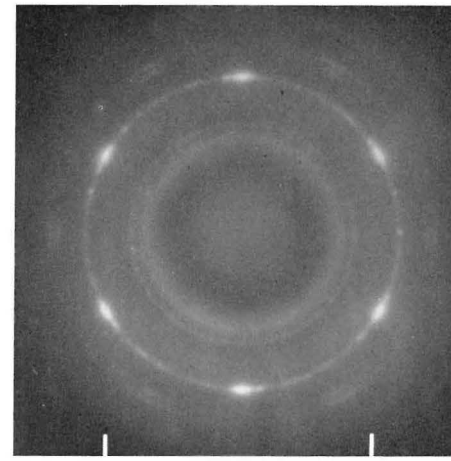

Fig. 63 d

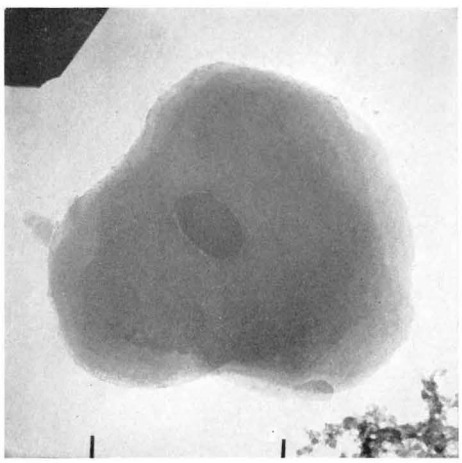

Fig. 64 a

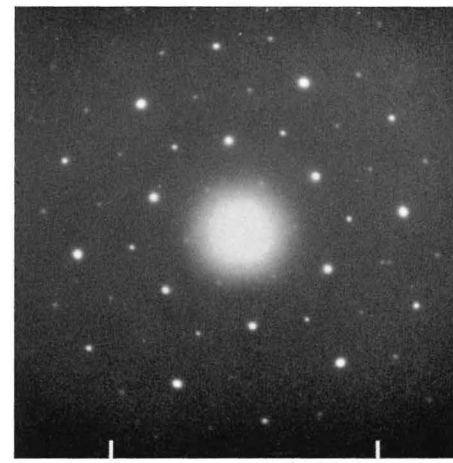

Fig. 64 b

23. C-A-H

Hexagonal-plate hydrates, transformations

Fig. 65. Sample Al—2A (cf. preceding pages).

EM (65a): Thin, hexagonal plate, covered with fibrous crust and surrounded by an interaction zone.

ED (65b): Corresponding ED, mainly hexagonal-symmetry spot pattern of $C_4A.aq.(hex.)$ type, $a_H = 5.73$ Å, inner spots ($(hk)=(10)$) almost absent.

EM (65c): Same particles, after heating for about one minute in beam of higher intensity.

ED (65d): Corresponding ED, mainly a spot-ring diagram of $C\bar{C}$, calcite, also six spots in regularly-hexagonal arrangement at about 1.70 Å from oriented aggregate of C crystals, and a glass phase ring at about 2.9 Å. The original formation is probably a calcium carboaluminate hydrate crystal, $C_4A\bar{C}$ aq(hex.), covered with an amorphous, $\bar{C}$-contaminated CH precipitate, similar to those of Figs. 7 to 11.

Fig. 66. Sample Al—2B.

EM: Aggregate of thin plates with certain signs of hexagonal structure and probable composition C_4A aq (hex.) (cf. Fig. 49).

ED: Diffuse glass-phase ring at 2.9 Å, and six spots at 1.70 Å from oriented C crystal aggregate, formed by thermal decomposition of original structure. All the plate crystals of this sample showed similar ED patterns and were thus already decomposed before EM inspection. It is suggested that the hexagonal-plate phase is gradually becoming more unstable prior to the expected, but slow conversion to C_3AH_6(cub.).

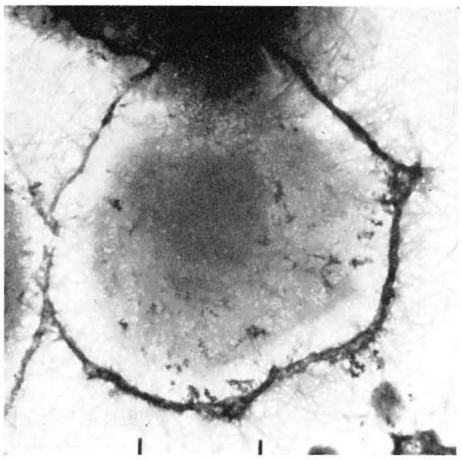

Fig. 65 a

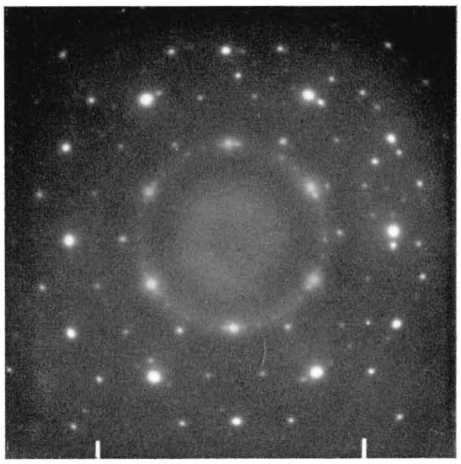

Fig. 65 b

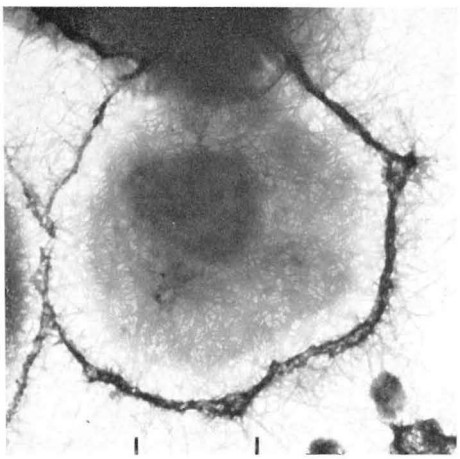

Fig. 65 c

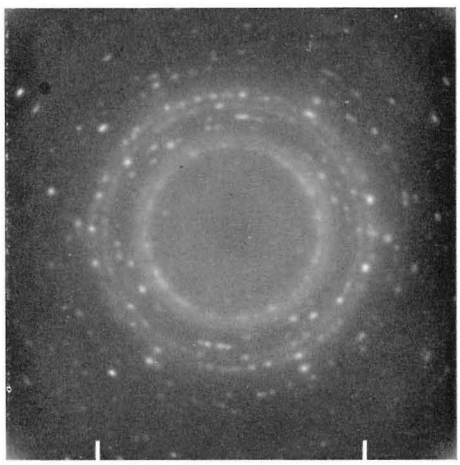

Fig. 65 d

Fig. 66 a

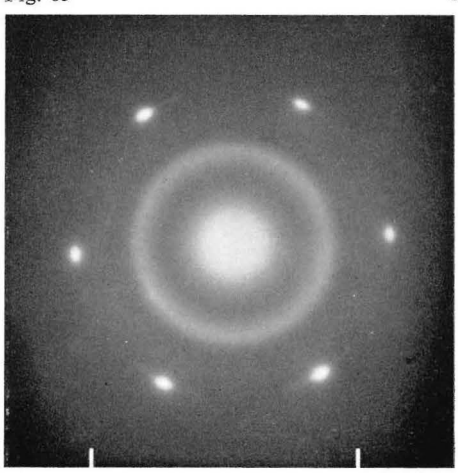

Fig. 66 b

24. C-A-H

Phases in C_3A suspension, various observations

Figs. 67—71. Sample Aw—2A.

EM (67a): Large, thin, regularly-hexagonal plates and hydrogarnet crystals (cf. Fig. 51).

ED (67b): Diffuse glass-phase ring at about 2.9 Å. None of the plate crystals in this sample could be observed in its original crystalline state, most certainly of regularly-hexagonal symmetry. Because of the transient nature of the hexagonal-plate phase, these crystals are easily vitrified by the combined action of heat and vacuum.

ED (68): Pattern given by particle similar to the plates of Fig. 67 a, diffuse ring at 2.9 Å., and C ring pattern without preferred-orientation effects. In this case, the internal vitrification has obviously been completed, before the C crystals were formed.

ED (69): Region similar to that of Fig. 67 heated in high-intensity beam until melting occurred, ED given by particles recrystallized upon cooling, consisting of C ring diagram, with 2.405 and 1.701 Å reflexions most prominent, superimposed by spot or spot-ring pattern of the anhydrous compound $C_{12}A_7$. Measurements give the following average values of observed lattice spacings, with $C_{12}A_7$ spacings and relative intensities given by *Midgley* 1957 in brackets (some of the weaker X-ray reflexions are omitted):
4.89 (4.89—10), 4.19 (4.24—2), 4.07(?), 3.78 (3.795—5), 3.21 (3.20—5), 3.01 (2.999—7), 2.82(?), 2.78 (C ring), 2.685 (2.680—10), 2.455 (2.445—8), 2.405 (C ring), 2.19 (2.186—7), 1.945 (1.944—7), 1.718 (1.729—4), 1.703 (C ring), 1.66 to 1.56 (1.662—7, 1.630—4, 1.601—7), 1.452 (C ring), 1.393 (C ring), 1.395 (1.393—6), 1.206 (C ring), 1.078 (C ring) Å.

ED (70): Similar to Fig. 69, but C rings weaker, $C_{12}A_7$ spot-rings more continuous and prominent.

ED (71): Similar to Fig. 69, mixture of C, $C_{12}A_7$, and $C\bar{C}$ (calcite) spot-ring patterns.

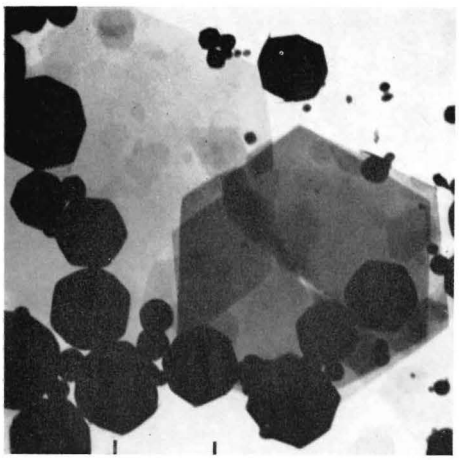

Fig. 67 a

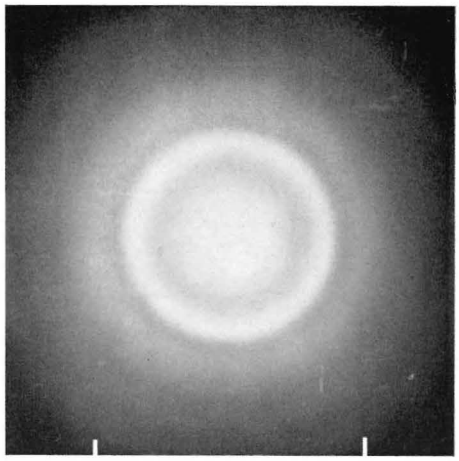

Fig. 67 b

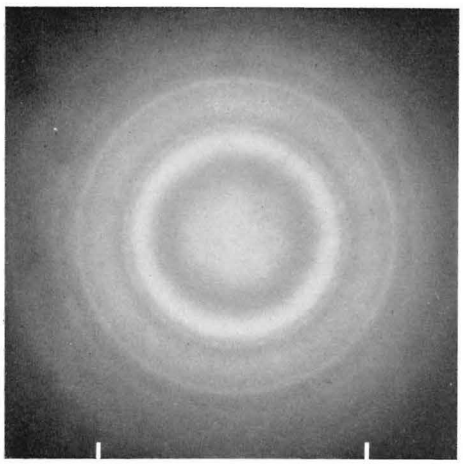

Fig. 68

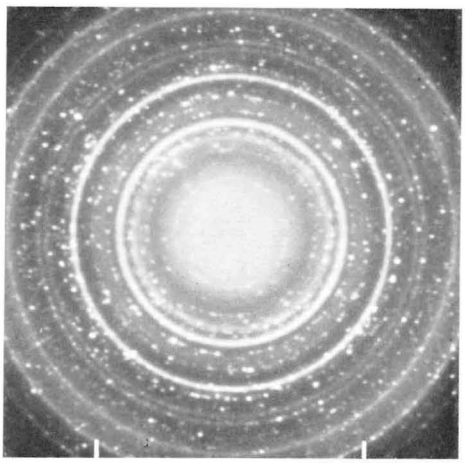

Fig. 69

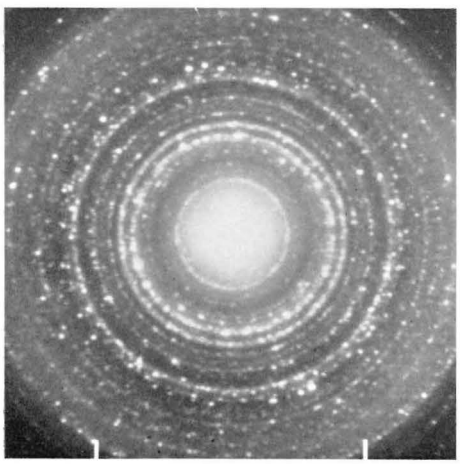

Fig. 70

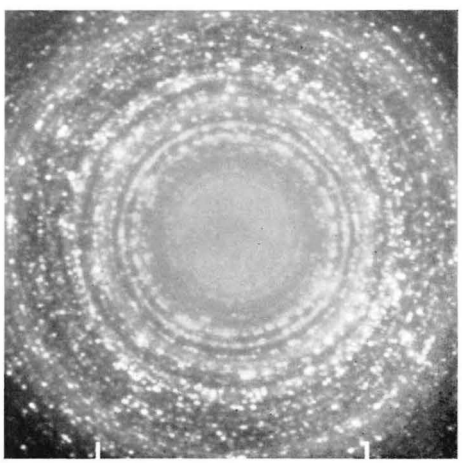

Fig. 71

25. C-A-H

Phases in C_3A suspension and paste

Figs. 72 and 73. Sample Aw—2B.

This sample consisted mostly of hydrogarnet phase (cf. Figs. 52 and 53), and contained much fewer hexagonal-plate crystals than the freshly-prepared sample (Aw—2A). The crystals observed were well-shaped and did not show any signs of decomposition, but were still found to consist of products of conversion, due to thermal dehydration.

EM (72a): Thin, hexagonal plate, hydrogarnet crystals, and fibers (obviously rolled-sheet particles, minor constituent of sample).

ED (72b): Diffuse glass-phase ring at about 2.85 Å, and six spots at 1.70 Å from oriented C crystal aggregate, probably product of thermal dehydration of hexagonal plate.

EM (73a): Superimposed C-A-H(hex.) plates, with some fibers attached.

ED (73b): Complicated oriented-aggregate spot pattern, containing CH, C, and $C\bar{C}$ spots, together with glass-phase ring at about 2.85 Å.

Fig. 74. Sample Ap—1A.

EM: Large, thin, almost regular hexagonal plate, with indications of spiral growth, probable composition $C_3A \cdot aq$ (hex.). The sample consisted almost exclusively of hexagonal-plate crystals.

ED: Spot pattern of hexagonal symmetry, $a_H = 5.76$ Å, inner spots ($(hk) = (10)$) weak but clearly visible.

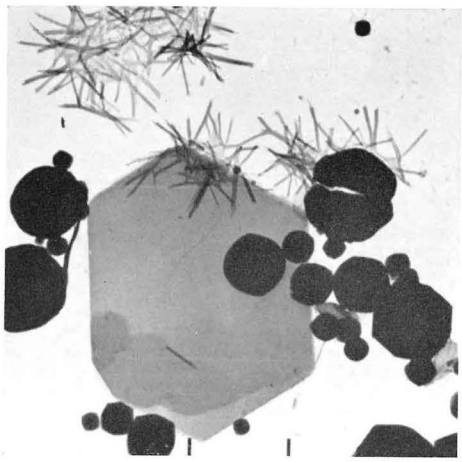

Fig. 72 a

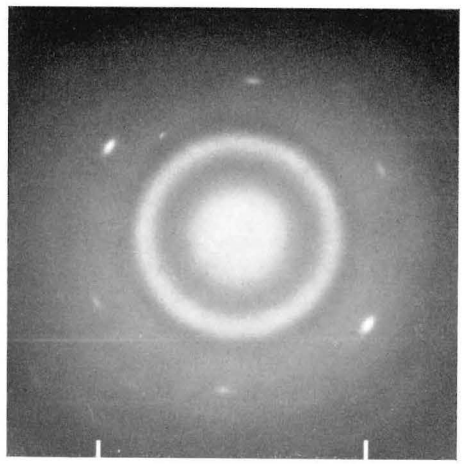

Fig. 72 b

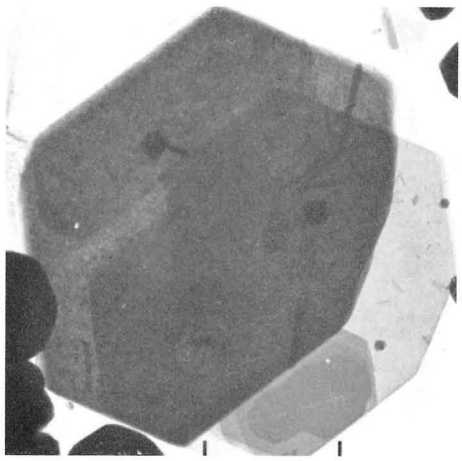

Fig. 73 a

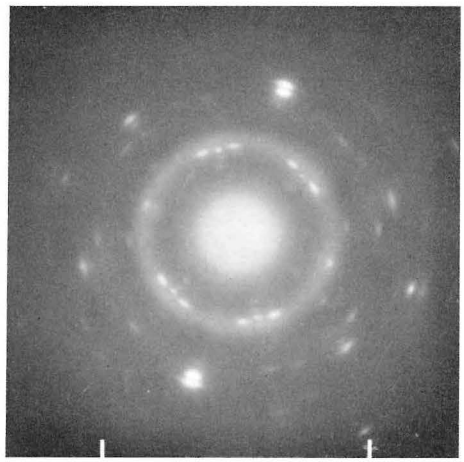

Fig. 73 b

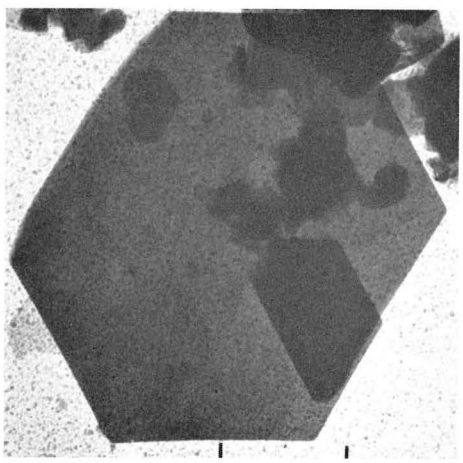

Fig. 74 a

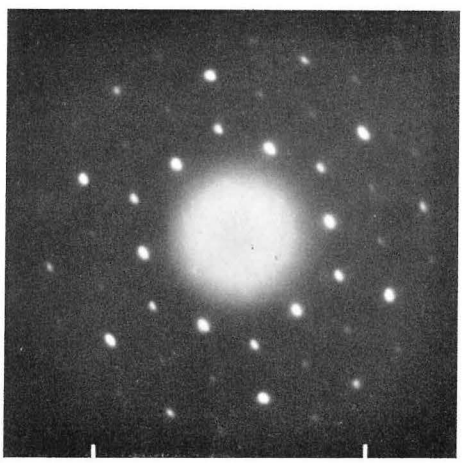

Fig. 74 b

26. C-A-H

Hexagonal-plate phases in portland cement suspensions

Fig. 75. Sample Pw—1A.

EM: Plates with regularly-hexagonal angles, C_4A aq.(hex.) or, more probably, $C_4A\bar{S}$ aq. (hex.) crystals. These plates, which were found to be common in this boiled cement suspension, were covered, especially around the edges, with fibers of a C-S-H(I) phase.

ED: Spot pattern, mainly C-A-H(hex.)-type hexagonal-symmetry pattern with $a_H = 5.72$ Å, also spot-ring at 1.805 Å, probably the fiber-axis repeat distance of C-S-H(I). Measurements on three other similar plates gave a_H values of 5.68 to 5.69 Å.

Fig. 76. Sample Pw—1B.

EM: Crystal plate similar to those of Fig. 75.

ED: Spot pattern of regularly-hexagonal symmetry, $a_H = 5.68$ Å, inner spots ($(hk)=(10)$) comparatively strong, also CH-type pattern of spots inside some of the spots of the main diagram, probably from product of thermal dehydration of the original crystal. The hexagonal unit cell of the latter pattern is 3.64 Å, or slightly larger than that of the pure CH lattice. This fact seems to disagree with the conception of partly-filled octahedral layers, described in the discussion of Figs. 57 and 58, and of the mechanism of formation of CH-type layers by thermal dehydration. It can be observed that *Buttler et al.* 1959 found a unit cell $a_H = 3.7$ Å for the CH-type lattice formed in crystals of natural hydrocalumite, of composition $C_4A\bar{C}_{1/4}$ aq., heated to 300 or 400° C and cooled. It is possible that, whether the octahedral sites of the CH-type conversion phase are occupied by only Ca ions or by Ca and Al ions in proportion 2:1, inclusions of $\bar{C}$ (as in hydrocalumite), or $\bar{S}$ (as in the present case) contribute to expand the hexagonal cell of the lattice.

Fig. 77. Sample Pw—4B.

EM: Thin plate crystal, one of a few found in this sample, probably $C_4A\bar{S}$ aq.(hex.). One of the major constituents of the sample, as seen in Figs. 244—48, consisted of ettringite-type particles. Immediately after mixing (sample Pw—4 A), no C-A-H (hex.) plates could be seen, and even after one day, the conversion of trisulfo- to monosulfoaluminate hydrate seemed to be in the beginning stage.

ED: Spot pattern of regularly-hexagonal symmetry, $a_H = 5.72$ Å, inner spots ($(hk)=(10)$) absent or extremely weak.

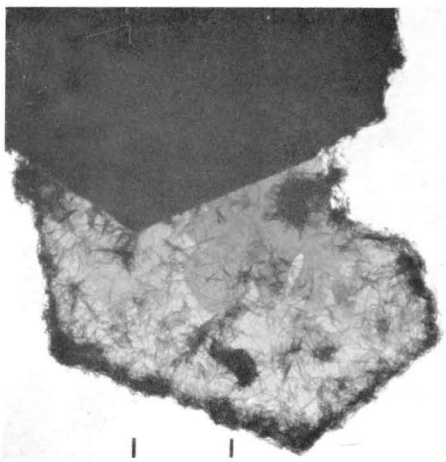

Fig. 75 a

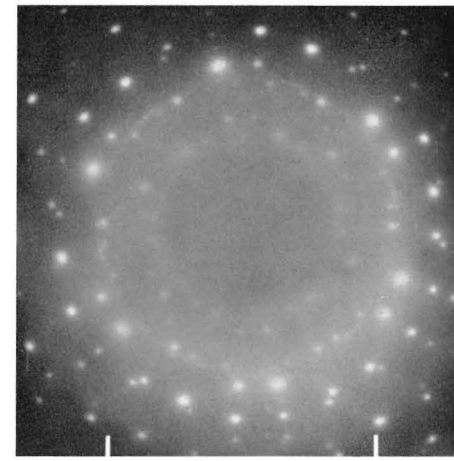

Fig. 75 b

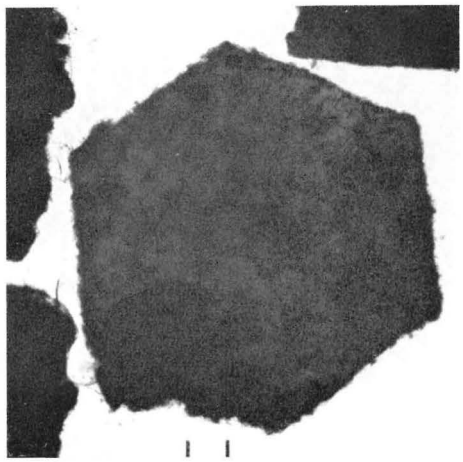

Fig. 76 a

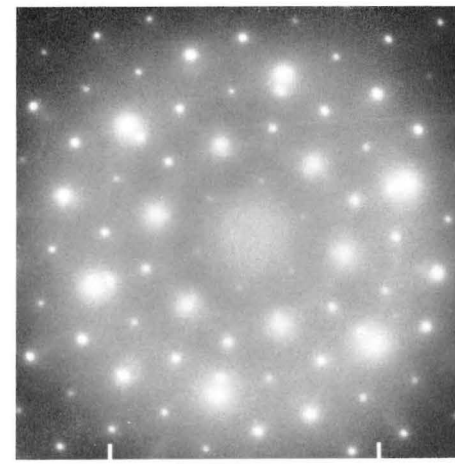

Fig. 76 b

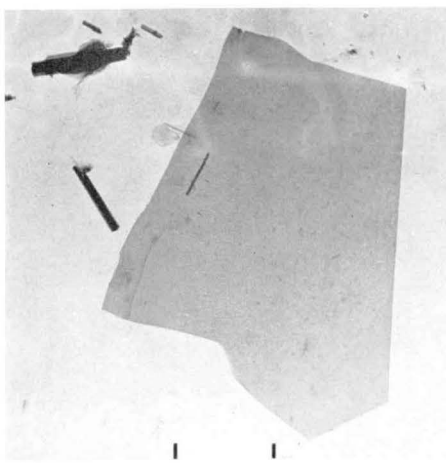

Fig. 77 a

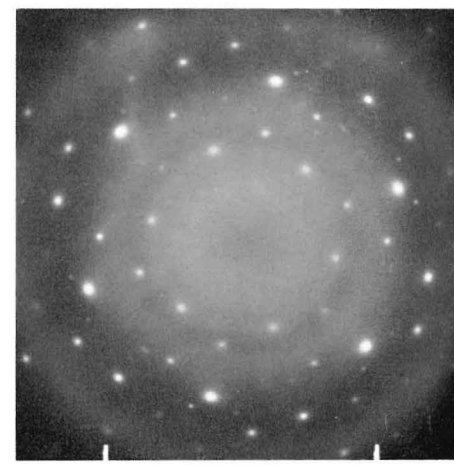

Fig. 77 b

27. C-A-H

Hexagonal-plate phases in portland cement suspensions (continued)

Figs. 78—81. Sample Pw—2.

EMs: (78, 79, 80a): Examples of hexagonal-plate particles rather commonly observed in this sample.

ED: (80b): Typical ED diagram given by one of these plates, diffuse glass-phase ring at about 2.9 Å, and C spot-rings showing no preferred-orientation effects, possibly originating from dehydrated, small CH crystals also present in Fig. 80a. Without being deliberately heated in the beam, all the plates of obviously hexagonal crystal symmetry seen in this sample were found to be dehydrated and vitrified, similar to the crystals of Figs. 67—72.

EM (81a): A large hexagonal flake was heated in a high-intensity beam, until it melted and recrystallized.

ED (81b): Composite spot-ring pattern, the most prominent rings of which can be indentified as C and C_3A reflexions. The following series of spacings has been measured, with the intensities of some more prominent reflexions indicated and with C_3A spacings and intensities observed by *Midgley* 1957 given in brackets: 5.42, 4.60, 4.21, 4.08—s (4.08—2), 3.70, 3.50, 3.33—ms (3.34—1), 3.07, 2.78—s (C reflexion), 2.70—vs (2.70—10), 2.405—s (C reflexion, 2.39—2), 2.29, (2.258—1), 2.205—m (2.200—s), 2.11, 2.03—m (2.039—4), 1.90—m (1.901—9), 1.825 (1.826—1), 1.70—s (C reflexion), 1.63, 1.555—s (1.556—8), 1.50, 1.45—m (C reflexion) Å, etc. These data indicate that the C/A ratio of the original structure (and of the intermediate glass phase) is higher than 3, and the probable composition is therefore C_4A aq., possibly with $\bar{S}$ in solid solution.

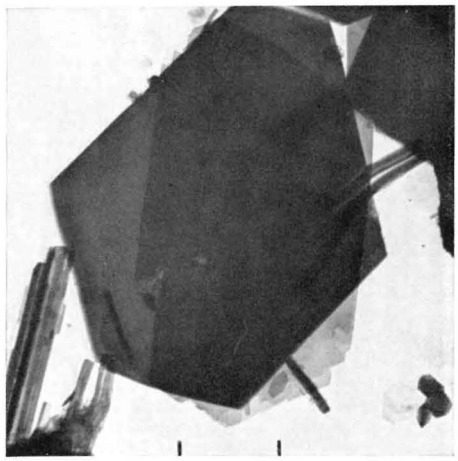

Fig. 78

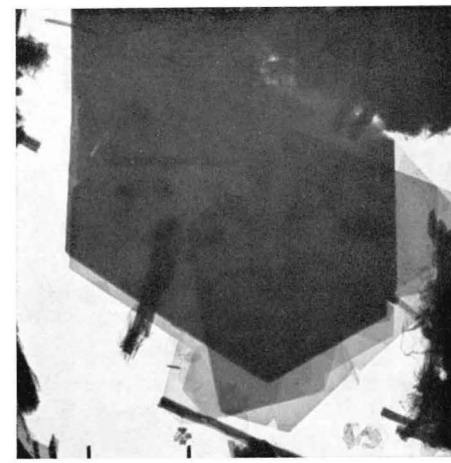

Fig. 79

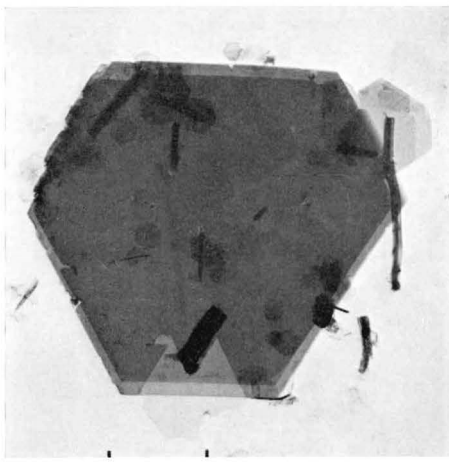

Fig. 80 a

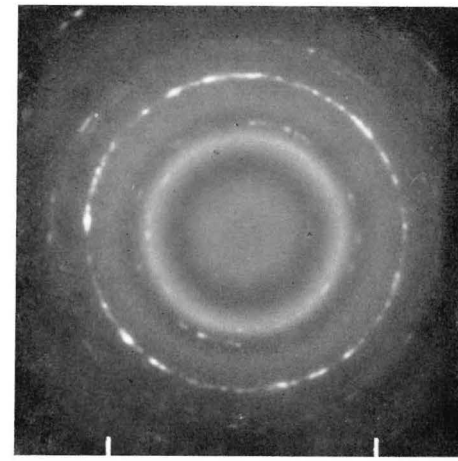

Fig. 80 b

Fig. 81 a

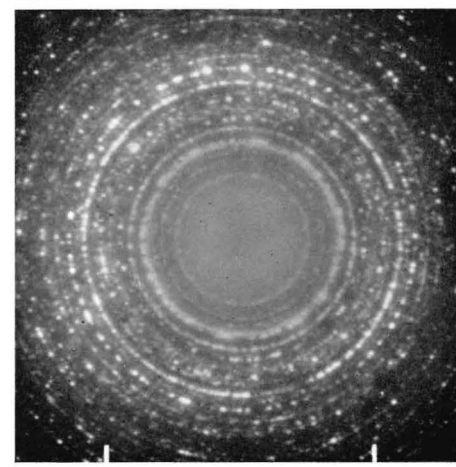

Fig. 81 b

28. C-A-H

Transformation products in portland cement suspensions

Figs. 82 and 83. Sample Pw—3A.

EM (82): Mainly network of fine fibers or crinkly foils. Judging from the appearance of the edge structure, where two straight edges at 120° angle can be discerned, the network has been formed from the material of a hexagonal-plate particle, probably of the identity of $C_4A\bar{S}$ aq.(hex.), similar to the plates on Figs. 78—80. This formation might represent a later stage of growth than that seen in Figs. 75 and 76, and the plate is not only covered with C-S-H(I) or C-S-H(II) fibers, but actually dissolved and incorporated in the fibrous phase (cf. Fig. 239).

EM (83): Various particles representative of the sample, among others a hexagonal-plate crystal covered with fibrous phase growing out over the edges.

Figs. 84 and 85. Sample Pw—3B.

EM (84a): Formation similar to that of Fig. 82, hexagonal angles clearly distinguishable.

ED (84b): Amorphous-phase pattern with diffuse rings, maxima at about 2.93, 2.09, and 1.17 Å.

EM (85a): Similar network of fibers, heated in the beam until melting occurred locally.

ED (85b): Composite diagram containing a rather strong C ring pattern, a hexagonal-symmetry cross-grating spot pattern with $(hk)=(10)$, (11), (20), (30), (22), and (40) spots observed and $a_H=7.46$ Å, given by compound of unknown identity, and some weaker spot-rings, also unidentified.

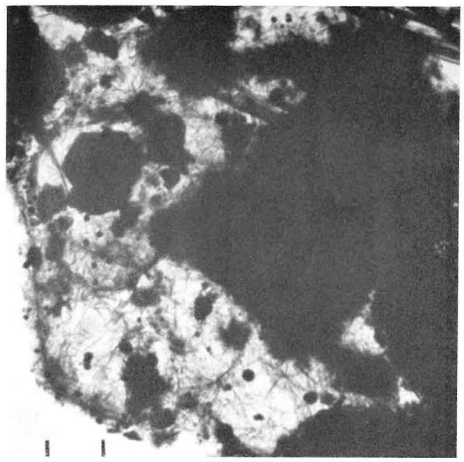

Fig. 82

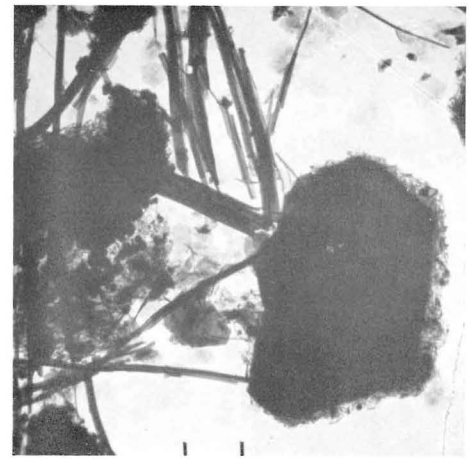

Fig. 83

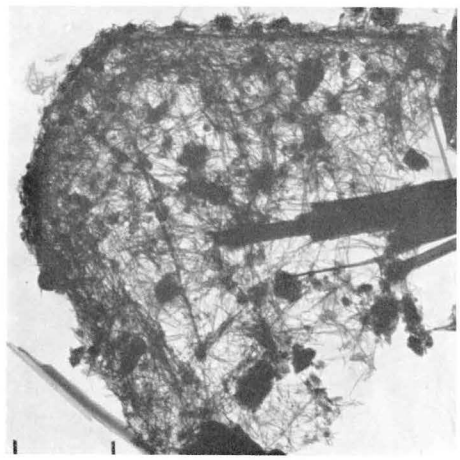

Fig. 84 a

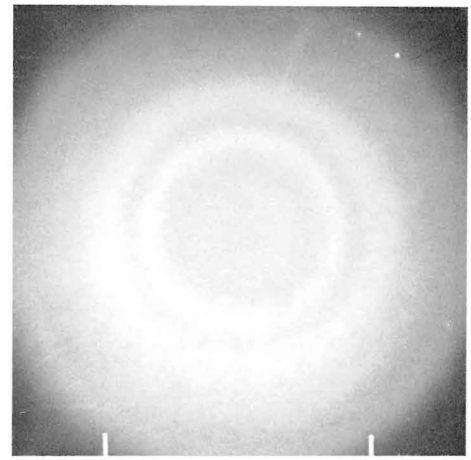

Fig. 84 b

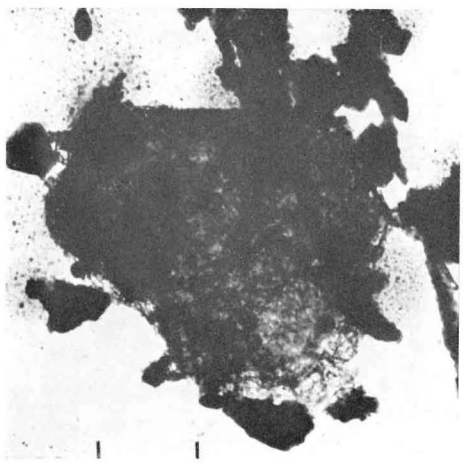

Fig. 85 a

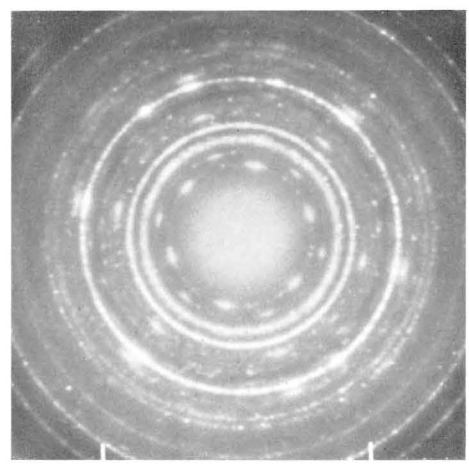

Fig. 85 b

29. C-A-H

Hexagonal-plate phases in portland cement suspensions (continued)

Fig. 86. Sample Pw—6A.

EM: Thin crust-like flake, probably C-A-H (hex.) particle in first stage of formation, with some rods or creased-sheet particles attached (cf. Figs. 134 and 135).

ED: Irregular spot-ring pattern, with reflexions at e.g. 3.86—3.82, 3.41—3.39, 3.06—3.04, 2.74, 2.50—2.47, 2.34, 2.09, 1.99 Å, etc., given by compound of unknown identity.

Figs. 87 to 89. Sample Pw—6B.

EMs (87, 88, 89a): Upon standing for about one day of the suspension treated in the high-speed mixer, large, thin crystal plates of hexagonal C-A-H phase, probably $C_4A\bar{S}$ aq. (hex.), had developed in appreciable amounts .Some fibrous-phase particles were mostly attached to the plates (cf. Figs. 136 and 137, 251—253).

ED (89b): Spot pattern, hexagonal (*hk*) cross-grating spots, $a_H = 5.68$ Å, inner spots ((*hk*)=(10)) of comparatively strong intensity.

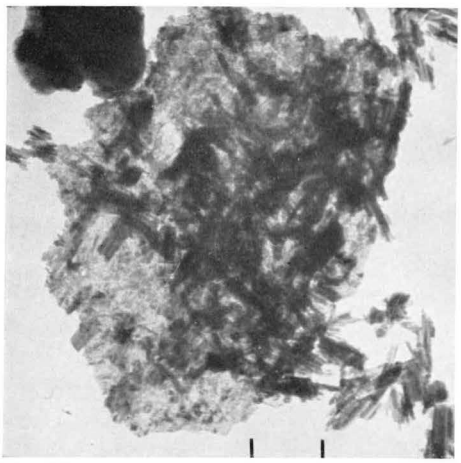

Fig. 86 a

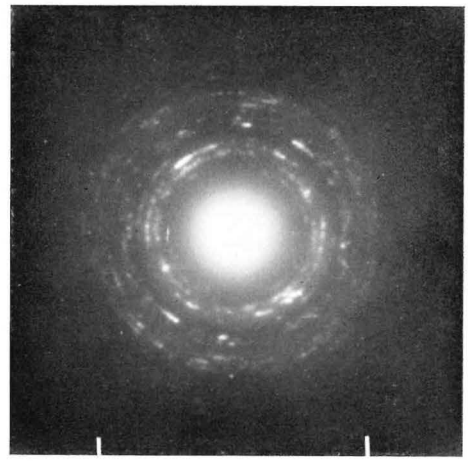

Fig. 86 b

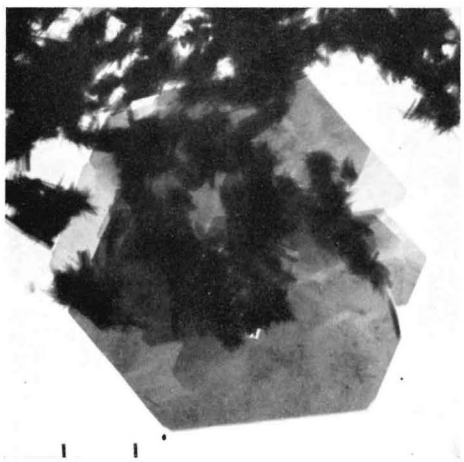

Fig. 87

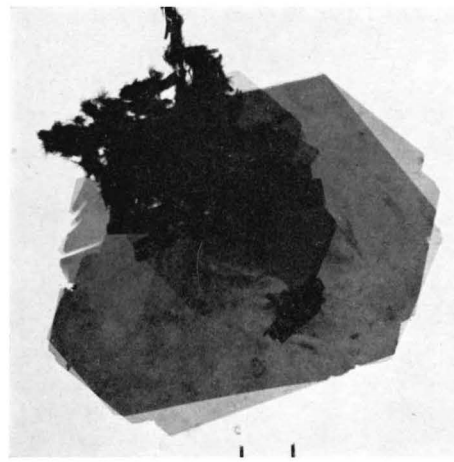

Fig. 88

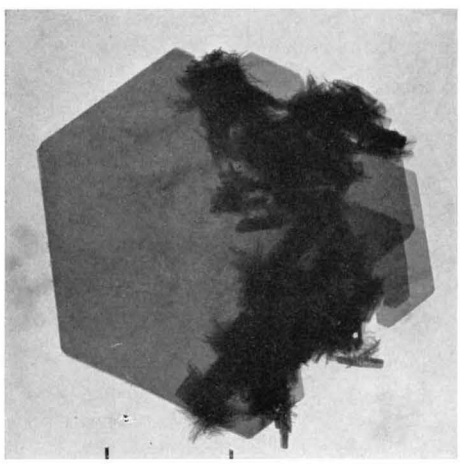

Fig. 89 a

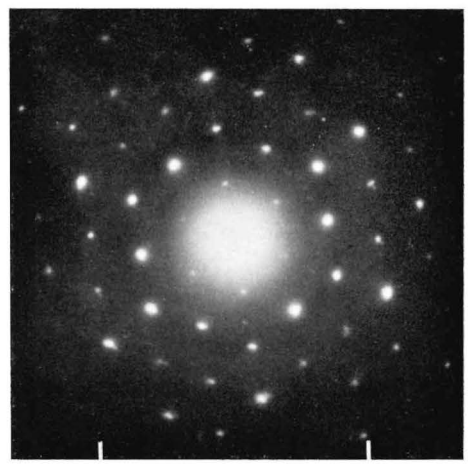

Fig. 89 b

30. C-A-H

Hexagonal-plate phases in portland cement suspensions (continued)

Figs. 90 and 91. Sample Pw—6C.

EM (90a): Hexagonal-plate crystal, similar to those of Figs. 87—89, attached to large aggregate of fibrous phase.

ED (90b): Mainly spot pattern similar to that of Fig. 89b, $a_H = 5.73$ Å.

EM (91a): Hexagonal-plate crystal, similar to the preceding ones, also some fibrous phase.

ED (91b): Spot pattern, similar to previous one, $a_H = 5.70$ Å, also weak ring at 2.99 Å (cf. Figs. 140, 261).

EM (91c): Same particle, heated in high-intensity electron beam. The outlines are un affected, but pores and bubbles have been formed in the interior.

ED (91d): The spot reflexions of Fig. 91b were observed to disappear gradually during heating, after which only glass-phase rings remained, at approximate spacings 2.9, 2.1, and 1.15 Å.

Fig. 90 a

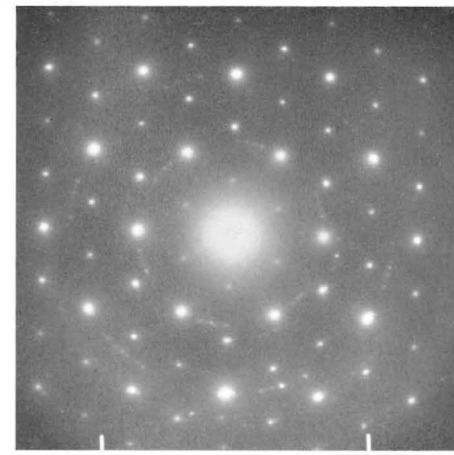

Fig. 90 b

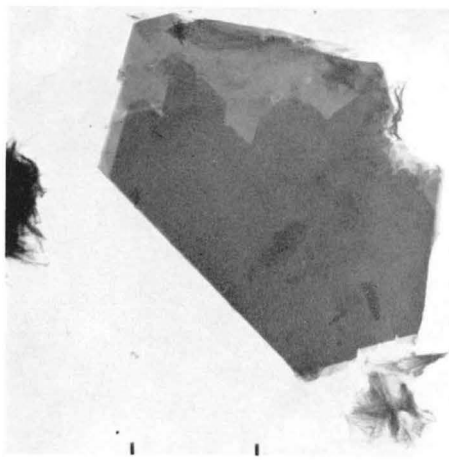

Fig. 91 a

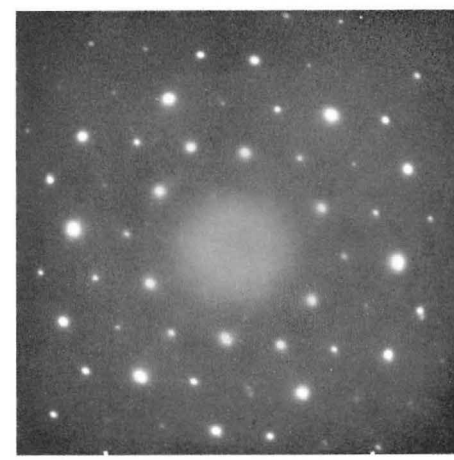

Fig. 91 b

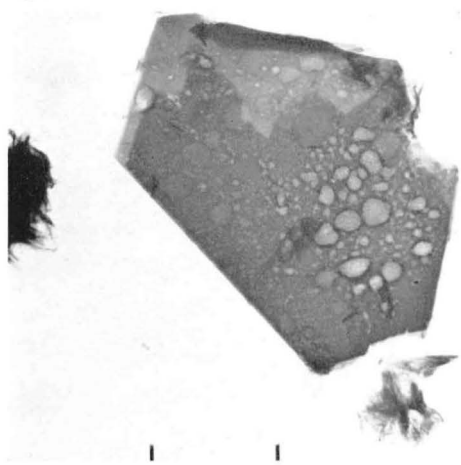

Fig. 91 c

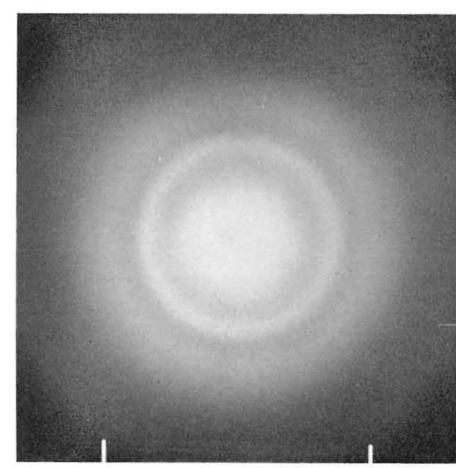

Fig. 91 d

31. C-A-H

Hexagonal-plate phases in portland cement suspensions (continued)

Figs. 92—94. Sample Pw—7B.

EMs (92—94a): Examples of hexagonal-plate crystals developed after one day of slow agitation of the suspension.

ED (94b): Spot pattern, regularly-hexagonal symmetry, $a_H = 5.68$ Å, inner spots ((*hk*)= =(10)) comparatively strong, also some CH (*hk*.0) reflexions at 3.112 (10.0) and 1.797 (11.0) Å.

EM (94c): After heating in beam of temporarily-raised intensity, only small changes noticeable.

ED (94d): Spot pattern of hexagonal symmetry, axes coinciding with those of original pattern, CH (10.0) and (11.0) reflexions, and a spot-ring at 1.71 Å, probably C (220) reflexions, also a diffuse glass-phase ring at about 2.9 Å.

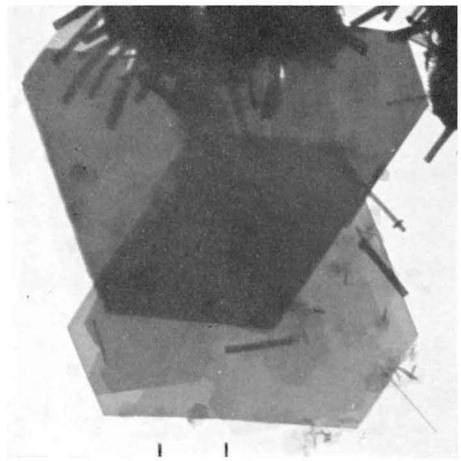

Fig. 92

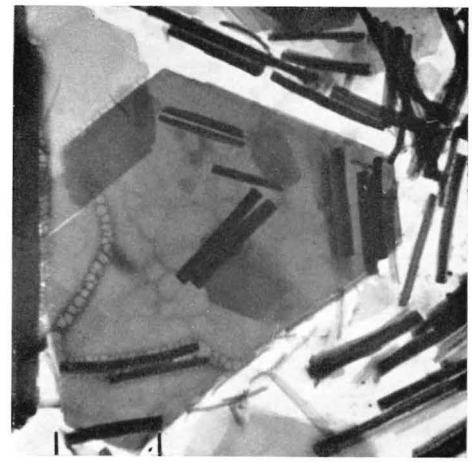

Fig. 93

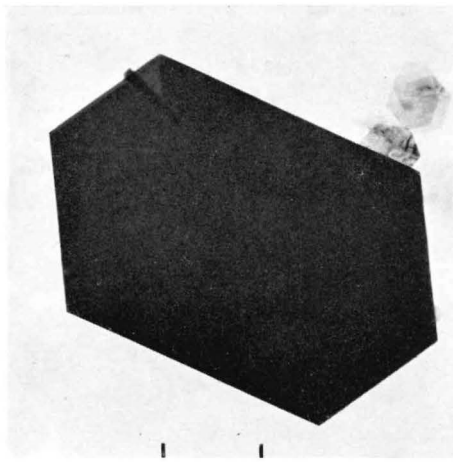

Fig. 94 a

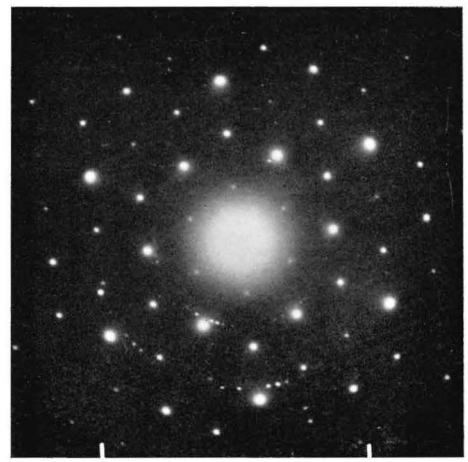

Fig. 94 b

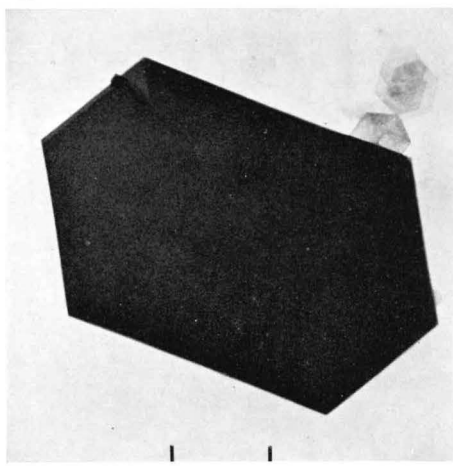

Fig. 94 c

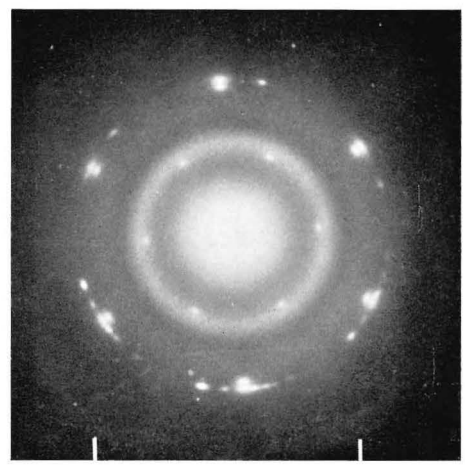

Fig. 94 d

32. C-A-H

Hexagonal-plate phases in portland cement suspensions (continued)

Figs. 95 and 96. Sample Pw—7B (cf. preceding page).

EM (95a): Hexagonal-plate crystal, attached to aggregate of radiating ettringite-type particles, also smaller CH crystals of hexagonal shapes (cf. Fig. 24).

ED (95b): Hexagonal-symmetry spot pattern, $a_H = 5.69$ Å, and CH (*hk*.0) spot rings at 3.112 (10.0) and 1.797 (11.0) Å.

EM (96a): Hexagonal-plate crystals, with angles deviating from 120° (maximum deviation 7°), probably due to the fact that the plane of the plates is tilted out of the plane perpendicular to the beam. The measured deviation is equivalent to a 30° angle of tilt.

ED (96b): Spot pattern of distorted-hexagonal symmetry, given by tilted crystal. The maximum hexagonal unit cell measurable in any direction of the diagram is $a_H = 5.66$ Å, and the angle of tilt calculated from the maximum deviation from hexagonality is 33°, in approximate agreement with the angle calculated above.

Figs. 97 and 98. Sample Pw—7C.

EM (97): Hexagonal-plate crystal, probably $C_4A\bar{S}$ aq.(hex.), with ettringite-type rods and C-S-H(I)-type foils attached to it. The ED pattern is a hexagonal-symmetry spot pattern with $a_H = 5.65$ Å, together with two rings originating from C-S-H(I) at 3.03 and 1.81 Å.

EM (98a): Hexagonal-plate crystal, similar to the previous one, attached to aggregate of foil-like particles.

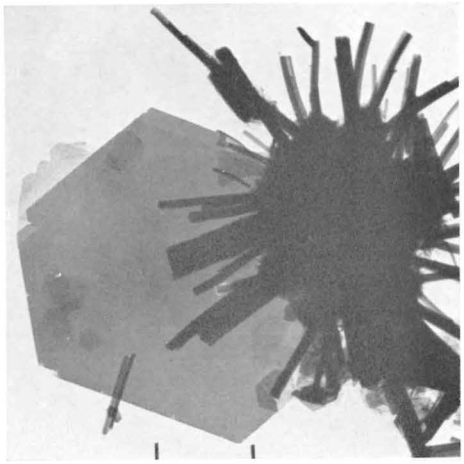

Fig. 95 a

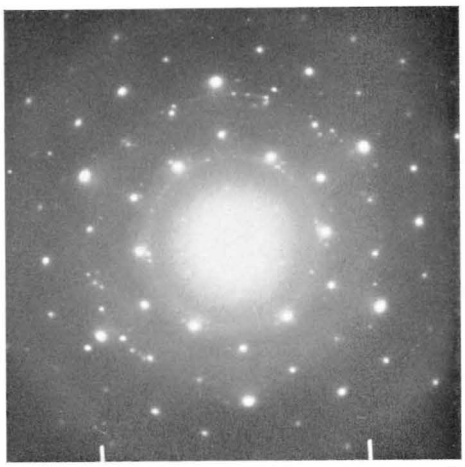

Fig. 95 b

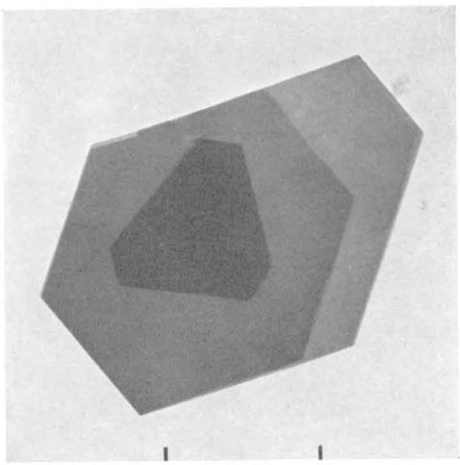

Fig. 96 a

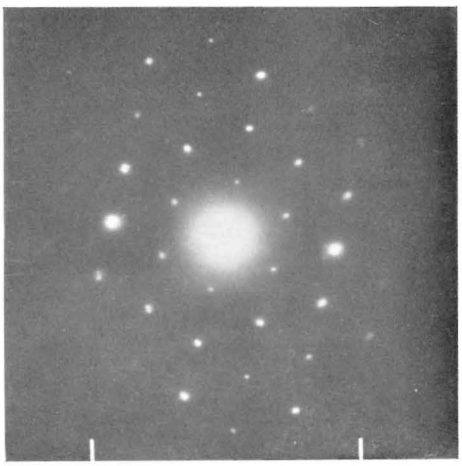

Fig. 96 b

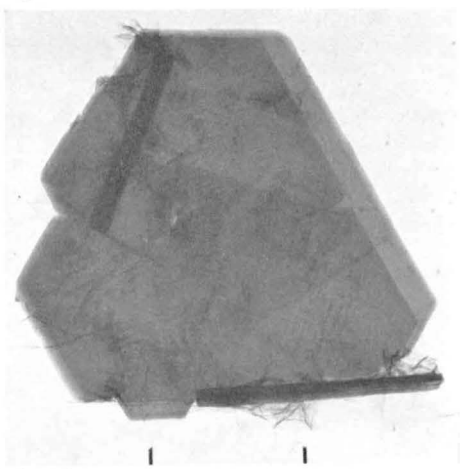

Fig. 97

Fig. 98 a

33. C-A-H

Hexagonal-plate phases in portland cement suspensions (continued)

Fig. 98 (continued) (Sample Pw—7C).

ED (98b): Hexagonal-symmetry spot pattern, very regular and with all spots in the same range of intensity, $a_H = 5.71$ Å.

ED 98c): Upon heating in beam of moderately-raised intensity, the original pattern became weaker, and inside certain spots there appeared new, diffuse spots from a CH-type lattice (cf. discussion of Figs. 57 and 58). It can be observed that original spots not associated with new spots have weakened more than the others. It is found that the original lattice spacing, $a_H = 5.71$ Å, is constant, and that the CH-type lattice has $a_H = 3.58$ Å.

EM (98 d): The hexagonal-plate crystal, after heating in a beam of higher intensity, shrank and loosened from the foil aggregate, but the externally visible changes, due to the heating, are still small.

ED (98 e): The corresponding ED pattern consists of a diffuse glass-phase ring between about 3.05 and 2.7 Å, and six weak, hexagonally-arranged spots at 1.70 Å, given by an oriented-aggregate residue of C crystals.

EM (98 f): After heating for some time in a beam of highest-possible intensity, the particles around the plate melted, and the plate itself became deformed and spotted with small crystals.

ED (98 g): The ED diagram of the recrystallized product is mainly a C ring pattern with certain hexagonally-arranged enhancements, and additional rings, the strongest ones at 3.73, 2.63, 2.14, and 1.85 Å, given by a compound of unknown identity.

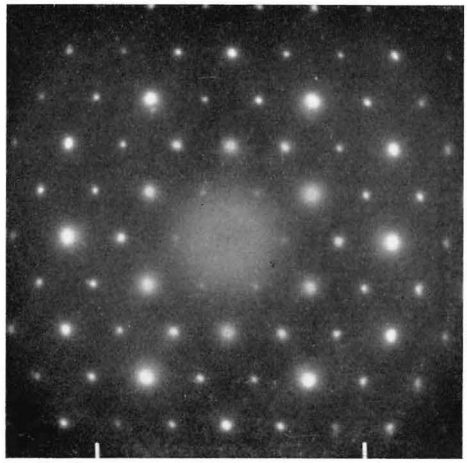

Fig. 98 b

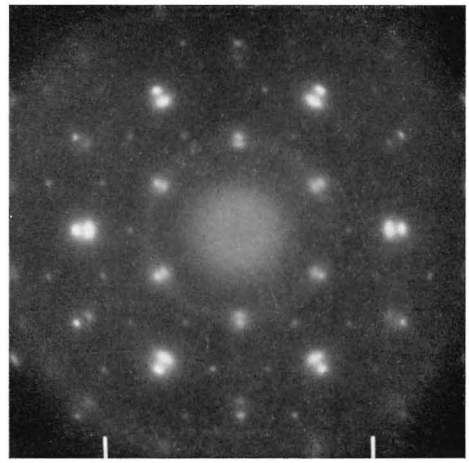

Fig. 98 c

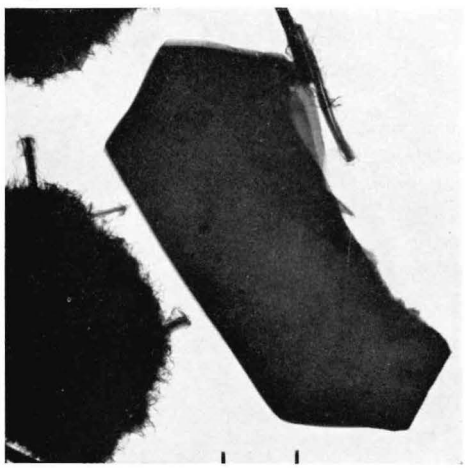

Fig. 98 d

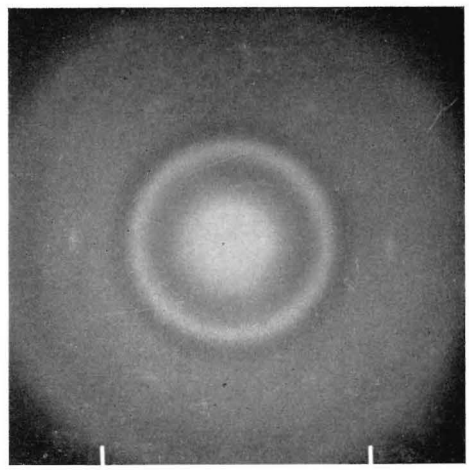

Fig. 98 e

Fig. 98 f

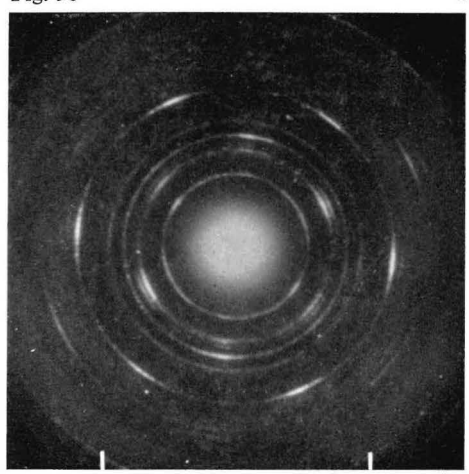

Fig. 98 g

34. C-A-H

Hexagonal-plate phases in hardened portland cement pastes

Fig. 99. Sample Pp—2.

EM: Thin flake, with certain indications of regularly-hexagonal angles, and with some fibrous material adsorbed on its surface.

ED: Spot pattern of nearly-regular hexagonal symmetry. Every second spot in any row is generally stronger, and this pattern of strong spots corresponds to a pseudohexagonal cell with a_H varying between 5.71 Å in a certain direction, and 5.63 Å in a direction perpendicular to this. Alternatively, one can use a face-centered orthorhombic pseudo cell of size about 5.7 by 9.7 ($5.6 \cdot \sqrt{3}$) Å, similar to the base cells of clay mineral structures. To obtain the true cell, defined by the combined strong and weak reflexions, these dimensions should be doubled. In this case, the cell dimensions are thus $a_0=11.42$, $b_0=19.50$ Å.

Also visible in the diagram is a pattern of slightly elongated spots, in face-centered orthorhombic symmetry and with spacings 3.03, 2.78, 1.82, 1.655, and 1.39 Å, representing the $(hk)=(11)$, (20), (02), (31), and (40) reflexions, respectively, of a tobermorite-type crystal with pseudo cell dimensions $a=5.56$ Å, $b=3.64$ Å.

Fig. 100. Sample Pp—3.

EM: Thin plate with adsorbed cement hydrate material, fibrous and irregular.

ED: Pattern similar to that of Fig. 99b, pseudo unit cell dimension varying between 5.70 Å in one direction and 5.63 Å in a direction perpendicular to this.

Fig. 101. Sample Pp—5.

EM: Thin plate with adsorbed fiber bundles.

ED: Two patterns similar to that of Fig. 99b, but with weak superstructure spots, pseudo unit cell dimensions 5.67 to 5.68 Å, also diffuse haloes at 3.02 and 1.81 Å from fibrous tobermorite gel phase.

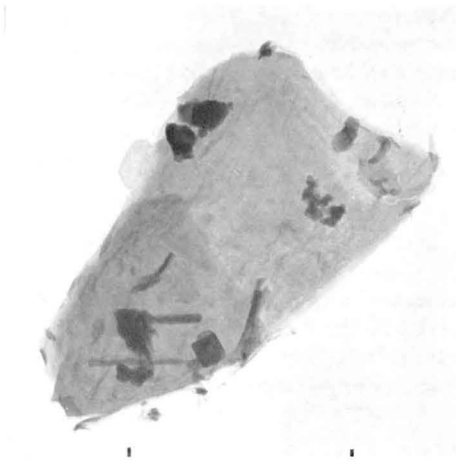

Fig. 99 a

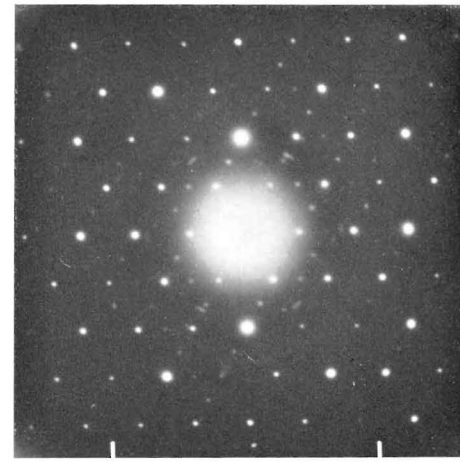

Fig. 99 b

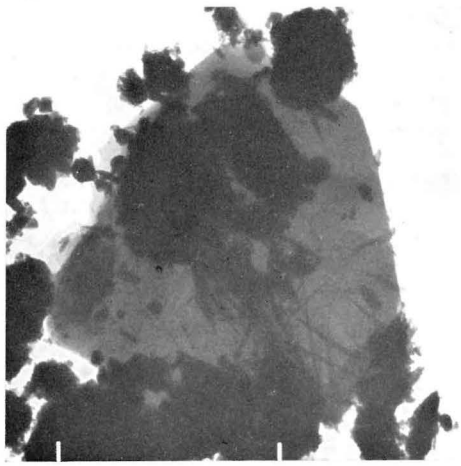

Fig. 100 a

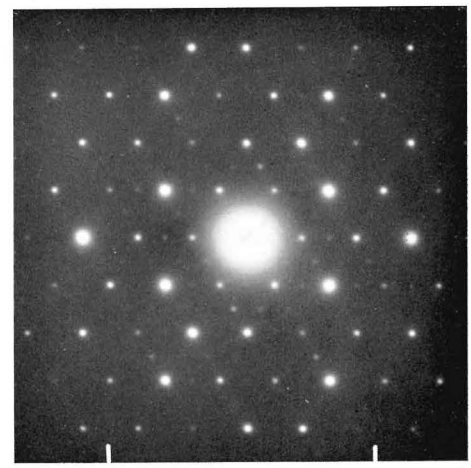

Fig. 100 b

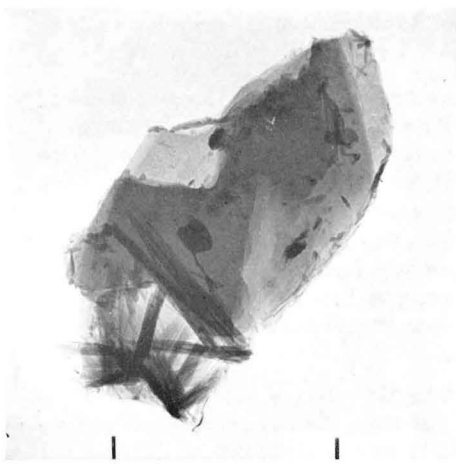

Fig. 101 a

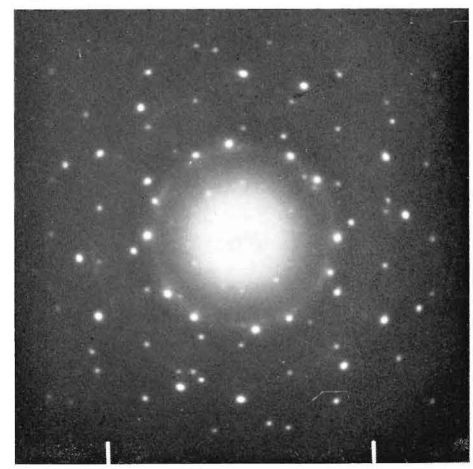

Fig. 101 b

The crystals of Figs. 99—101 may be regarded as prototypes of a constituent found in minor quantities in various samples of hardened Type I cement pastes. One characteristic feature of this constituent is a pseudo cell dimension which may be nearly constant, normally between 5.68 and 5.70 Å, as measured in different directions of the diagram, or which, as is most common, may vary from a maximum of about 5.70 Å in one direction down to 5.60—5.64 Å in some cases, much smaller in a few others, in a perpendicular direction. This deviation from regular hexagonality can of course be observed also with a regularly-hexagonal layer lattice turned out of the normal position perpendicular to the electron beam (as is exemplified in e.g. Fig. 96). The frequent observation of deviation effects in C-A-H gel phase crystals found in hardened pastes, but not in the C-A-H phases described earlier, seems to indicate, however, that at least some cases of lattice distortion are real, not just projection effects (although these can occur simultaneously). Of 30 ED patterns from C-A-H phase crystals in paste samples (Pp—1 to 7) observed in the present study, 14 showed 1 to 3 percent deviation, 3 showed larger deviation, and 13 were regularly-hexagonal, within the limits of accuracy of measurement.

Another feature of the C-A-H gel phases of hardened pastes is the frequent occurrence of lattice superstructures in the form of a solid solution of certain cations distributed in an ordered pattern over a set of pseudo unit cells, or partially replacing other cations in an orderly fashion. In ED patterns, the superstructure manifests itself in the appearance of additional, mostly weaker reflexions in a pattern of interstitial positions. Of the 30 C-A-H patterns mentioned above, 19 contained superstructure spots of stronger or weaker intensities, all situated halfway between the spots of the primary, pseudo cell pattern.

Of the 17 patterns with deviations from regular hexagonality, 9 contained superstructure spots of strong to medium general intensities, whereas only 2 weak and atypical patterns lacked such spots. Of the 13 regularly-hexagonal patterns, on the other hand, the superstructure spots were absent or at most weak in 11 patterns, of medium intensity in the two remaining ones. These statistical data indicate that there is a correlation between deviations from regular hexagonality and superstructure effects, which is also natural since both phenomena are presumably caused by ordered lattice substitutions. It is implied by the arrangement of superstructure spots that every fourth pseudo unit cell (every second cell along each direction of the basal *a* axes) differs from the others. Taking into account the composition and possible reactions of ordinary cement, the difference can conceivably consist in one of a few alternatives: a substitution of Fe (ferric ion) for Al in tetrahedral or octahedral positions, an introduction of extra Al or Fe in octahedral or tetrahedral voids (substituting for three protons), or an introduction of S (sulfuric ion) in tetrahedral voids or possibly other sites (substituting for six protons).

The substitution possibilities in the model structures of C_4A aq.(hex.) are best described in terms of the repeat units of cationic sites along the orthohexagonal axis (the long diagonal of the 5.7 Å. unit cell). In the structure assumed by *Buttler et al.* 1959 the repeat unit in the octahedral layer is Ca-Ca-Al-, and the most probable substitutions are F for A in every 4th cell, and (or) $\bar{S}$ for 3H in interstitial water layers and in two positions of every 4th cell (to get the monosulfate composition $C_4(A, F)\,\bar{S}$ aq. (hex.)). In the structure proposed by *Grudemo* 1962, 1964b the repeat unit of the octahedral layer is Ca-Ca-void-, and in the tetrahedral layer Al-void-hole- (the hole may be occupied by a water molecule). There are several possibilities for substitutions in this lattice, as indicated above. The most probable site of the S ion seems to be the tetrahedral void.

The composition of the cement used for preparing the pastes of samples Pp—1 to 7 is such that the molar ratios $A/F/\bar{S}$ is 1/0.22/0.47. Assuming that at equilibrium about one-third of the Al ions are incorporated in the C-S-H gel phase, the rest of the ions in a $C_4(A, F)\,(\bar{S}, 3H)$aq.(hex.) solid-solution phase, the composition of the latter phase would be

very nearly to $C_4A_{3/4}F_{1/4}\bar{S}_{1/2} \cdot aq$. Thus, whichever structure is actually present, the data indicate a substitution of one Fe for one Al ion and an introduction of one S ion in every fourth pseudo cell. It is likely that these are only average figures, since observations show considerable variation in the character of the ED patterns.

It remains to consider the deviations from regularly-hexagonal unit cells. Either of the substitutions just suggested can be made in such a way that the hexagonal symmetry of the substituted layer is maintained, although with the size of the unit cell doubled, but the combination leads inevitably to a lower symmetry. This is best described as orthorhombic, in terms of the two-dimensional unit cell observable in ED diagrams, but the true cell is most probably of monoclinic symmetry.

The reason for the appearance of these deviations, as well as superlattice effects, in old Type I cement pastes but not in the corresponding fresh slurries (Fig. 87 ff.) is not quite clear. Possibly, the hexagonal-plate hydrate crystallizing at a comparatively early age and persisting for at least a few days, is a pure C_4A aq.(hex.) phase, whereas the suggested introduction of Fe ions, from a slowly-hydrating anhydrous phase, and S ions, from a decomposing ettringite-type hydrate formed initially, occurs first in later stages of the reaction.

35. C-A-H

Hexagonal-plate phases in hardened portland cement pastes (continued)

Fig. 102. Sample Pp—1A.

EM: Edge of large plate, with bundles of fibrous material.

ED: Pattern similar to that of Fig. 99b, with pseudo unit cell size varying between 5.72 Å in one direction and 5.65 Å in perpendicular direction, also tobermorite fiber reflexion (streak) at 1.825 Å.

Figs. 103 and 104. Sample Pp—6A.

EM (103a): Large, thin plate with indications of regularly-hexagonal angles, and with fibrous material adsorbed on its surface.

ED (103b): Pattern similar to the preceding one, strong superstructure spots, maximum pseudo unit cell dimension $a_H = 5.67$ Å, with only small (0.5 percent) deviations towards smaller values, also rings from fibrous tobermorite phase at 3.03 and 1.81 Å.

EM (104a): Plate with adsorbed, fibrous or ribbon-like crystals.

ED (104b): Pattern similar to those above, superstructure spots rather weak, pseudo unit cell size $a_H = 5.68$ Å, with very small deviations from regularly-hexagonal symmetry. Also spot-rings at 3.03, 2.77, 1.805, 1.645, and 1.385 Å, representing the reflexions with (*hk*) =(11), (20), (02), (31), and (40), respectively, from the orthorhombic cell of the adsorbed tobermorite crystals, of dimensions 5.54×3.62 Å.

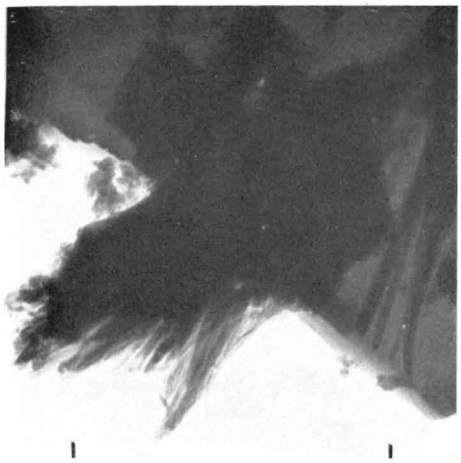

Fig. 102 a

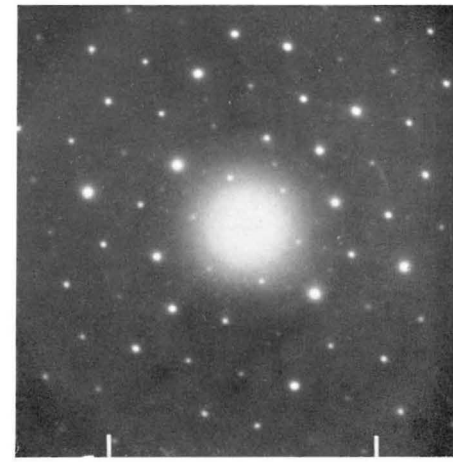

Fig. 102 b

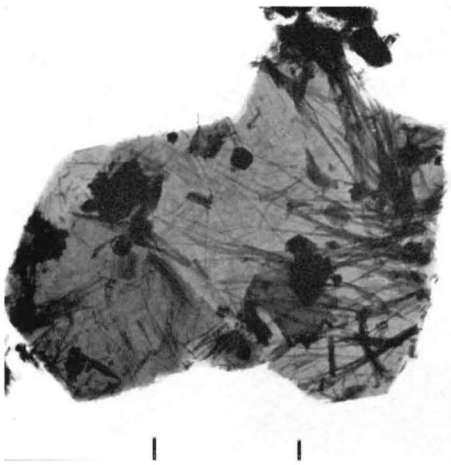

Fig. 103 a

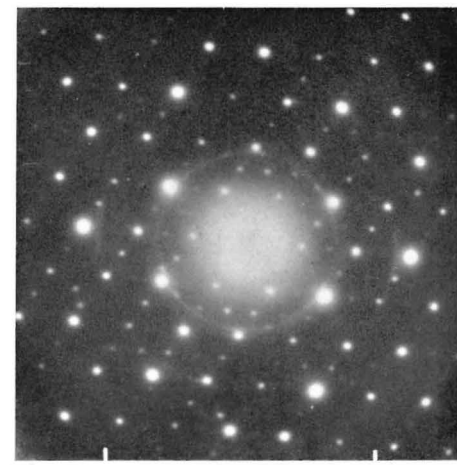

Fig. 103 b

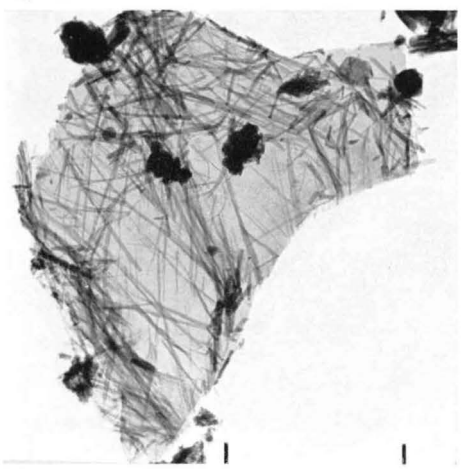

Fig. 104 a

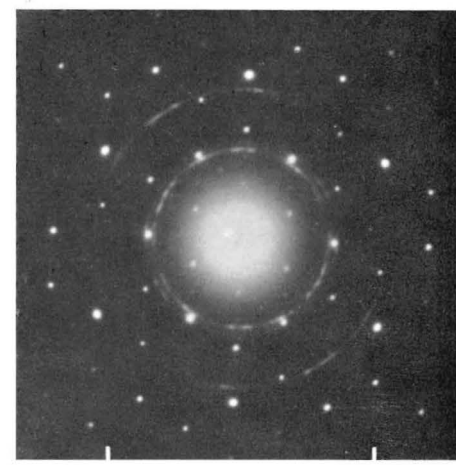

Fig. 104 b

36. C-A-H

Hexagonal-plate phases in hardened portland cement pastes (continued)

Fig. 105. Sample Pp—6B.

EM: Regularly-hexagonal plate (half).
ED: Regularly-hexagonal spot pattern, $a_H = 5.68$ Å, no superstructure spots.

Figs. 106 and 107. Sample Pp—6A.

EM (106a): Thin plate, covered with a basket-like network of fibers.

ED (106b): Pseudohexagonal spot pattern, weak superstructure spots, large deviation from hexagonal symmetry, $a_H = 5.70$ Å in one direction, about 5.0 Å in direction perpendicular to this; crystal plate probably tilted with respect to electron beam, angle of tilt about 28°. Also rings from tobermorite fibers, at 3.02 and 1.81 Å.

EM (107a): Plate similar to that of e.g. Fig. 103, after heating for some minute in a high-intensity electron beam, treatment which did not cause any appreciable change in outer shape.

ED (107b): Diffuse glass-phase ring with maximum at about 2.9 Å, and additional weak CH and oriented-aggregate C spots (cf. e.g. Fig. 94) (the original pattern of this crystal was a pseudohexagonal spot pattern with a_H (max.) = 5.70 Å, about 5 percent deviation from regularly-hexagonal symmetry, and superstructure spots).

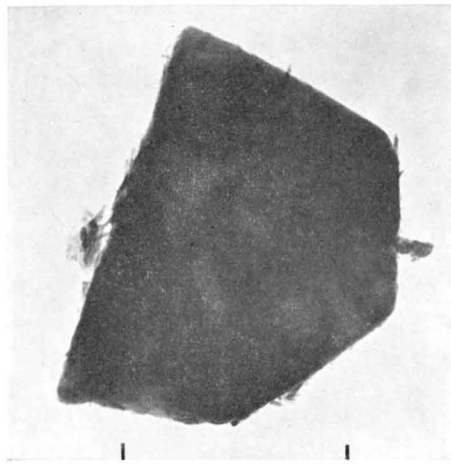

Fig. 105 a

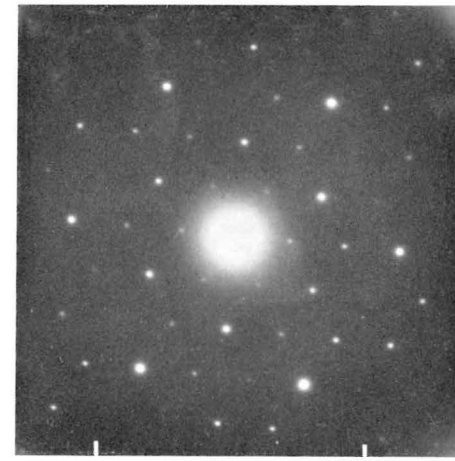

Fig. 105 b

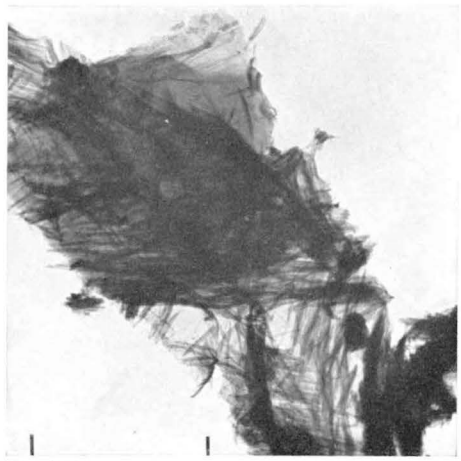

Fig. 106 a

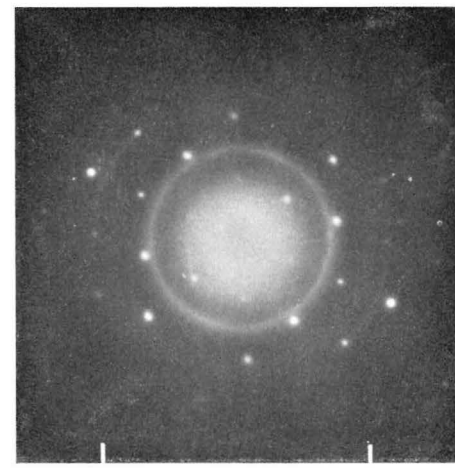

Fig. 106 b

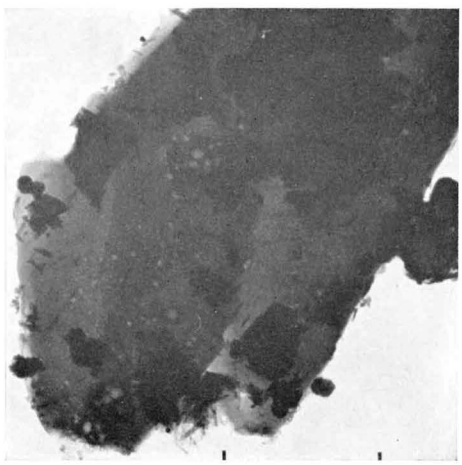

Fig. 107 a

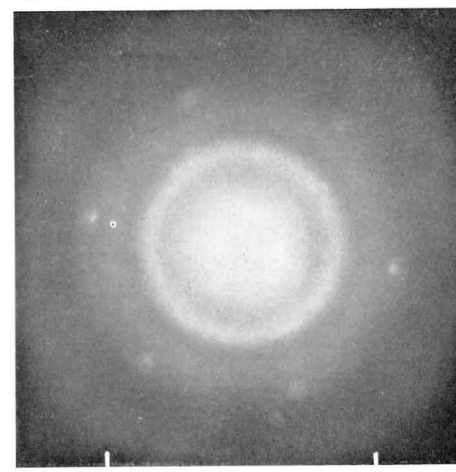

Fig. 107 b

37. C-A-$\bar{S}$-H

Ettringite structures in portland cement suspensions

Figs. 108—110. Sample Pw—2.

EM (108): Characteristic growth in Type I cement suspension, ettringite rods, about 2 to 3μ long and 0.2 to 0.3μ across, radiating from the surface of a hydrating cement particle.

EM (109): Bundle of ettringite rods with characteristic striations parallel to fiber axis, and sharply cut-off end faces, also thin, hexagonal CH plates.

EM (110a): Large C-A-H (hex.) plate (cf. Figs. 78—80), smaller CH plates, and ettringite rods.

ED (110b): Diffuse ring, 3.0—2.7 Å, and C spot-rings, both effects given by dehydrated structures.

Fig. 111. Sample Pw—3A.

EM: Aggregate of striated, ettringite-type rods.

Fig. 112. Sample Pw—3B.

EM: Bundle of rod-like structures, similar to those of Fig. 109.

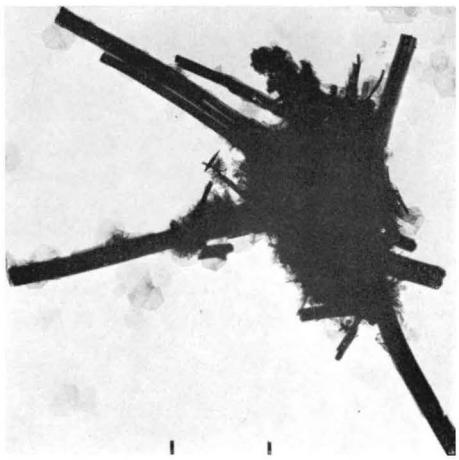

Fig. 108

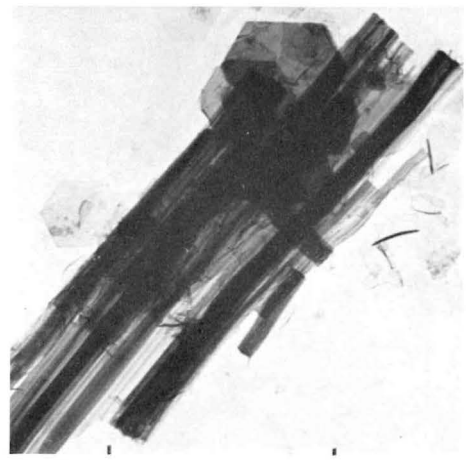

Fig. 109

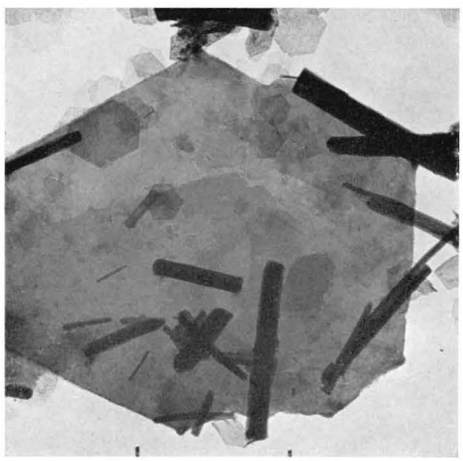

Fig. 110 a

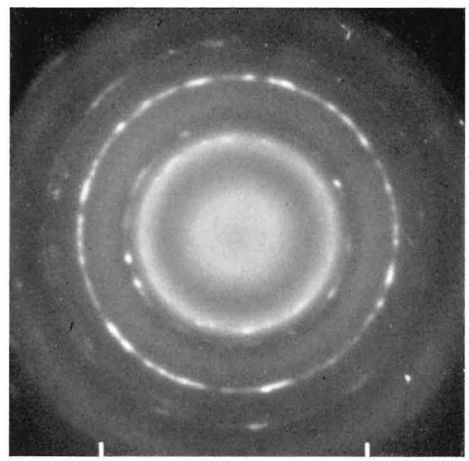

Fig. 110 b

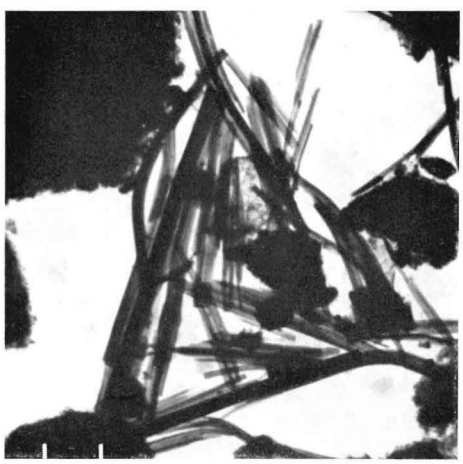

Fig. 111

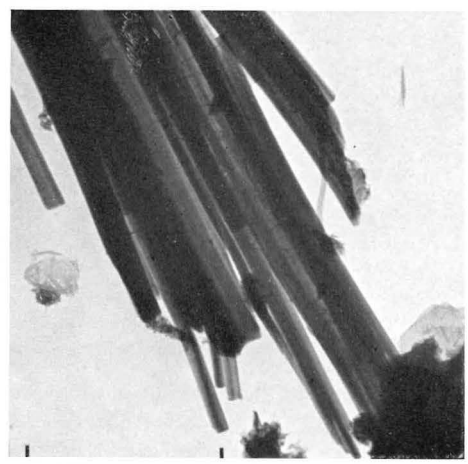

Fig. 112

38. C-A-$\bar{S}$-H

Ettringite structures in portland cement suspensions (continued)

Figs. 113 and 114. Sample Pw—3B.

EM (113a): Network of fibers with internal striations, probably ettringite formations. Some particles seen in this sample appear as curved fibers rather than the usual straight rods or slender prisms typical of ettringite phases. This difference in morphology is probably due to different conditions of formation. These particles are either precipitated in the boiling suspension, and are then likely to contain silica to stabilize the ettringite-type C-A-$\bar{S}$-H lattice, or they are formed secondarily during cooling from temperatures at which high-sulfate sulfoaluminate phases are unstable, according to several investigators.

ED (113b): Diffuse haloes with maxima at about 2.95, 2.07, and 1.18 Å from dehydrated and vitrified structure, also spot-ring at 1.475 Å from unknown substance.

EM (114a): Fibers similar to those of preceding figure, after heating in high-intensity beam.

ED (114b): Mainly C ring diagram, and additional weak ring at 3.50 Å, probably the very strong (020) and (002) 3.50 Å reflexion of C$\bar{S}$, anhydrite (*Swanson et. al.* 1955), also diffuse densities (but sharper than in preceding ED) at about 2.85, 2.05, and 1.18 Å.

Fig. 115. Sample Tw—2.

EM: Network of fibers, of appearance resembling that of Fig. 113a (*ED:* strong, diffuse ring at 2.90—2.95 Å).

Fig. 116. Sample Tl—2.

EM: Similar to preceding EM, rods with sharply cut-off or angular end faces. (*ED:* strong, diffuse ring at 2.90—2.95 Å.)

As indicated in the introduction (Section 4), the "trisulfate" or ettringite is only one member of a whole group of compounds which are isostructural or structurally related, and which are derivable by substitution of such complexes as $\bar{S}$ or $\bar{C}$ for water in the model substance C_6AH_{33} prepared and studied by *Flint* and *Wells* 1944. The fibrous or acicular nature of the crystals of compounds within the group does not seem to be compatible with the layer lattice structures proposed for e.g. ettringite, originally by *Bannister* 1936 and recently by *Grudemo* 1962. As suggested by *Taylor* 1960, the crystal structure of the mineral thaumasite, $C_3S\bar{S}\bar{C}H_{14}$, determined by *Welin* 1957, may provide some clues for establishing the character of the structural element common to these lattices. The thaumasite structure contains chains of the trigonal-symmetry repeat unit — $Ca_3O\ SiO_3$ — running parallel to the hexagonal c_H axis, at a mutual distance of about 11 Å (10.95 in thaumasite, 11.2 in ettringite). It is possible that similar chains, with Al ions replacing all or part of the Si ions in tetrahedral coordination, constitute the important structural elements of the C_6AH_{33}-type compounds. In analogy to thaumasite, $\bar{S}$ or $\bar{C}$ groups may replace the water molecules that complete the CaO_6 octahedra and fill out the spaces between the hexagonally-arranged chains.

The general composition of this group of compounds may be written $C_6(A,S_2)\ (\bar{S},H_3)_3\ (\bar{C},H_2)_3\ H_{23-24}$. Ettringite, $C_6A\bar{S}_3H_{30}$, is one member, and the existence of the corresponding carboaluminate, $C_6A\bar{C}_3H_{33}$, has also been confirmed, according to *Taylor* 1960. It is suggested that the formations of Figs. 115 and 116, appearing in $\bar{C}$-contaminated suspensions of C_3S

Fig. 113 a

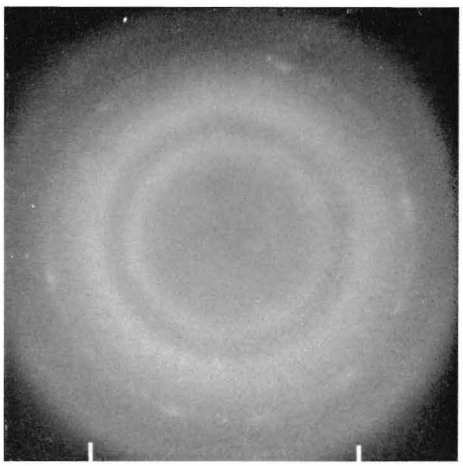

Fig. 113 b

Fig. 114 a

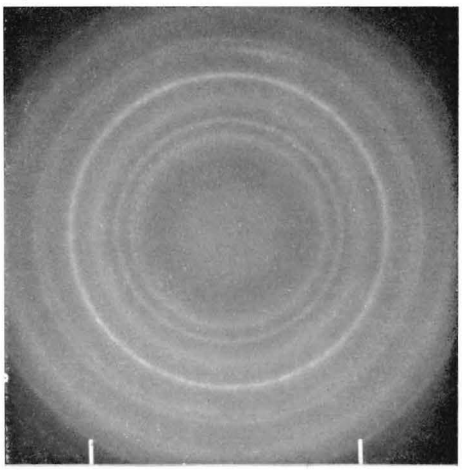

Fig. 114 b

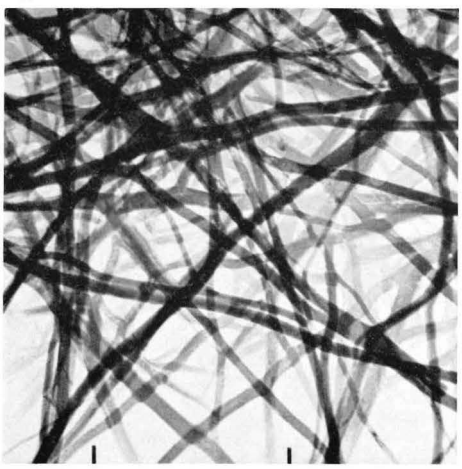

Fig. 115

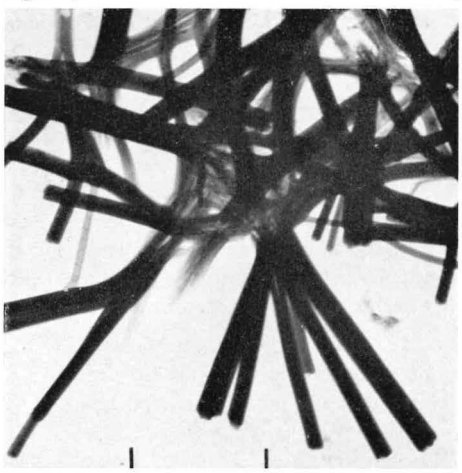

Fig. 116

in water or lime solution, may represent the corresponding carbosilicate, of possible composition $C_6S_2\bar{C}_3H_{32}$.

As stated in the introduction (Section 6), all these materials are highly hydrous substances. In saturated conditions, the thaumasite-type chains are kept in place in a pattern of hexagonal symmetry by interstitial water molecules which form, together with the oxygens of the chain, nearly coplanar oxygen layers, four per unit distance of about 10.5 Å along the chain, perpendicular to the chain axis. Most of the water molecules are easily removed upon drying (e.g. in EM examinations), and the hexagonal structure collapses. It seems, however, that the chains remain unbroken, only packed together in some kind of irregular pattern. Judging from the habits of structures shown in Figs. 108 ff., the chains condense into puckered and rolled layers, causing the dehydrated crystal to appear as a striated rod. All ED diagrams from unheated particles of this type have shown at most a couple of diffuse rings, and there seems to be no fixed repeat unit, even in the direction of the chains.

---

39. C-$\bar{S}$-H

Development of sulfate phases in portland cement suspension

Figs. 117—120. Sample Pw—7A.

EMs (117—119 a): Various forms of rod-like or rolled crystals in parallel-oriented aggregates. These are early products of hydration and disappear completely later on (Pw-7B). They seem to be formed from sheets or ribbons, rolled up into tubular or scroll-like particles. It can further be observed that most rod ends are cut off obliquely at approximately 60° angles. Other formations present are loosely-wrinkled foils (see Figs. 22 and 23).

ED (119b): Composite diagram, rings in agreement with those of Fig. 23b, additional spot pattern from fiber aggregate, resembling X-ray layer line diagram. The distances between layer lines correspond to a repeat unit 6.24 Å in the direction of the fiber axis. This distance is recognized as one of the unit cell lengths of either $C\bar{S}H_2$, gypsum, $C\bar{S}$, anhydrite, or possibly some intermediate hydrate phase, $C\bar{S}H_x$ (see further discussion on next page).

EM (120a): Ribbon-like or tubular particles similar to those above, protruding parallel to one pair of edges of a larger crystal plate. The angles between these edges and the two other edge directions are estimated to be about 53° and 66° (acute angles taken), thus deviating from regular 60° angles. A comparison with the gypsum, $C\bar{S}H_2$, lattice (*Wooster* 1936) shows that the angles between the fiber axis of fibrous varieties of gypsum and two other crystallographically important directions in the basal (010) plane of the layer lattice of gypsum are 52°5 and 65°9. It is therefore most likely that the formations shown on this page are dehydrated pseudomorphs of gypsum crystals, reprecipitated from an early solution phase and growing as rolled sheets or laths of the gypsum layer lattice. Obviously, there is not yet enough alumina present in solution to take care of all the dissolved sulfate, by formation of a high-sulfate sulfoaluminate.

ED (120b): Ring diagram, essentially equal to the previous one, from the wrinkled-foil particles also present in the EM, and an indistinct pattern of diffuse spots from the particles assumed to be gypsum pseudomorphs.

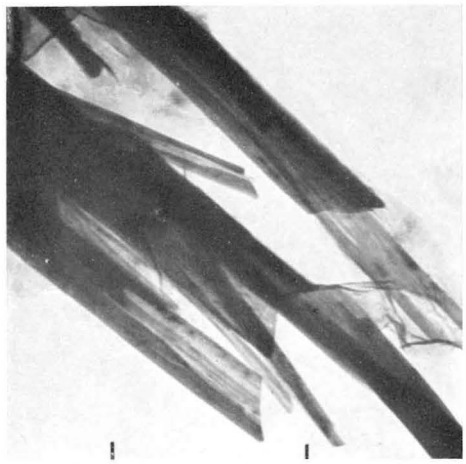

Fig. 117

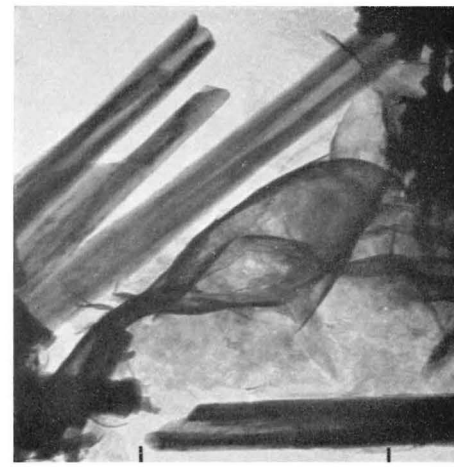

Fig. 118

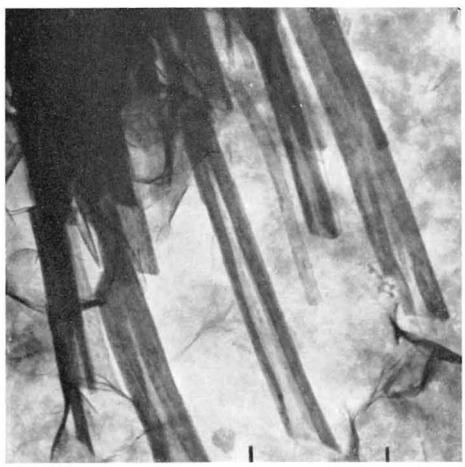

Fig. 119 a

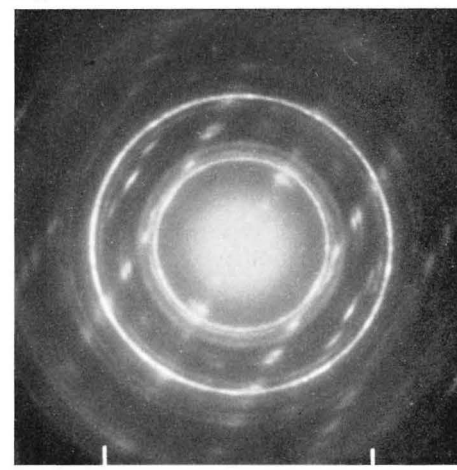

Fig. 119 b

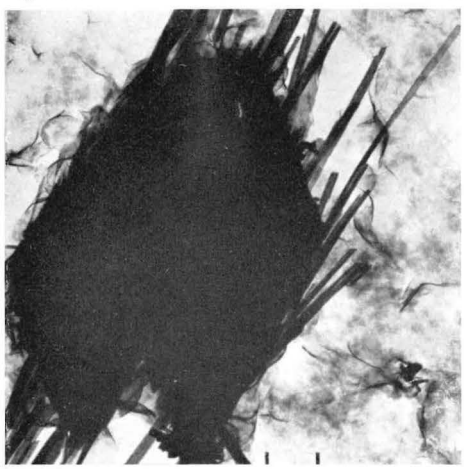

Fig. 120 a

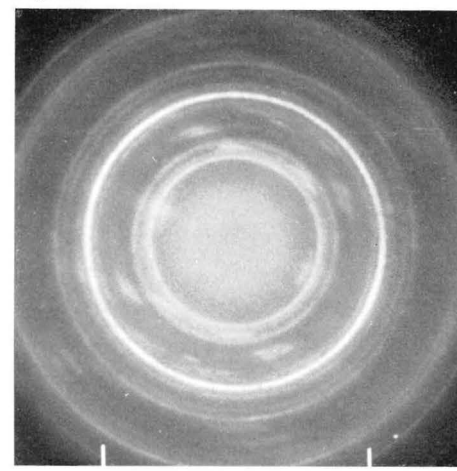

Fig. 120 b

40. C-$\bar{S}$-H and C-A-$\bar{S}$-H

Development of sulfate phases in portland cement suspension (continued)

Figs. 121—125. Sample Pw—7A.

EM (121a): Rolled-sheet or tubular particle, similar to those on preceding page, gypsum pseudomorph.

ED (121b): Layer-line spot pattern, with distances between layer-lines corresponding to a fiber axis unit of 6.17 Å. Most of the spots can be indexed on the basis of a two-dimensional, orthorhombic unit cell 6.17×6.89 Å, the second distance being the average of 12 measurements along the layer-lines. In the zero layer-line, there are two reflexions at 6.0 and 3.0 Å., possibly the first and second order reflexions from a spacing $6.93 \cdot {}^1/_2\sqrt{3}$ Å (cf. below).

ED (122): Pattern similar to that of preceding ED, and given by similar particle. There is no orthorhombic symmetry in this projection of the lattice, and there seems to be no regularity in the distribution of spots along the layer-lines, except that of zero order, which contains the 2nd—6th order reflexions from a spacing about 6.9 Å. The distances between layer-lines corresponds to a fiber repeat unit of 5.94 Å. The ring elements are CH reflexions.

ED (123): Pattern very similar to that of Fig. 121b, and given by similar particle. Nearly all the reflexions can be indexed on the basis of a simple orthorhombic cross-grating cell of dimensions 6.24×6.92 Å., the former spacing corresponding to the distance between the weakly-pronounced layer-lines. However, there is one set of reflexions outside the simple orthogonal pattern, viz. the outer spots of the pair of reflexions in the second layer-line. If the main pattern is taken to represent the (*hk*0) zone of the crystal, the pair of spots can be indexed (220) and (221), and the corresponding spacings are 2.315 and 2.20 Å (measured values). It can be inferred from the data given below that these reflexions, which can also be observed on Figs. 119b and 121b, are the comparatively strong (202) or (220), and (212) spacings of anhydrite.

EMs (124 and 125): Examples of general appearance of sample, showing, in addition to the long rods of the gypsum pseudomorphs, also the short, stumpy prisms of ettringite formations starting to grow outwards from the surfaces of the anhydrous crystals, and the wrinkled foils or thin sheets also shown in Figs. 22 and 23.

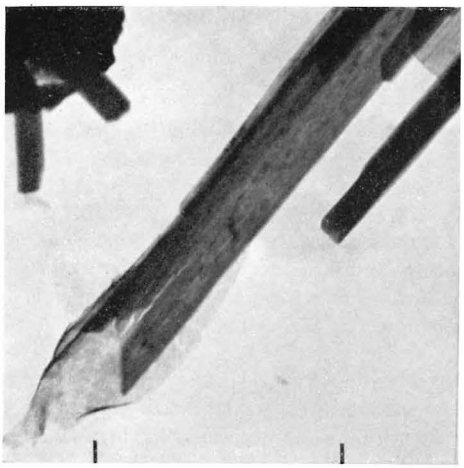

Fig. 121 a

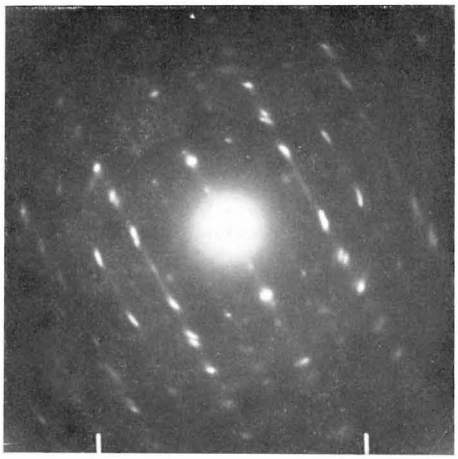

Fig. 121 b

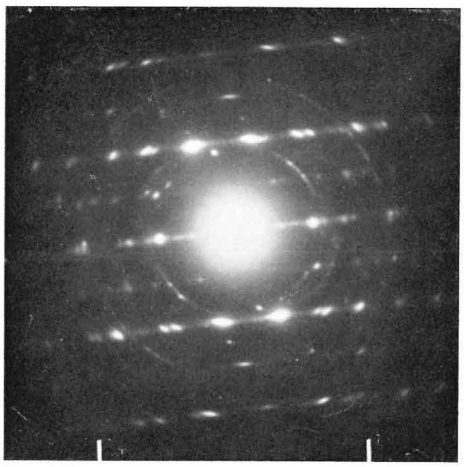

Fig. 122

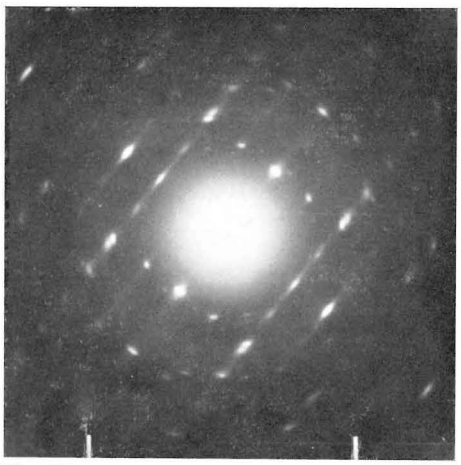

Fig. 123

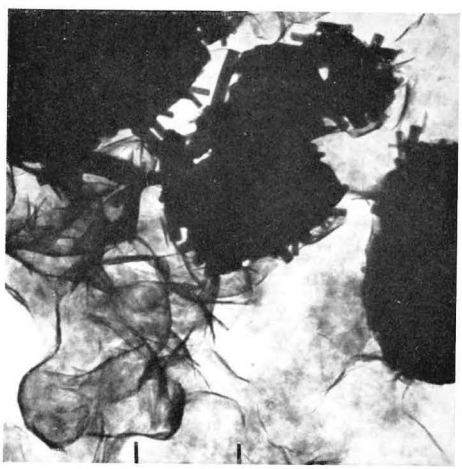

Fig. 124

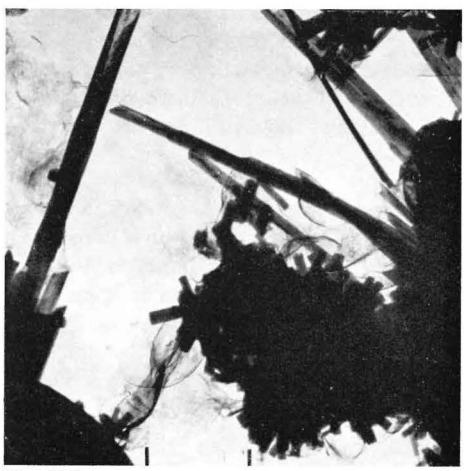

Fig. 125

The following lattices are of interest for the interpretation of the ED patterns now described:

β-$C\bar{S}$, anhydrite, is of orthorhombic symmetry, with space group D_{2h}^{17}—Bbmm, $a=6.238$, $b=6.991$, $c=6.996$ Å (26° C), according to *Swanson et. al.* 1955. The cell dimensions given by earlier investigators are in general slightly smaller. In the powder pattern, the strongest reflexions are found at 3.498 (002) (020), 2.849 (210), 2.328 (202) (220), 2.208 (212), 1.869 (230), 1.749 (004), 1.748 (040), and 1.648 (232) Å. The symmetry is very nearly tetragonal, and the lattice structure is best described by giving the arrangement of ionic groups along the pseudotetragonal (a) axis: SO_4 tetrahedra, oriented with two edges perpendicular to the axis, alternating with Ca ions which are also coordinated in an approximately tetrahedral manner between the perpendicular edges of the two nearest SO_4 tetrahedra.

γ-$C\bar{S}$, soluble anhydrite, and the calcium sulfate subhydrate series, "hemihydrate", $C\bar{S}H_x$ with x varying from nearly zero up to about $^2/_3$, possess closely related lattices of hexagonal or pseudohexagonal symmetry. Some values for the cell dimensions given in the literature, are for γ-$C\bar{S}$: $a_H=6.99$, $c_H=6.34$ Å (*Flörke* 1952), for $C\bar{S}H_{0\cdot02}$: $a_H=6.959$, $c_H=6.32$ Å and for $C\bar{S}H_{2/3}$: $a_H=6.929$, $c_H=6.36$ Å (*Bunn* 1941), for $C\bar{S}H_{1/2}$: $a_H=6.83$, $c_H=6.25$ Å, (*Caspari* 1936), or $a_H=6.93$, $c_H=6.35$ Å (*Khol* 1948). The water contained in these substances is assumed to be zeolitic and fixed in lattice pores or channels running parallel to the c_H axis. These water molecules evaporate rather easily in dry conditions, but the open, hexagonal structure seems to persist until the last trace of water is removed. The arrangement of Ca and SO_4 ions along the c_H axis is closely similar to the one described above for β-$C\bar{S}$. Thus, the formation of the pseudotetragonal β-$C\bar{S}$ structure from the collapsing hexagonal structure can be visualized simply as a close-packing of the parallel-oriented $C\bar{S}$ chains.

$C\bar{S}H_2$, gypsum, has a layer lattice of monoclinic symmetry, space group C_{2h}^6—C 2/c, $a=10.49$, $b=5.18$, $c=6.52$ Å, $\beta=151°55$. The b axis is perpendicular to the plane of the layers, and there are two layer units per cell, each unit consisting of a central, anhydrous $C\bar{S}$ layer, with the ions arranged in a rather complex, double-layer pattern, and two water layers, the latter forming networks of distorted hexagons, in the meshes of which certain O—O edges of SO_4 tetrahedra are accommodated. The a and c axes are in the plane of the layers. The a axis given above is not particularly suitable for describing the crystal elements, and two alternative units can be chosen (*Flörke* 1952), by means of which the layer can be divided in roughly equilateral, triangular units with the sides 6.28, 5.66, and 6.52 Å. The direction of the 6.28 Å cell is the fiber axis of gypsum crystals growing in fibrous or elongated- prismatic habits, and is occupied by Ca ions, alternating with SO_4 tetrahedra arranged in such a way that only slight shifts of the atomic positions are needed for the formation of $C\bar{S}$ chains identical with those of anhydrite and the subhydrates, as described above.

Of the examples of ED patterns shown for these particles, which are undoubtedly dehydration pseudomorphs of gypsum, those in Figs. 119b, 121b, and 123 are most probably anhydrite patterns, projections of the ($hk0$) or ($h0l$) zones, with the a axis varying from 6.24 Å and down to about 6.1 Å. in these and other patterns (may be due to tilts of the fibers out of the plane perpendicular to the beam), and with the b or c axes generally between 6.9 and 6.95 Å. The c_H axis of the subhydrates, at about 6.35 Å, has not been observed. On the other hand, a few patterns (among them that of Fig. 121b) show the first and higher order reflexions of a unit spacing 6.02 Å ($6.95 \cdot {}^1/_2\sqrt{3}$), possibly the (10.0) spacing of a hexagonal $C\bar{S}H_x$ (subhydrate) lattice also present. In one ED diagram (not shown here) complete patterns from two cells of sizes 6.23×6.95 Å and 6.23×6.02 Å occur simultaneously and with

the same direction of the 6.23 Å fiber axis. The less symmetrical pattern of Fig. 122 is probably given by a crystal of related type, although with some kind of anomaly with regard to dehydration or direction of fiber axis.

The gypsum crystals shown in Figs. 117—125 are obviously pseudomorphs, observed in different stages of dehydration. An example of an ED pattern from the (*h*0*l*) zone of an undehydrated crystal needle of gypsum is given by *Chatterji* and *Jeffery* 1963b, who suggest that such crystals are formed by the hydration of "hemihydrate" originally present in the cement.

41. C-A-$\bar{S}$-H

Development of ettringite-type phase in portland cement suspension

Figs. 126—128. Sample Pw—7B.

EMs: (126 and 127): Particles in cement suspension covered with ettringite formations protruding in all directions from the surface (cf. Fig. 95a, Figs. 108 ff). As stated earlier, these rods are most probably vitrified pseudomorphs of original ettringite-type crystals. A comparison with Figs. 124 and 125 shows that the crystals have continued to grow from a length of about 0.2μ after one hour to about 1μ or more after 24 hours. There are also signs of a villous surface hydration product growing between the ettringite rods.

EM (128a): Isolated rod particle, showing the characteristic striated, columnar appearance of these particles.

ED (128b): There is no sign of any ED effects given by this seemingly well-organized structure. The spot pattern is a CH (*hk*.0) pattern originating from the crystal plate attached to one end of the rod.

Figs. 129 and 130. Sample Pw—7C.

EMs: After a few days' hydration, the surface coat, barely visible in Figs. 126 and 127, has grown out in the form of loosely-wrinkled foils, partly covering and gradually wrapping up the ettringite rods.

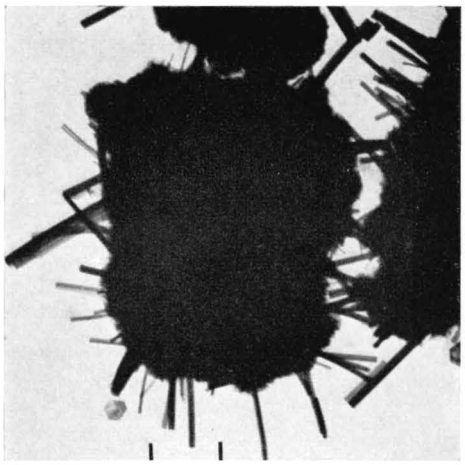

Fig. 126

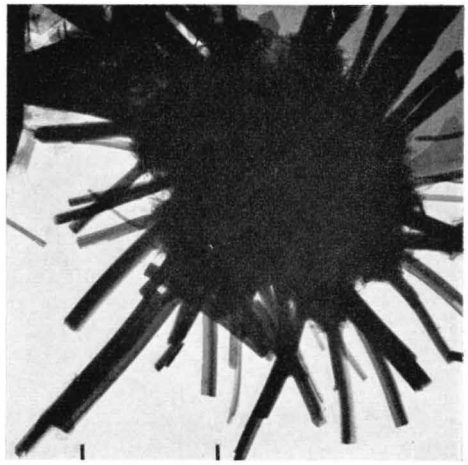

Fig. 127

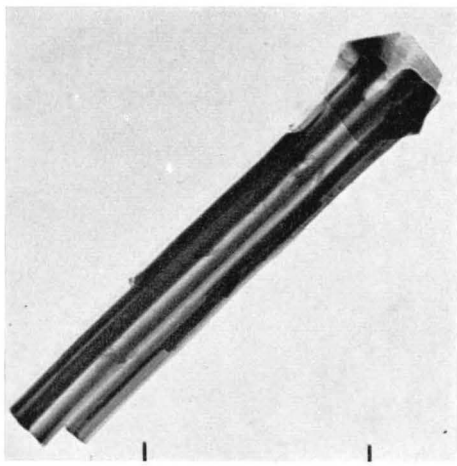

Fig. 128 a

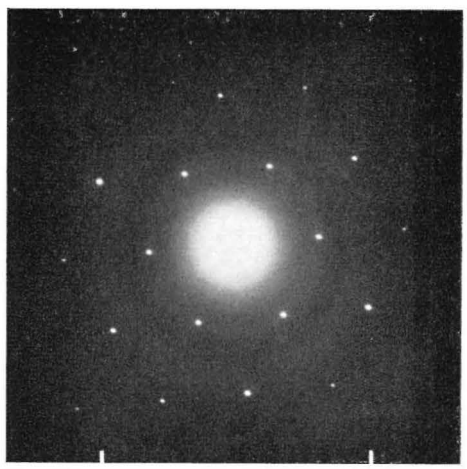

Fig. 128 b

Fig. 129

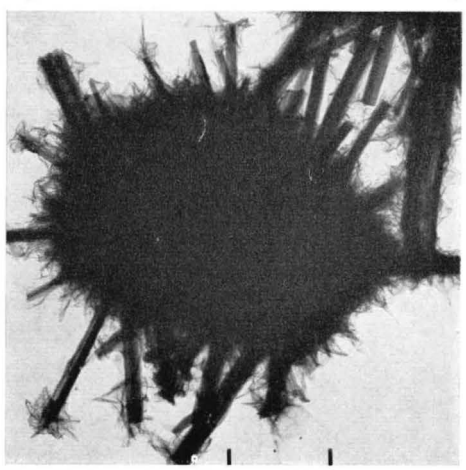

Fig. 130

42. C-A-$\bar{S}$-H

Development of ettringite-type phase in portland cement suspension (continued)

Fig. 131. Sample Pw—7C.

EM: Bundled aggregate of ettringite-type pseudomorphs, covered with thin, wrinkled foils.

ED: Weak, but rather sharp ring at 2.96 Å., probably from C-S-H(I) foils, and some scattered spots from CH crystals.

Figs. 132 and 133. Sample Pw—5.

EMs: Disorganized masses of cement particles, shattered into fragments by the strongly dispersing action of high-speed mixer. Some amounts of rod-like or prismatic particles resembling ettringite can be seen, but these may also be columnar fragments of still unhydrated cement constituents.

Figs. 134 and 135. Sample Pw—6A.

EMs: After ten minutes of vigorous mixing, the hydrated mass has become better organized, and seems to be composed of a practically homogenous phase, with particles of the habit of irregular rods or rolled-sheet elements, about 0.2 or 0.3μ long and 0.05μ wide. It is suggested that the homogenizing action of the mixing procedure has caused the transient formation of a single cement hydrate phase, containing all the oxide ingredients of the starting material, and essentially of the character of a mixed $C_3S-C_6(A, F)$-hydrate stabilized by incorporation of $\bar{S}$, i.e. an ettringite-type phase. The ED patterns recorded for this phase are indistinct and difficult to interpret (cf. Fig. 86).

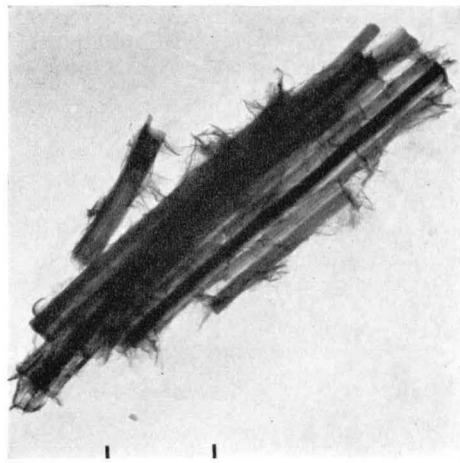

Fig. 131 a

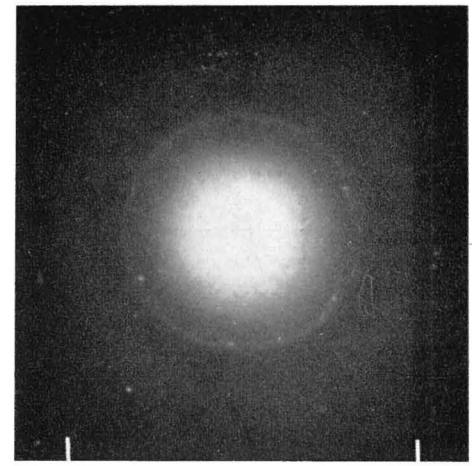

Fig. 131 b

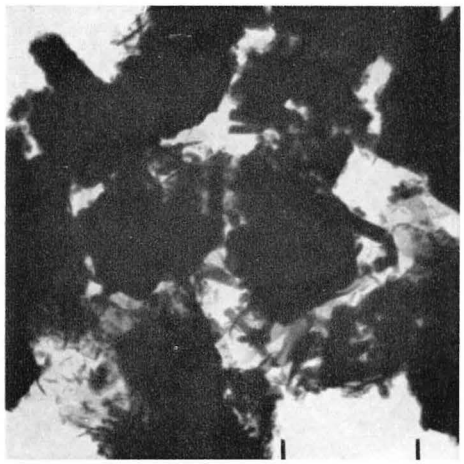

Fig. 132

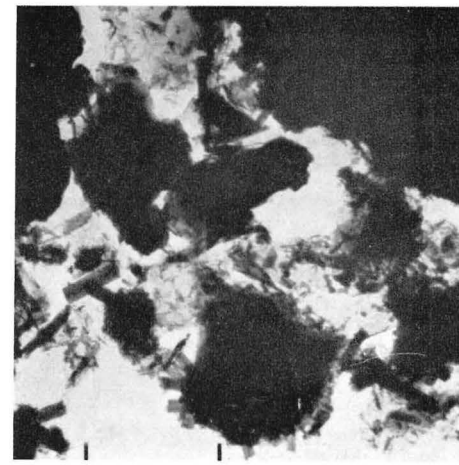

Fig. 133

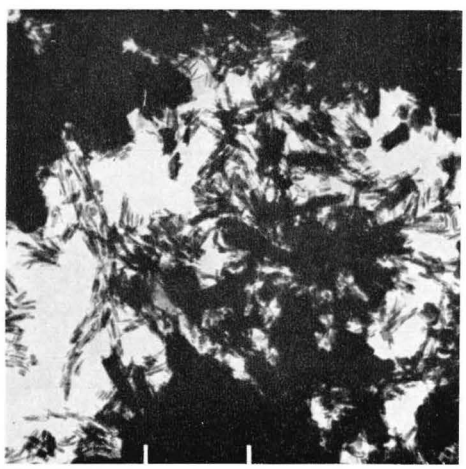

Fig. 134

Fig. 135

43. C-A-$\bar{S}$-H

Development of ettringite-type phase in portland cement suspension (continued)

Figs. 136 and 137. Sample Pw—6B.

EMs: After standing for one day, the homogenous, hydrated phase of Figs. 134 and 135 has separated into at least two phases, one of the striated-rod type assumed to be characteristic of ettringite and similar structures, one of the crinkly-foil, C-S-H(I) type. At this stage, the sample resembles Pw—7 C (cf. e.g. Fig. 130). However, since the original cement grains have been dispersed by the mechanical treatment, the EMs do not show hydrated particles growing outwards from surfaces of larger grains, but a more intimate mixture of hydrated phases, of which the CH crystal phase is remarkably scarce.

Figs. 138—140. Sample Pw—6C.

EMs (138—140): In the next few days, the C-S-H(I) foils continue to grow and cover up the ettringite phase. The EMs show some parts of the specimen where the bundled or striated rods are still clearly visible. In other particle aggregates, this phase is absent, and seems to have become loosened-up by or dissolved in the felted mass of C-S-H(I) foils (cf. Figs. 259—262).

ED (140b): Weak ring at 2.95 Å from C-S-H(I) phase, no reflexions from the ettringite particles which, as stated before, are obviously pseudomorphs resulting from vacuum dehydration.

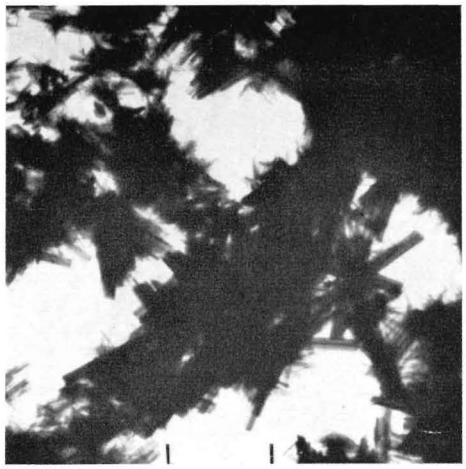

Fig. 136

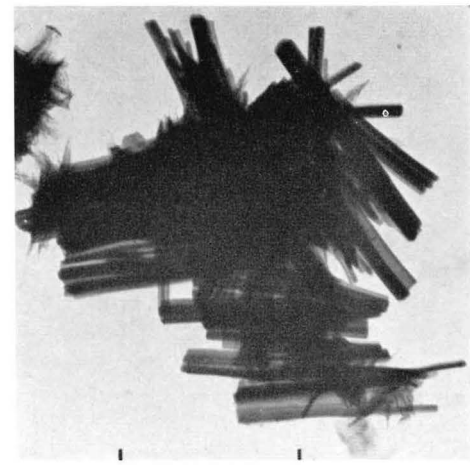

Fig. 137

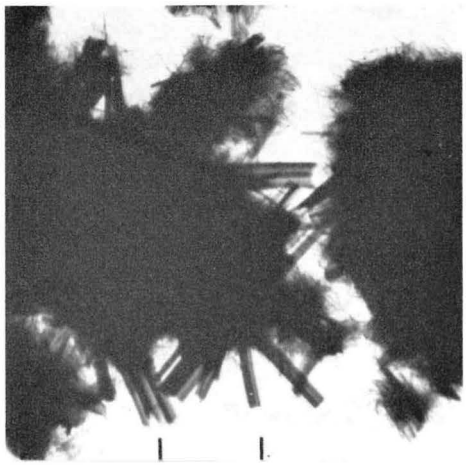

Fig. 138

Fig. 139

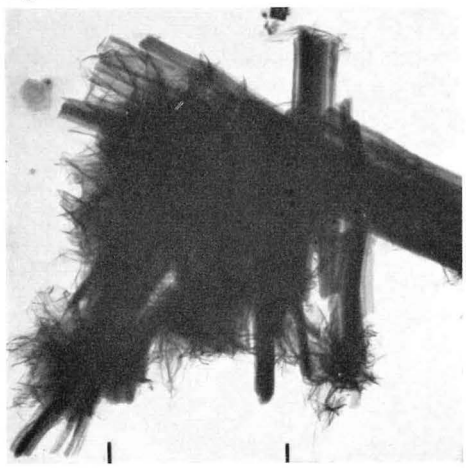

Fig. 140 a

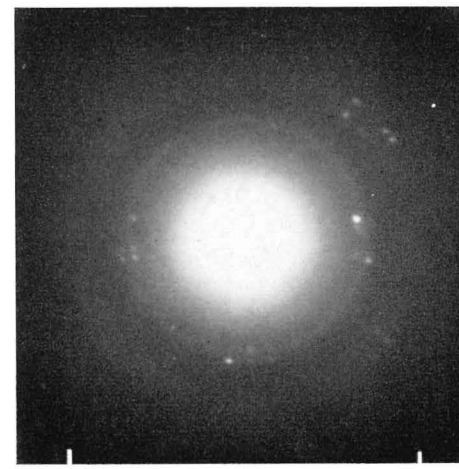

Fig. 140 b

44. C-A-$\bar{S}$-H

Development of sulfoaluminate phases in C_3A paste with gypsum admixture

Figs. 141 and 142. Sample Ap—2A.

EM (141): Ettringite crystals growing on the C_3A and gypsum crystals of the starting material, in the form of rods with sharply cut-off ends, about 0.5—1μ long and about 0.02—0.1μ wide.

EM (142): Ettringite rods adsorbed on plate particle of unknown identity. No significant ED effects are given by these particles.

Figs. 143 and 144. Sample Ap—2B.

EMs: The ettringite phase has developed further, and appears in many parts of this preparation as loose masses detached from the anhydrous particles. The X-ray powder diagram of this sample shows ettringite and gypsum reflexions of moderate intensities, together with a strong C_3A pattern, and a few unidentified reflexions.

Figs. 145 and 146. Sample Ap—2C.

EMs: After 14 days, the ettringite phase has disappeared completely, and the hardened paste consists of plate particles, some of which show hexagonal angles and shapes. The ED diagrams from isolated plates show simple, regularly-hexagonal spot patterns, similar to those of e.g. Figs. 59 and 60, with hexagonal cells $a_H = 5.72-5.74$ Å. The X-ray powder diagram contains a C_3A pattern of moderate intensity, and a pattern coinciding well with that given for $C_4A\bar{S}H_{13}$ by *Midgley* 1957. This pattern is of still higher intensity in the 3-month sample, in which C_3A is nearly absent. The equilibrium composition of the paste would correspond to a lower content of $\bar{S}$, about one-third solid solution, $C_4A\bar{S}_{1/3}$ aq. Judging from the presence of weak basal reflexions at 10.7, 8.1, and 7.7 Å, in addition to the very strong one at 8.85 Å, characteristic of the sulfate solid-solution phase, the hardened product seems to consist of a mixture of phases.

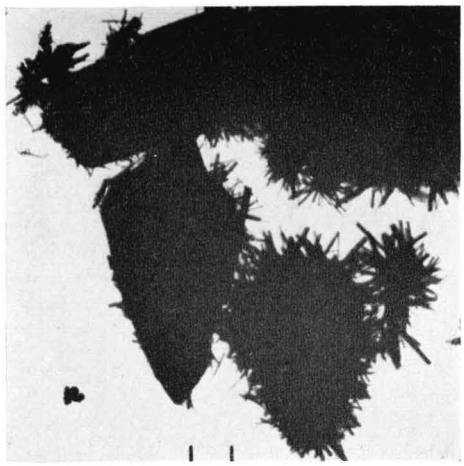

Fig. 141

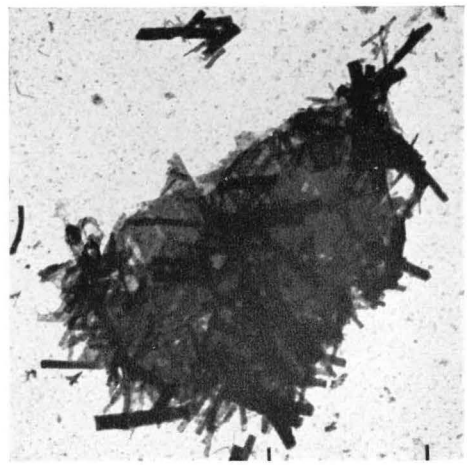

Fig. 142

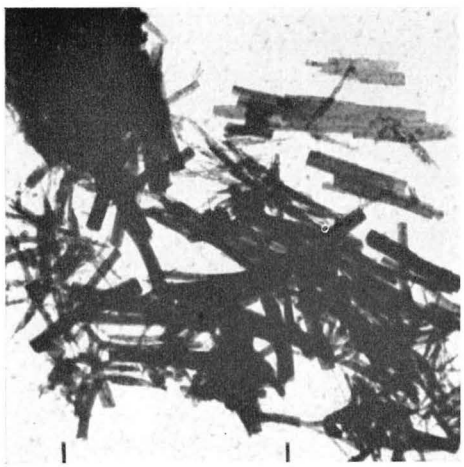

Fig. 143

Fig. 144

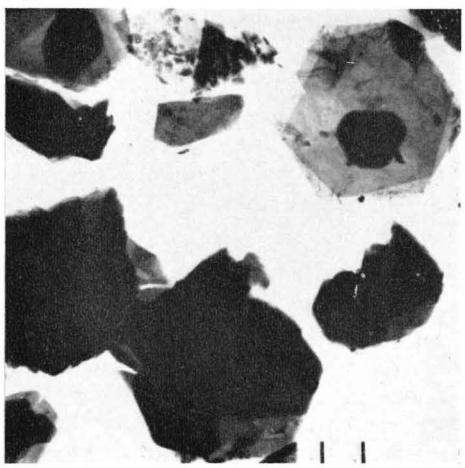

Fig. 145

Fig. 146

45. C-S-H

Well-crystallized tobermorite varieties

Figs. 147 and 148. Sample CSwq—1.

EM (147a): Thin crystal plate with pseudohexagonal angles.

ED (147b): Single-crystal pattern of pseudohexagonal character, indexable on the basis of a face-centered, orthorhombic cell with axes $a=11.05$, $b=7.33$ Å (another, similar diagram gave the values 10.86 and 7.26 Å, which may indicate the magnitude of variation due to differences in shrinkage, angle of tilt and experimental error, that can be expected). The pattern of strong spots corresponds to a pseudo cell with these values halved. There is a certain tendency to "layer-line" formation perpendicular to the b^* direction (vertical), and reflexions with k odd are slightly drawn-out along these layer lines, indicating a certain degree of polymorphic stacking disorder in the crystal. Similar tobermorite patterns and effects have been described by *Akaiwa* and *Sudoh* 1956, *Gard* and *Taylor* 1957, *Grothe, Schimmel,* and *Zur Strassen* 1962, and *Kurczyk* and *Schwiete* 1962.

EM (148): Collection of representative crystals, mostly thin plates, some elongated or lath-like habits are also observed.

Figs. 149 and 150. Sample TSwq—1.

EM (149): Thin plate crystals, of a more or less elongated or lath-like habit typical of this sample, which consists of almost pure tobermorite. X-ray diagram: 11.5 (ms), 5.5 (m), 4.52, 4.2, 3.53, 3.30, 3.20, 3.08 (s), 3.03, 2.98 (m), 2.81 (m), 2.52, 2.48, 2.42, 2.28, 2.23, 2.14, 2.08, 2.00, 1.835 (m), 1.67 (mw), 1.625, 1.60, 1.535, 1.405 Å, etc. (intensities weak, if not given). Most reflexions are comparatively diffuse, indicating a moderate degree of crystallinity.

EM (150a): Large, thin crystal plate with pseudohexagonal angles, partly covered with smaller misaligned plates.

ED (150b): Single-crystal pattern, similar to the preceding one, $a=11.20$, $b=7.35$ Å, with strong pseudohalving, but no signs of stacking disorder. A couple of other diagrams from lath-like crystals gave smaller a values: $a=11.05$, $b=7.38$ Å, and $a=10.92$, $b=7.30$ Å, and in addition showed streaky reflexions in the a^* direction of especially the rows of spots with k odd.

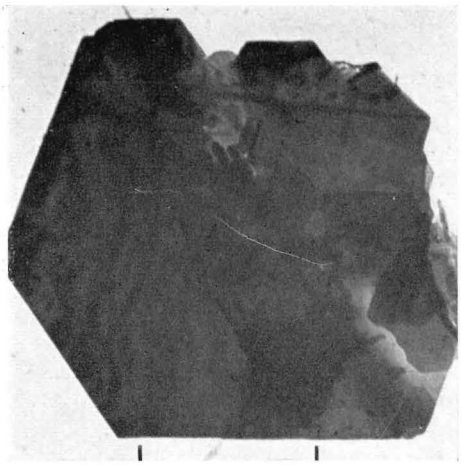

Fig. 147 a

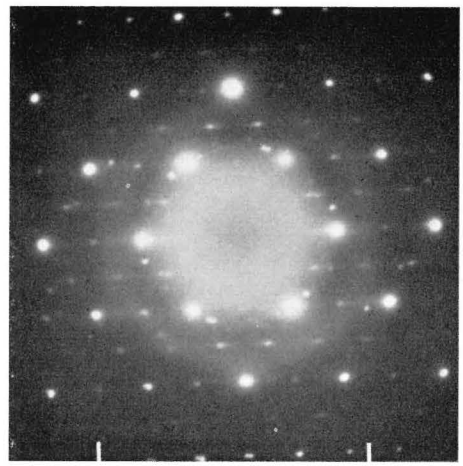

Fig. 147 b

Fig. 148

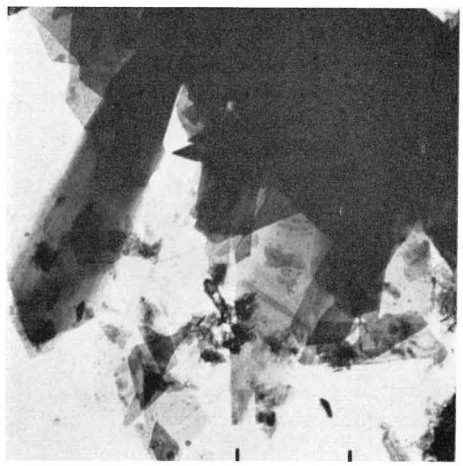

Fig. 149

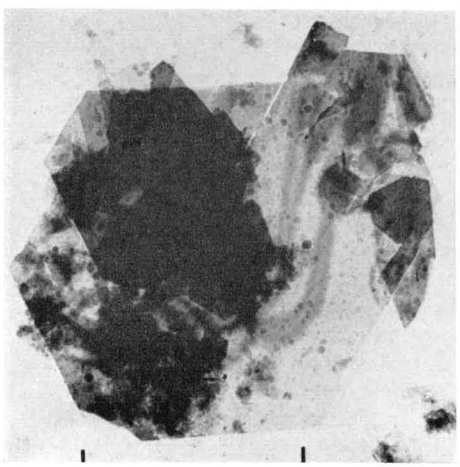

Fig. 150 a

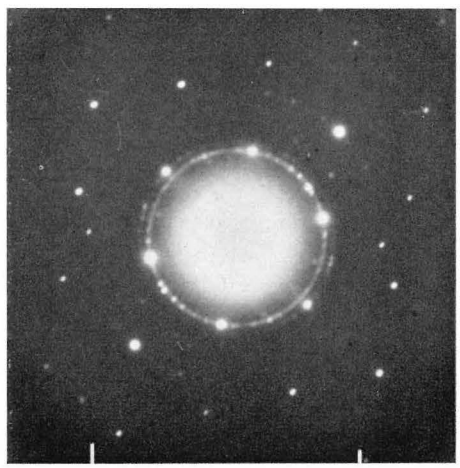

Fig. 150 b

46. C-S-H

Well-crystallized tobermorite varieties (continued)

Fig. 151. Sample DSpq—1.

EM: Crystal plate with approximately 60° angles.

ED: Single-crystal pattern similar to that of Fig. 147b. reflexions not belonging to the face-centered pseudo cell are weak, with k odd streaky, indicating a disordered displacement along the a axis in the stacking of adjacent layer units, unit cell $a \times b = 11.02 \times 7.34$ Å, pseudo cell with half these values. Other values measured for five similar patterns were 11.00×7.34, 11.06×7.22, 11.08×7.38, 11.15×7.40, and 11.10×7.38 Å. The corresponding crystals were generally of a more elongate habit and splintered appearance than the one shown. Such crystals were not uncommon, but most of the sample consisted of flocs of fibrous particles, possibly formed from creased or rolled sheet crystals. The X-ray diagram contained, in addition to a weakened β-C_2S pattern, a small number of more or less diffuse reflexions from the hydrated phases at about 16 (very diffuse), 11.4, 8.4, 5.5, 4.2, 3.38, 3.07 (rather sharp line superimposed on diffuse region of about 0.1 Å width), 2.97, 2.80, 1.835 and 1.815 Å (the two last reflexions form a well-resolved doublet with lines of about equal intensity and width). These data indicate the simultaneous presence of two related tobermorite gel phases. One of these would be "normal" tobermorite, as shown in the micrograph, with an interlamellar spacing about 11.4 Å, a fiber unit 7.34 Å (4×1.835) and a comparatively well-defined unit spacing about 2×5.6 Å perpendicular to these ((220) and (400) spacings at 3.07 and 2.80 Å, respectively). The other phase would have an interlamellar spacing about 8.4 Å, with a second-order reflexion at 4.2 Å (and perhaps a double-layer unit at about 16 Å), a slightly shorter fiber unit ((040) reflexion at 1.815 Å), and a less well-ordered arrangement of units in the a direction (diffuse (220) reflexion). This hypothesis is supported by the X-ray diagrams of another sample, with the β-C_2S-silica mixture in a suspension of thin slurry consistency, but otherwise equal to the paste sample. After 24 hours of autoclaving, a weak pattern of the second phase described above could be seen together with the reflexions from unreacted β-C_2S. After 72 hours, however, the X-ray diagram contained a strong pattern of the 11.4 Å tobermorite phase, with reflexions in general agreement with those given under Fig. 149, together with a β-C_2S pattern of much-weakened intensity. EMs from the 72 hour sample showed fascicular aggregates of tobermorite fibers, or tobermorite crystals in the process of splitting into laths or needles.

Figs. 152 and 153. Sample Dwq—1.

EM (152a): Aggregate of slender, lath-like particles, formation characteristic of this sample, a large part of which consisted of loosely-felted masses of a fibrous constituent. Another phase was α-C_2SH, in the form of block-shaped, rectangular crystals, as seen in Figs. 219 and 220. This phase dominated the X-ray diagram, which also contained some additional, slightly diffuse lines, the most prominent at 3.03, 2.71, 1.91 and 1.89 Å., in general agreement with patterns quoted by *Heller* and *Taylor* 1956 for a substance called dicalcium silicate hydrate (C) (or C_2S γ-hydrate). According to *Taylor* 1962, 1964, the latter substance is probably a mixture of two phases with related structures, calcio-chondrodite and kilchoanite, of probable compositions C_5S_2H and $C_3S_2H_{0-1}$, respectively. The model structure for both compounds is the orthorhombic, olivine-type structure of γ-C_2S. These structures seem to have two of the orthorhombic unit cell dimensions in common, viz. a about 5.05 Å and b about 11.3 Å. By analogy with the γ-C_2S structure, even the hydrated structures are likely to contain discrete SiO_4 tetrahedra as structural elements, which is also indicated by the absence of the 7.3 Å cell distance that is otherwise the characteristic chain repeat unit in fibrous C-S-H compounds.

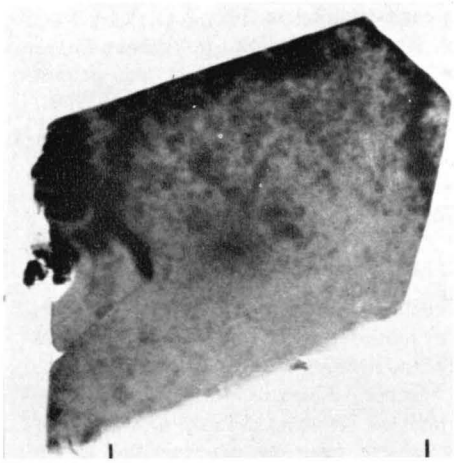

Fig. 151 a

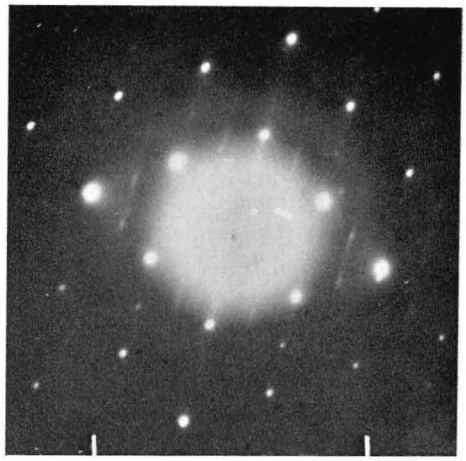

Fig. 151 b

Fig. 152 a

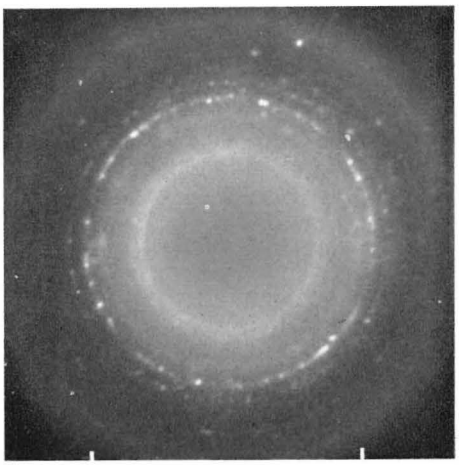

Fig. 152 b

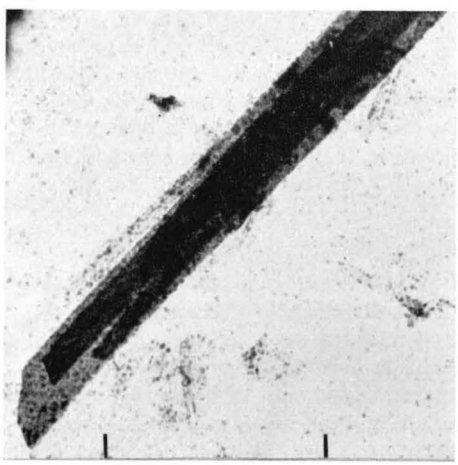

Fig. 153 a

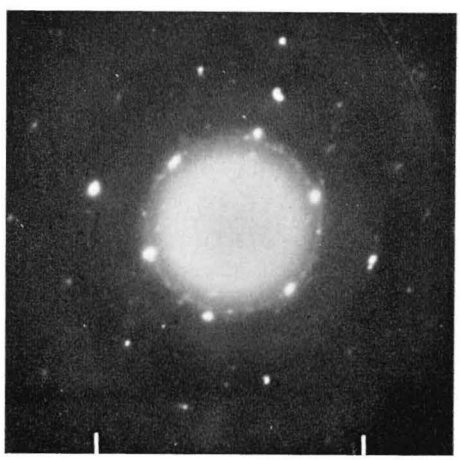

Fig. 153 b

ED (152b): Spot-ring pattern, with reflexions corresponding to 3.09, 2.82, 1.88, 1.71, 1.55, and 1.42 Å, the spacings of an orthogonal, face-centered cell $a \times b$ of about 5.65×3.75 Å. With respect to the relative distribution of spacings and intensities, this pattern resembles ordinary tobermorite gel or C-S-H(I) ED powder patterns (*Grudemo* 1955, cf. below, e.g. Figs. 160, 172), but the cell dimensions are a few percent larger than is normal. This is a case where the ED data show the presence of one seemingly major phase which is not found in the X-ray diagram, and vice versa. Essentially the same observations were made for the paste sample Dpq−3, processed similarly (cf. Fig. 275).

EM (153a): Aggregate of parallel-oriented, lath-like crystals.

ED (153b): Single-crystal pattern, unit cell face-centered, orthogonal, $a \times b = 5.66 \times 3.74$ Å. In this pattern, there are certain weak indications of spot rows in the a^* direction, with three spots evenly distributed between each pair of adjacent stronger spots of the same k index. These effects, which are better visible in a couple of other patterns recorded, indicate a true unit cell which is primitive, orthogonal, with a doubled (11.32 Å). Similar spot rows, for k even in a cell $b = 2 \times 3.65$ Å, and with closely spaced reflexions corresponding to an 11.3 Å repeat distance, occur in ED patterns for the end product of the series of tobermorite materials formed in sand-lime brick preparations studied by *Grothe et al.* 1962. One difference seems to be that there are continuous streaks for k odd, whereas in the case shown here, there are no diffraction effects in the corresponding positions, indicating that the true unit cell is half the ordinary fiber unit distance of 7.3 Å.

It remains to consider the nature of the structural transformations that may give rise to the observed changes in the diffraction patterns. In discussing the possible structures of tobermorite varieties, the model structure of well-crystallized, natural tobermorite mineral of low C/S ratio, advanced by *Megaw* and *Kelsey* 1956, as the result of a tentative, but reasonably complete synthesis of X-ray single-crystal data, can be used as a basis of reference.

In this structure, as well as in several other C-S-H compounds with a fibrous crystal habit, a special type of metasilicate chain composed of units, of length $b_0 = 7.3$ Å (approximately) and containing three tetrahedral links each, is the most important structural element. These chains are associated sideways in layers, with calcium ions acting as linking elements. The distance $a_0/2$ between adjacent chains is about 5.6 Å, and their mutual displacement in the chain direction is $b_0/2$. The twodimensional unit cell of the layers is therefore best described as orthogonal, face-centered, with dimensions $a_0 \times b_0$. Further, it may be noted that the layer is asymmetrical, the oxygen ions on one side of the unit being only half as densely packed as on the other side, with pairs of hydroxyl ions parallel to the layer, but at right angles to the chain direction, forming a pattern of ridges.

Two such layers, superimposed with the sides containing the high oxygen density facing each other, form the unimolecular sheet unit of the *Megaw-Kelsey* structure of tobermorite. The mutual displacements along the a_0 and b_0 directions, that occur in this superposition, is $a_0/4$ and $b_0/4$, respectively. In this way, an orthogonal, face-centered pseudo unit cell of dimensions $a_0/2 \times b_0/2$ is formed. The X-ray and ED patterns of tobermorite are dominated by reflexions indexable in a simple way on the basis of this pseudo cell.

The C/S ratio of the two-layer structure element is only 2/3, or less than the actual value for the natural mineral, which is 0.8−1.0. It was observed by *Megaw* and *Kelsey* that in their model much space is left between the protruding tetrahedral edges or ridges of OH-OH in the outer surfaces of the unimolecular sheet unit. Ca ions and water molecules can be accommodated in interstitial positions in these surfaces, causing the C/S ratio to rise towards 1.0. The arrangement of these interstitial groups, which is unknown, is also likely to influence the basal spacing between unimolecular two-layer units. The normal value of this spacing is $c_0 = 11.3$ Å for the well-crystallized tobermorite mineral, but other values such

as 14.0, 12.6, 10.0, and 9.35 Å have been observed for different species of tobermorite in various states of hydration (*Taylor* 1962).

As is demonstrated by Figs. 151—153, crystalline C-S-H phases with a strong resemblance to tobermorite can appear under steam-curing conditions even in systems with an over-all C/S ratio of 1.5 to 2. The colloidal C-S-H varieties formed in the same C/S range at lower temperatures, viz. C-S-H(I) with a maximum C/S ratio of about 1.5, and C-S-H(II) with a C/S ratio approaching 2, are also generally assumed to be closely related to tobermorite with respect to their crystal structures. However, this assumption may not be true, as will be discussed further below.

In order to maintain a tobermorite structure, the structural changes connected with the increase in C/S ratio should leave the base unit cell $a_0/2 \times b_0/2$ essentially unchanged, i.e. both the characteristic unit along the chain, and the distance between the chains should remain the same. Several alternatives for the nature of these changes have been suggested, in addition to the probable filling of voids in the corrugated surfaces, as indicated above.

Gard, *Howison*, and *Taylor* 1959, and *Grudemo* 1956 suggest structural modifications derived from the *Megaw-Kelsey* model by stripping off the metasilicate chains on one side of the unimolecular sheet, and replacing them by hydroxyl groups to saturate the valences of one half of the calcium ions in the central layer. The structure would then change from the symmetrical one, with a content of cations in layers with the schematic sequence (Ca)3Si—4Ca—3Si(Ca) to an asymmetrical one, with the sequence (2Ca)3Si—4Ca, where the brackets denote possible amounts of interstitially fixed Ca ions. Analogous sequences of layers can be found in the clay minerals of the so-called 2:1 and 1:1 types, respectively where the sequence is 2Si—2Al—2Si (or 2Si—3Mg—2Si) in pyrophyllite (or talc), 2Si—2Al in kaolinite. The maximum value of the C/S ratio would be 2.0, and the basal c spacing of superimposed units could be expected to assume a value of about 10 Å, with a reasonable mutual displacement of ionic groups in the adjoining surfaces. These data agree rather well with those found for C-S-H(II) (cf. *Taylor* 1962, 1964), and the asymmetrical unit is therefore considered as one alternative for the C-S-H(II) structure.

According to another theory, advanced by *Taylor* and *Howison* 1956, and supported by *Brunauer* and *Greenberg* 1962, the change in the tobermoritic structure connected with an increasing C/S ratio is likely to consist in a bilateral removal of SiO_2 groups from the tetrahedra which constitute the ridges in the outer surfaces of the monolayer. Such a removal would result in a layer with a C/S ratio of 1.0, and possibly a smaller basal spacing. Alternatively, the transformation could be imagined as taking place by a replacement of S by C+H, or of S by 2H, the latter similar to replacements in the grossularite-hydrogarnet series. In both cases, the volume changes would be small, since the space requirements are about the same for the three groups (the equivalent of two oxygens). The C/S ratio would rise above 1.

When the outer Si ions are missing, there are no longer any continuous metasilicate chains, but rows of dimeric Si_2O_7 groups, possibly tied together by hydrogen bonds formed by the protons that are liberated when the outer SiO_2 groups are removed. Even in layers in this hypothetical, stripped state, the surface hydroxyls form ridges. However, these ridges run parallel with, instead of perpendicular to, the b axis. The closest possible packing of such stripped layers, with ridges and grooves fitting into each other, gives a minimum basal spacing of about 6.2 Å. The C/S ratio of this structure is 1.0. However, the close-packed arrangement is not the most likely one. An expansion of the interlamellar distance up to about 8.4 Å would be just enough to allow for the introduction of Ca and OH ions in appropriate positions between the ridges, in amounts which would correspond to an increase in the C/S ratio up to a probable maximum of 1.5. These data fit in well with those of one of the phases described in connection with Fig. 151.

In the tobermorite structures suggested by *Kurczyk* and *Schwiete* 1962, $c_0 = 17.15$ Å is considered to be the minimum interlamellar distance between (presumably) double-layer units of tobermorite of low C/S ratio, as observed in ED patterns of a sample prepared at 140° C and consisting of thin crystals of the habit of needles or laths. X-ray patterns indicate a spacing $c_0 = 22.4$ Å (2×11.2), as usual for normal, well-crystallized tobermorite. The difference is explained by the loss of water layers upon dehydration in the electron microscope. In another sample of a tobermorite-like phase with a C/S ratio of 1.8 to 1.9, the X-ray spacing is $c_0 = 27-28$ Å, the difference being ascribed to the intercalation of complete CH layers, of distorted or disorganized structure, between the regular tobermorite layers.

It seems that the spacing of 17.15 Å is too small to be possible for a double-layer unit of tobermorite of the *Megaw-Kelsey* structure, even in the lowest state of dehydration, preceding a complete collapse of the structure. The minimum value acceptable for steric reasons is probably well over 18 Å, or 2×9.35 Å observed for the riversideite variety of tobermorite (cf. *Taylor* 1962, 1964). The lattice distance 17.15 Å may not be a c spacing at all, but the a (100) spacing of xonotlite. This compound could well be formed in small amounts under the conditions indicated. Certain patterns given by *Kurczyk* and *Schwiete* are in close agreement with those occurring in the ($hk0$) zone of xonotlite, as shown in Figs. 201 and 204, whereas others show the 11.2×7.3 Å, face-centered cell. The corresponding preparation may therefore be a mixture of phases, xonotlite and tobermorite, both giving ED patterns from their ($hk0$) zones.

On the other hand, the increase of the 22.4 Å c spacing by about 5 Å, observed for the high-lime tobermorite-like phase, could well be due to the introduction of C-H layers in interlamellar positions. However, it seems reasonable to assume a distribution such that there is one C-H layer, about 2.5 Å thick, per interlamellar space between adjacent tobermorite base units of 11.2 Å thickness. If this is the case, it is evident that there is no place for fully developed CH layers of hexagonal symmetry, with Ca ions between two sheets of close-packed OH ions, analogous to the $Mg(OH)_2$ layers between 2:1 clay (talc) layers in chlorite or vermiculite (*Grudemo* 1954). As is further pointed out by *Kurczyk* and *Schwiete*, these incomplete CH layers must be distorted and their structure adapted to fit in, as assumed, with the undistorted structure of tobermorite layers of the *Megaw-Kelsey* type.

According to certain solubility data, quoted by *Brunauer* and *Greenberg* 1962, the degree of polymerization, or metasilicate chain formation in C-S-H gel phases produced under various conditions, shows a general increase with decreasing C/S ratio and with increasing temperature. The authors arrive at the conclusion that the gel phases formed at room temperature, even C-S-H(I) with a low C/S ratio, contain no three-link metasilicate chains, only monomeric groups of silica tetrahedra. The supposed analogies between the structures of tobermorite and the gel phases C-S-H(I) or C-S-H(II) would therefore be limited, firstly to an incidental resemblance of the face-centered pseudo unit cells $a \times b$, of nominal size 5.6×3.6 Å, and with ranges of variation of about 5.6 to 5.4 Å, and 3.6 to 3.75 Å, respectively, and secondly to similarities in habits of the crystal elements, which are sheet-like or foil-like at low C/S ratios, lath-like or fibrous towards higher C/S values.

The morphological properties of the low-temperature C-S-H phases suggest the presence of chains arranged in layers even in these structures. According to *Brunauer* and *Greenberg* 1962, the chains are likely to be of the type proposed by *Bernal* 1954. The *Bernal* chain consists of monomers of $SiO_2(OH)_2$ tetrahedra, simply arranged in rows with one twofold axis of the tetrahedra coinciding with the axis of the row. The tetrahedra are linked together by hydrogen bonds, arranged tetrahedrally in nearly the same way as the four oblique O—O edges in the tetrahedra themselves. The repeat unit along the chain axis could be expected to fall within the range 3.62 to 3.76 Å, as calculated from an edge length of 2.56 Å in the SiO_4 tetrahedron, and a hydrogen bond length of 2.76 Å.

It is observed that such hydrogen-bonded *Bernal* chains have two planes of symmetry at right angles to each other, both containing the chain axis. With respect to the oxygen positions, but not to the silicon positions, there are even pseudo planes of symmetry perpendicular to the chain axis.

There are several ways of arranging the chains in parallel, either in layers or in patterns of tetragonal symmetry in cross-section.

A simple layer arrangement would be one in which symmetry planes in each chain coincided with the plane of the layer, and in which also the identical pseudo symmetry planes coincided. In the layer thus obtained, it would be possible to place Ca ions between the chains in sites surrounded by a rectangular group of four oxygens, nearly identical with the group surrounding the Ca ions in the *Megaw-Kelsey* tobermorite structure. The distance between the chains would also be about the same, namely, 5.5 to 5.6 Å. The Si ions of neighbouring chains are not likely to be in positions directly opposite each other, but are probably displaced to each side of the common pseudo symmetry plane. The true unit cell would therefore be about 11.2×3.6 Å, covering a width of two chains in the *a* direction. It can be noticed that this is the cell observed for the crystal in Fig. 153, as well as for crystals of the material prepared by *Grothe et al.*, and mentioned in this connection.

Other arrangements within the layers of hydrogen-bonded orthosilicate chains could be produced by turning each chain about its axis out of the position just described. A rotation of 45° would, at least hypothetically, permit a very close packing of the chains, with the distance between adjacent chains approaching the theoretical minimum of about 3.6 Å. Of course, such a structure is quite impossible, since there would be no space left for the Ca ions. At an intermediate angle of rotation of the chains, Ca ions could be located in distorted-octahedral positions in a group of six chain oxygens. The chain-to-chain distance in this case would be only slightly smaller than that of the structure described in the preceding paragraph. In both cases, the C/S ratio of the layer would be 1. Consequently, in a C-S-H batch synthesized with this C/S ratio, there would be no ionic material left for the interlamellar space, which, however, could possibly be taken up by more or less regular water layers.

The association of chains sideways, by means of Ca ions in rectangular or distorted-octahedral oxygen groups, can be imagined as taking place not only in one plane, but in two perpendicular directions. A complete, idealized structure of this kind would consist of chains arranged in a pattern of tetragonal symmetry. The C/S ratio of this structure would be 2. It is conceivable that real structures of the C-S-H(I) or C-S-H(II) types possess more or less disordered structures that are intermediate between the two extreme cases, the unimolecular layer with $C/S=1$, and the tetragonal fiber with $C/S=2$.

47. C-S-H

C-S-H(I) from ethyl silicate in lime solution

Figs. 154—157. Sample Sl—1A.

EM (154): Representative structures from main precipitate, agglomerates of thin, wrinkled foils of C-S-H(I).

EM (155): Edge of large agglomerate. The foils are so thin that they can hardly be resolved from the general background intensity.

EM (156a): In some areas of the specimen, the wrinkles were strongly pronounced, giving the structure a fibrous character.

ED (156b): Rather sharp reflexion at 2.95 Å, and weak diffuse halo at about 2.1 Å.

EM (157a): Rounded agglomerate of rather well-developed foils.

ED (157b): Diffuse halos at about 2.95 and 2.1 Å.

The ED effects given by these foils do not include any fiber reflexion at 1.82 Å. This indicates that the tendency to formation of long chains, whether metasilicate or hydrogen-bonded, must be slight.

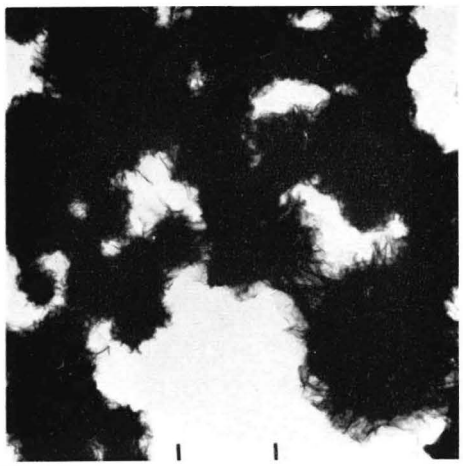

Fig. 154

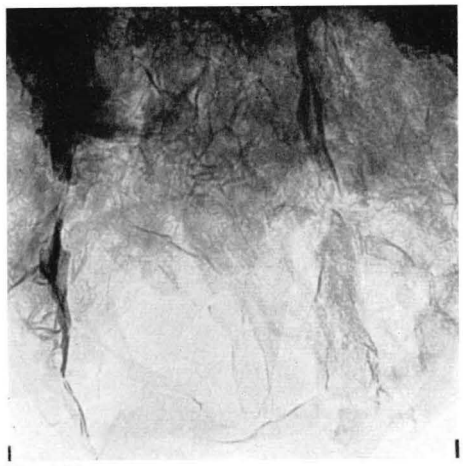

Fig. 155

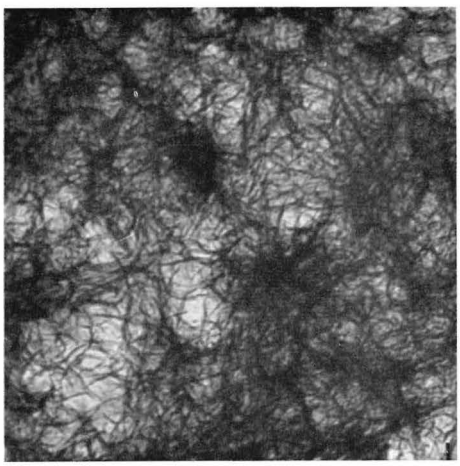

Fig. 156 a

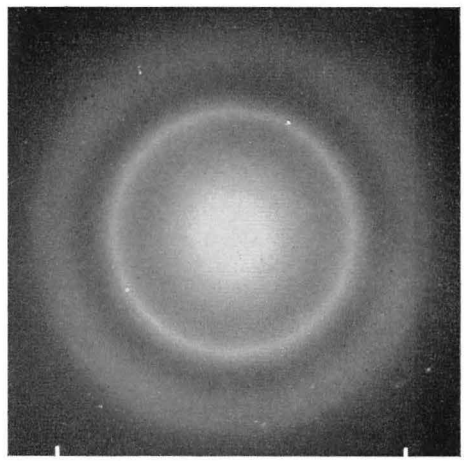

Fig. 156 b

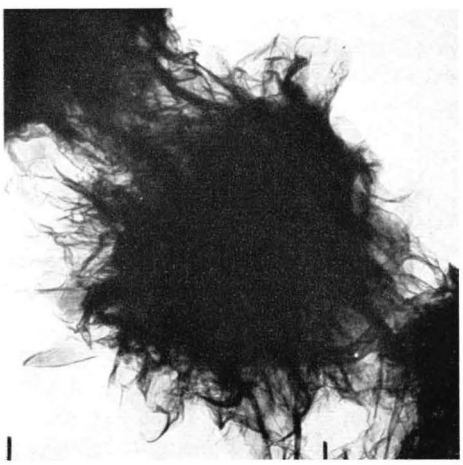

Fig. 157 a

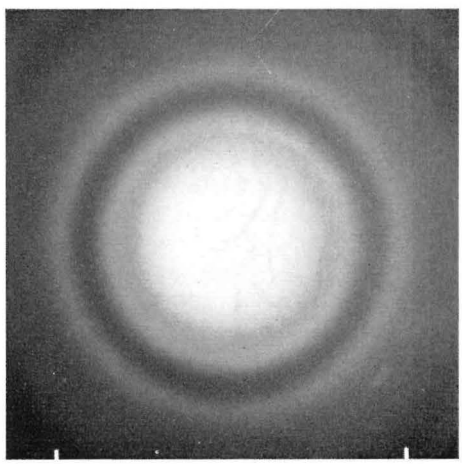

Fig. 157 b

48. C-S-H

C-S-H(I) from ethyl silicate in lime solution (continued)

Figs. 158 and 159. Sample Sl—1A.

EM (158a): The particles in Fig. 156, after heating in high-intensity beam for about 30 sec., recrystallized into elongated crystal particles.

ED (158b): Spot pattern of distorted type, reflexions at 3.22, 2.81, 2.75—2.72, 2.28, 2.08, 1.98, 1.78—1.74, 1.61, 1.55 Å, etc. The general distribution of lattice spacings shows a certain conformity to that of afwillite, according to *Midgley* 1957 (cf. Figs. 184 ff.), but this similarity may be incidental.

EM (159a): Particles similar to those of, for example Fig. 154, after heating in high-intensity beam until partial melting occurred. The melted and resolidified particles are rounded and drop-shaped.

ED (159b): Irregular spot pattern, probably given by anhydrous substance. The most prominent feature is a spot-ring at about 2.78 Å. It may be noted that this is the region of strongest intensities in the powder patterns of C_3S and β-C_2S.

Fig. 160. Sample Sl—1B.

EM: Representative structures from the film formed on the surface of the solution, consisting of thin, loosely wrinkled foils, and occasional CH crystals. One or two of the latter particles are seen in the figure as hexagonal plates, one as a pile of plates, viewed from the edge (cf. Fig. 28).

ED: Powder pattern of the (*hk*0) zone of C-S-H(I), and scattered spot reflexions from the CH crystals. The (00.1), (00.2), and (00.3) CH reflexions at (nominally) 4.91, 2.455, and 1.637 Å, respectively, are visible in the original, as well as (11.0) reflexions at 1.797 Å., and others. Using the latter CH reflexion as calibration standard, the following series of C-S-H(I) spacings have been measured: 3.02 (110), 2.77 (200), 1.810 (020), 1.648 (310), 1.51 (?) (220), 1.388 (400), corresponding to a face-centered unit cell $a \times b$ of 5.55×3.62 Å. The measurements on the (00.*l*) CH spot reflexions give a c spacing that is about 0.6 percent dilated from the nominal value at 4.91 Å. It is suggested that this could be due to the anisotropic thermal expansion of the CH lattice. The expansion along the c_H axis is about 0.3—0.4 percent per 100°, as against only about 0.1 percent per 100° in directions perpendicular to this. From these figures, the temperature of the sample can be estimated to be 200—300° C, which is a reasonable value.

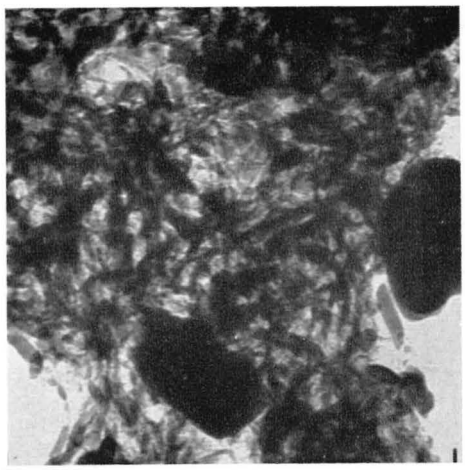

Fig. 158 a

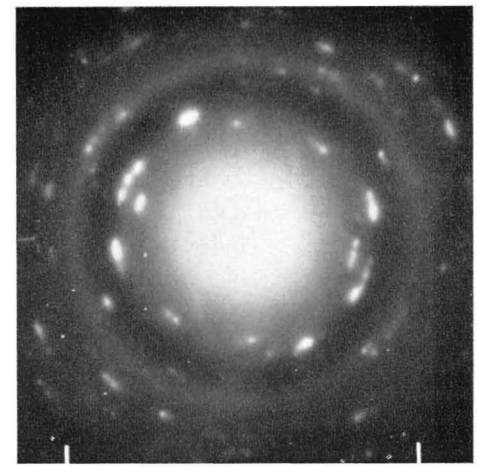

Fig. 158 b

Fig. 159 a

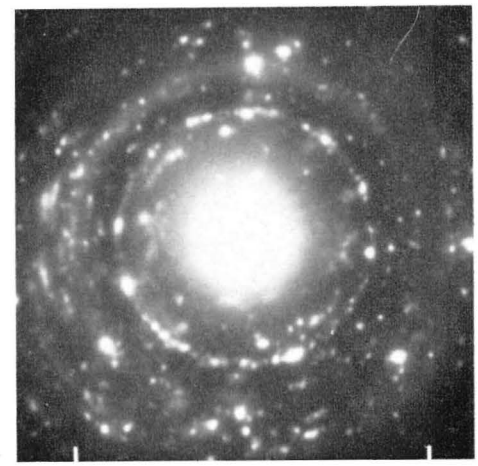

Fig. 159 b

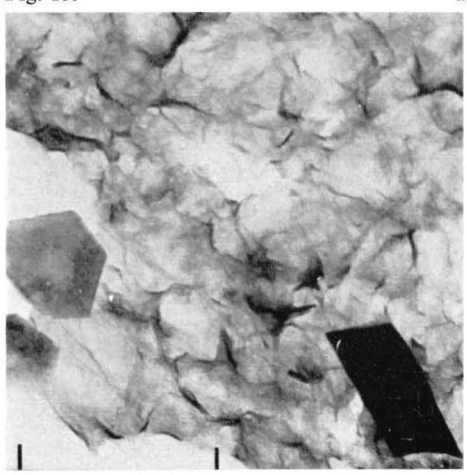

Fig. 160 a

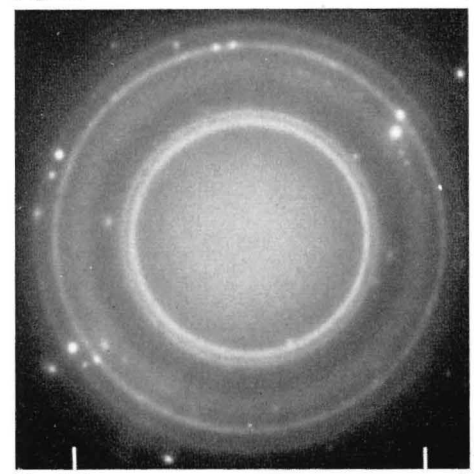

Fig. 160 b

49. C-S-H

Structures in hardened and ground C_3S paste after brief redispersion in water

Figs. 161—163. Sample Tp—1C.

EM (161): Representative, large aggregate of rehydrated paste, with the central parts transparent, revealing an internal structure in the form of a network of intersecting needles or fibers (cf. also Figs. 276—279).

EMs (162a,b): Thin veils or loosely wrinkled foils, developing at some places between the rehydrating paste aggregates, probably C-S-H(I) formations.

ED (162c): Mainly a strong, but very diffuse halo with its maximum at about 2.95 Å.

EM (163a): Paste aggregates consisting of bundles of fibers, of a mottled appearance, observed in minor quantities in the sample.

ED (163b): $C\bar{C}$ (calcite) ring pattern, reflexions at 3.035, 2.495, 2.285, 2.095, 1.928/1.912/1.875 Å (unresolved triplet) clearly visible, with traces of other reflexions. With water used as suspension medium, some CO_2 contamination occurs very easily, in spite of the precautions taken to avoid this, rapid handling, etc.

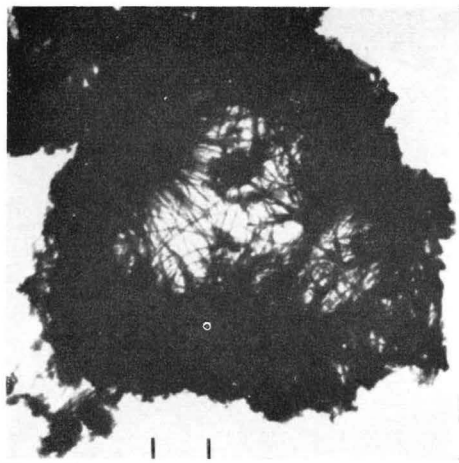

Fig. 161

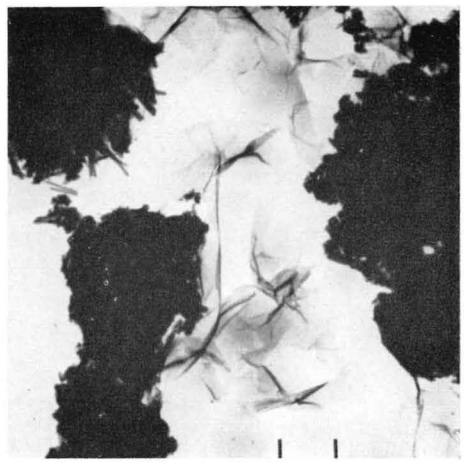

Fig. 162 a

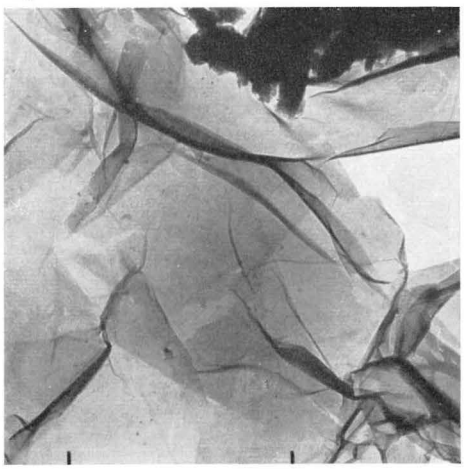

Fig. 162 b

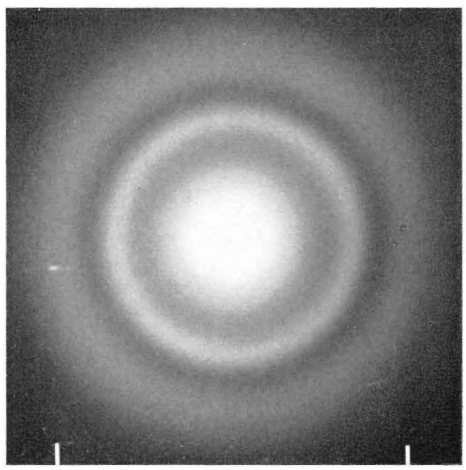

Fig. 162 c

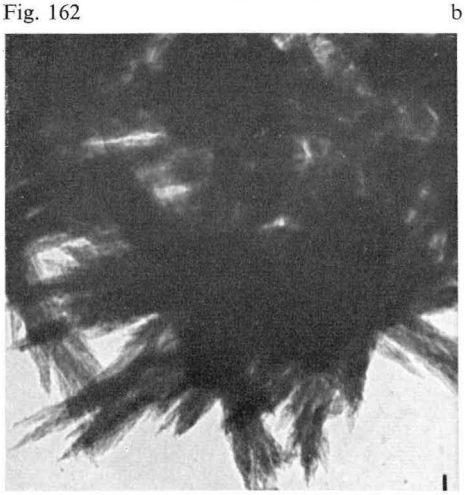

Fig. 163 a

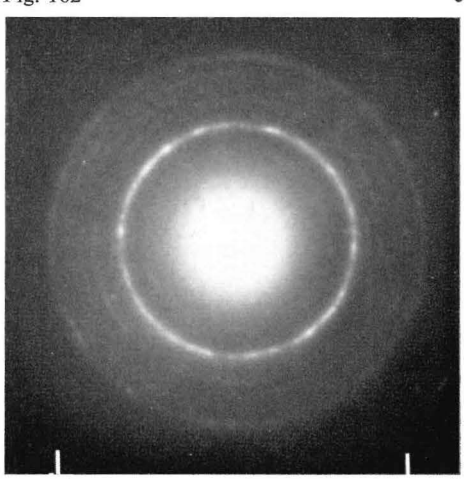

Fig. 163 b

50. C-S-H

Structures in hardened and ground C_3S paste, after some time of rehydration

Figs. 164—167. Sample Tp—1D.

EM (164a): Thin, wrinkled foils, with many indications of a parallel-orientation of the striations into structures resembling bundled fibers.

ED (164b): C-S-H(I) pattern, with rings at 3.00, 2.75, and 1.81 Å.

EM (165a): Structure resembling a network of fibers, foils with pronounced effects of wrinkling and rolling.

ED (165b): One rather sharp reflexion at about 2.92 Å.

EM (166): Characteristic agglomerate of C-S-H(I) foils (ED: One rather sharp, somewhat spotty reflexion ring at 2.97 Å).

EM (167): Bundles of fibers of appearance similar to that of C-S-H(II) particles (cf. *Grudemo* 1955, *Brunauer* and *Greenberg* 1962). (ED: $C\bar{C}$ (calcite) pattern, similar to that of Fig. 163b).

Fig. 164 a

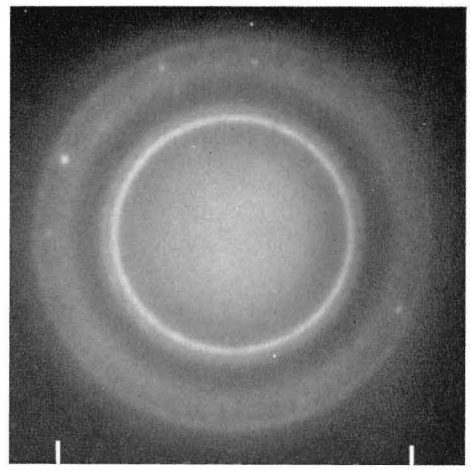

Fig. 164 b

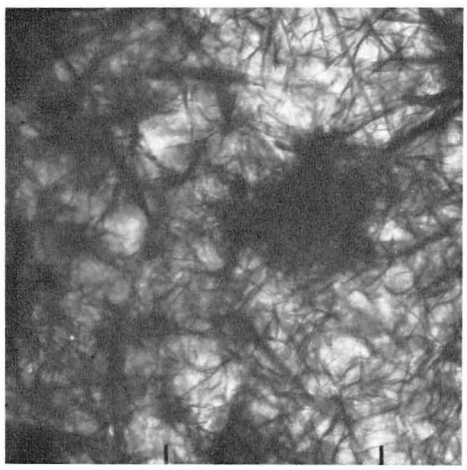

Fig. 165 a

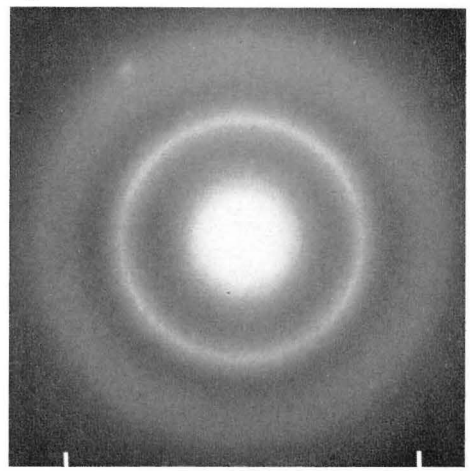

Fig. 165 b

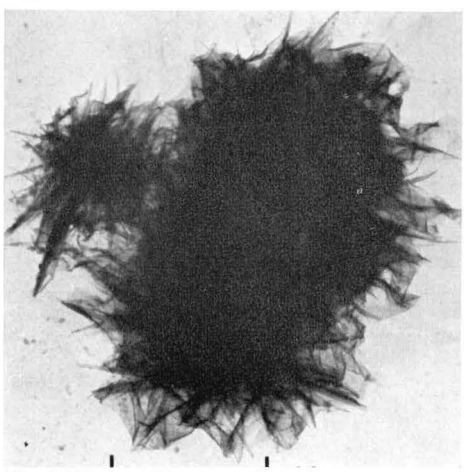

Fig. 166

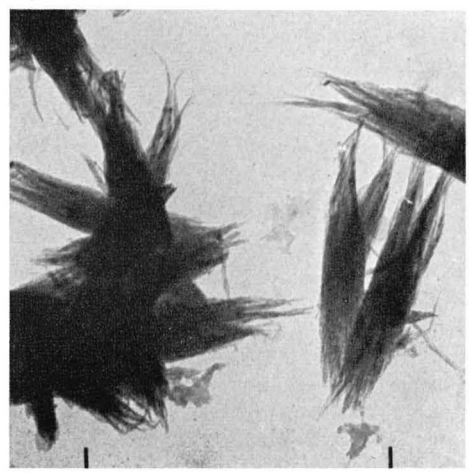

Fig. 167

51. C-S-H

Structures in rehydrated C_3S paste and in C_3S suspension

Figs. 168 and 169. Sample Tp—1D.

EM (168a): Edge structures of large, rehydrated paste aggregates, with protruding, needle-like particles.

ED (168b): $C\bar{C}$ (calcite) pattern of rather spotty appearance.

EM (169): Characteristic appearance of large, rehydrated paste aggregates, with edge structures of rolled foils and needles, probably partly $\bar{C}$-contaminated, as shown in Fig. 168.

Figs. 170 and 171. Sample Tw—3C.

EM (170): Aggregates similar to those of Figs. 168—169, from suspension of C_3S in water. (ED: In the original state, these formations gave only diffuse ED effects, cf. also Figs. 235—238).

EM (171a): Other characteristic formation of this batch, large C-S-H(I) foils, loosely wrinkled or twisted.

ED (171 b): Diffuse ring at about 2.85 Å.

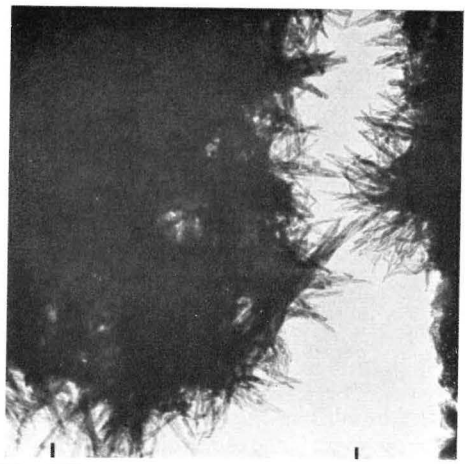

Fig. 168 a

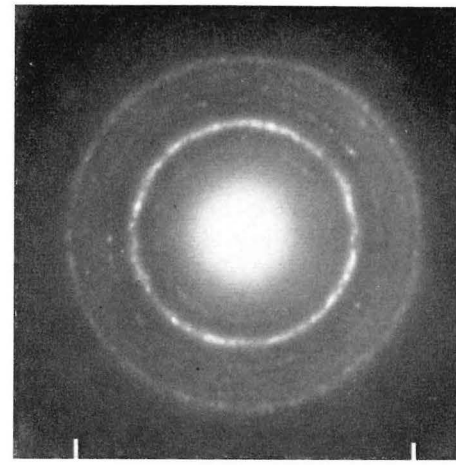

Fig. 168 b

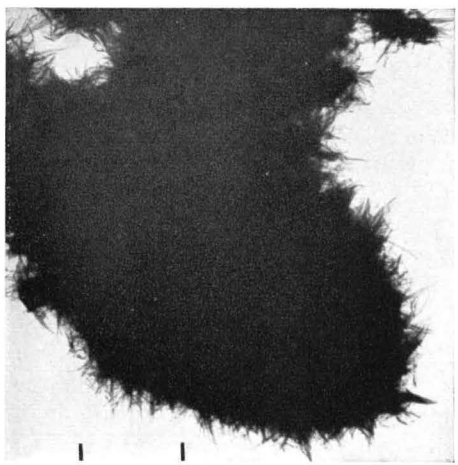

Fig. 169

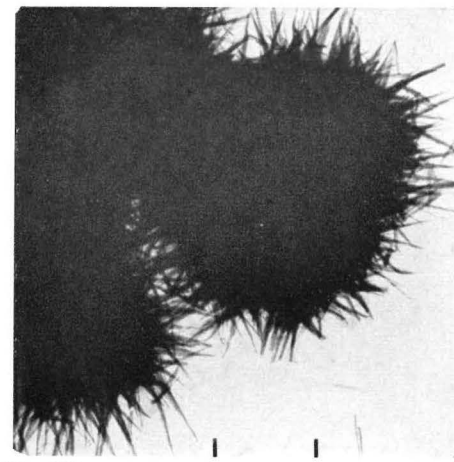

Fig. 170

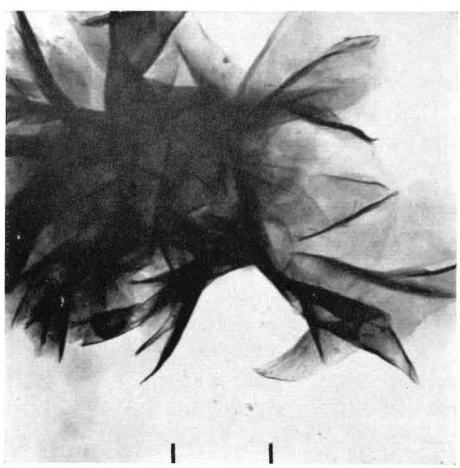

Fig. 171 a

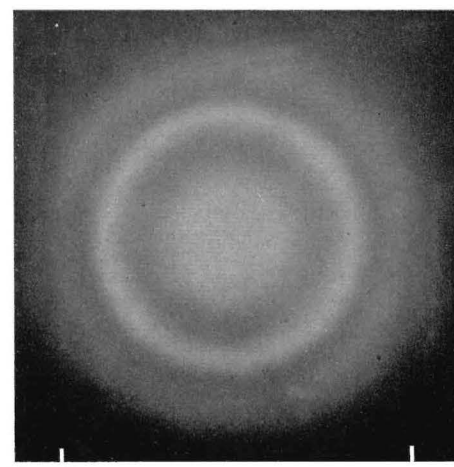

Fig. 171 b

52. C-S-H

C-S-H(I) formed from silica in lime solution

Fig. 172. Sample Sl—5.

EM: Product of reaction of silica gel in a lime solution of low concentration, wavy C-S-H(I) foils of C/S ratio about 1.0.

ED: C-S-H(I) pattern with reflexion rings of slightly spotty appearance, indicating a comparatively high degree of crystallinity. Reflexions at 3.02, 2.76, 1.805, 1.645, 1.51, 1.385, and 1.212 Å, corresponding to the (*hk*0) reflexions with $h+k$ even from a cell $a \times b = 5.52 \times 3.61$ Å.

The phase compositions at equilibrium of three batches made with silica gel in lime solution are given under Sl—5 in the list of samples. The two lowest points fall almost on the equilibrium curve obtained by *Grudemo* 1955 by adding ethyl silicate very slowly to lime solutions of a number of concentrations which are kept constant in the course of the C-S-H(I) synthesis. The highest point falls on the rising portion of the corresponding curve obtained by *Taylor* 1950, most probably due to the presence of a precipitated CH phase in the solid.

Figs. 173 and 174. Sample Sl—4.

EM (173a): Product of reaction of ethyl silicate in a lime solution of low concentration, C-S-H(I) particles in the form of small, irregular plates or wrinkled foils. The material is partly well-dispersed, partly aggregated in clusters.

ED (173b): Rather sharp reflexion at 2.98 Å, and a very weak indication of a 1.80 Å reflexion.

EM (174a): Thin plates and twisted foils.

ED (174b): C-S-H(I) pattern, reflexions at 2.98, 2.72, (about 2.1, very diffuse), 1.80, 1.63, and 1.36 Å, corresponding to the (*hk*0) reflexions with $h+k$ even from a cell $a \times b = 5.45 \times 3.60$ Å. A comparison with the pattern in Fig. 172b indicates a certain contraction of the C-S-H(I) lattice of sample Sl—4, preferably in the direction of the a axis, an effect which is in agreement with earlier observations made by *Grudemo* 1955.

The phase composition at equilibrium of the samples Sl—2 to 4, all prepared by mixing ethyl silicate with lime solutions of varying concentrations, are given in the list of samples. The three points fall somewhat above the equilibrium curve given by *Taylor* 1950. Even taking into due account some uncertainty with regard to the amounts of silica added at the start, it is clear that the C/S ratios of these C-S-H(I) preparations have attained values close to maximum. The reason for this is not known, but it can be tentatively suggested that the special form of silica developed in a rapid hydrolysis of ethyl silicate is capable of taking up more calcium ions than is normal in the formation of C-S-H(I) products.

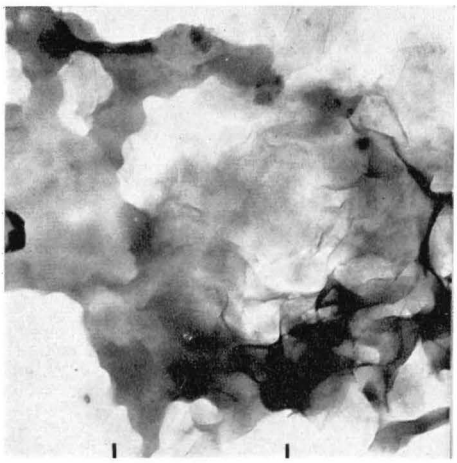

Fig. 172 a

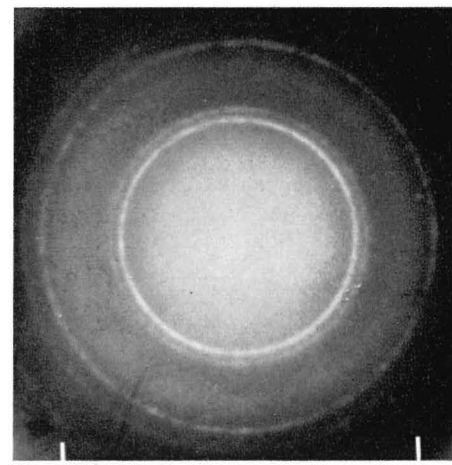

Fig. 172 b

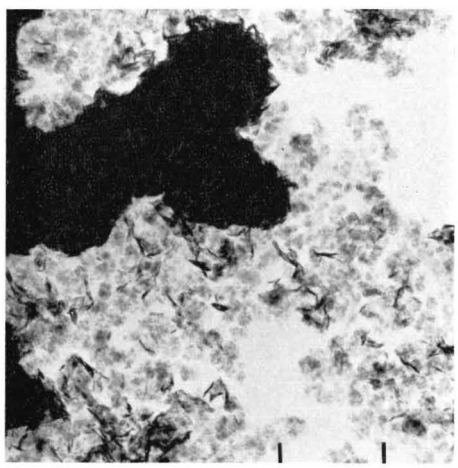

Fig. 173 a

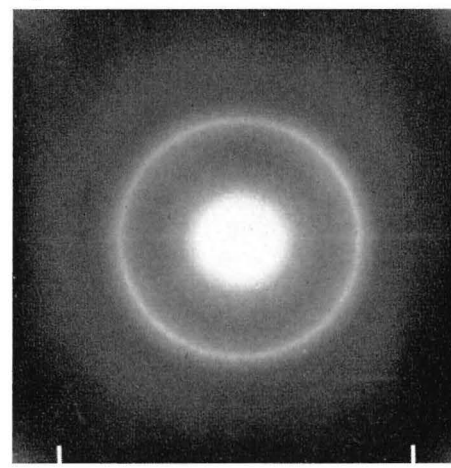

Fig. 173 b

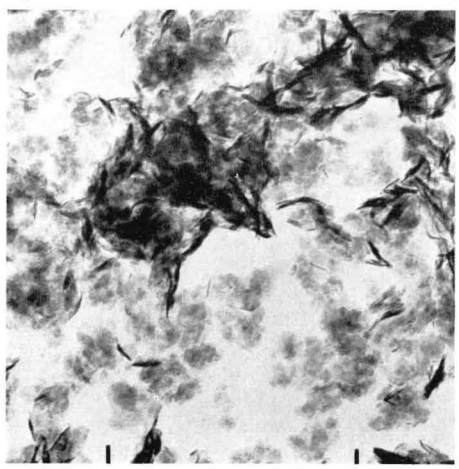

Fig. 174 a

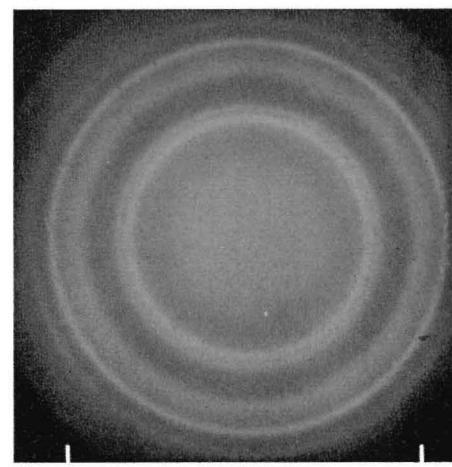

Fig. 174 b

53. C-S-H

C-S-H(I) formed from silica in lime solution (continued)

Fig. 175—177. Sample Sl—3.

EM (175): Product of reaction of ethyl silicate in a saturated lime solution, representative phase consisting of dense agglomerates of C-S-H(I) foils.

EMs (176, 177a): Certain parts of the sample had a looser texture, with foils or flocs of irregular shape and thickness.

ED (177b): Rather sharp, strong reflexion at about 2.95 Å, very weak indication of reflexion at 1.80 Å.

Figs. 178 and 179. Sample Sl—2.

EMs: Product of reaction in supersaturated solution, otherwise as above. The structures are also very similar to the ones immediately preceding.

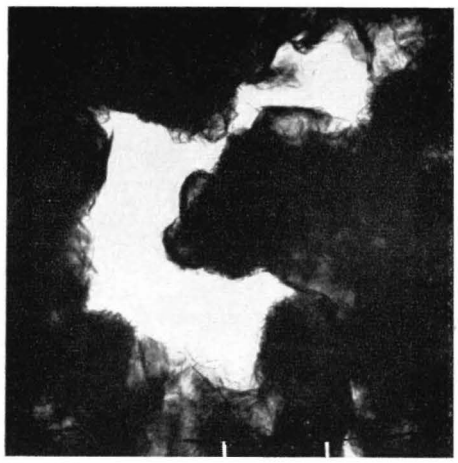

Fig. 175

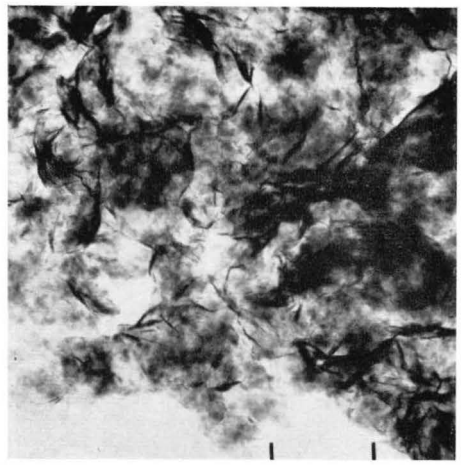

Fig. 176

Fig. 177 a

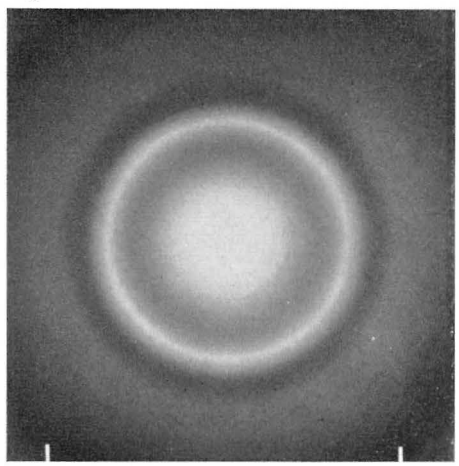

Fig. 177 b

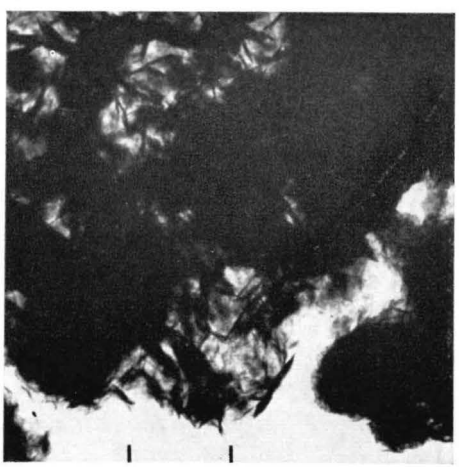

Fig. 178

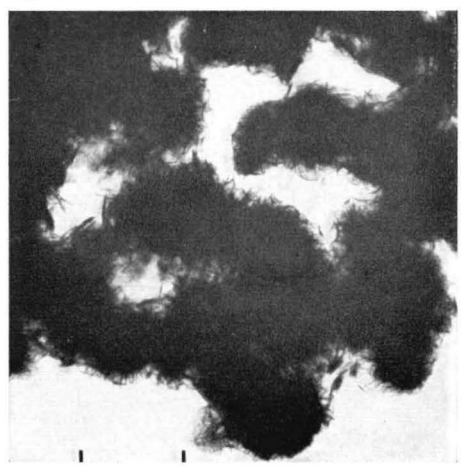

Fig. 179

54. C-S-H

C-S-H(I) formed from silica in lime solution (continued)

Fig. 180. Sample Sl—2.

EM: Well-dispersed part of sample, flocs and twisted foils of C-S-H(I). In addition, there are also numerous particles resembling very thin (less than 50 Å) needles or threads which were observed only in this preparation, made with originally supersaturated lime solution.

ED: Weak C-S-H(I) rings at 2.96, 2.71, and 1.80 Å, (*hk*0) reflexions from a unit cell $a \times b$ of about 5.4×3.6 Å.

Fig. 181. Sample CSw—2A.

Figs. 182 and 183. Sample CSw—2B.

EMs (181—183a): Aggregates of small, irregular particles, probably plates or foils.

ED (183b): Reflexions at 2.78, 2.40, and 1.70 Å from C crystals (product of dehydration in the electron microscope), and a diffuse halo at about 2.9 Å, from disorganized C-S-H gel.

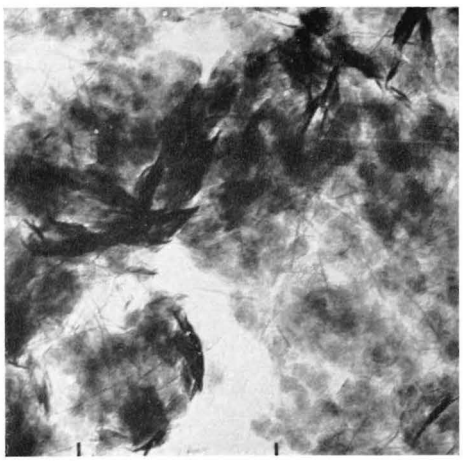

Fig. 180 a

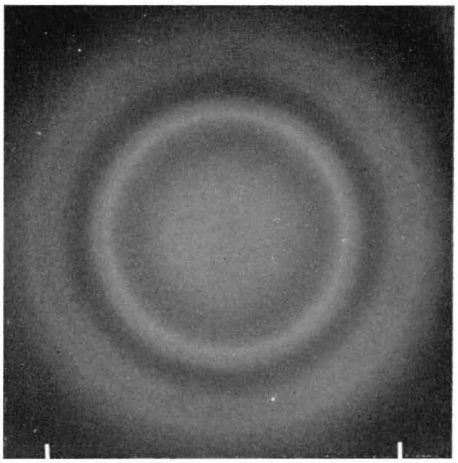

Fig. 180 b

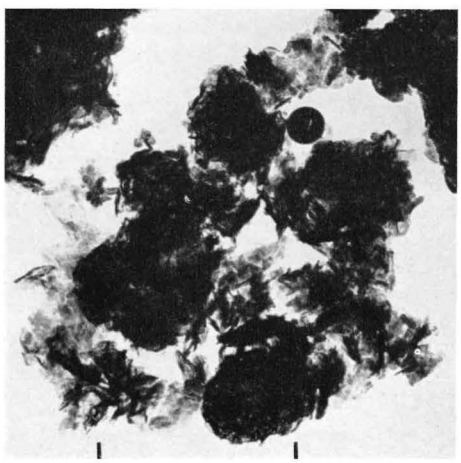

Fig. 181

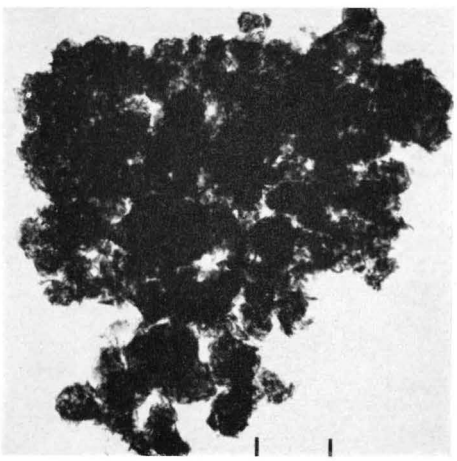

Fig. 182

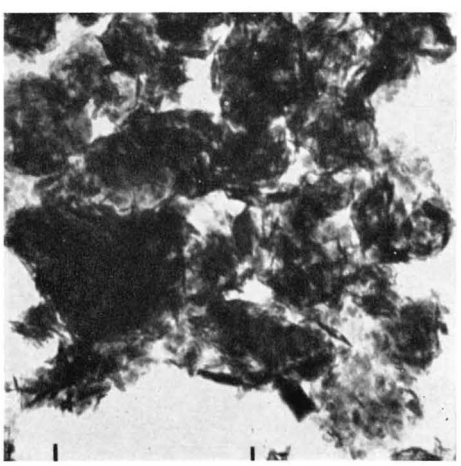

Fig. 183 a

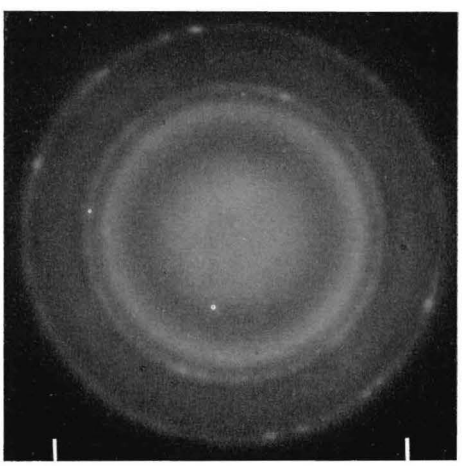

Fig. 183 b

55. C-S-H

Products formed in lime-silica mixture

Figs. 184—189. Sample CSw—1.

EMs (184—186): Mainly plate-like particles, some irregular, some showing straight edges and crystalline angles.

EDs (187—188): Mostly CH single-crystal reflexions, (00.1), (11.0), (10.1), (10.2), (11.0), (11.1), etc. visible, also a diffuse intensity region at about 2.9—2.7 Å, containing a few spots at 2.80—2.85 Å. This type of diagram may indicate the presence of afwillite (cf. Figs. 190 ff.)

ED (189): From recrystallized region of sample (exposed to a high-intensity beam), large number of reflexions with more or less irregular distribution. C rings at 2.40 and 1.70 Å can be observed, and a region of strong reflexions at about 2.83—2.72 Å. These reflexions, together with some other features of more indistinct character, indicate that afwillite is still present, although in a recrystallized state.

As stated in the list of samples, the X-ray analysis of sample CSw—1 showed that it consisted mainly of afwillite. In ED diagrams, this compound does not show up nearly as readily as CH, in the form of thin plate crystals, as is also shown in Figs. 190 ff.

The samples CSw—1 and CSw—2 (Figs. 181—183) were prepared in almost the same way with respect to composition and treatment, the only disparity being the brand of silica used. The distribution of silica groups, and the manner in which they are liberated and reassociated in the course of the reaction, are obviously different, and this results in the formation of (presumably) hydrogen-bonded silica chain elements in a highly disorganized structure in one case, separate silica groups in a relatively well-crystallized afwillite structure in the other. According to the structure analysis made by *Megaw* 1952, the silica tetrahedra in the afwillite lattice occur in groups of two tetrahedra, between which there is a single hydrogen bond. This is very short, 2.52 Å, but is still among the bonds broken in the formation of a cleavage plane, according to *Megaw*.

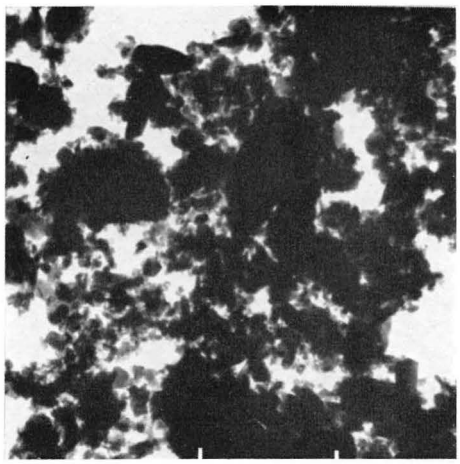

Fig. 184

Fig. 185

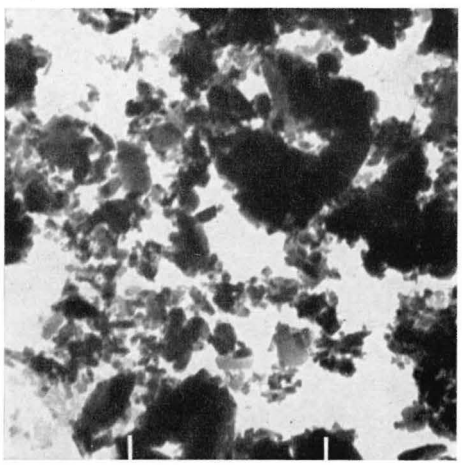

Fig. 186

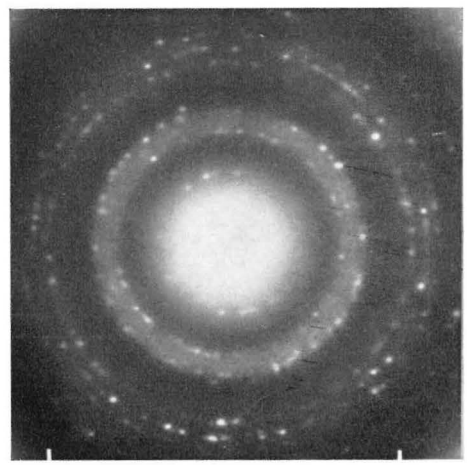

Fig. 187

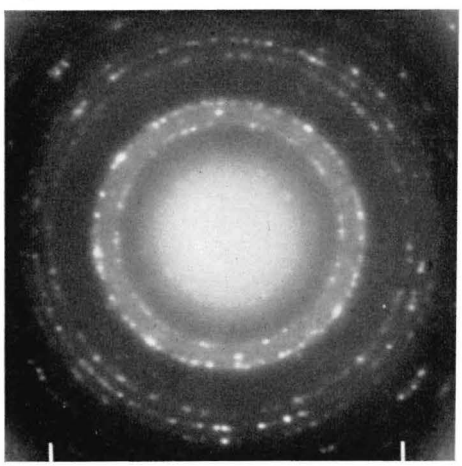

Fig. 188

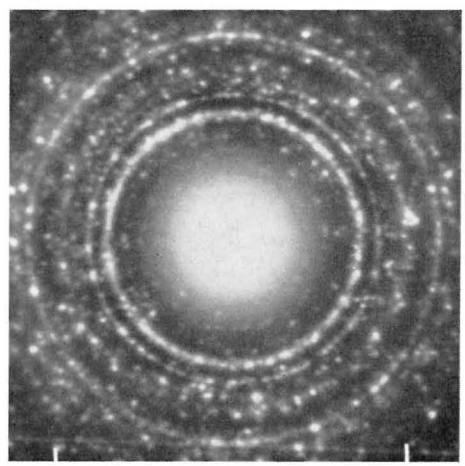

Fig. 189

56. C-S-H

Afwillite in ball-milled C_3S suspensions

Figs. 190 and 191. Sample Tw—4.

EM (190a): Aggregate of small plates, of rather uniform size.

ED (190b): Spot-ring reflexions, incomplete afwillite pattern with some CH reflexions. The measured spacings are (corresponding spacings and intensities given by *Midgley* 1957 in brackets): 5.06 (5.08—5), 4.10 (4.15—5), 3.18 (3.19—10), 3.11 (CH), 2.80 (2.84—10), 2.71 (2.74—10, 2.67—5), 2.63 (CH), 2.13 (2.145—8), 1.785 (1.805—8, 1.776—8, 1.797—CH) Å, etc. Several important afwillite reflexions are missing in this list, but the agreement is still sufficiently good to warrant an identification of the material as afwillite.

In similar ED patterns from this sample, reflexions were observed at 6.49, 5.03, 3.20—3.17, 2.83—2.79, 2.74 Å, etc., in addition to CH reflexions. These reflexions are obviously those which show up most readily in ED patterns of this variety of afwillite.

EM (191): Specimen area containing rather large plate crystals, without very pronounced crystalline habits.

Figs. 192—194. Sample Tw—6A.

EM (192): Survey of various formations observed in the sample, prismatic crystals of afwillite, in the 1000 Å size range, plate crystals of CH, with irregular and flaky edges, and some long slender ribbons of a tobermorite variety (cf. Figs. 199 and 200).

EM (193): Crystals of afwillite, plates or prisms with rounded corners, and of CH, plate with irregular edge.

ED (194): This pattern, which is representative of the sample, contains CH reflexions at 3.11, 2.63, and 1.80 Å, together with a number of scattered, weak spot reflexions from afwillite crystals, at 5.06, 4.71, 4.11, 3.19, 2.81, and in the 2.20—1.94 Å region.

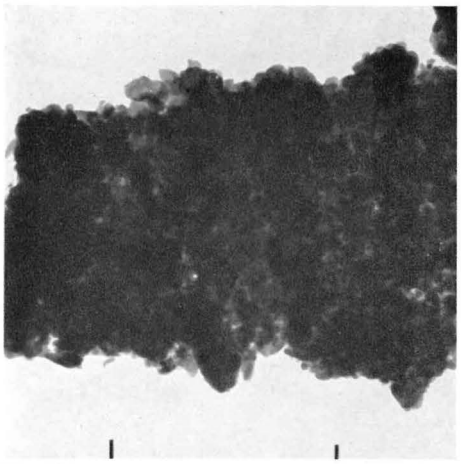

Fig. 190 a

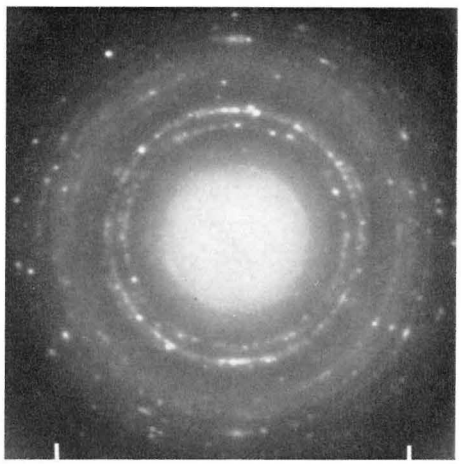

Fig. 190 b

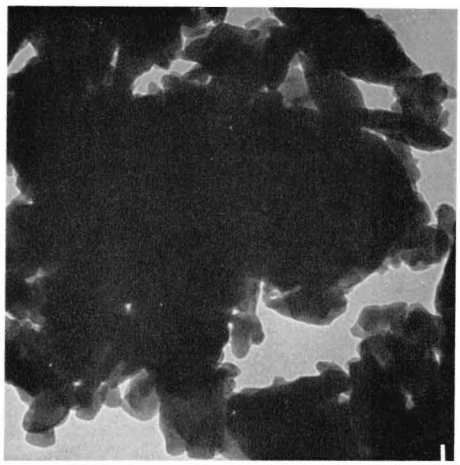

Fig. 191

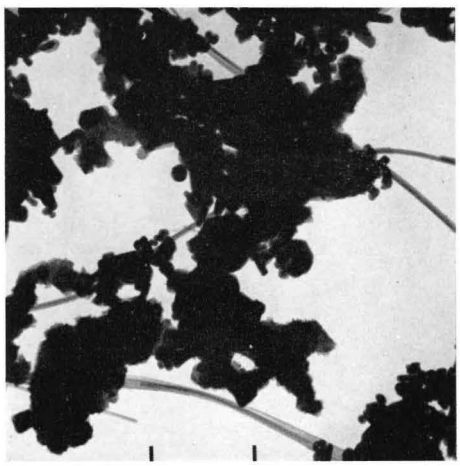

Fig. 192

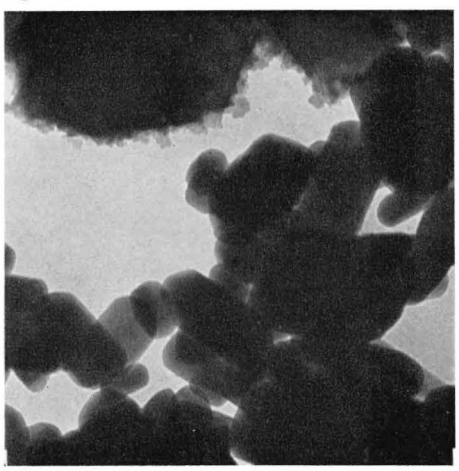

Fig. 193

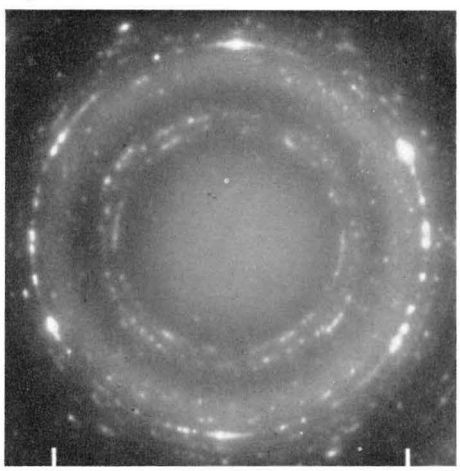

Fig. 194

57. C-S-H

Afwillite in ball-milled C_3S suspensions (continued)

Figs. 195 and 196. Sample Tw—5.

EM (195a): Flaky aggregates, mixture of CH and afwillite crystals.

ED (195b): Mainly CH spot-ring pattern, with additional spot reflexions at 4.12, 3.88, 2.805, 2.135 Å. These spacings, as well as others given earlier (cf. Fig. 190b), which have been determined with the CH spacings used as standards for determining the parameter of the diagrams, are in general 0.5 to 1 percent smaller than certain characteristic spacings of the afwillite crystal lattice. The discrepancies may be caused by differences in dehydration shrinkage and in thermal expansion of the CH and afwillite crystals.

EM (196a): Area with three phases: rounded-prismatic particles of afwillite, regularly-hexagonal plates of CH, and aggregates of large, very thin, rounded plates of unidentified substance.

ED (196b): Composite diagram, in which the following features can be distinguished:
(a) scattered spot reflexions from afwillite, at 6.48. 4.12, 2.83—2.79 Å,
(b) (10.0) and (11.0) spot reflexions from CH crystals,
(c) spot-ring reflexions at 2.67 and 1.54 Å (the latter very prominent), probably the (10.0) and (11.0) reflexions from a lattice of hexagonal symmetry and with $a_H=3.08$ Å,
(d) diffuse spots in the 2.45—2.35 Å region, and at 1.50 Å, probably from a product of dehydration of the phase described under (c). This phase (c) is very similar to those shown in Figs. 424—429, and believed to consist of a clay-type silicate hydrate with a true hexagonal unit cell at 5.34 Å, and a strongly pronounced sub-cell 3.08 Å ($5.34/\sqrt{3}$). Crystals of this type were observed in a few areas of the EM specimen.

These could possibly be a spurious formation of clay-type C-S-H compound with a deficient layer lattice, similar to the C-A-H(hex.) compunds discussed in connection with Figs. 57—58. However, it is more likely that they represent a contamination phase, such as a magnesium silicate hydrate of talc or vermiculite type, both of which have pseudohexagonal unit cells of sizes near 5.34 Å. Magnesium hydroxide, gibbsite, with a unit cell $a_H=3.15$ Å. is another possible alternative (cf. Figs. 418—429).

Figs. 197 and 198. Sample Tw—6B.

EM (197): Survey of various formations observed in the sample, mainly aggregates of prismatic crystals of afwillite, of sizes mostly between 0.1 and 0.3μ, together with plate crystals of CH, with irregular and flaky edges, and long, thin ribbons or laths of a tobermorite variety.

EM (198): Afwillite, crystals of rounded, prismatic or slab-like habits. As stated in the list of samples, the sample Tw—6 was processed for the purpose of increasing the size and improving the crystallinity of the afwillite crystals. It is evident that the treatment by boiling and refluxing has been successful in this respect. However, the afwillite seems to be unstable in relation to another phase that develops slowly under the conditions chosen for the treatment (cf. next page).

The samples shown on this page are closely similar to the afwillite samples shown by *Copeland et al.* 1960, 1962a.

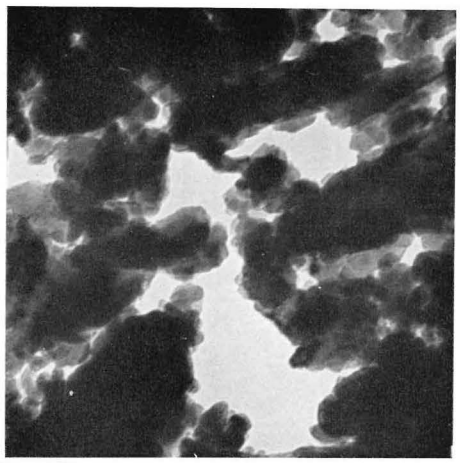

Fig. 195 a

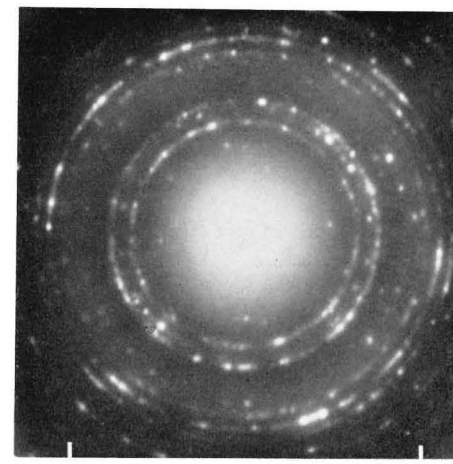

F g. 195 b

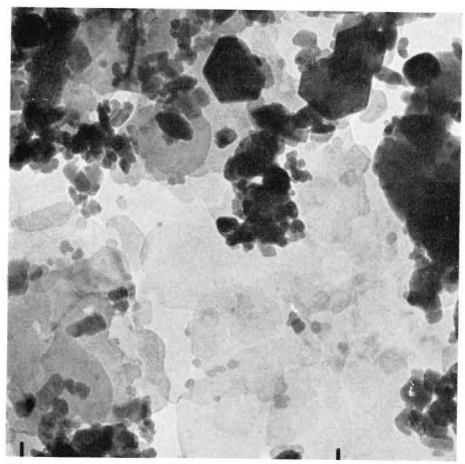

Fig. 196 a

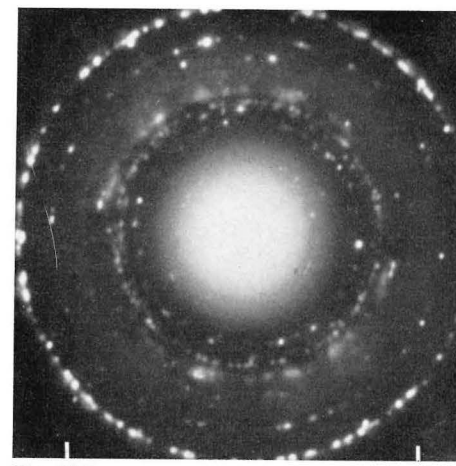

Fig. 196 b

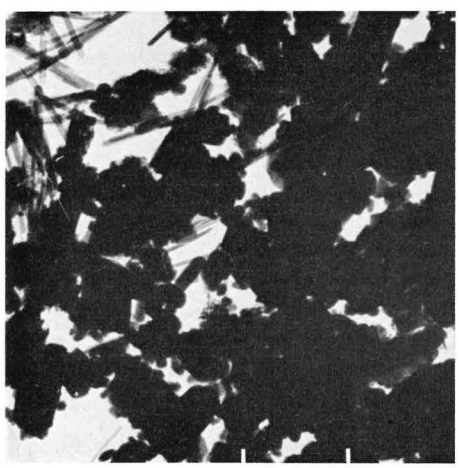

Fig. 197

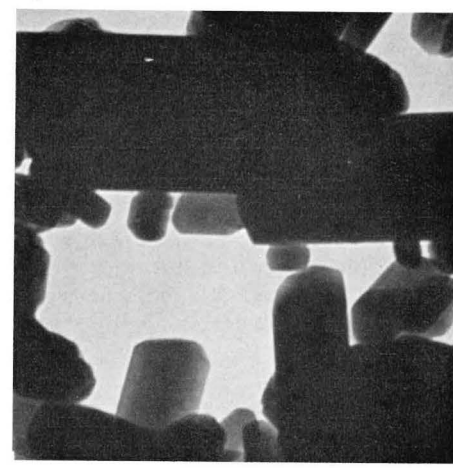

Fig. 198

58. C-S-H

Recrystallization in ball-milled and boiled C_3S suspension

Figs. 199 and 200. Sample Tw—6B.

EMs (199, 200a): Network of lath-like or ribbon-like crystals, with straight, parallel edges and fairly uniform thickness and width, the latter about 500 Å. These formations were observed in several areas of the EM specimen, and seemed to have crystallized out from the afwillite-CH mixture.

ED (200b): Spot-ring powder diagram given by crystals in a $5\times5\mu$ area (about the size of Fig. 199).

EDs (200c—e): Single-crystal spot patterns given by crystals isolated by selective screening.

In the ring diagram, the following series of spacings is found, (three prominent spacings in italics), and compared with the spacings of a primitive, orthogonal cell $a\times b=5.38\times3.60$ Å (spacings and indices in brackets): 5.38 (5.38 (10)), 3.56 (3.60 (01)), *2.96* (2.99 (11)), 2.69 (2.69 (20)), 2.45 (weak spots), 2.15 (2.155 (21)), 1.95 (spots), *1.797* (1.800 (02)), 1.793 (30)), 1.702 (1.707 (12)), *1.616* (1.612 (31)), 1.54—1.53 (weak spots), 1.490 (1.496 (22)), 1.350 (1.345 (40)), 1.256 (1.260 (41)), 1.167 (1.172 (13)), 1.082 (1.078 (42), 1.076 (50)), 1.038 (1.032 (51)) Å, etc. The agreement between measured and calculated values is satisfactory, even if some of the less prominent reflexions fall outside the main pattern. Thus the principal component of the material in Figs. 199 and 200 is a layer-lattice phase with a cross-grating unit cell of size about 5.4×3.6 Å. This phase has been described earlier (*Grudemo* 1962), and was then considered to be an example of the hypothetical high-lime tobermorite phase with an asymmetrical unit layer, as described in the discussion following Fig. 153. So the observed unit cell must be only a pseudo cell, a strongly pronounced sub-unit of a face-centered 10.8×7.2 Å cell. Another alternative is that it corresponds to a structure containing hydrogen-bonded chains, arranged sideways in a simple manner that does not give a doubling of the *a* dimension, as suggested in the discussion following Fig. 153. From this limited amount of experimental data, it is impossible to decide which alternative is the most likely, or if there is a third one.

Only one example was recorded of a single crystal with the simple cell. This is reproduced in the pattern of Fig. 200 c, which corresponds to a cell of dimensions $a\times b=5.18\times3.59$ Å. It is not known whether the reduction in the *a* dimension is caused by differential dehydration shrinkage, or if the pattern is given by a crystal with the *a* axis tilted about 15° out of the image plane. The distributions of strong reflexions is somewhat reminiscent of that of patterns of C-S-H particles in certain paste preparations, such as those shown in Figs. 271—272, and is indicative of a tendency towards face-centered arrangement of important ionic groups within the unit cell.

The two other single-crystal patterns shown, Fig. 200d—e, are of a different type. The reflexions are arranged in rows, similar to the layer-lines of ordinary X-ray rotation diagrams. It is believed that this phenomenon is generally associated with, or even caused by, the

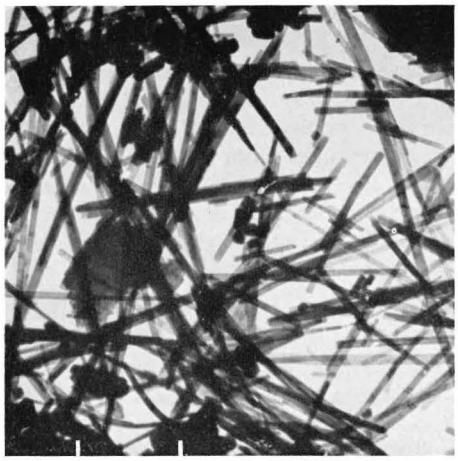

Fig. 199

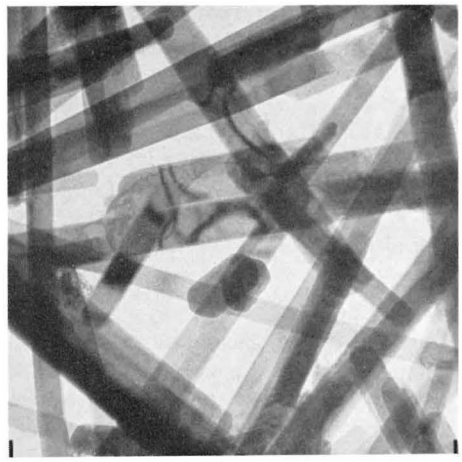

Fig. 200 a

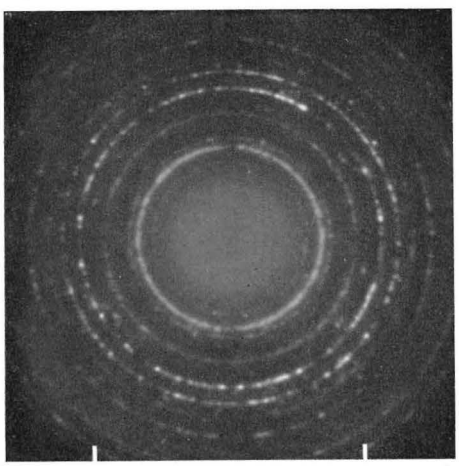

Fig. 200 b

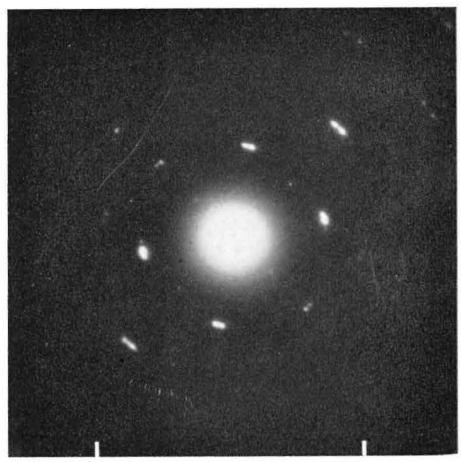

Fig. 200 c

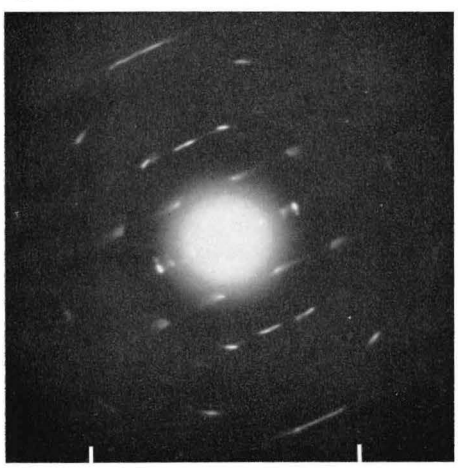

Fig. 200 d

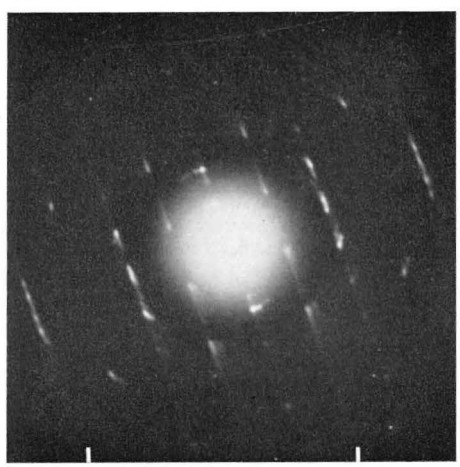

Fig. 200 e

presence of curved or rolled lattice layers (cf. the gypsum patterns in Figs. 121–123) in a structure containing chain elements running perpendicularly to the layer-lines. In this case the distance between layer-lines corresponds to a chain unit of 5.25 Å. In the zero-order layer-line, there is a series of spot reflexions which corresponds to sub-multiples of a spacing of 7.25 Å. There is no such orderly pattern observed in the layer-lines of higher orders. The layer-lines of odd orders consist of streaks rather than spots, which is usually considered to be indicative of some kind of polymorphic disorder of stacking of layer units or, as is probable in the present case, the existence of more than one alternative for the mutual displacement of adjacent chain units in the structure. Patterns of similar appearance and spacings were also recorded for particles of the fibrous phase seen in Fig. 192.

The detection of a 5.25 Å chain repeat unit in these crystals immediately suggests the presence of metasilicate chains of the most usual type, the pyroxene chain with only two tetrahedral links per repeat unit, corresponding to a length of two oxygen diameters. This unit has not yet been observed in combination with Ca ions. It has been suggested (cf. e.g. *Liebau* 1963), and also verified by analysis of several structures that the two-link chain does not fit together well with chains or layers of oxygen polyhedra coordinated around Ca ions. However, the Ca ion is also known to be adaptable in coordination polyhedra of very irregular or distorted types, and although the existence of a stable, crystalline compound with Ca ions incorporated between pyroxene chains in a regular structure must be regarded with some suspicion, it is not entirely impossible. Figs. 200d–e may be examples of ED patterns given by such a structure. Further, it may be noticed that the distance between the two planes containing the "free" tetrahedral edges on opposite sides of the pyroxene chain is about 3.6 Å. This distance may be related in some way to the observed repeat unit, 7.25 Å perpendicular to the fiber axis.

Thus it would seem that the ring diagram of Fig. 200b, although dominated by the reflexions from the 5.38×3.60 Å cell, should also contain some reflexions which may be related to this latter phase. There are some indications of such reflexions at 2.45 and 1.54–1.53 Å. These reflexions can be found as prominent spots in Figs. 200d–e, the first one in the second-order layer-lines, and the second one as spots arranged in a regularly-hexagonal fashion in the zeroth- and third-order layer-lines. The crystalline material shown in Figs. 199 and 200 a is probably a mixture of two phases, both with silica chain structures, although of different types.

(continued from following page)

As indicated above, the sample contained appreciable amounts of the compound CSH(A) (*Bogue* 1953, first described by *Flint et al.* 1938). This material is structurally very similar to the C-S-$\bar{C}$-H mineral scawtite (cf. *Taylor* 1962), and it has been suggested that CSH(A) is a monocalcium silicate hydrate which has taken up small quantities of $\bar{C}$ (atmospheric carbon dioxide) in its lattice, probably by simple replacement of S by $\bar{C}$, and which has then assumed a crystal structure similar to that of scawtite. The composition may be $CS_{1-y}\bar{C}_yH_x$, with a maximum y of the order of $0.15-0.20$. The C/S ratio is thus more than 1.0. If $\bar{C}$ is introduced by atmospheric contamination of a batch with a C/S ratio of 1.0, it would be natural to have the formation of CSH(A) balanced by a simultaneous formation of a constituent with C/S less than unity. As demonstrated in Fig. 203, this constituent could well be gyrolite, with a C/S ratio of 2/3 (or possibly 3/4). At still lower C/S ratios, about 0.5, other phases of the gyrolite family may be formed, such as Z-phase (*Assarsson* 1962) or reyerite, according to data obtained by *Funk* 1961, who also shows the electron-optical appearance of these products.

59. C-S-H

Xonotlite and gyrolite, autoclaved preparations

Fig. 201. Sample CSwq−2.

EM: Aggregate of xonotlite crystals of fibrous or lath-like habits. According to X-ray diagrams, the sample consists of pure xonotlite with very small crystals (all reflexions are rather diffuse). The composition of xonotlite, according to various sources (cf. *Taylor* 1962), is CSH_x, with $x=0.2$ or a little less.

ED: Spot-ring pattern with the following series of spacings, the two strongest reflexions in italics (corresponding spacings given by *Heller* and *Taylor* 1956 in brackets): 4.25 (4.27—mw), 3.65 (3.65—ms), *3.08* (3.07—vs), 2.82 (2.83—m), 2.51 (2.51—mw), 2.04 (2.04—s), 1.95 (1.95—s), *1.84* (1.84—mw), 1.685 (1.687—vw), 1.53 (1.52—w), 1.41 (diffuse) (1.43—vw, 1.39—vw). The relative intensities deviate considerably from those observed by X-ray diffraction, and some X-ray reflexions of about medium intensity are not recorded in the ED patterns. These effects can probably be ascribed to the presence of textured and disordered lattices in the xonotlite crystals.

Figs. 202 and 203. Sample TSwq−2.

EM (202a): Single crystal of xonotlite, or possibly oriented aggregate of lath-like unimolecular layers.

ED (202b): Single-crystal spot pattern of layer-line type, from (*hk*0) zone of the xonotlite crystal. The unit cell corresponding to this pattern is orthogonal, face-centered, of size $a\times b=17.15\times 3.74$ Å., or somewhat larger, especially along the fiber axis, than the pseudo cell given by *Heller* and *Taylor* 1956. In this pattern as well as in a few others of similar type, there is no sign of a doubling of the 3.74 Å repeat unit, but in a couple of patterns there are weak, more or less continuous streaks halfway between the layer-lines, indicating a true unit cell of 7.48 Å and a very pronounced kind of polymorphic disorder in the lateral association of the xonotlite chains (double three-link metasilicate chains of composition Si_6O_{17}).

EM (203a): Aggregate of thin plate crystals with regularly-hexagonal edge angles, together with fibrous crystals. The plates are probably gyrolite crystals, the fibers are particles of xonotlite or CSH(A) (*Flint's* CSH). X-ray diffraction diagrams of this sample show a mixture of the two latter phases, and certain indications of tobermorite. Gyrolite reflexions are not present in the X-ray diagrams, and only a few particles similar to those of Fig. 203 a were observed in the EM analysis. Thus this compound is a minor constituent of the sample.

ED (203b): Spot diagram, containing mainly one strong pattern of regularly-hexagonal symmetry. The most prominent reflexions are those with indices (20.0) (disappear in the central background intensity of the reproduction), (21.0), (22.0), (41.0) (strongest spots in the pattern), and (52.0), with hexagonal permutations. Measurements on a number of diameters of these spot reflexions give an average value $a_H=9.75$ Å, in good agreement with the value 9.73 Å given by *Taylor* 1962 for gyrolite and related minerals.

(continued on preceding page)

Fig. 201 a

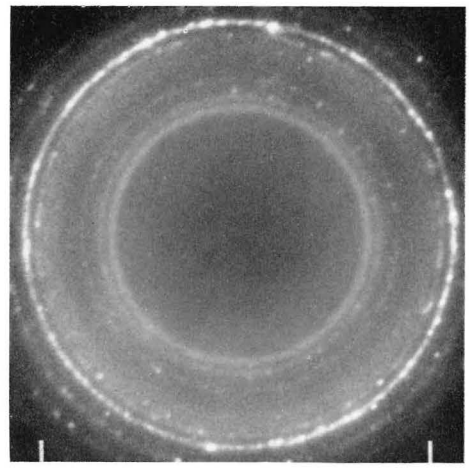

Fig. 201 b

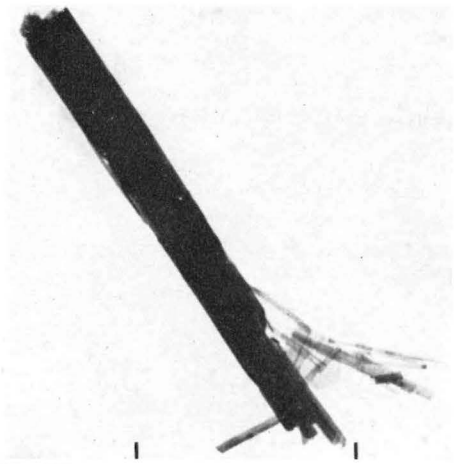

Fig. 202 a

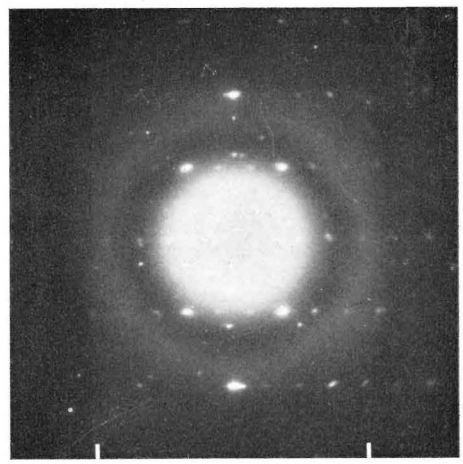

Fig. 202 b

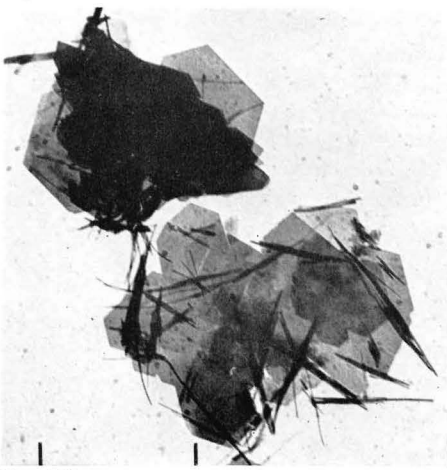

Fig. 203 a

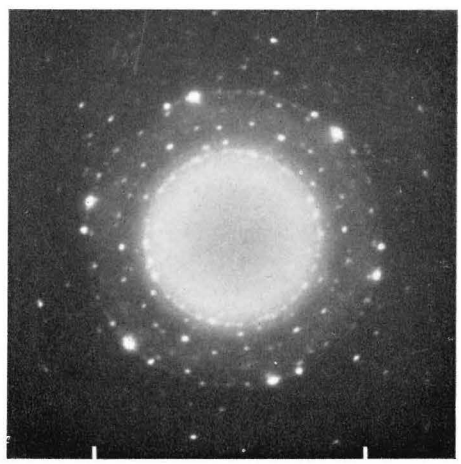

Fig. 203 b

60. C-S-H

Xonotlite, tobermorite, and foshagite, autoclaved preparations

Fig. 204. Sample TSwq—2.

ED: Part of pattern, similar to that of Fig. 202 b, and given by a long, slender xonotlite crystal strip. Measurements give a unit cell $a \times b = 17.38 \times 3.75$ Å. There are faint indications of streaks halfway between the layer-lines.

Figs. 205—207. Sample DSwq—1.

ED (205): Pattern given by a long, thin crystal needle. The sharp reflexions correspond to a primitive, orthogonal cell of dimensions 3.75×7.18 Å, but the streaks and some diffuse spots indicate a true cell $b \times c = 7.50 \times 7.18$ Å. The X-ray diagram of this sample is a mixture of xonotlite and tobermorite (11.4 Å. basal spacing) (cf. Figs. 206 and 207), with xonotlite spacings in good agreement with those given by *Heller* and *Taylor* 1956. Some measured spacings are 8.55(200), 7.05(001), 4.27(400), 3.09(320), 2.35(003), and 1.838(040) Å. The unit cell dimensions calculated from the X-ray spacings are thus $a \times b \times c = 17.1 \times 7.34 \times 7.35$ Å. The explanation for the values measured in ED patterns being about 2 percent higher is not known. It could be that the calibration substance used in this case (very thin Ag layer) is essentially unheated in the electron beam, whereas the isolated crystals of the sample are heated to a couple of hundred degrees (cf. discussion of Fig. 160) and are thus thermally expanded.

EMs: General appearance of sample, mixture of xonotlite and tobermorite. The elongated plate crystals of tobermorite (which is formed after a few hours' autoclaving, according to X-ray diagrams) are gradually transformed to xonotlite, and are then splitting up in bundles of lath-like or needle-like particles (cf. *Kalousek* and *Prebus* 1958).

Figs. 208 and 209. Sample CSwq—3.

EMs: Thick bundles of needle-like or lath-like crystals. The X-ray diagram of this sample indicated a mixture of foshagite, C_4S_3H, and hillebrandite, C_2SH, with the foshagite pattern as the predominant one. The phases and transitions observed in this sample, with C/S 1.5 at 200° C, were CSH(I) up to 10 hours, a mixture of CSH(I) and hillebrandite at 24 hours, and the foshagite-hillebrandite mixture at 48 hours, which is possibly the minimum time needed for the development of a stable phase mixture under the given conditions.

The crystal aggregates seen in the EMs thus consist mostly of foshagite crystals. Since the two patterns are fairly well resolved in the X-ray diagrams, there seems to be no intimate intergrowth of the two crystal species, as suggested by *Heller* and *Taylor* 1956, and as may be expected from the close similarities with respect to the arrangement of structure elements in the wollastonite-foshagite-hillebrandite series, postulated by *Gard* and *Taylor* 1959.

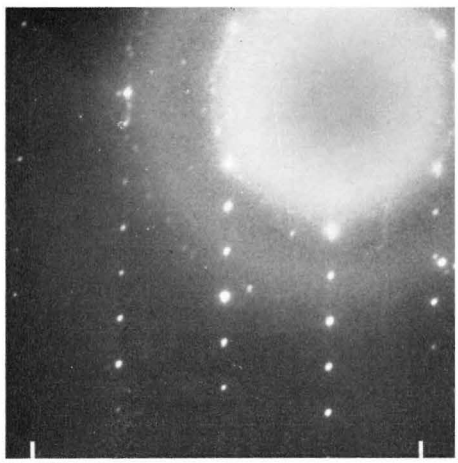

Fig. 204

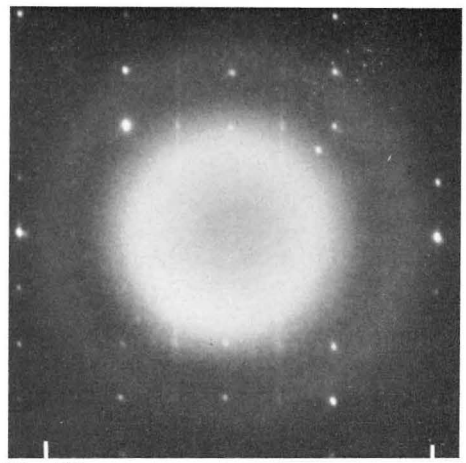

Fig. 205

Fig. 206

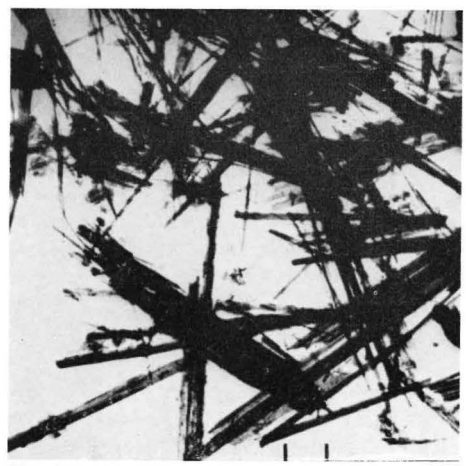

Fig. 207

Fig. 208

Fig. 209

61. C-S-H

Foshagite and hillebrandite, autoclaved preparations

Figs. 210 and 211. Sample CSwq—3.

ED (210): Single-crystal pattern given by long crystal needle, similar to those seen in Figs. 208 and 209. The reflexions can be indexed on the basis of a primitive, orthogonal cell $a \times b = 10.3 \times 3.71$ Å, the latter distance corresponding to the distance between layer-lines. As usual, the true cell is probably twice this value, or 7.42 Å, as indicated by weak, diffuse streaks halfway between the layer-lines in a few ED patterns of similar crystals. The data agree well with the corresponding cell dimensions of foshagite, $a \times b = 10.32 \times 7.36$ Å, observed by *Gard* and *Taylor* 1960.

ED (211): Pattern similar to the preceding one, given by bundle of parallel-oriented needles. The distance between layer-lines and the weak streaks for k odd indicate a fiber axis unit $b = 7.46$ Å. The layer-lines contain many reflexions with general (hkl) indices, but a pattern corresponding to a unit cell $a = 10.15$ Å. predominates.

Figs. 212—215. Sample CSwq—5.

EMs: Bundles of fibrous or needle-like crystals, often radiating out at the ends in broom-like fashion. These are crystal aggregates of hillebrandite. According to X-ray diffraction, this sample consists of pure hillebrandite, with lattice spacings and intensities in excellent agreement with those recorded by *Heller* and *Taylor* 1956. The first-formed products of hydration found in this batch were agglomerates of finely-fibrous C-S-H(I), together with CH. In the period between 3 and 6 hours of autoclaving, there occurred a complete transformation to hillebrandite, which remained stable up to the longest time of autoclaving used in this case, 48 hours.

ED (214): Part of spot pattern, given by long, narrow crystal needle of hillebrandite. The pattern corresponds to a face-centered, orthogonal cell $a \times b = 16.9 \times 3.68$ Å. The presence of diffuse streaks halfway between the layer-lines of certain patterns indicates a true cell $b = 7.36$ Å. Another, similar pattern gave the values $a \times b = 16.65 \times 7.37$ Å. The values given by *Heller* and *Taylor* 1956 are $a \times b \times c = 16.60 \times 7.26 \times 11.85$ Å, cell orthorhombic, with a pronounced pseudo-halving of the b unit. The distances measured in the ED patterns are thus somewhat expanded with respect to the normal ones.

ED (215): Spot pattern given by a hillebrandite crystal of the habit of a thin, transparent strip, about 0.4μ wide. The pattern corresponds to a primitive, orthogonal cell $b \times c = 7.34 \times \times 11.9$ Å. The layer-lines with k odd contain mainly diffuse spots with l even, and are streaky in a way that indicates some degree of polymorphic stacking disorder along the c axis.

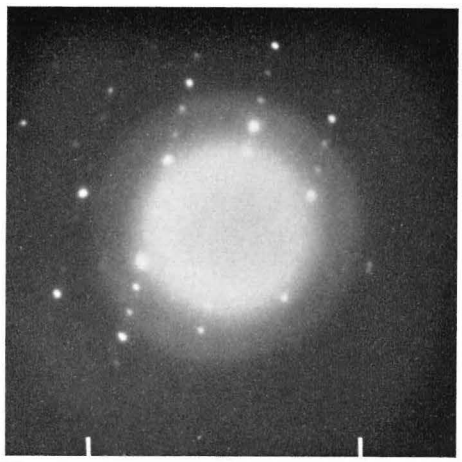

Fig. 210

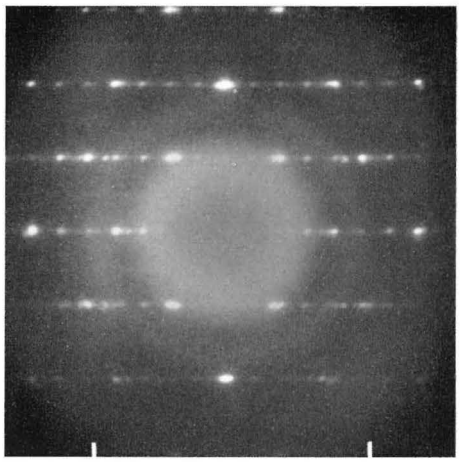

Fig. 211

Fig. 212

Fig. 213

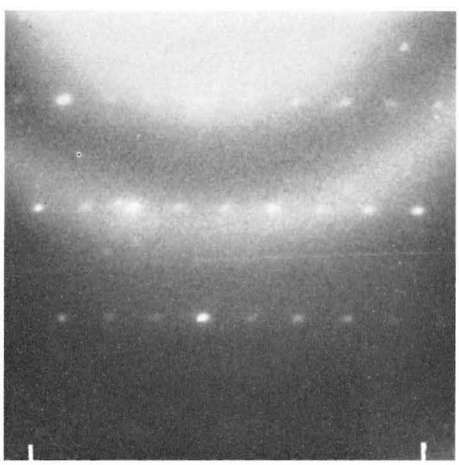

Fig. 214

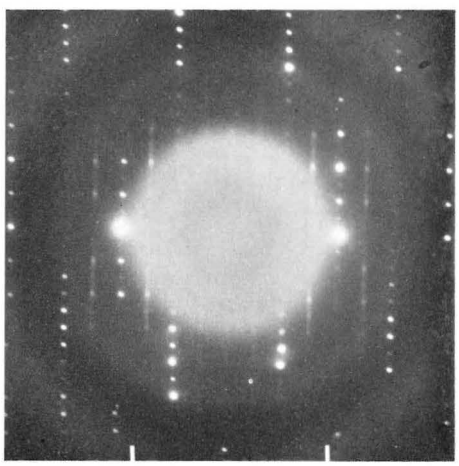

Fig. 215

62. C-S-H

Dicalcium silicate α-hydrate and tricalcium silicate hydrate

Figs. 216–218. Sample Twq–3.

EMs (216, 217): Mixture of crystal phases, block-like crystals of α-C_2SH and needles or rods of $C_6S_2H_3$. The X-ray diagram is also a mixture of patterns from these two phases, together with CH reflexions. The X-ray patterns are in general agreement with those given for α-C_2SH by *Heller* and *Taylor* 1956 and for $C_6S_2H_3$ by *Buckle*, *Gard*, and *Taylor* 1958.

EM (218a): Part of $C_6S_2H_3$ crystal rod. These crystals seem to consist of bundles of thinner units, often with sharply cut-off end faces and internal striations, similar to those observed in ettringite-type particles (cf. e.g. Figs. 109 and 112).

ED (218b): Layer-line diagram from the parallel-oriented aggregate, nearly single-crystal pattern. The distance between the layer-lines correspond to even-order reflexions from a spacing 7.55 Å.

In a number of other diagrams, c spacings varying between 7.50 and 7.64 Å have been measured. The (00.4) reflexion is very prominent in these diagrams. In Fig. 218b, there is no obvious order in the reflexions along the layer-lines. In a few other diagrams from $C_6S_2H_3$ particles, reflexions of various orders from a spacing 10.0 Å can be observed (cf. Fig. 400b).

The exact crystal structure of $C_6S_2H_3$ is unknown. *Buckle et al.* 1958 suggested a structure with a hexagonal or trigonal unit cell $a_H=10.0$ Å, $c_H=7.48$ Å. The silicate anions are probably dimeric Si_2O_7 groups, arranged with their trigonal axes in parallel in some kind of hexagonal pattern. An alternative structure proposed by *Mamedov*, *Klevtsova*, and *Belov* 1959 also contains Si_2O_7 groups with their trigonal axes in parallel along the fiber axis. However, they are not arranged in a hexagonal pattern, but built together with Ca-O octahedra into so-called tilleyite bands, arranged in parallel and linked together by pairs of Ca-OH octahedra. The structure is orthorhombic with $a\times b\times c=17.2\times 10.5\times 7.63$ Å, but can be regarded as pseudohexagonal, since the ratio a/b is not too far from the orthohexagonal ratio ($\sqrt{3}$). The strong X-ray reflexion at about 8.8 Å, which is characteristic of $C_6S_2H_3$, would in this representation be interpreted as an unresolved doublet of reflexions at 8.95 and 8.6 Å ((110) or ($1\bar{1}0$), and (020), respectively). According to the X-ray diagrams recorded in the present study, the region of appreciable intensity of this reflexion is about 0.15 Å. (8.85–8.7 Å), and there is no indication of a double peak.

Figs. 219 and 220. Sample TSwq–4.

EMs: Rectangular, block-like α-C_2SH crystals and $C_6S_2H_3$ rods (in Fig. 219), together with aggregates of fine fibers, representing the C-S-H(I) phase initially formed from the silica gel mixed with the C_3S. The X-ray diagram of this sample contains an α-C_2SH pattern and some of the stronger $C_6S_2H_3$ reflexions, but no CH. A couple of weak and diffuse C-S-H(I) reflexions present after 7 hours had disappeared at 72 hours.

A number of single-crystal ED patterns, or in most cases only small parts of the complete patterns, were recorded in various samples containing α-C_2SH, for crystals of an appearance similar to that of the block-shaped crystals in Figs. 219 and 220. Unit cells similar to that of α-C_2SH (orthorhombic, $a\times b\times c=9.34\times 9.22\times 10.61$ Å, according to *Heller* 1952) were observed only rarely. The corresponding ED patterns indicated primitive, orthogonal cells, in one case with dimensions 9.3×9.2 Å, in three other cases with dimensions 4.8×9.35 (2) and 4.7×9.1 Å. However, several other patterns given by block-shaped particles corresponded to a face-centered, orthogonal unit cell of dimensions 15.6×4.42 Å. The crystallographic identity of these particles is unknown.

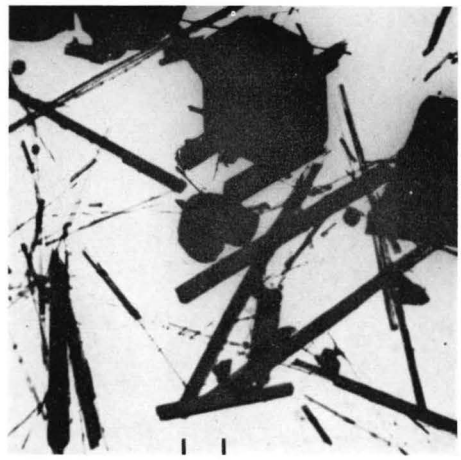

Fig. 216

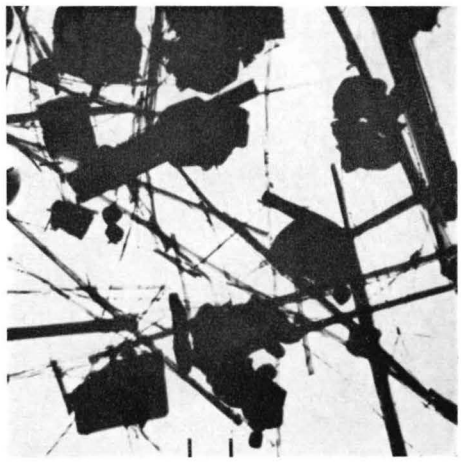

Fig. 217

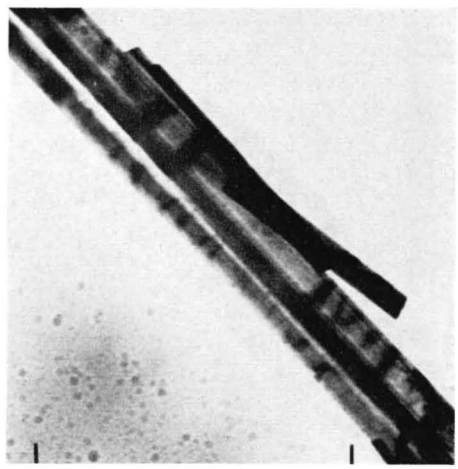

Fig. 218 a

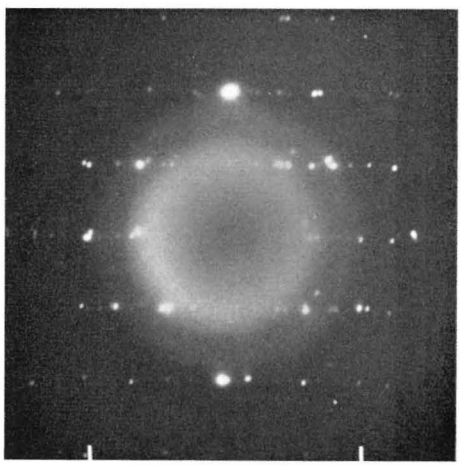

Fig. 218 b

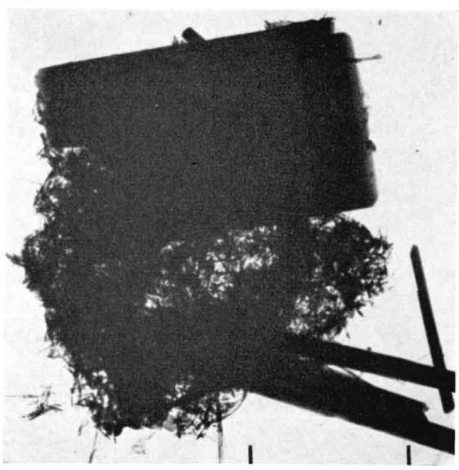

Fig. 219

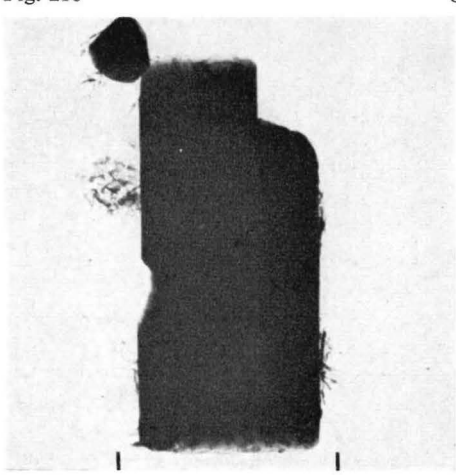

Fig. 220

63. **C-S-H**

C-S-H(I) formed from C_3S suspended in water

Figs. 221—224. Sample Tw—1.

EM (221): Large aggregate of densely-packed C-S-H(I) foils.

EM (222): Transparent part of aggregate, with loosely-wrinkled foils.

EMs (223a, 224a): Flocs of aggregated foils, with appearance characteristic of this sample.

EDs (223b, 224b): Rather strong and sharp reflexion at 2.98 Å, weak indications of rings at 2.76 and 1.81 Å. This pattern is characteristic of badly-crystallized C-S-H(I) of the foil variety, without pronounced fibrosity.

Since a certain amount of CH crystals was observed in this sample, the C/S ratio of the C-S-H(I) phase is probably about 1.5.

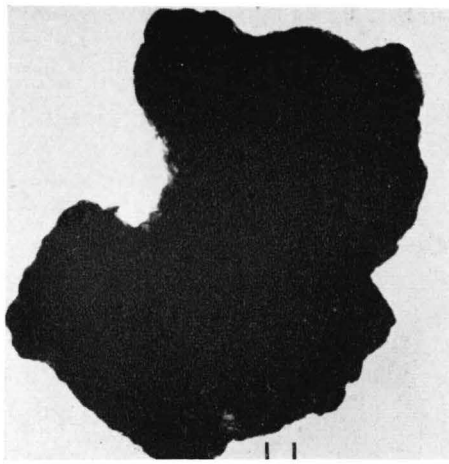

Fig. 221

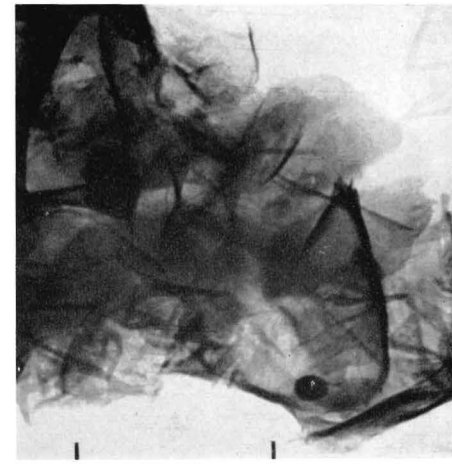

Fig. 222

Fig. 223 a

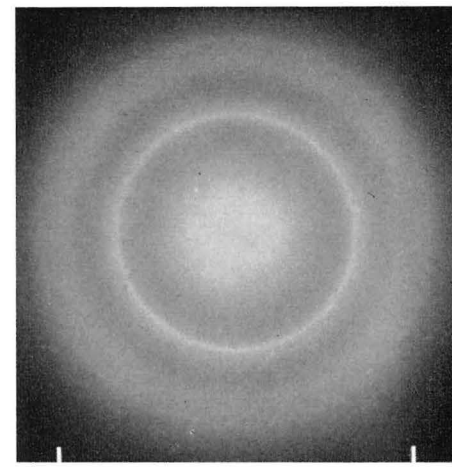

Fig. 223 b

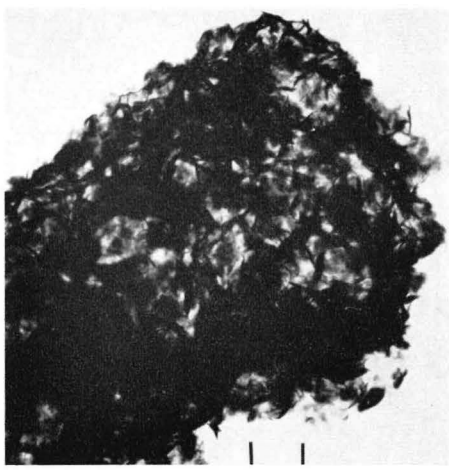

Fig. 224 a

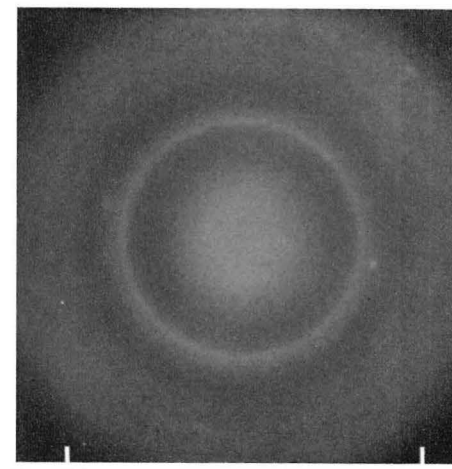

Fig. 224 b

64. C-S-H

C-S-H(I) and (II) formed from C_3S suspended in lime solutions

Figs. 225 and 226. Sample Tl—2.

EM (225a): One type of particle formed from C_3S in a saturated lime solution, thin sheets or foils with rounded contours, which are seen in different stages of rolling or twisting into distorted, scroll-shaped formations.

ED (225b): Diffuse halo in the 3.2—2.6 Å region, with scattered CH and $C\bar{C}$ spots.

EM (226a): Another type of formation characteristic of this sample (and the next one), tapering, cigar-shaped bundles of fibrous elements, resembling the C-S-H(II) structures described by *Grudemo* 1955 and by *Brunauer* and *Greenberg* 1962.

ED (226b): Mainly $C\bar{C}$ (calcite) spot-ring pattern. The C-S-H(II)-type formations are very easily attacked by atmospheric CO_2 slowly penetrating the walls of the polyethylene bottles used in these preparations.

In addition to these two types of formations, the sample contained some quantities of CH precipitates of certain $\bar{C}$-contaminated varieties (cf. Figs. 11, 30, and 31).

Figs. 227 and 228. Sample Tl—1.

EM (227): Lanceolate particle, similar to those shown in preceding EM, protruding from the edge of a large particle.

EM (228): Characteristic edge structures of the larger aggregates of C_3S hydrated in a temporarily supersaturated lime solution, showing a coat of fine fibers covering the original crystals of the anhydrous phase (cf. next page).

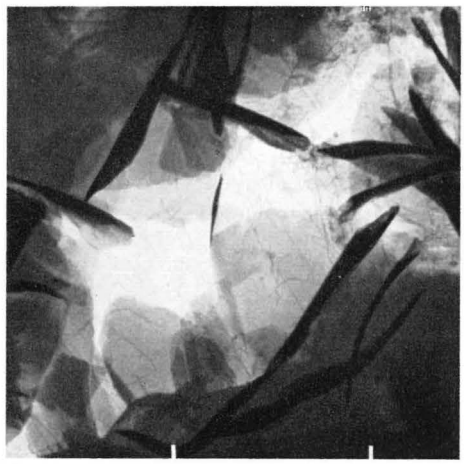

Fig. 225 a

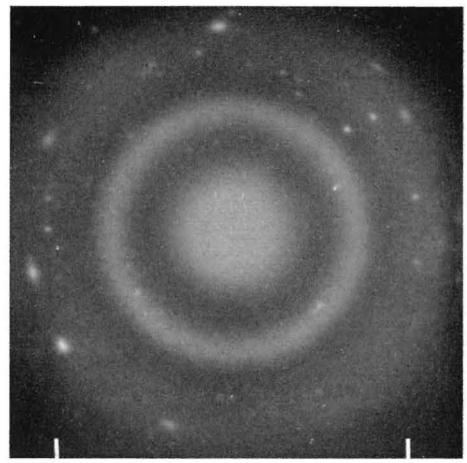

Fig. 225 b

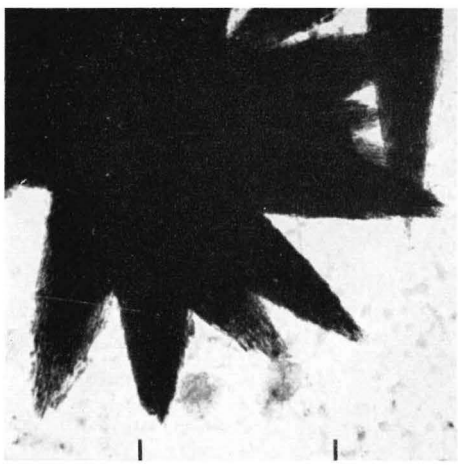

Fig. 226 a

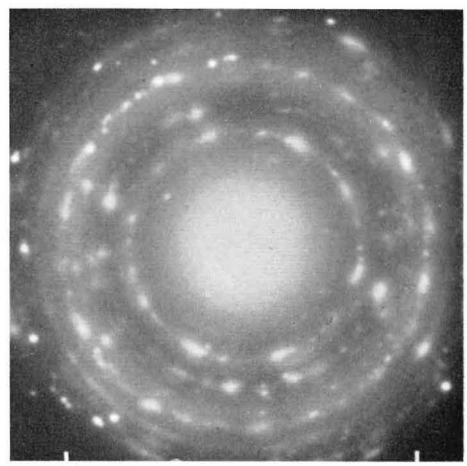

Fig. 226 b

Fig. 227

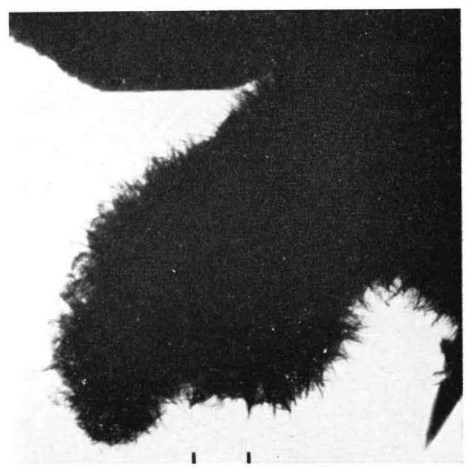

Fig. 228

65. C-S-H

C-S-H(I) and (II) formed from C_3S (continued)

Figs. 229 and 230. Sample Tl—1.

EMs: Characteristic structures formed from C_3S in supersaturated lime solution, larger aggregates covered with a surface coat of fine fibers, in some places with lanceolate, C-S-H(II)-type particles. Other formations are angular particles (Fig. 229, possibly regular calcite crystals), and a background precipitate of thin, crust-like particles (Fig. 230, probably $\bar{C}$-contaminated CH structures).

Figs. 231 and 232. Sample Tw—3A.

EMs: With C_3S shaken vigorously in a concentrated water suspension, the original crystals could not be dispersed as readily as the corresponding cement slurries (cf. e.g. Figs. 132—135). On some particles, a thin coat of fibers had started to grow out from the surface (Fig. 232), and hexagonal plates of dissolved and reprecipitated CH crystals could also be observed (Fig. 231).

Figs. 233 and 234. Sample Tw—3B.

EMs: After one day, the C_3S crystals were covered with a rather thick coat of finely fibrous particles, similar to those seen in e.g. Fig. 228. This structure was the only one observed in the sample. The ED patterns were diffuse and indistinct.

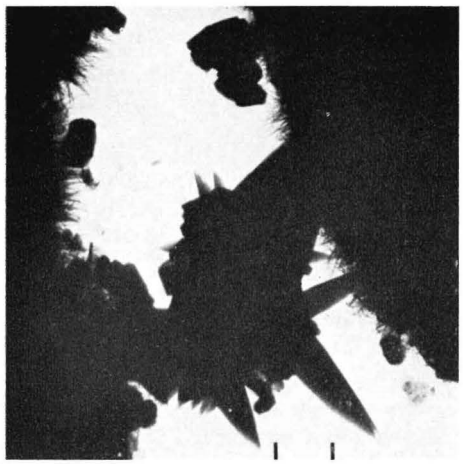

Fig. 229

Fig. 230

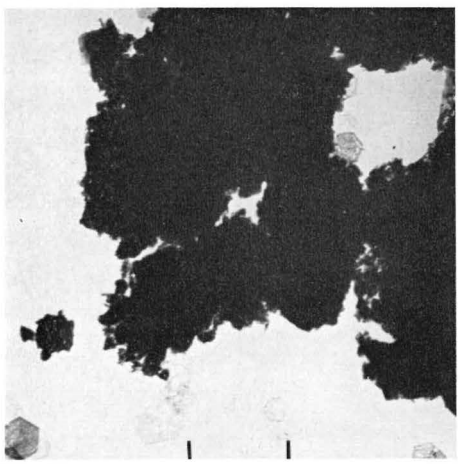

Fig. 231

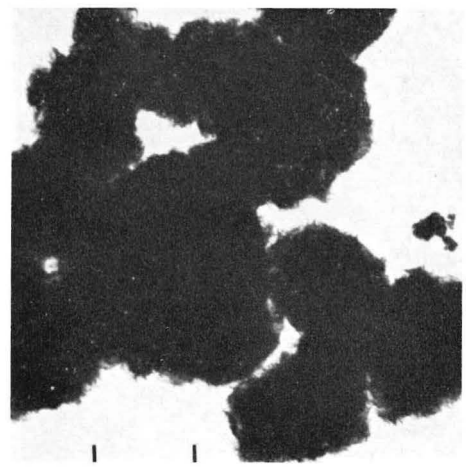

Fig. 232

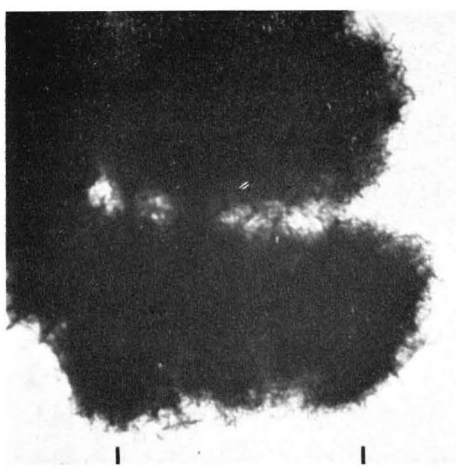

Fig. 233

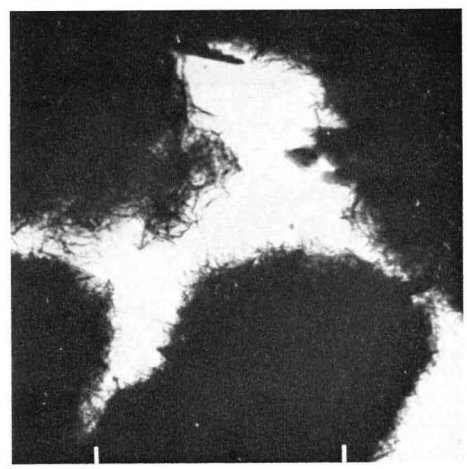

Fig. 234

66. C-S-H

Fibrous forms of C-S-H(I) or (II), from C_3S or cement suspensions

Figs. 235—238. Sample Tw—3C.

EMs: After some weeks, the hydration of sample Tw-3 (cf. preceding page) appeared complete, and the only structures observed were distorted foils and slender fibers of either C-S-H(I) or (II).

EDs: The ED patterns given initially by all these various formations were diffuse rings at 3.2—2.6 Å (Fig. 237). However, especially the diffuse patterns from the fibrous particles (Figs. 236 and 170) were extremely unstable, when exposed to the electron beam, and converted readily to a type of spot-ring pattern shown in Fig. 238. This conversion seemed to occur suddenly during the ED inspection, and was not accompanied by any definite change of particle habits. The new pattern contains the following reflexions: 3.97, (3.48), 3.22, (2.96), *2.85—2.76* (strong reflexion, probably incompletely resolved doublet), 2.46, (2.34), 2.26, 2.09, 1.98, 1.75, and 1.61 Å (less certain reflexions in brackets). These reflexions do not agree with the X-ray pattern of any known C-S-H compound, but there is a certain resemblance to the patterns listed by *Heller* and *Taylor* 1956 under the formulae $C_6S_3H_2$ (dicalcium silicate hydrate (D)) and $C_2SH_{1/2}$, the phases later reviewed by *Taylor* 1962, 1964 under the collective denomination "phase Y".

Fig. 239. Sample Pw—3A.

EM: Finely fibrous C-S-H(I) or (II) compound formed in a boiling cement suspension.
ED: Diffuse halo at 3.1—2.7 Å, and some spot reflexions at 1.70 Å (C (220) reflexion).

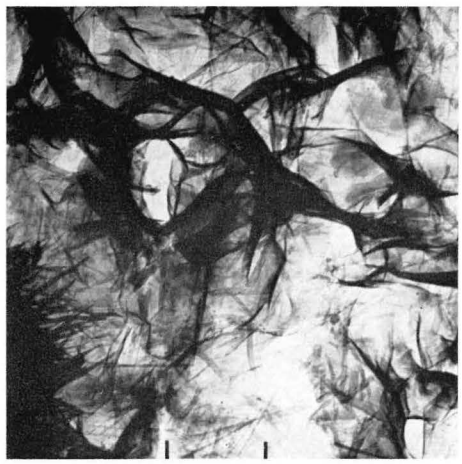

Fig. 235

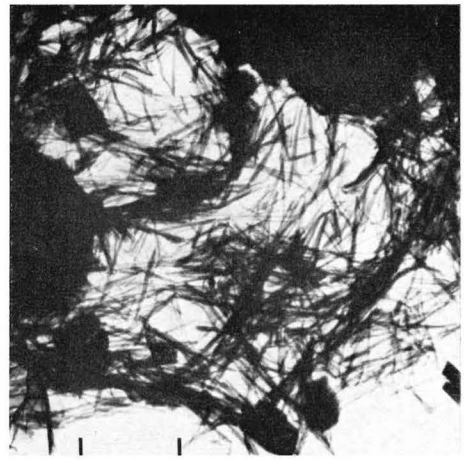

Fig. 236

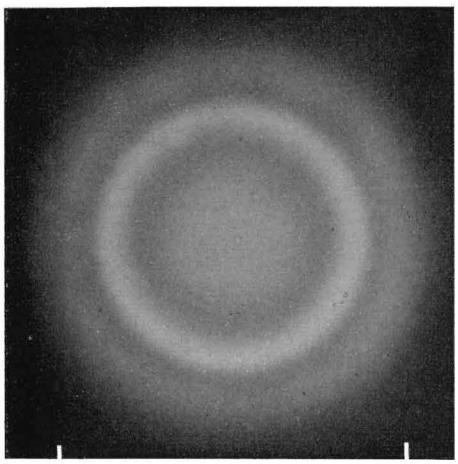

Fig. 237

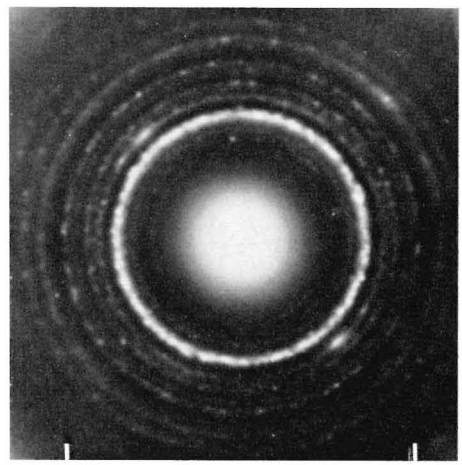

Fig. 238

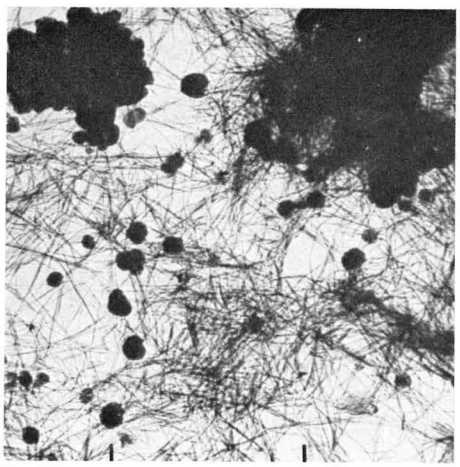

Fig. 239 a

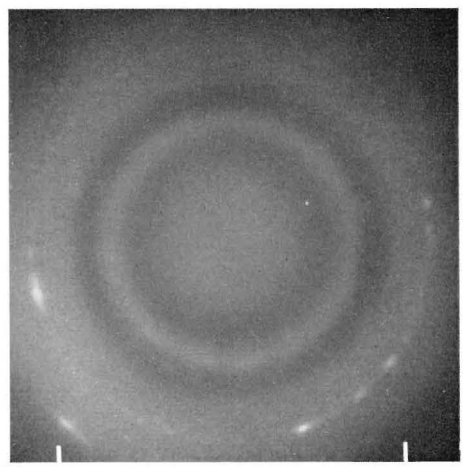

Fig. 239 b

67. C-S-H

Various structures formed at 100° C in C_3S or cement suspensions

Figs. 240—242. Sample Tw—2.

EM (240a): Structure characteristic of the sample, large, thin foils, partly open, partly crumpled at the edges, or twisted together in rolls.

ED (240b): Diffuse halo at about 3.05—2.7 Å, and weak rings at 2.40 and 1.70 Å (C (200) and (220) reflexions).

EMs (241 and 242): Other characteristic formations, curvilinear and branched, fibrous particles (Fig. 241), and fan-shaped aggregate of foils (Fig. 242).

Fig. 243. Sample Pw—1A.

EM: Fibrous C-S-H phase formed in boiling cement suspension. As inferred from Figs. 75 and 76, most of the fibrous phase found in this preparation occurred on and around the C-A-H(hex.)-type plates also formed. This is one case where fiber aggregates were observed without association to hexagonal plate crystals.

ED: Weak, diffuse ring at about 2.96 Å, together with CH spot-ring reflexions (3.11, 2.63, 1.80 Å reflexions).

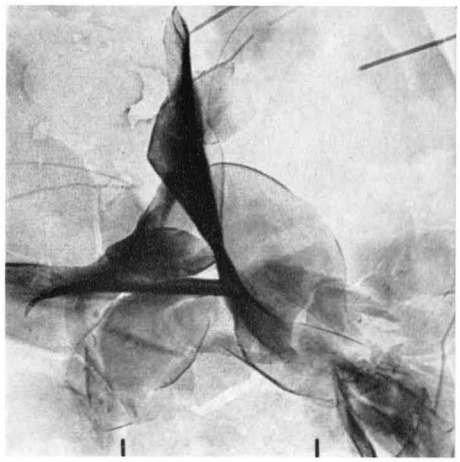

Fig. 240 a

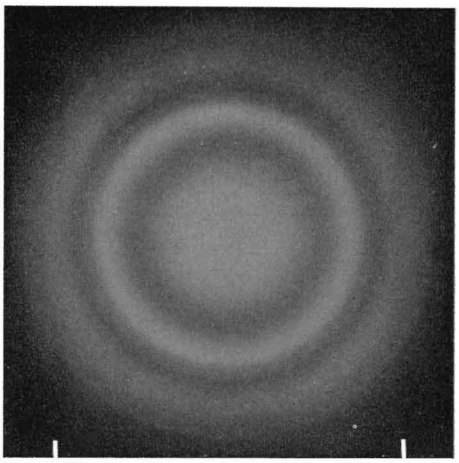

Fig. 240 b

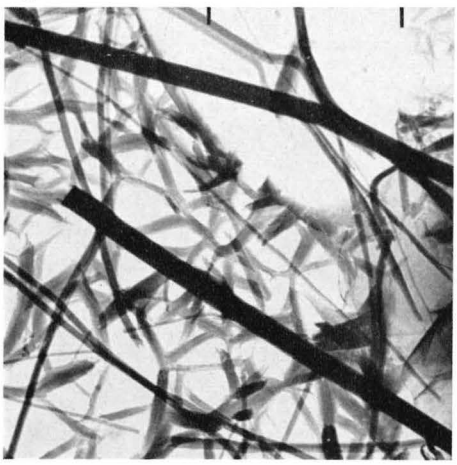

Fig. 241

Fig. 242

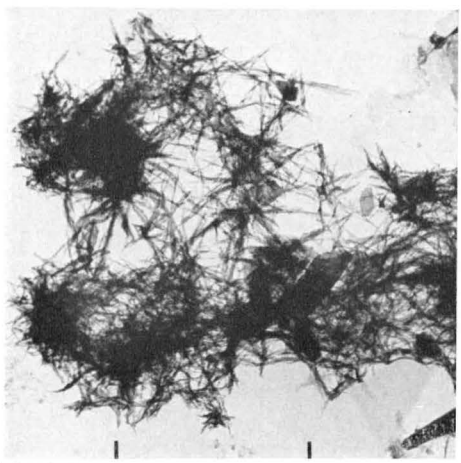

Fig. 243 a

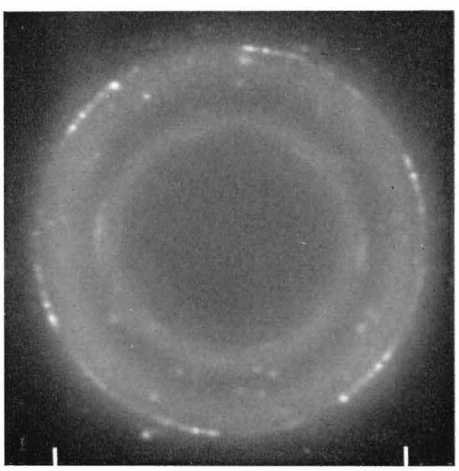

Fig. 243 b

68. C-S-H and C-A-$\bar{S}$-H

Development of C-S-H(I) phase in cement suspensions

Figs. 244 and 245. Sample Pw—4A.

EMs: This sample, prepared immediately after a period of vigorous mixing, seemed to contain mainly ettringite-type rods (cf. Figs. 126—128) and CH plate crystals. At some places, however, the rod formations were partly overgrown by thin, wrinkled foils, probably of C-S-H(I).

Figs. 246—248. Sample Pw—4B.

EM (246): After some hours, the C-S-H(I) foils had grown out further, covering the ettringite-type rod aggregates more or less completely.

EM (247): Aggregates of foils with a more open, less distorted texture were also observed.

EM (248a): Well-developed ettringite-type rods, partly covered with wrinkled foils.

ED (248b): The only ED effect given by this combination of structures was a weak, rather diffuse ring at about 2.95 Å.

Fig. 244

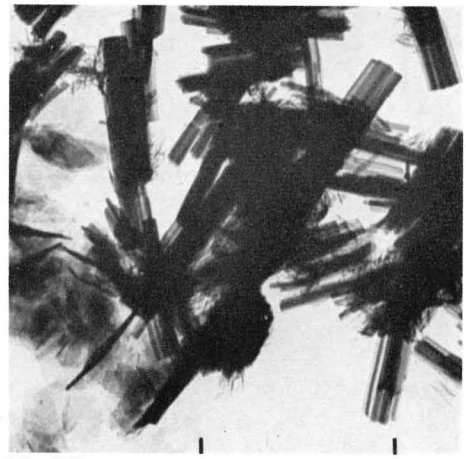

Fig. 245

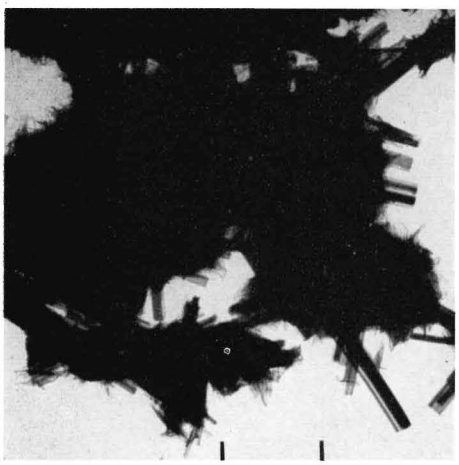

Fig. 246

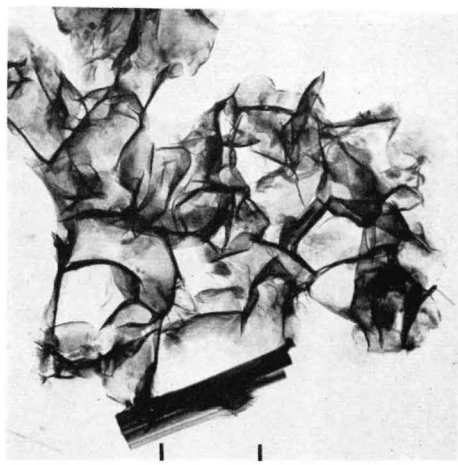

Fig. 247

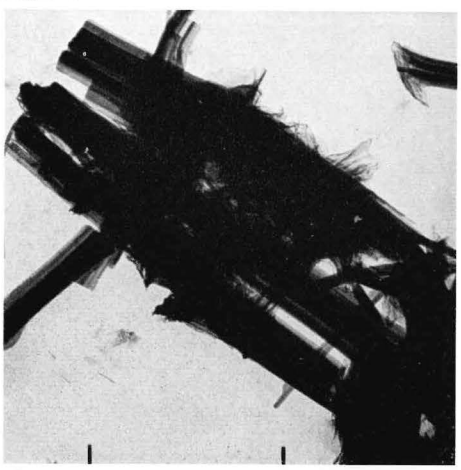

Fig. 248 a

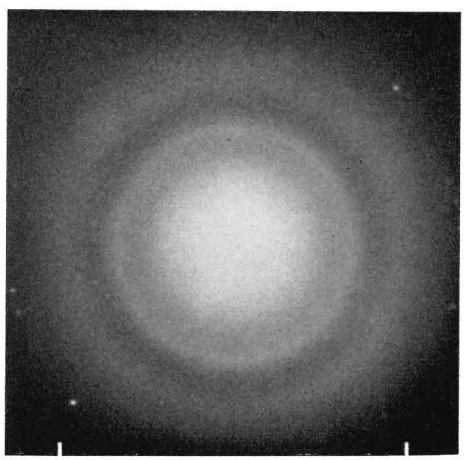

Fig. 248 b

69. C-S-H and C-A-$\bar{S}$-H

Development of C-S-H(I) phase in cement suspensions (continued)

Figs. 249 and 250. Sample Pw—7B.

EMs: After one day's agitation of the cement suspension, a coat of thin, distorted C-S-H(I) foils has started to grow on the surfaces of the original cement crystals, and between the ettringite-type rods formed earlier (cf. Fig. 127).

Figs. 251—253. Sample Pw—6B.

EMs (251a, 252, 253): Ettringite-type formations, covered by C-S-H(I) foils, in later stage of development. The evolution of foils has been accelerated considerably by the initial, vigorous mixing. Fig. 252 is a survey at smaller magnification, intended to show the uniformity of this two-phase mixture.

ED (251b): Weak, somewhat diffuse reflexion at about 2.98 Å, and a few weak CH spots.

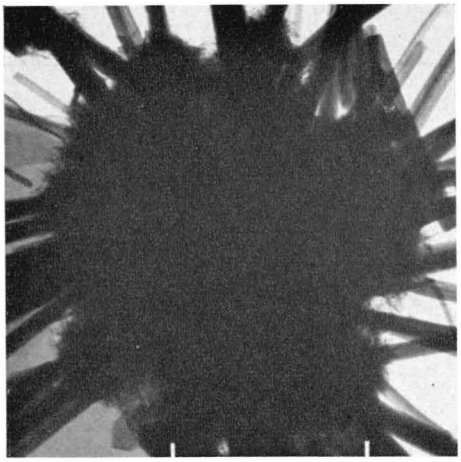

Fig. 249

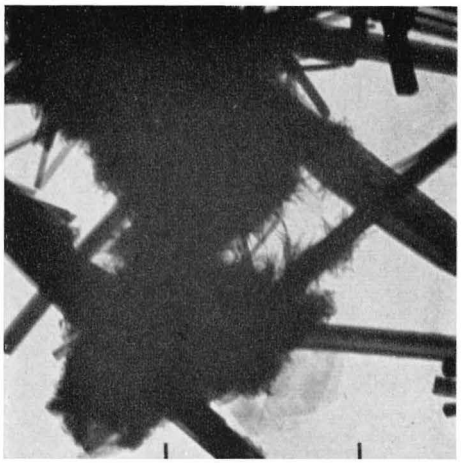

Fig. 250

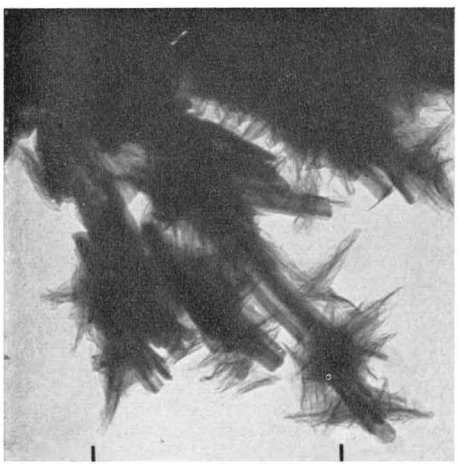

Fig. 251 a

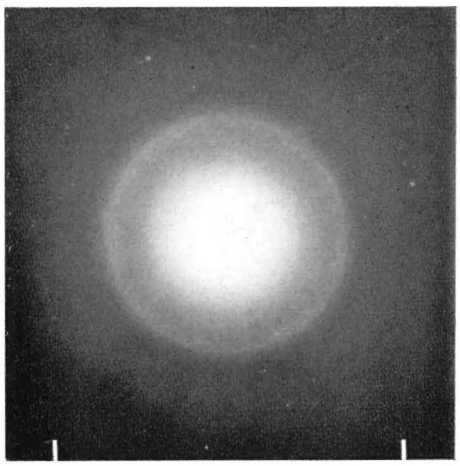

Fig. 251 b

Fig. 252

Fig. 253

70. C-S-H and C-A-$\bar{S}$-H

Development of C-S-H(I) phase in cement suspensions (continued)

Figs. 254—258. Sample Pw—7C.

EMs (254, 255): Survey micrographs of slowly-agitated cement suspension, after 4 days' curing in the sedimented state. The C-S-H(I) foils have grown out further and cover most of the ettringite-type rods. The latter have not grown during the period of standing, but seem to have begun to deteriorate. C-A-H(hex.) plates are still present.

EMs (256, 257, 258a): Various parts of the sample, showing representative structures with rod-like structures wrapped in loosely-wrinkled foils. The appearance of the ettringite rods indicates that they are in the process of dissolution, the material being partly used up for the C-S-H(I) foils growing on them.

ED (258b): C-S-H(I) reflexion at about 2.95 Å.

Fig. 254

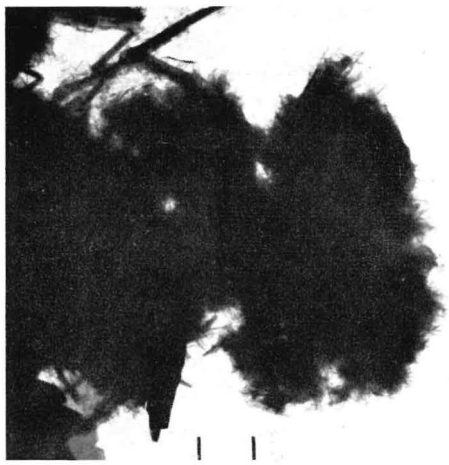

Fig. 255

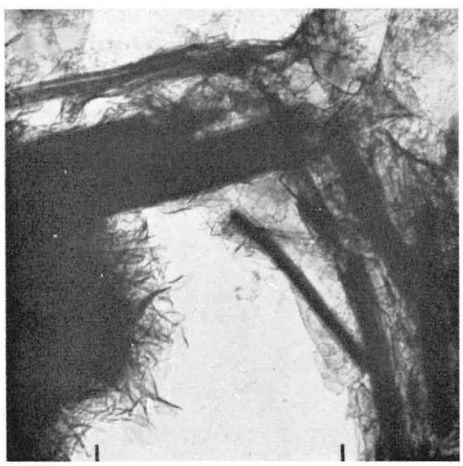

Fig. 256

Fig. 257

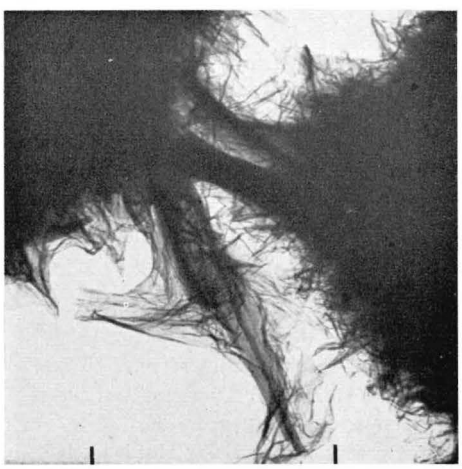

Fig. 258 a

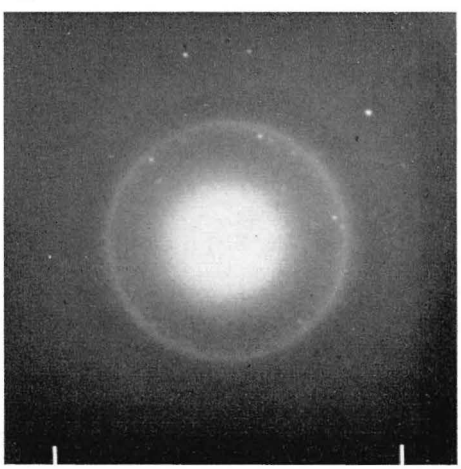

Fig. 258 b

71. C-S-H and C-A-$\bar{S}$-H

Development of C-S-H(I) phase in cement suspensions (continued)

Figs. 259—262. Sample Pw—6C.

EMs (259, 260): Survey micrographs of rapidly-agitated cement suspension, after 3 days' curing in the sedimented state. The ettringite-type rod structures present after one day (Figs. 251—253) were almost completely covered by the C-S-H(I) foils.

EM (261a): The structure has become converted to C-S-H(I) foils, showing at various places an internally corrugated texture, with parallel striations, indicating that the structure has been formed from a matrix of rod-like aggregates.

ED (261b): Rather sharp, prominent reflexion at 2.95 Å, and (in the original) a weak ring at 1.80 Å. This indicates that the degree of crystallinity of the C-S-H(I) phase, although still very low, increases with time (cf. Fig. 251b).

EMs (262a, b): C-S-H(I) foil aggregates and a hexagonal CH plate, same part of sample, before and after heating for about a minute in an electron beam of highest possible intensity. The C-S-H(I) particles move around a little due to this treatment, but are not essentially changed in appearance, nor is there any noteworthy change in the ED pattern before and after the heating. The CH crystal maintains its hexagonal shape but has obviously lost much substance due to dehydration, and is probably converted to C (cf. Fig. 21).

An extrapolation of the data given by *Tamaru* and *Siomi* 1932, shows that the reaction CH→C+H may occur already at 150—120° C at 10^{-3}—10^{-4} mm Hg, which is the range of water vapour pressure that can be expected in the column of the electron microscope. *Tamaru* and *Siomi* observed that the dissociation of CH becomes increasingly sluggish below about 400° C. Thus it is very likely that CH crystals, as well as other hydrates of comparable dehydration characteristics, may reach temperatures of 200—300° C before beginning to decompose at any appreciable rate.

As inferred from the data of Fig. 160, the temperature of the sample can reach this level even in a beam of normal intensity. The temperatures attained with a high-intensity beam are certainly a few hundred degrees higher. However, as indicated by the observations of Fig. 262, the C-S-H(I) structure seems remarkably stable, even at temperatures of about 500—600° C. According to *Taylor* 1964, the structure becomes increasingly vitrified at 400—600° C, and is converted to wollastonite first at about 800° C.

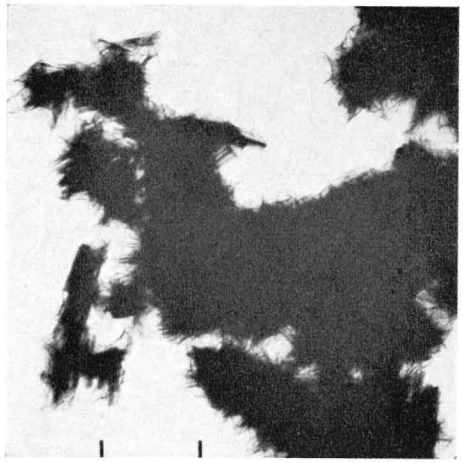

Fig. 259

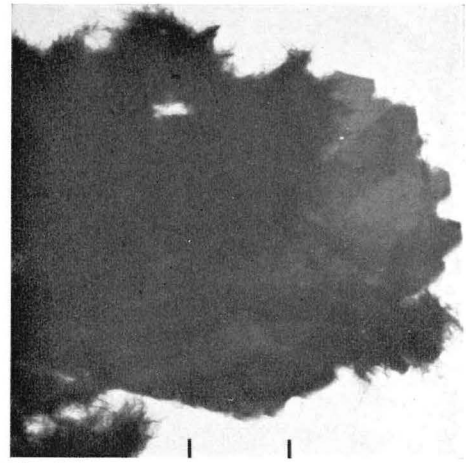

Fig. 260

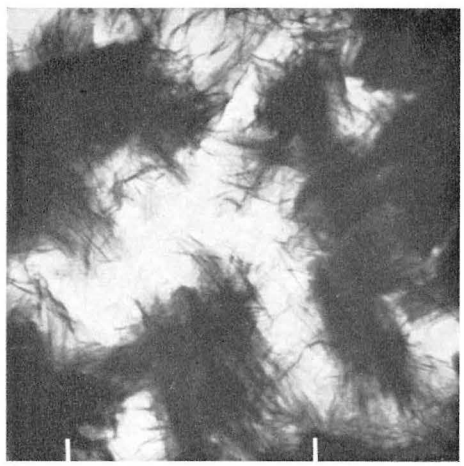

Fig. 261 a

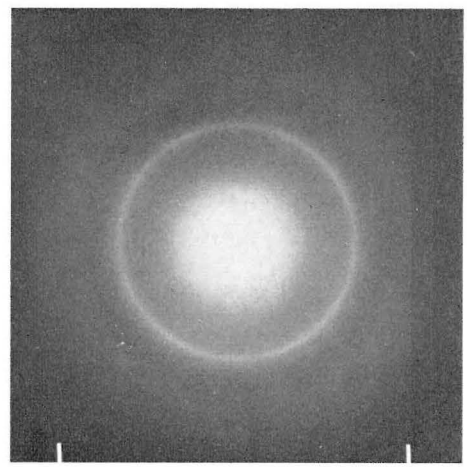

Fig. 261 b

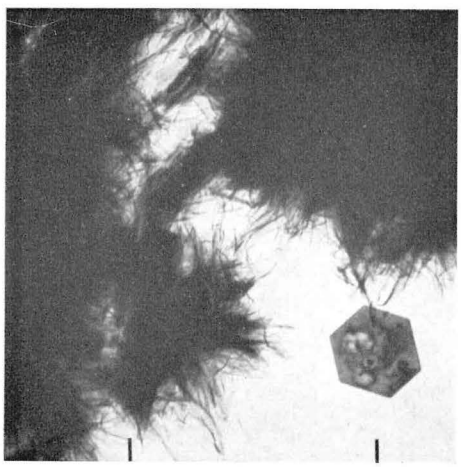

Fig. 262 a

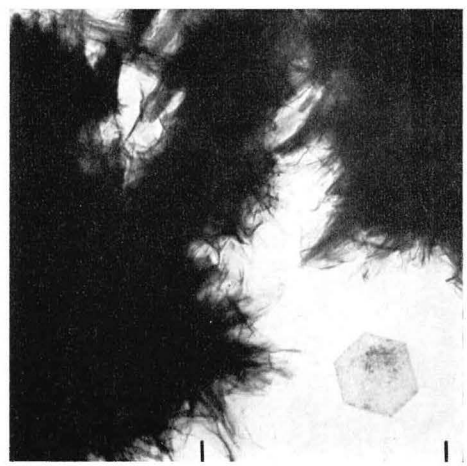

Fig. 262 b

72. C-S-H

Structures formed in β-C_2S paste

Figs. 263—267. Sample Dp—1C.

EM (263): Survey micrograph of representative hydrated structures, from cured, dried, and ground sample redispersed in water for a few minutes. The sample consists partly of elongated, rod-like or needle-like particles, partly of flocky aggregates of irregular particles, but very few CH crystals.

EM (264): Coarsely-fibrous particles and irregular fragments.

EM (265a): Mainly thick bundles or rolls of sheet-like elements, probably with a reed-like internal structure. These particles, as well as similar ones shown on the next two pages, are possibly identical with the columnar or prismatic fragments observed by *Funk* 1960, 1962 in certain products of hydration of β-C_2S. According to *Funk*, these particles are obtained as cleavage fragments in the topotactical conversion of hydrating β-C_2S crystals.

ED (265b): Strong, diffuse halo reflexion at 3.15—2.7 Å.

EDs (266, 267): Two examples of patterns from either unhydrated or recrystallized parts of the sample. From the spot-ring reflexions in Fig. 267, the following series of spacings is obtained: 3.84, 3.39, 3.15, 2.88, *2.78—2.74* (C (111) reflexions and others), 2.41 (C (200) reflexion), 2.21, 2.05, 1.93, 1.70 Å (C (220) reflexion), etc. (most prominent ring in italics). The spacings of Fig. 266 are almost the same, except for the C reflexions, which are missing. The patterns show a certain resemblance to the X-ray diffraction patterns given for various species of β-C_2S, (except for the missing 2.60 Å reflexion), but there is a corresponding degree of likeness to the pattern of afwillite. Moderate heating in the electron beam could well cause this compound to crystallize out in the unstable gel mass.

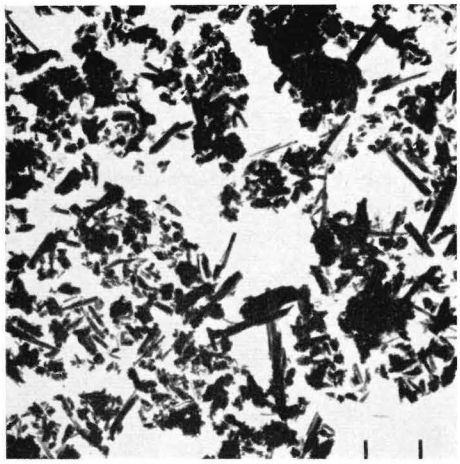

Fig. 263

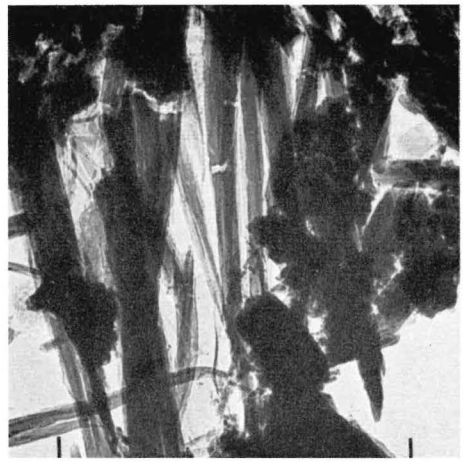

Fig. 264

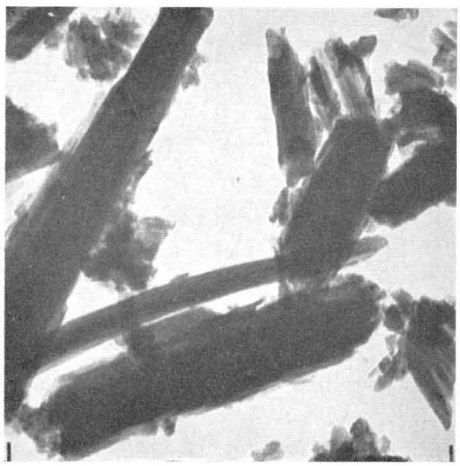

Fig. 265 a

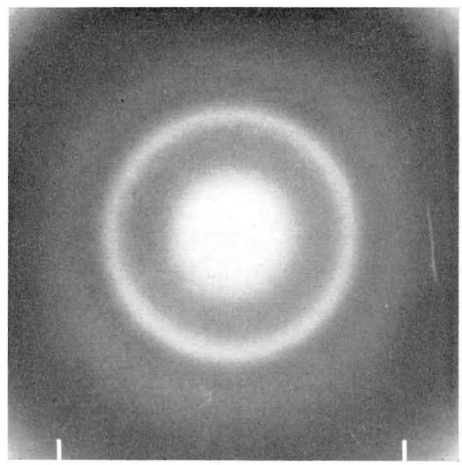

Fig. 265 b

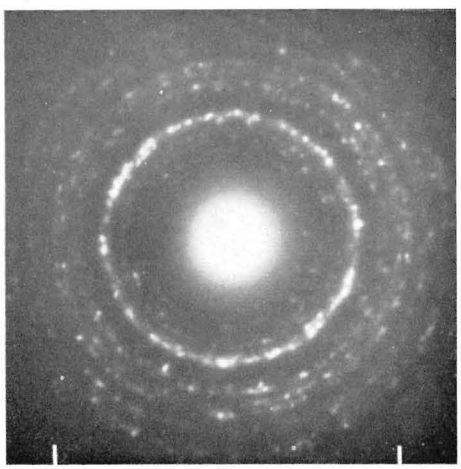

Fig. 266

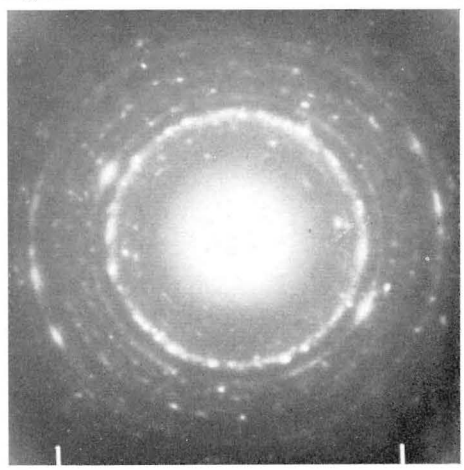

Fig. 267

73. C-S-H

Structures formed in β-C_2S paste (continued)

Figs. 268 and 269. Sample Dp—1B.

EMs: Representative gel structures, bundles of varying thickness, showing characteristic striations parallel to the fiber axis. An unrolled flap of a sheet element can be seen in Fig. 268, some amounts of amorphous material in Fig. 269.

Figs. 270 and 271. Sample Dp—1A.

EM (270a): Particles similar to those above.

ED (270b): Diffuse ring with somewhat irregular and streaky intensity distribution, maximum at about 3.02 Å, and weak but sharp reflexion at 1.82 Å.

EM (271a): Loose aggregate of parallel-oriented, reed-like particles, and some material of irregular structure.

ED (271b): Six diffuse spots at 3.0—2.9 Å, arranged approximately in a regular hexagon, and a fiber unit reflexion at 1.805 Å.

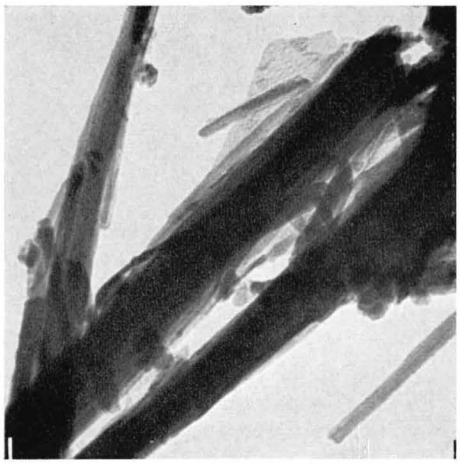

Fig. 268

Fig. 269

Fig. 270 a

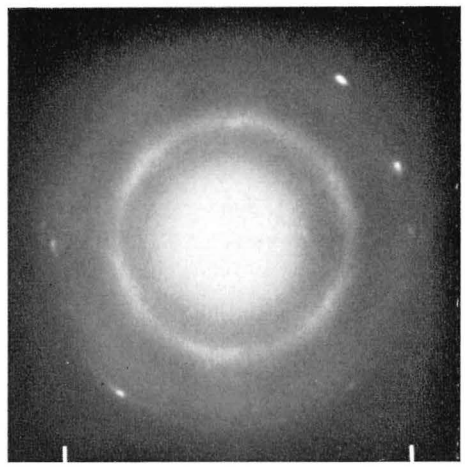

Fig. 270 b

Fig. 271 a

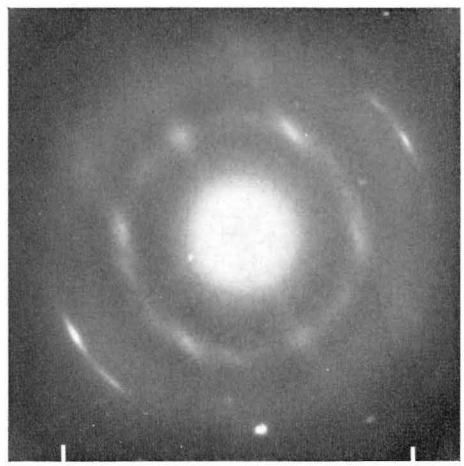

Fig. 271 b

74. C-S-H

Structures formed in β-C_2S paste (continued)

Fig. 272. Sample Dp—1A.

EM: Fiber bundle of characteristic, striated appearance.

ED: Well-developed C-S-H(I) or C-S-H(II) fiber pattern, with six diffuse spots in approximately regular, hexagonal arrangement at about 3.0 Å, and a fiber reflexion streak at 1.825 Å. The spots are somewhat elongated in the direction of the streak, in a fashion reminiscent of layer-lines. This type of pattern (Figs. 271b, 272b) is related both to the single-crystal pattern of Fig. 153b, and the oriented-fiber pattern of Fig. 320b. The degeneration of the single-crystal pattern can be due either to lattice distortions such as the curving of lattice planes in the rolled sheet elements of the particle in e.g. Fig. 272a, or lattice restrictions in one or two directions, as is probably the case in very narrow band elements or thin fibers.

Fig. 273. Sample Dpq—1.

Fig. 274. Sample Dpq—2.

EMs: These samples, β-C_2S paste autoclaved for three days at 100 and 150° C respectively, are similar with respect to morphologic appearance of the hydrated phase developed. This consists of a growth of fine fibers around the initial, anhydrous particles. The ED patterns contain mainly a diffuse halo at about 3.0 Å. In sample Dpq—2, occasional crystals of other types were observed. The X-ray diagrams consist of β-C_2S powder patterns of intensities comparable to those of unhydrated material, without any sign of the development of hydrated phases.

Fig. 275. Sample Dpq—3.

EM: Characteristic appearance of main hydrated phase, elongated, splintered sheets or lath-like crystals, similar to those found in sample Dwq—1 (Figs. 152 and 153).

ED: Single-crystal pattern from an isolated, lath-shaped crystal. The diagram of stronger spots corresponds to a face-centered unit cell $a \times b = 5.60 \times 3.73$ Å, and thus strongly resembles an ordinary tobermorite diagram.

The pattern also contains weaker spots (best visible on the original microfilm) distributed in exactly the same way as described for Fig. 153b. The true unit cell therefore seems to be primitive, orthogonal, of cell dimensions $a \times b = 11.2 \times 3.73$ Å. As was suggested in the discussion following Fig. 153, this cell can be associated with the presence of hydrogen-bonded chains, of the type described by *Bernal* 1954.

The X-ray diagram of this sample contains a β-C_2S pattern of weakened intensity, and a number of additional, slightly broadened lines at 3.04 (s), 2.69 (vw), 2.59 (w), 2.48 (w, diffuse), 2.33 (vw), 1.91 (m), 1.89 (m) 1.80 (mw) Å. These are reflexions characteristic of compounds of the calcio-chondrodite or γ-C_2SH family, as discussed further in connection with Fig. 152. The strong reflexion of α-C_2SH at 3.27 Å is also present as a weak line. A moderately strong α-C_2SH pattern is present in the X-ray diagram at 24 hours, but seems to be replaced by the γ-C_2SH pattern in the later stages of curing. There is no sign of X-ray reflexions corresponding to the tobermorite-like phase identified in several ED patterns.

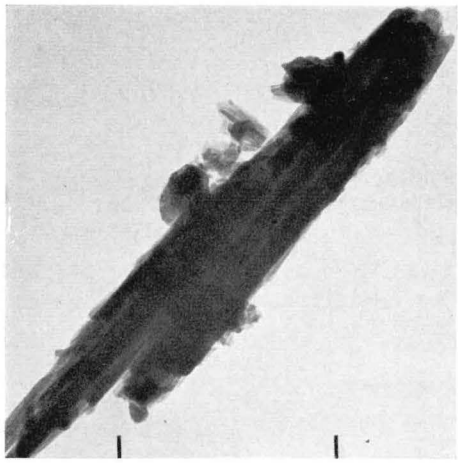

Fig. 272 a

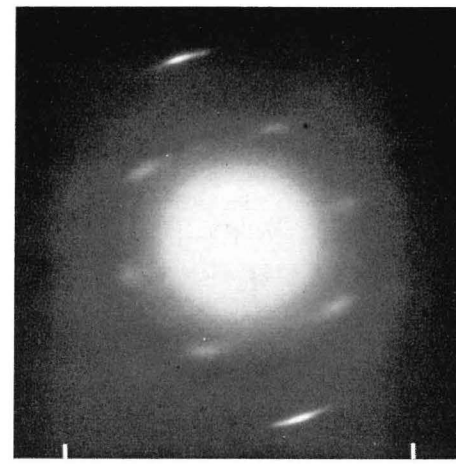

Fig. 272 b

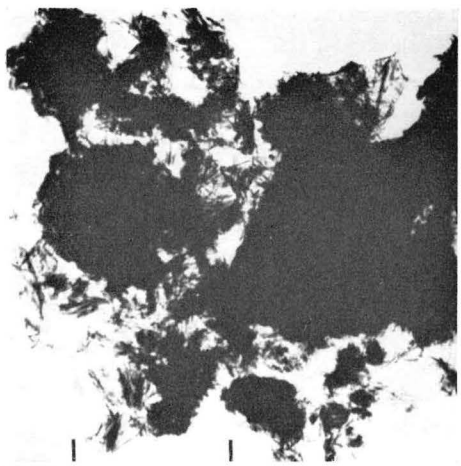

Fig. 273

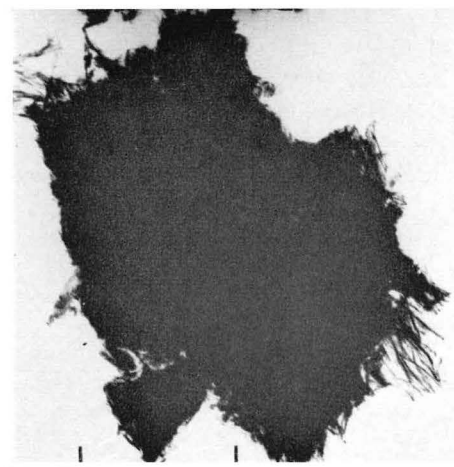

Fig. 274

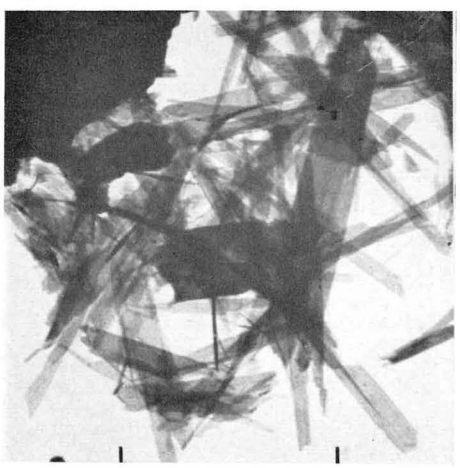

Fig. 275 a

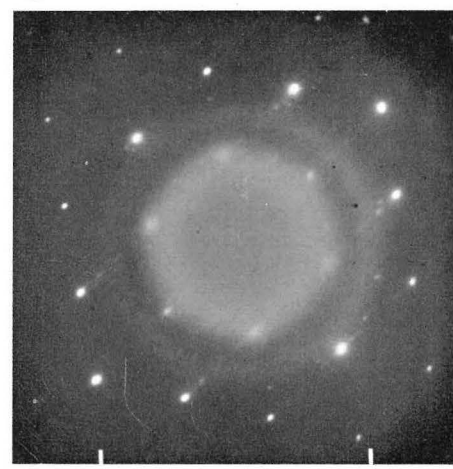

Fig. 275 b

75. C-S-H

Structures formed in C_3S paste

Figs. 276—279. Sample Tp—1C.

EM (276a): Structures in fully hydrated C_3S paste, revealed by the brief redispersion in water. The plate with interference fringes and certain hexagonal contours is a CH crystal, the sheet with parallel striations and other, more amorphous particles are C-S-H gel phases.

ED (276b): CH single crystal pattern, mainly (11.0), (20.0), and (22.0) reflexions, and a C-S-H fiber pattern with a diffuse ring at about 3.0 Å and fiber reflexion streaks at 1.81 Å.

EM (277a): Gel structure representative of this sample, network of needle-like or reed-like particles.

ED (277b): Typical pattern from C-S-H gel fibers oriented in various directions, diffuse halo at about 3.0 Å, with irregular intensity distribution, and weak but sharp fiber streaks at 1.815 Å, forming a broken ring reflexion.

EM (278): Network of intersecting fibers, similar to Fig. 277a. The thin, rounded particles in the background are probably secondary, lime-rich precipitate.

EM (279): Particle aggregate with an internal structure resembling an interlocking framework of laths or reeds, oriented in three directions at angles of about 60°. These structures are probably formed by topotactical conversion of the C_3S structure in the interior of a crystal grain, due to the influence of the successive replacement of part of the Ca ions by protons.

C_3S paste structures similar to those shown in Figs. 276—284 have also been observed by *Copeland* and associates 1960, 1962a, by *Brunauer* and *Greenberg* 1962, and by *Grudemo* 1962, 1964a.

Fig. 276 a

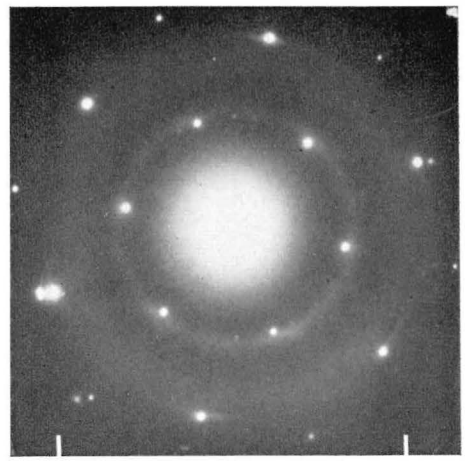

Fig. 276 b

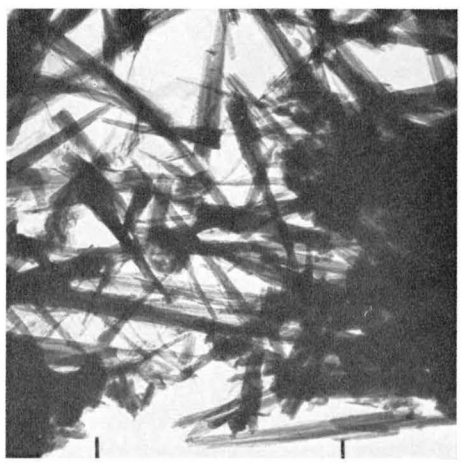

Fig. 277 a

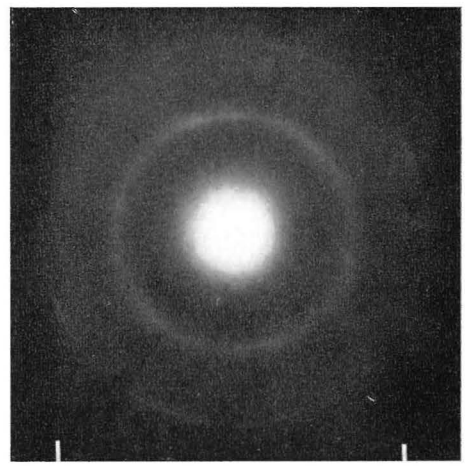

Fig. 277 b

Fig. 278

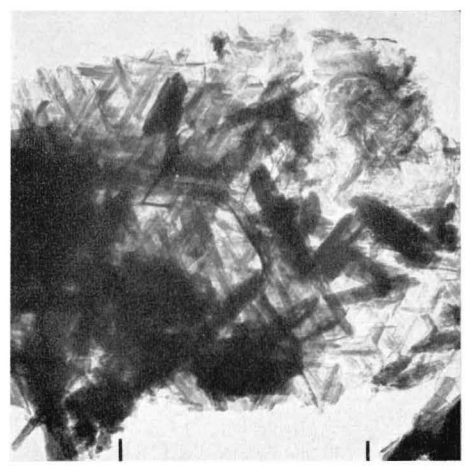

Fig. 279

76. C-S-H

Structures formed in C_3S paste (continued)

Fig. 280. Sample Tp—1E.

EM: Rather thick bundles of fibers, resembling those found in β-C_2S paste. (ED: Similar to those below, with additional CH pattern due to the plate crystal).

Figs. 281 and 282. Sample Tp—1B.

EM (281): Needles intersecting each other at various angles.

EM (282a): Needles radiating from a common point of intersection, and flocs of amorphous material.

ED (282b): Similar to patterns on preceding page, diffuse ring at about 3.0 Å, and weak though sharp fiber reflexion at 1.82 Å.

Fig. 283. Sample Tp—1A.

EM-ED: Similar to Fig. 282 and others, structures protruding from edge of large aggregate.

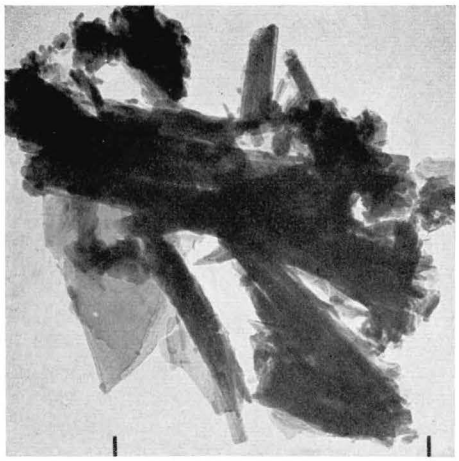

Fig. 280

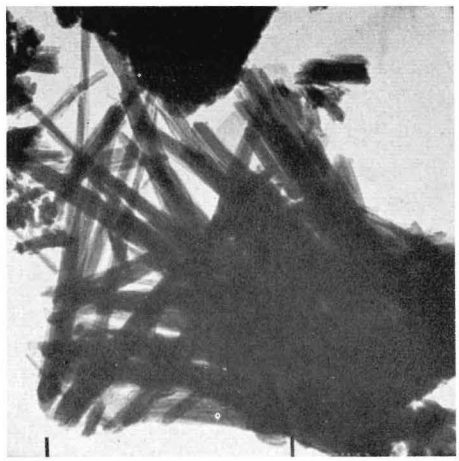

Fig. 281

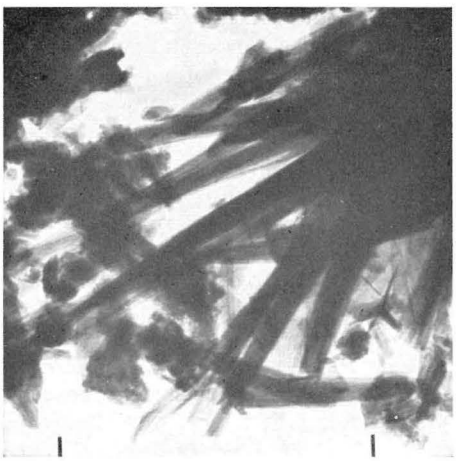

Fig. 282 a

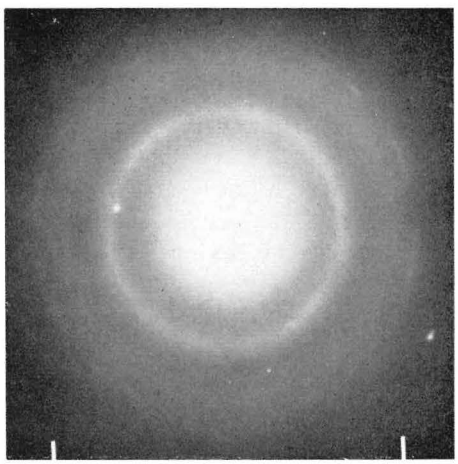

Fig. 282 b

Fig. 283 a

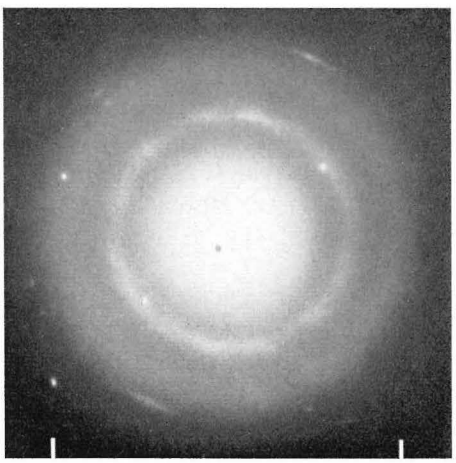

Fig. 283 b

77. C-S-H

Structures formed in C_3S paste (continued)

Fig. 284. Sample Tp—1B.

EM: Large aggregate of hydrated paste, with surfaces covered by radiating, long needles or reeds, with some particles of more irregular appearance.

ED: Similar to preceding patterns, diffuse ring at about 3.0 Å, and fiber streaks at 1.81 Å. The pair of spots is probably a CH (10.1) reflexion at 2.63 Å.

According to *Brunauer* and *Greenberg* 1962, the X-ray patterns of these samples (Tp—1) show only three broadened reflexions, one strong line at about 3.05 Å, two weaker lines at 2.79 and 1.82 Å. However, no 2.79 Å reflexion can be detected in any of the ED patterns. This reflexion corresponds to half the unit distance between silica chains, which can vary to a certain extent in lattice sheets with a variable radius of curvature in the *a* direction. The ED patterns are given by particles in the surface layers of the larger aggregates, whereas the X-ray patterns originate from the bulk material in the interior of the hydrated particles. It is conceivable that the tendency to curving and rolling of lattice planes in certain preferred directions is more pronounced in the looser structures of aggregate surfaces than in the topochemically formed core structures. This effect may serve to explain the general lack of definition in the 3.1—2.7 Å region of the ED patterns given by the C_3S paste hydration products.

Fig. 285. Sample Twq—1.

EM: The C_3S paste cured at 100° C contains mainly large particles of the initial C_3S crystals, coated with a hydrate phase with very long, thin fibers. In a few ED patterns, weak rings at 3.0 and 1.83 Å are observed. The corresponding X-ray diagram contains a weak pattern of C_3S, still remaining after 72 hours, a strong CH pattern and a few additional, diffuse lines at 3.04, 2.98, 2.78, and 1.825 Å originating from the fibrous C-S-H gel phase. There is no sign of any basal reflexion. Except for the more fibrous structure of the gel phase formed at 100° C, there is thus no great difference between this substance and the one formed at a much slower rate at normal temperature.

Figs. 286 and 287. Sample Twq—2.

EM (286): Survey micrograph, showing rectangular block crystals of α-C_2SH and aggregates of bundled $C_6S_2H_3$ crystal fibers. The X-ray diagram is a mixture of α-C_2SH and CH patterns, with certain indications of the presence of $C_6S_2H_3$, e.g. a reflexion at 8.8 Å.

EM (287): Representative aggregate of the fibrous $C_6S_2H_3$ phase. A few aggregates gave indistinct ED patterns similar to that of Fig. 399b, featuring a strong (00.4) reflexion corresponding to a c_H spacing of 7.5—7.6 Å in the direction of the fiber axis.

Fig. 288. Sample Twq—3.

EM: Survey micrograph, showing angular block of α-C_2SH crystals, and long, slender rods or needles of $C_6S_2H_3$ crystals, similar to those illustrated in Figs. 216 and 217. The X-ray diagram is a mixture of α-C_2SH, CH, and $C_6S_2H_3$ patterns, the latter with reflexions at 8.8 (m), 5.0 (vw), 3.29 (partly masked by the strong 3.26 Å. reflexion of α-C_2SH), 3.03 (ms), 2.99 (m), 2.89 (m), 2.83 (m), 2.46 (m), 2.08 (m), 1.98 (w), 1.87 (m), 1.75 (mw), 1.685 (m) Å, etc., in general agreement with the reflexions listed by *Buckle et al.* 1958.

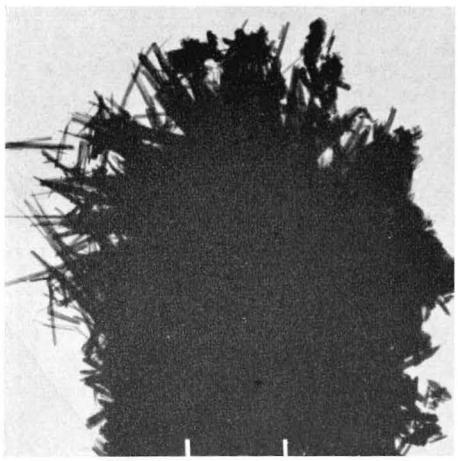

Fig. 284 a

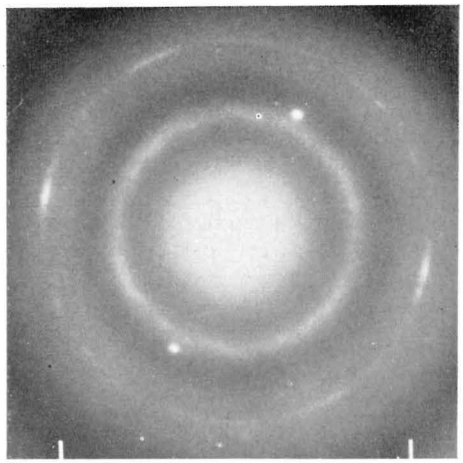

Fig. 284 b

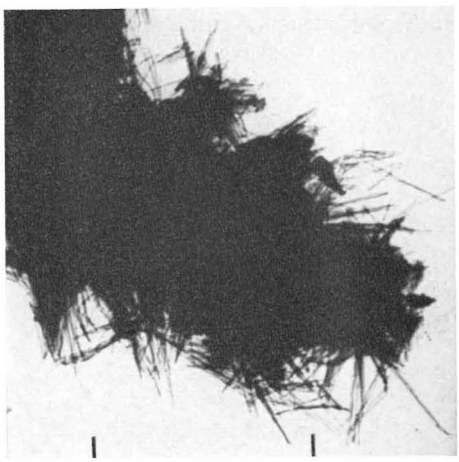

Fig. 285

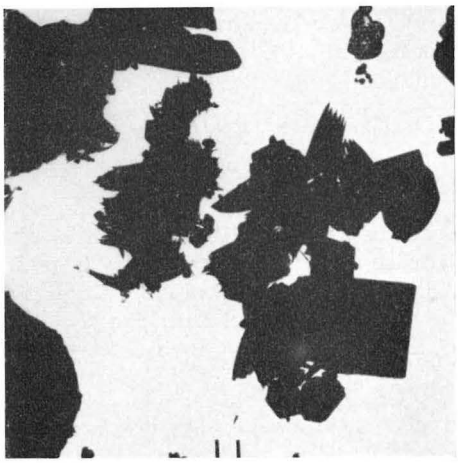

Fig. 286

Fig. 287

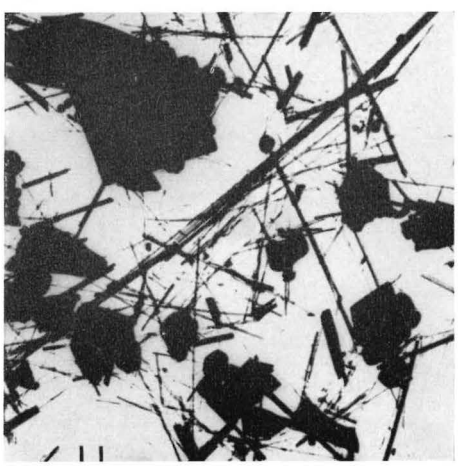

Fig. 288

78. **Hydrated cement**

Gel structures in standard portland cement paste

A comparatively large number of subsequent pages are taken into account to demonstrate representative gel structures in ordinary portland cement pastes of variable type, water-cement-ratio, age, fineness of grinding, etc. These structures do not vary much in general appearance from one sample to another, and most of them are nearly void of remarkable features. It has been considered appropriate to include a rather broad picture material here, mainly to emphasize the structural similarities and the general lack of definition of the gel materials.

Figs. 289 and 290. Sample Pp—1B.

EM (289): Gel particle aggregates representative of normal paste samples, rounded clusters of small particles of variable and irregular shape, some of them plate-like, others elongated or fibrous. A couple of thin plates of C-A-H(hex.) phase can also be observed.

EM (290): Thick bundle of fibrous, striated particles, a phase found in minor quantities in the sample.

Figs. 291 and 292. Sample Pp—2.

EMs: Aggregates of mainly fibrous particles, with a certain amount of more amorphous material.

EDs: Weak C-S-H(I) patterns, diffuse ring at about 3.0 Å, and sharp (040) fiber unit reflexion at 1.82 Å, similar to the patterns of e.g. Figs. 270b and 277b. It is commonly observed that the appearance of a 1.82 Å. reflexion is connected with the presence of some amount of fibrous gel material in the selected ED area, whereas amorphous gel aggregates give only a broad ring at about 3.0—2.9 Å.

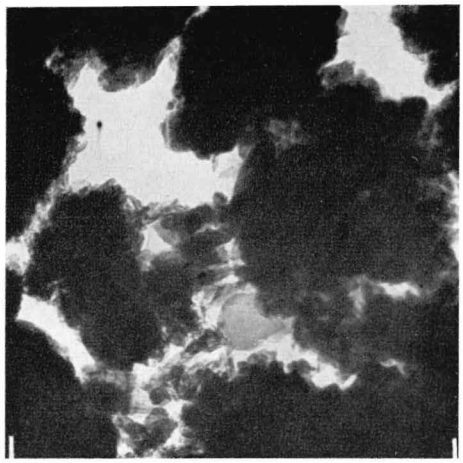

Fig. 289

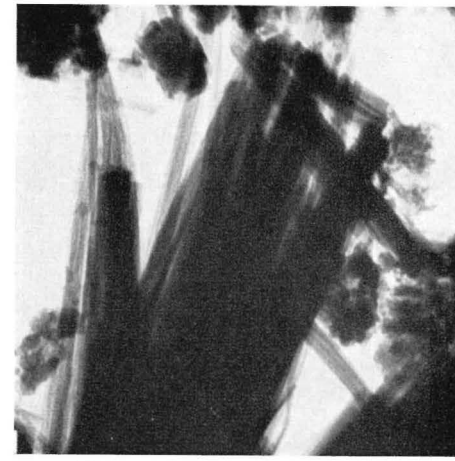

Fig. 290

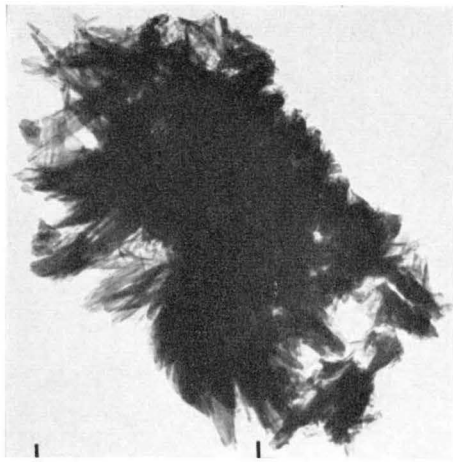

Fig. 291 a

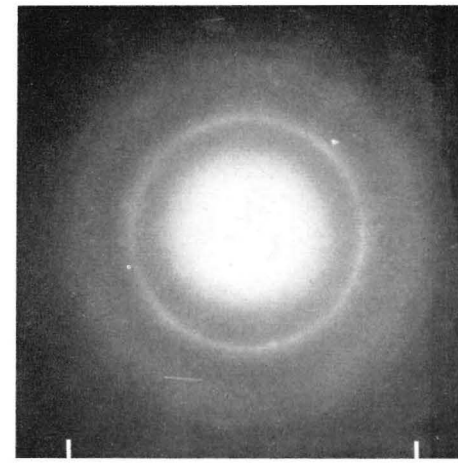

Fig. 291 b

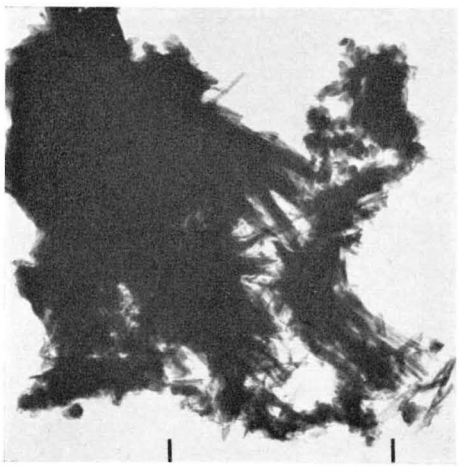

Fig. 292 a

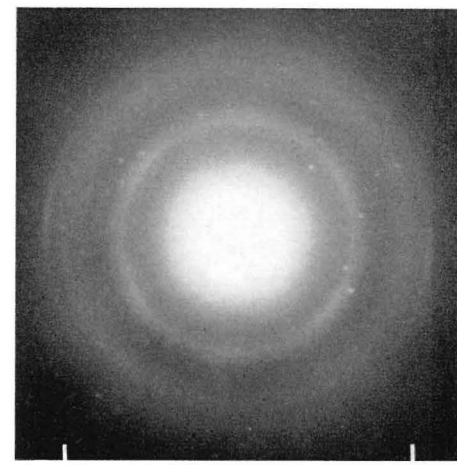

Fig. 292 b

79. **Hydrated cement**

Gel structures in standard portland cement paste (continued)

Figs. 293—296. Sample Pp—1A.

Figs. 297 and 298. Sample Pp—7.

EMs: Various examples of gel structures of representative appearance. These are aggregates or networks of comparatively fine fibers, associated with larger plates (Fig. 293), large clumps of amorphous material with some plates (Figs. 294, 296, 297), and similar material together with coarse bundles of fibers (Fig. 295) or with large CH plate crystal, striated by interference fringes of characteristic type (Fig. 298).

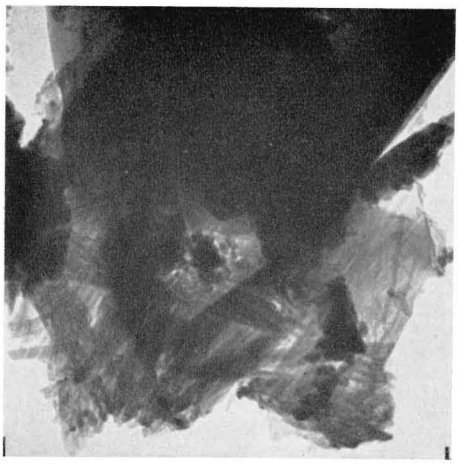

Fig. 293

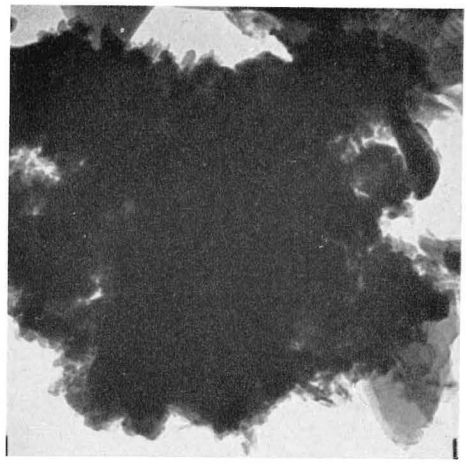

Fig. 294

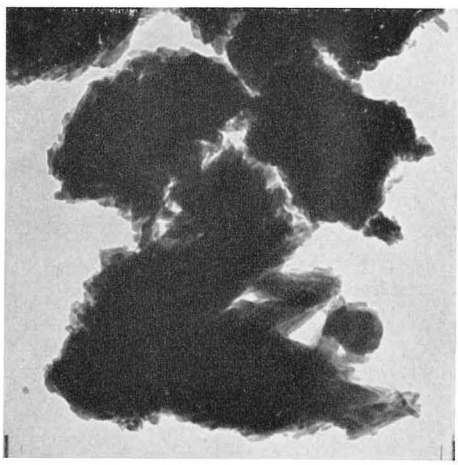

Fig. 295

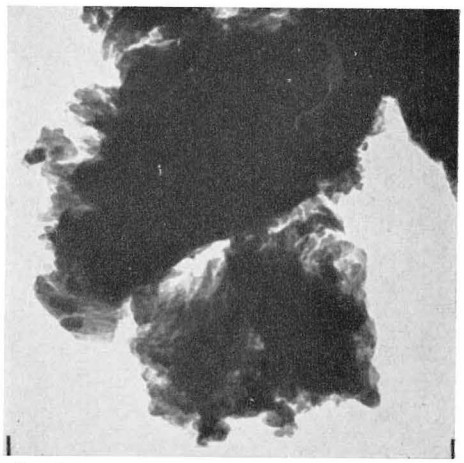

Fig. 296

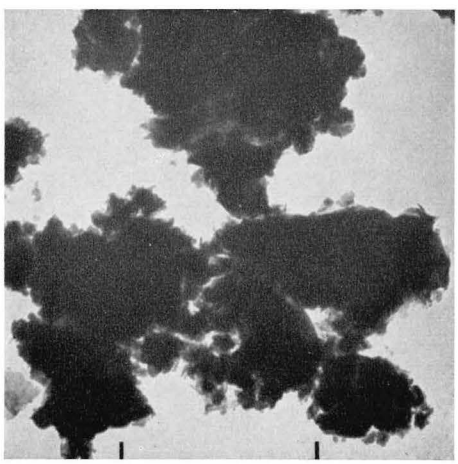

Fig. 297

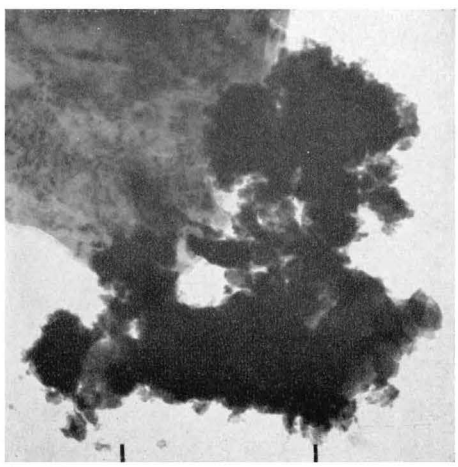

Fig. 298

80. **Hydrated cement**

Gel structures in standard portland cement paste (continued)

Figs. 299—301. Sample Pp—3.

Figs. 302 and 303. Sample Pp—4.

EMs: These are examples of the gel structures observed in old samples of both high and low water-cement ratio (0.70 in Pp—3, 0.35 in Pp—4). There is no obvious difference between the two structures, both consisting chiefly of shapeless, sponge-like aggregates of irregular fragments of gel material. A fibrous growth of the gel is observed only rarely, except in the vicinity of occasional C-A-H(hex.) plates (cf. Fig. 100).

The data indicate that, at least in standard cement pastes, the structure of the gel is practically the same for all water-cement ratios between 0.35 and 0.70, the range normally used in cement and concrete materials. This observation also supports the conclusions arrived at by *Powers* 1962, 1964, that the gel developed in the paste hydration of ordinary portland cement has a certain characteristic density of 1.76, counted as weight of dry (non-evaporable) material per cm^3, and a characteristic gel porosity of 0.28, counted as volume of gel pores per total volume. The effect of a moderate increase in the initial water-cement ratio, above a certain lower limit of about 0.35 required to reach complete hydration, is therefore only an increase in the residual volume of capillary pores remaining in the completely reacted paste.

It can also be noted that, even after ten years' curing there is no sign of a slow transformation of the colloidal gel substance into new phases of a considerably increased degree of crystallization, as postulated by some investigators.

ED (301b): Micrograph typical of ED effects usually obtained from representative areas containing colloidal C-S-H gel in cement paste, strong background scattering and diffuse enhancements at about 3.0, 2.1, and 1.2 Å. An extremely weak fiber reflexion at 1.80 Å is also observed in this case, corresponding to the presence of some fibrous material in Fig. 301a.

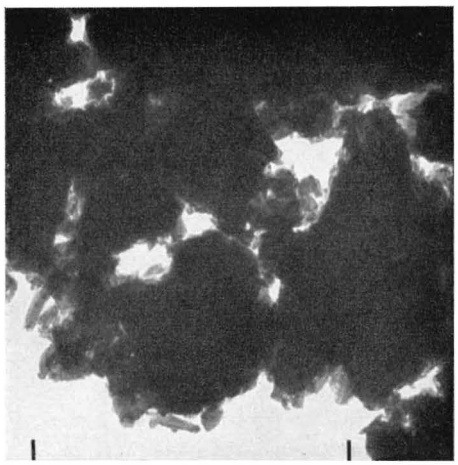

Fig. 299

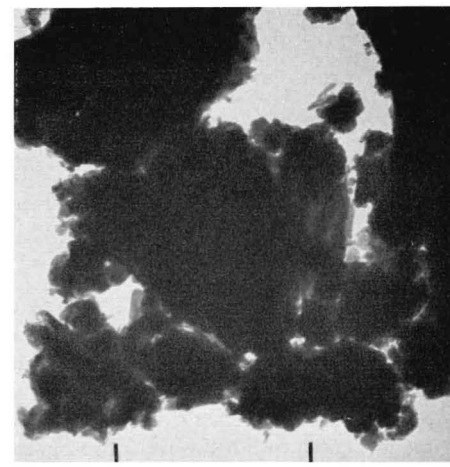

Fig. 300

Fig. 301 a

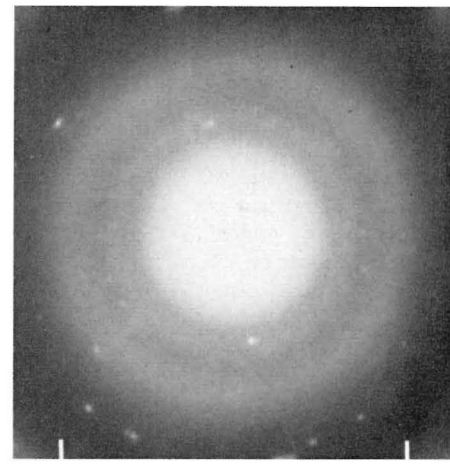

Fig. 301 b

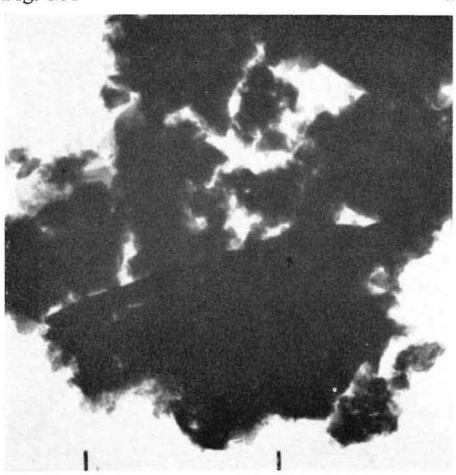

Fig. 302

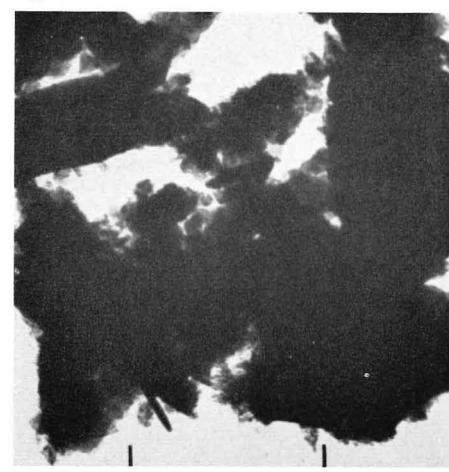

Fig. 303

81. **Hydrated cement**

Gel structures in various portland cement pastes

Figs. 304 and 305. Sample Pp—8.

EMs: The gel aggregates of this paste sample (ASTM Type II cement) consist of particles of the type resembling rods or reeds (cf. Figs. 280—283) in a much higher proportion than in the Type I cement paste samples shown in preceding pages. A few recorded ED patterns are indistinct, of the type shown in Fig. 301b.

The potential compound composition computed from the chemical analysis given by *Copeland, Kantro*, and *Verbeck* 1962 is about 52—25—3—13 percent for C_3S-C_2S-C_3A-C_4AF, respectively, as compared to about 45—28—13—7 percent for the Type I cement pastes of samples Pp—1 to 5. Disregarding the somewhat higher proportion of C_3S which, incidentally, is also higher than that allowed by the ASTM specifications for Type II cement, the main difference between the two cement types is the low content of C_3A in the Type II cement. The natural conclusion would be that some of the Al ions liberated in the hydration of C_3A are taken up in the structure of the C-S-H gel, thereby disturbing the regular crystallization process and especially preventing the formation of silica chains of one type or another.

Figs. 306 and 307. Sample Pp—9.

EMs: The C-S-H gel of this paste sample (ASTM Type III cement) has a much finer texture and higher degree of subdivision than the corresponding phase in the Type I cement pastes. A large part of the gel is decidedly fibrous, showing creased-foil structures as well as minute reeds or splines. The ED patterns recorded for this sample are indistinct. The compound composition, given by *Powers* and *Brownyard* 1948, is about 60—12—10—8 percent for C_3S-C_2S-C_3A-C_4AF, respectively. The structural characteristics of the gel material can thus be associated with a high proportion of C_3S in combination with the disturbing influence, as indicated above, of Al ions from the relatively large amount of C_3A, and the greater degree of fineness of grinding, generally used in the rapid-hardening Type III cements.

Fig. 308. Sample Pp—10A.

EM: Survey micrograph of gel aggregates of an ASTM Type IV cement paste. The particle elements are mostly irregular fragments of colloidal material.

ED: The ED pattern is of the usual, indistinct type, with a heavy background scattering, a diffuse ring at about 3.0 Å, broad halos at about 2.1 and 1.2 Å, and a weak fiber reflexion ring at 1.82 Å.

The compound composition, given by *Powers* and *Brownyard* 1948, is about 33—54—2—6 percent for C_3S-C_2S-C_3A-C_4AF, respectively. The morphological properties of the gel are possibly determined mainly by the development of the hydrates formed from the belite phase.

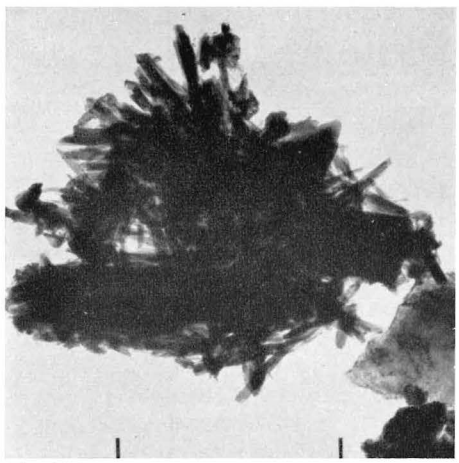

Fig. 304

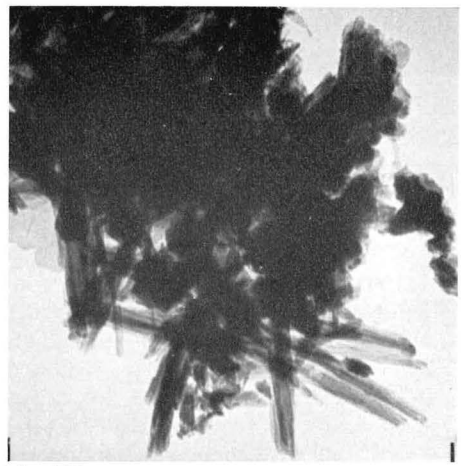

Fig. 305

Fig. 306

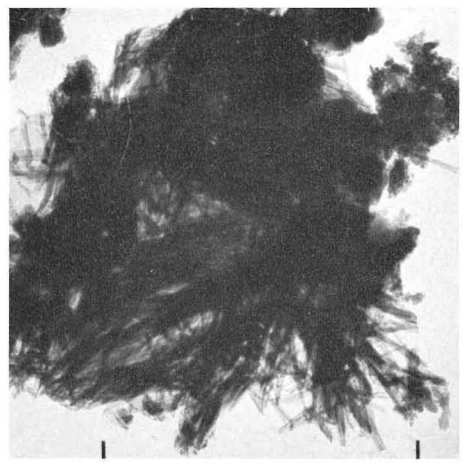

Fig. 307

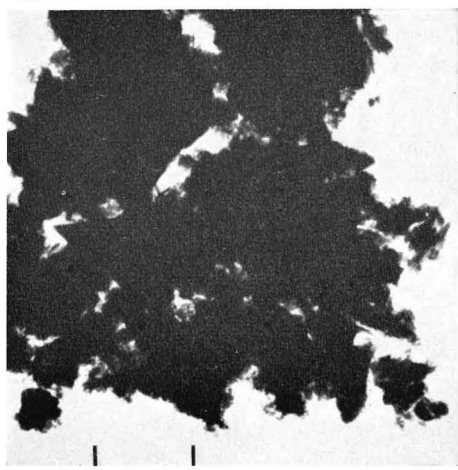

Fig. 308 a

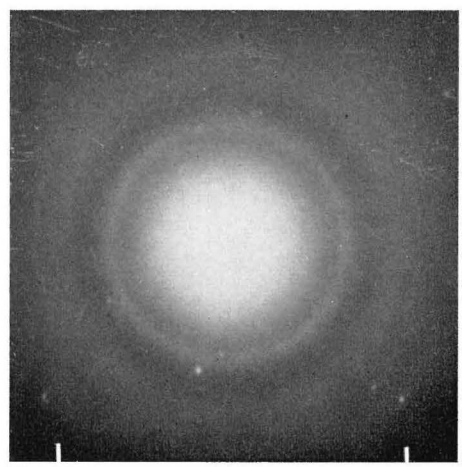

Fig. 308 b

82. **Hydrated cement**

Gel structures in low-heat portland cement paste

Figs. 309—311. Sample Pp—10A.

Figs. 312 and 313. Sample Pp—10C.

Fig. 314. Sample Pp—10B.

EMs: Structures of gel particles in different preparations of a hydrated Type IV (low-heat) cement paste. Fig. 313 is a survey micrograph of low magnification, showing various structures, among them large, thin plates and fibrous aggregates, the other EMs show mainly the rather shapeless gel structures of this sample. In Figs. 311 and 314, several particles show the habit of short, stubby rods or fiber bundles, resembling the structure found in β-C_2S pastes (cf. e.g. Figs. 265, 269, and 270). The plate visible in Fig. 310 is not a C-A-H (hex.) crystal, but probably a clay-type particle (cf. Figs. 427—429). The C-A-H(hex.) crystals found in standard cement pastes seemed to be missing in the low-heat cement paste samples. This can be explained as an effect of the low C_3A and C_4AF content. The small amounts of Al and Fe ions liberated in the course of hydration can probably be easily accommodated in the C-S-H gel phase.

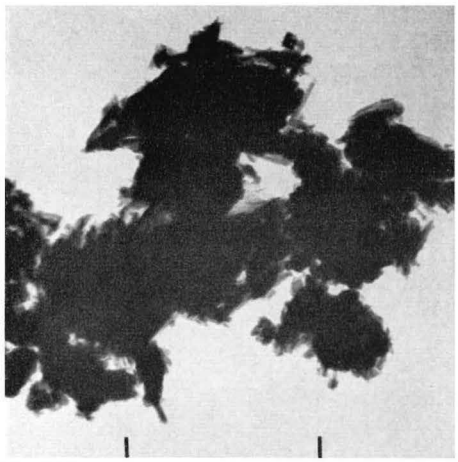

Fig. 309

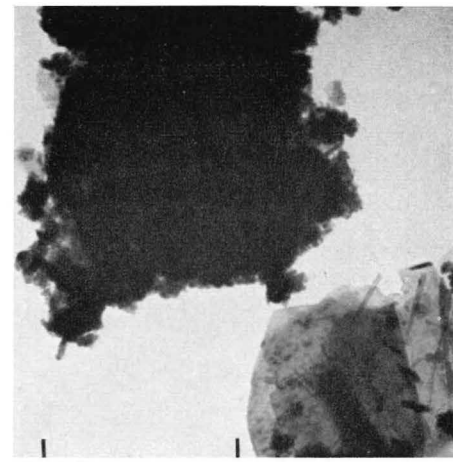

Fig. 310

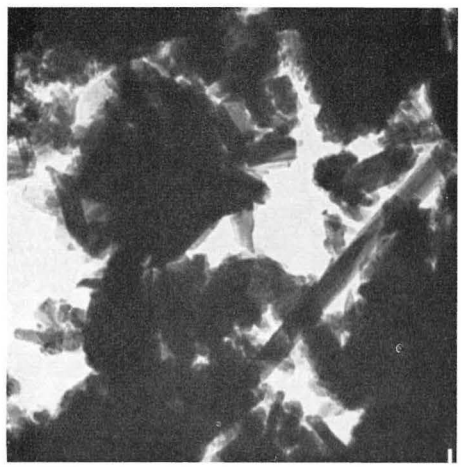

Fig. 311

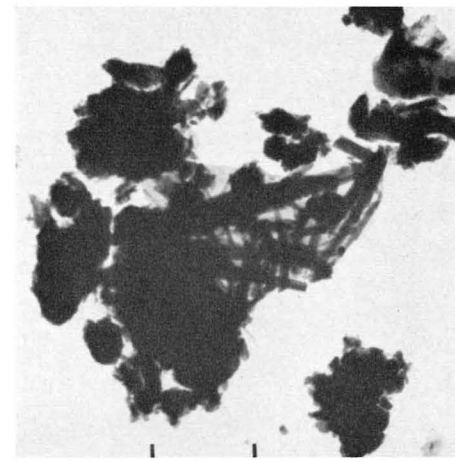

Fig. 312

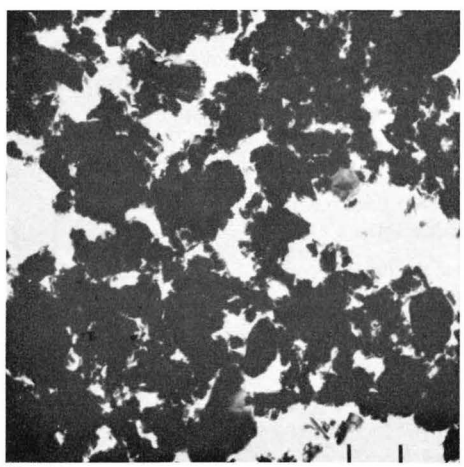

Fig. 313

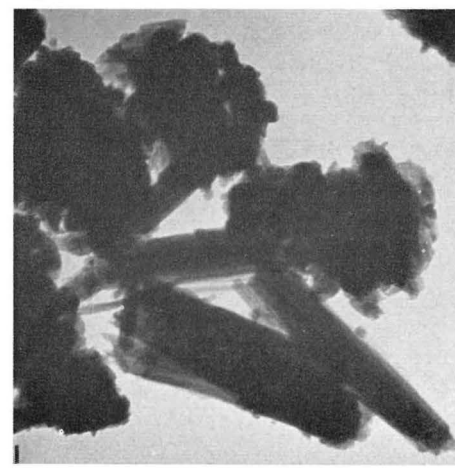

Fig. 314

83. **Hydrated cement**

Gel structures in low-heat portland cement paste (continued)

Figs. 315—317. Sample Pp—10C.

These are examples of various types of gel structures and the ED effects given by them.

EM (315a): Representative gel aggregates, similar to those of preceding page.

ED (315b): Mainly a diffuse halo at about 2.9 Å, and some scattered spots or streaks at 2.40 and 1.70 Å, originating from C crystals in dehydrated lime phase.

EM (316a): Aggregates of fibrous or reed-like particles, observed in small amounts in the samples.

ED (316b): Mainly a pattern characteristic of fibrous C-S-H gel phase, with a diffuse halo at 3.1—2.8 Å, containing some enhanced parts at about 3.0 Å, and a sharp fiber unit reflexion at 1.82 Å, and further some scattered spots of unknown origin.

EM (317a): Thick bundle of lath-like or rolled-sheet structures.

ED (317b): Oriented-fiber pattern, similar to those observed for certain gel particles in β-C_2S paste (cf. Figs. 271 and 272). Four of the six diffuse inner spots, indexable as (*hk*) =(11) and permutations, contain enhanced intensities at about 3.03 Å, the two others, indexable as (*hk*)=(20) and ($\bar{2}$0), are more diffuse outwards, extending down to spacings of about 2.7 Å. The strong fiber reflexion streak ((*hk*)=(02)) corresponds to 1.814 Å. In the original pattern, there is also a second-order reflexion ((*hk*)=(04)) at 0.907 Å. The pair of sharp spots at 3.11 Å is probably the (10.0) reflexion from a CH crystal.

Of the ED patterns from ordinary cement paste particles recorded by the author so far, this is the only one showing clearly resolved C-S-H(I) or (II) (*hk*) reflexions. Such well-crystallized particles are obviously rare, and are also difficult to locate and isolate for ED recording purposes.

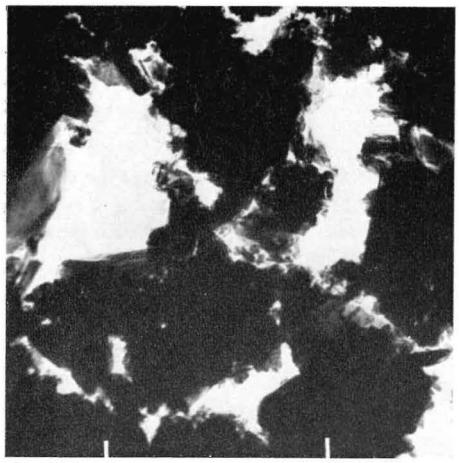

Fig. 315 a

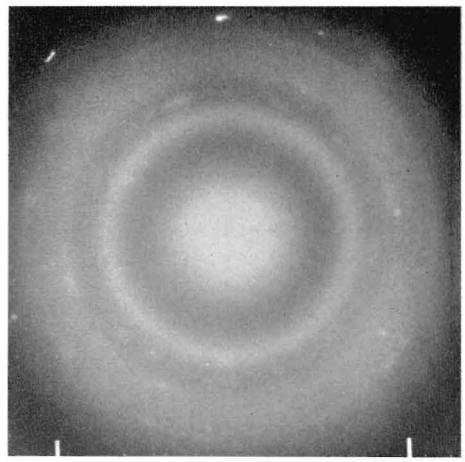

Fig. 315 b

Fig. 316 a

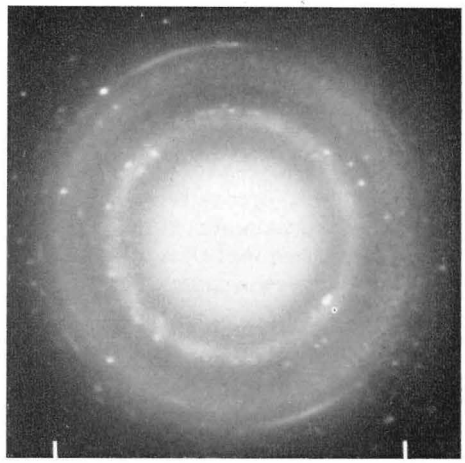

Fig. 316 b

Fig. 317 a

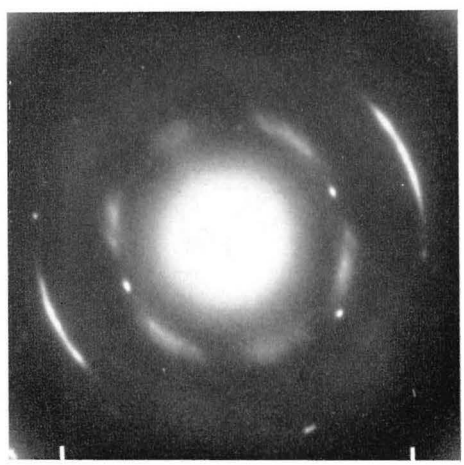

Fig. 317 b

84. **Hydrated cement**

Gel structures in pastes made from fine fraction of standard cement

Figs. 318 and 319. Sample Pp—5.

EMs: Gel structures in paste of water-cement ratio 0.70, aggregates of very minute particles, showing only slight signs of a fibrous texture, together with thin plates of C-A-H (hex.) phase. Finely fibrous structures were found in small amounts in this sample, but only associated with or adsorbed on C-A-H(hex.) plates (cf. Fig. 101).

Fig. 320. Sample Pp—6A.

Figs. 321 and 322. Sample Pp—6B.

EMs: Gel structures in paste of water-cement ratio 1.5. These samples consisted mainly of bundles or networks of long, slender fibers, together with certain amounts of C-A-H (hex.) phase (cf. Figs. 103—107.).

ED: C-S-H(I) fiber pattern given by bundle of fibers, six diffuse spots in approximately hexagonal arrangement at about 3.0 Å, with the (11) and ($1\bar{1}$) reflexions somewhat stronger and sharper than the (20) reflexions, and a strong fiber unit reflexion at 1.815 Å. The pattern is strongly reminiscent of those of e.g. Figs. 272b and 317b.

It is of some interest to note that no CH plate crystals could be found in samples Pp—5 and Pp—6 by means of EM—ED examination. However, the X-ray diffractometer records of these samples are dominated by a very strong and sharp CH pattern, whereas the reflexions from other gel substances are very diffuse and indistinct. The reason for the absence of CH crystals in the EM preparations is not clear. It is possible that this phase consists of large crystals which separate easily from the rest of the material in the course of preparation of EM specimens.

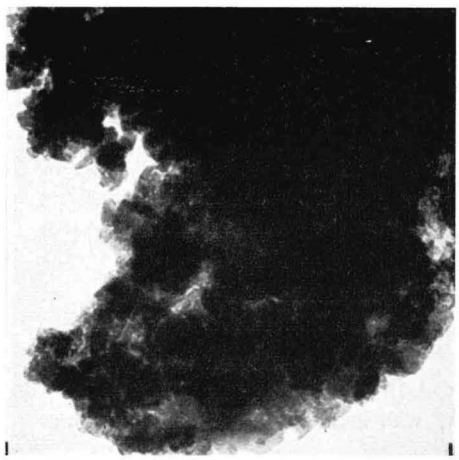

Fig. 318

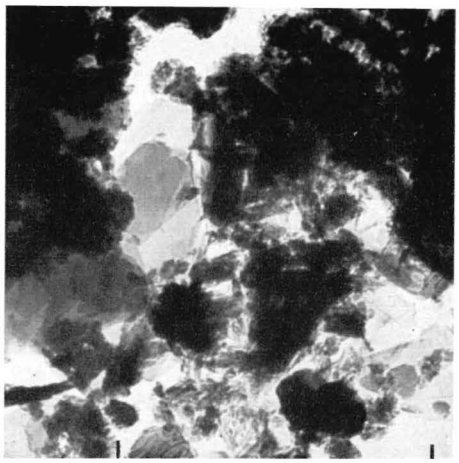

Fig. 319

Fig. 320 a

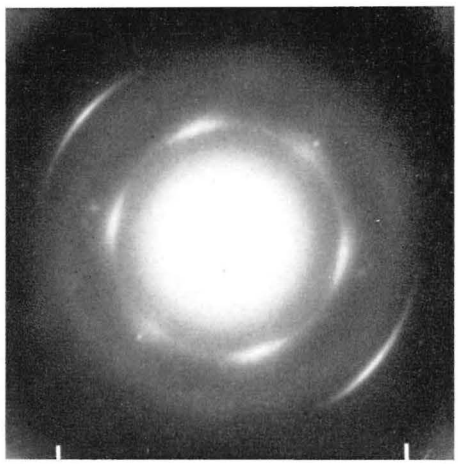

Fig. 320 b

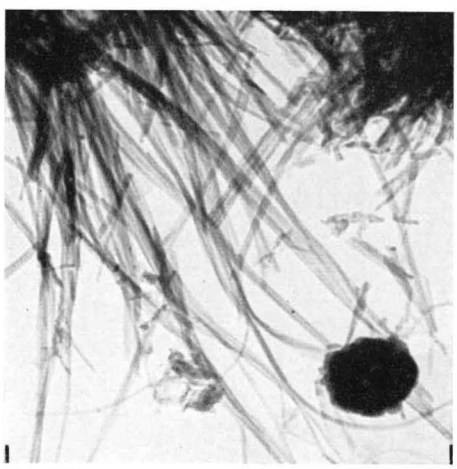

Fig. 321

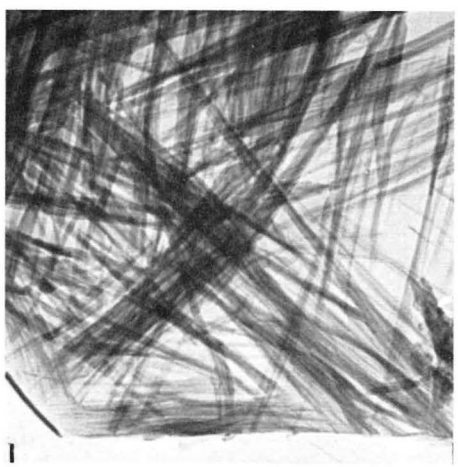

Fig. 322

85. Hydrated cement

Gel structures in paste of extremely high porosity

Figs. 323—325. Sample Pp—6B.

EMs: Networks or loose bundles of fibrous C-S-H particles, more or less adsorbed or attached to thin C-A-H(hex.) plates. The C-A-H(hex.) plate of Fig. 323a is rather thick and clearly visible, that of Fig. 324 a is almost covered by a thick network of fibers, and that of Fig. 325 a is very thin and nearly invisible.

ED (323b): Composite diagram, (1) C-A-H(hex.) spot pattern of hexagonal type, but with some deviation from regularity, measured a_H variable between 5.67 and 5.55 Å, (2) C-S-H gel reflexion at 2.98 and 1.80 Å.

ED (324b): Similar to preceding diagram, (1) C-A-H(hex.) spot pattern with $a_H = 5.70-5.66$ Å, (2) C-S-H reflexions at 3.02 and 1.82 Å, with indications of a third ring about 2.8 Å.

ED (325b): Fiber pattern from comparatively well crystallized C-S-H(I) phase. The arcs of strongest intensity correspond to the (*hk*) reflexions from the parallel-oriented fibers in Fig. 325a, but there are also reflexions from fibers running at about 60° angles to the main fiber direction. The measured (*hk*) spacings are 3.04 (11), 2.78 (20), 1.815 (02), 1.650 (31), 1.522 (22), 1.392 (40), 1.176 (13), 1.103 (42), and 1.065 (51) Å, agreeing well with spacings calculated from a face-centered, orthogonal cell $a \times b = 5.56 \times 3.63$ Å: 3.04, 2.78, 1.815, 1.650, 1.520, 1.390, 1.183, 1.105, and 1.063 Å.

Fig. 323 a

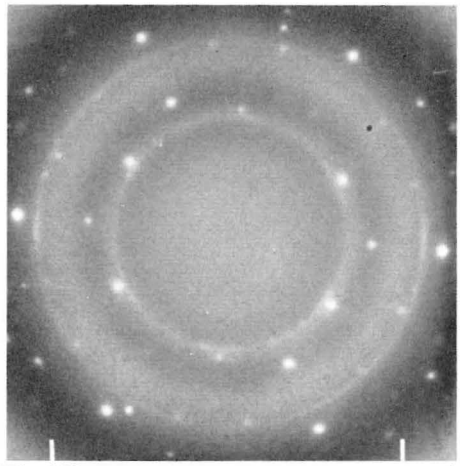

Fig. 323 b

Fig. 324 a

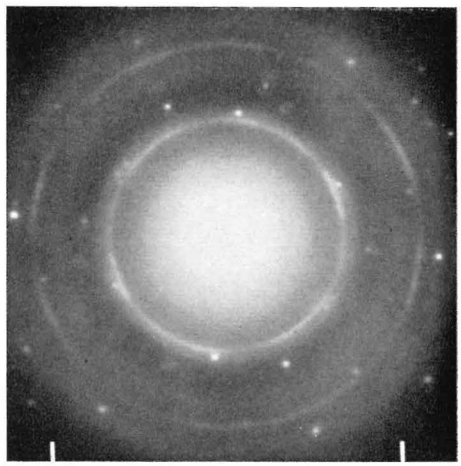

Fig. 324 b

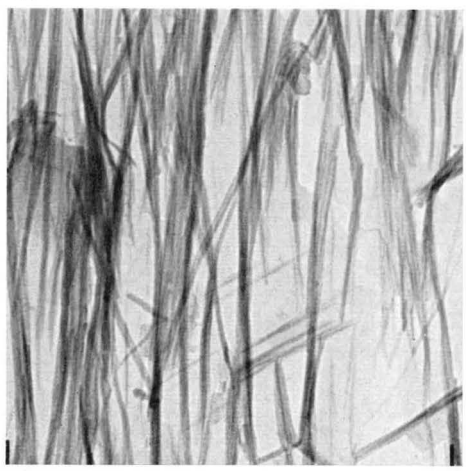

Fig. 325 a

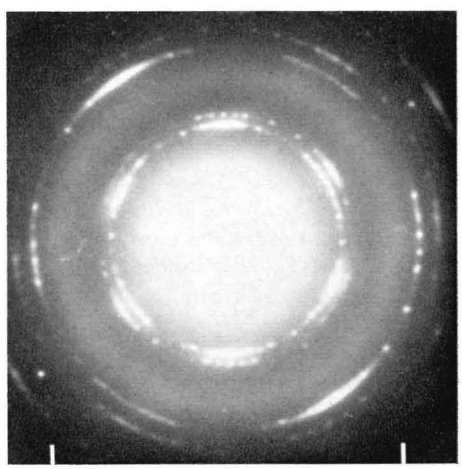

Fig. 325 b

86. **Hydrated cement**

Development of gel structures in fresh standard cement paste

Figs. 326 and 327. Sample Pp—12A.

EMs: Standard cement paste, two hours after mixing, showed mainly the original anhydrous particles, with only slight indications of being superficially attacked by the water.

Figs. 328 and 329. Sample Pp—12B.

EMs: The same paste as above, six hours after mixing. Many cement crystals are covered by radiating, acicular particles, which seem to form bridges to other crystal grains. Some surfaces are still smooth and unattacked by the mixing water.

The crystallographic identity of the acicular phase is not quite certain. It is probably a high-lime C-S-H compound, the morphological development of which is affected by the presence of A, F, and $\bar{S}$. No ED effects could be observed from it.

Figs. 330—333. Sample Pp—12 C.

EMs: After 4 days, most of the acicular edge structures observed during setting had disappeared or been replaced by more shapeless structures consisting of aggregates of small, irregular or possibly plate-like fragments of hydrated material, together with a certain amount of rod-like particles, as seen e.g. in Fig. 332.

The course of evolution of various hydrated structures, as observed in these samples of ordinary cement paste, is closely analogous to the one described by *Copeland* and *Schulz* 1962 a, b. There are also some similarities to the hydration processes described by *Chatterji* and *Jeffery* 1963b for various cement pastes. The latter investigators observed "spherical reaction products" (possibly $\bar{C}$-contaminated CH formations) at a very early stage of reaction, and later on splines of C-S-H and ettringite covering the original cement crystals and persisting even after 14 days.

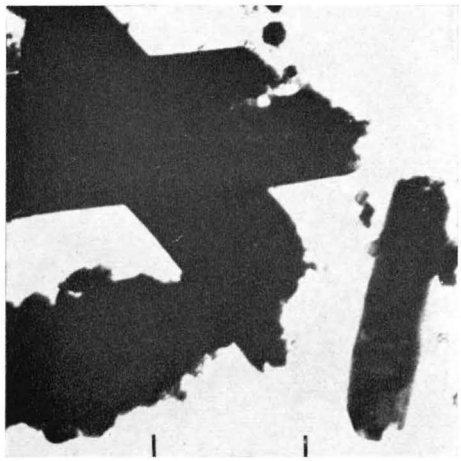

Fig. 326

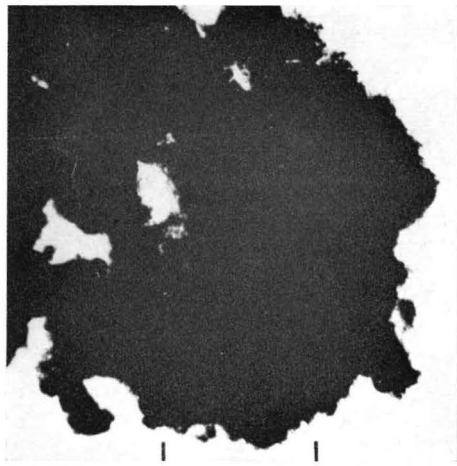

Fig. 327

Fig. 328

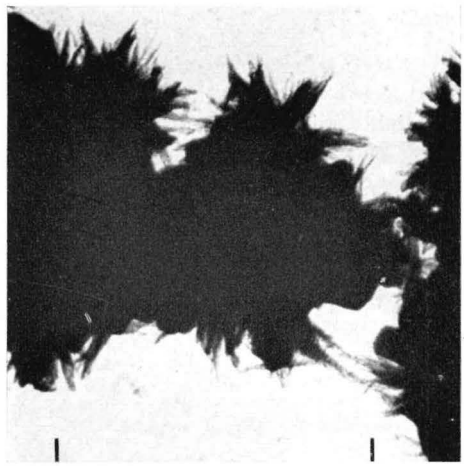

Fig. 329

Fig. 330

Fig. 331

87. **Hydrated cement**

Gel structures in standard cement pastes

(*Figs. 332 and 333, see preceding page*).

Figs. 334—336. Sample Pp—11.

EMs (334, 335): A Swedish standard cement paste, of low water-cement ratio and mineral composition similar to that of sample Pp—12, showed in the hardened state a structure mainly consisting of small, irregular flakes or chips, together with a certain amount of large, thin plates (CH and possibly C-A-H crystals) and a few coarse, rod-like particles.

EM (336a): Large CH plate surrounded by gel fragments.

ED (336b): CH spot-ring pattern, (*hk*.0) and (*hk*.1) reflexions (cf. e.g. Figs. 24b and 40b).

Fig. 332

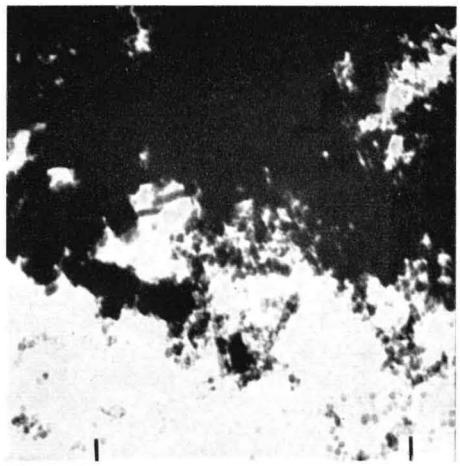

Fig. 333

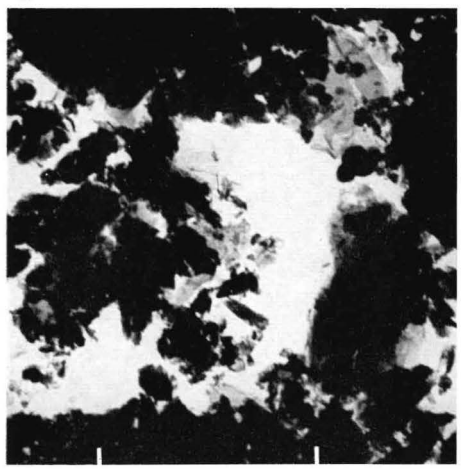

Fig. 334

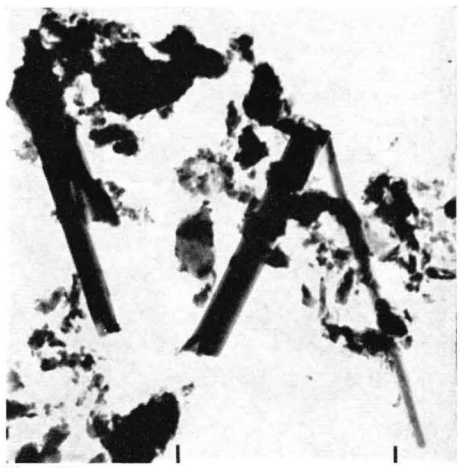

Fig. 335

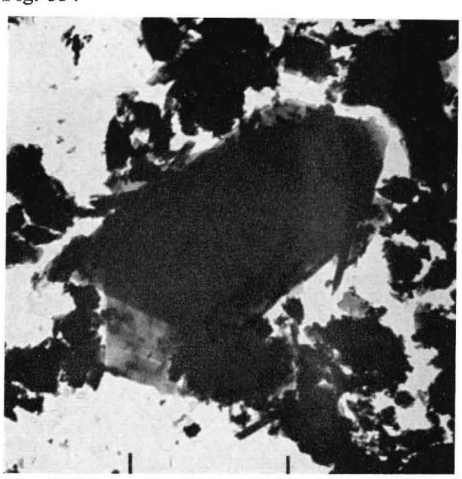

Fig. 336 a

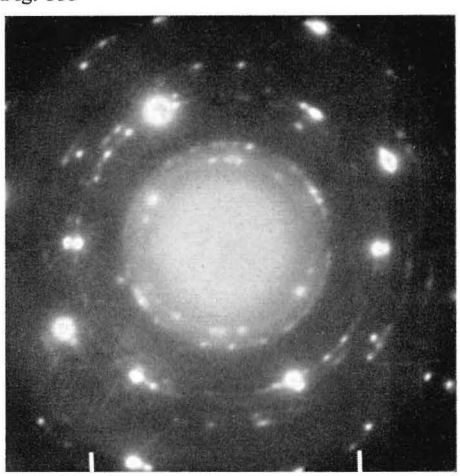

Fig. 336 b

88. **Hydrated cement**

Development of gel structures in fresh clinker paste

Figs. 337—340. Sample Pp—13A.

EMs: Representative structures in clinker paste two hours after mixing. Although this paste did not set much quicker than the corresponding cement paste (sample Pp—12), in spite of the absence of gypsum admixture, considerable amounts of hydration products had already formed at this stage. These consisted of long, curved rods or rolls, often branching out from bundles similarly to the formations in Figs. 111—116, and in rather large, thin plates. None of these phases gives any distinct ED effects, and their identity is uncertain. The plates could be residues of unstable C-A-H(hex.) crystals, and the rods could be an alkali-containing C-A-H phase. The occurrence of both these phases is obviously conditioned by the absence of $\bar{S}$.

Figs. 341—344. Sample Pp—13B.

EMs: After six hours of hydration of the clinker paste, the bundles of rods and the thin plates were still present. Around the edges of the original cement particles a growth of wrinkled foils had started to develop. The latter phase resembles the foil-like phases developing at very early ages in certain artificial paste mixtures with alite as main ingredient, prepared and examined by *Chatterji* and *Jeffery* 1963a.

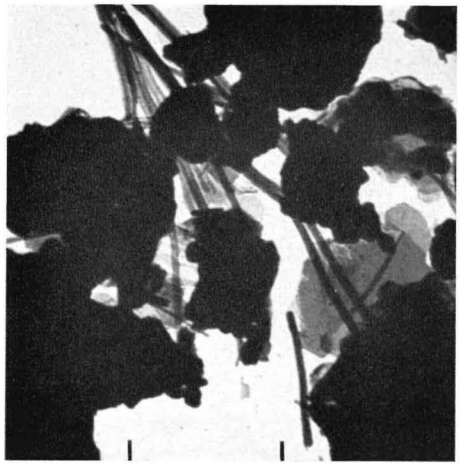

Fig. 337

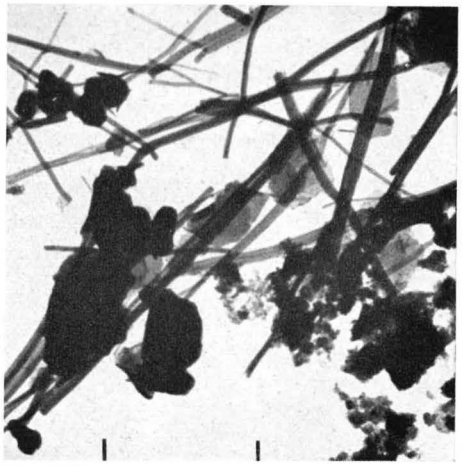

Fig. 338

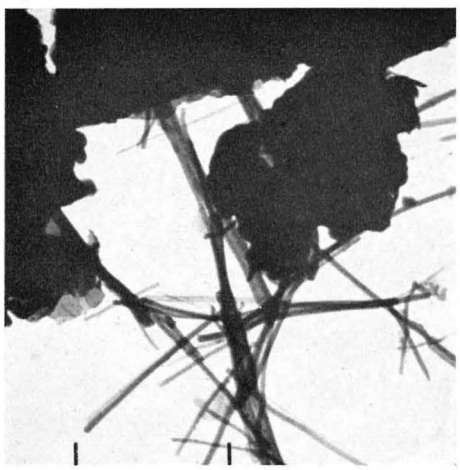

Fig. 339

Fig. 340

Fig. 341

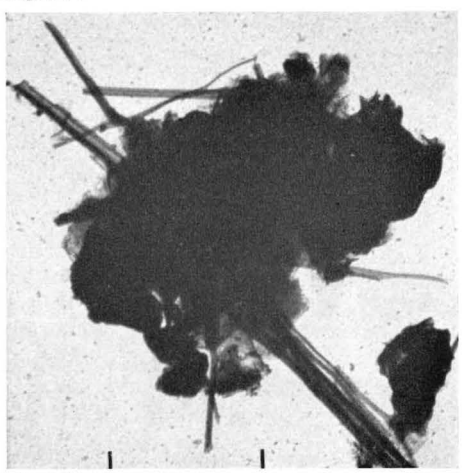

Fig. 342

89. **Hydrated cement**

Development of gel structures in fresh clinker paste (continued)

(Figs. 343 and 344, see preceding page).

Figs. 345 and 346. Sample Pp—13C.

EMs: After one day, the rod-like structures had disappeared almost completely, and also the number of thin plates had diminished considerably. Most of the gel consisted of aggregates of small, irregular fragments, possibly distorted and cracked foils.

Figs. 347 and 348. Sample Pp—13D.

EMs: After one week, the whole gel mass consisted of clusters of small, irregular fragments.

The examples of paste structures given in the last few pages show that the course of development of hydrated structures during setting and early stages of hardening can vary greatly in different samples, probably depending on the relative amounts present of certain minor ingredients such as aluminate and alkali, or admixtures such as sulfate. However, the subsequent stages of hardening are probably conditioned by the successive evolution of the major gel phase, consisting mainly of some kind of ill-defined C-S-H substance. The first-formed phases, which often have easily recognizable habits (such as the rods and the thin, flat plates observed in the last sample), seem to be dissolved and their material incorporated in the main C-S-H gel phase, probably in the state of a solid solution of some type. The inclusions may disturb the formation of a regular C-S-H lattice, causing the gel phase elements to develop as very ill-defined crystal fragments.

Similar effects of dissolution of a primarily formed hydrate phase and incorporation of it in a secondary phase has been shown earlier in this paper, e.g. in Figs. 256—258.

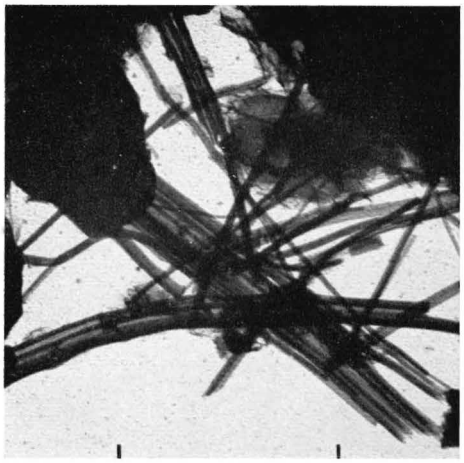

Fig. 343

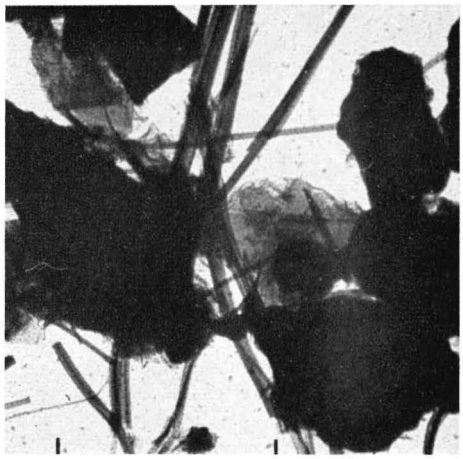

Fig. 344

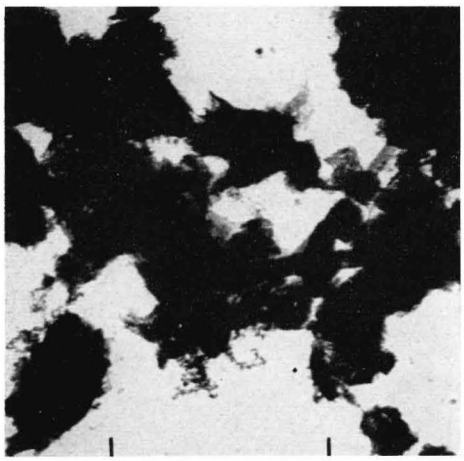

Fig. 345

Fig. 346

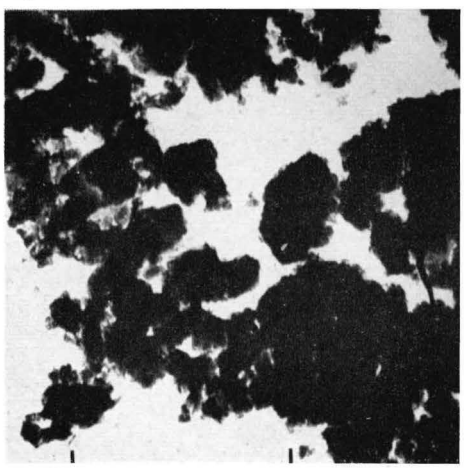

Fig. 347

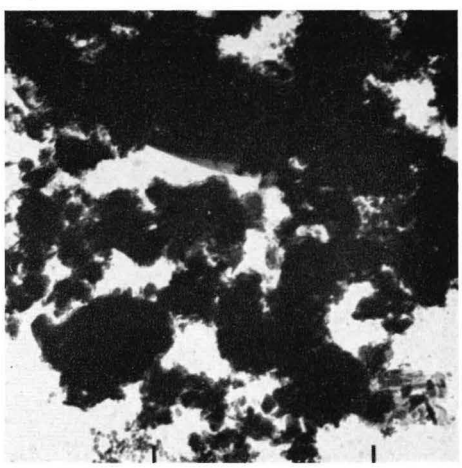

Fig. 348

90. **Hydrated cement**

Development of gel structures in alite paste

Figs. 349—351. Sample Tp—2A.

An EM sample of this paste, observed after three hours, showed only slight signs of reaction products.

EMs: Sample after 24 hours, all surfaces of the original alite crystals were covered by a radial growth of fibrous structures, consisting of irregularly rolled foils. The only ED effect given by these edge structures is a more or less weak ring in the range 3.05—3.00 Å. The X-ray powder diagram shows an alite pattern and a rather weak CH pattern.

Figs. 352—354. Sample Tp—2 B.

EMs: Sample after 14 days, the surface structures were still present, and were somewhat longer and more needle-like than after one day. The ED patterns showed the 3.0 Å. ring and a very weak ring at 1.82 Å. The X-ray diagram contained a strong CH pattern and a weakened alite pattern. The presence of possible, weak reflexions from a C-S-H gel constituent is uncertain, since these are masked by certain alite reflexions.

The X-ray diagram taken after 3 months' paste hydration of this sample showed mainly a strong CH pattern. A couple of the strongest alite reflexions were barely visible, indicating that the hydration was nearly complete. Weak, diffuse reflexions from the C-S-H gel, at 3.04 and 1.815 Å, were also observed, as well as a diffuse band at 4.6—4.0 Å, which seems always to accompany the development of C-S-H gel products of very low degree of crystallinity.

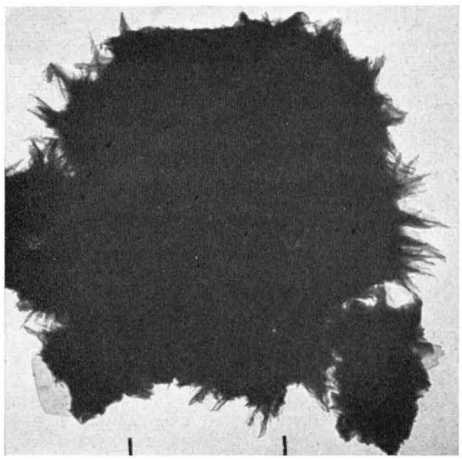

Fig. 349

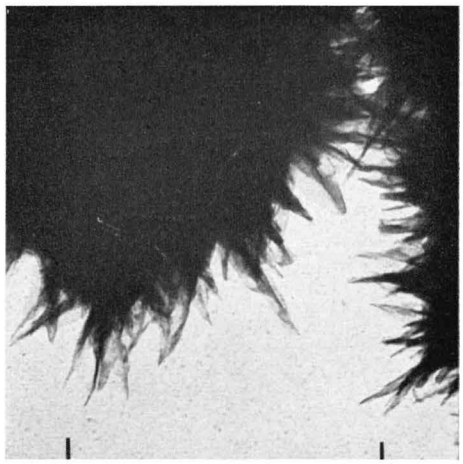

Fig. 350

Fig. 351

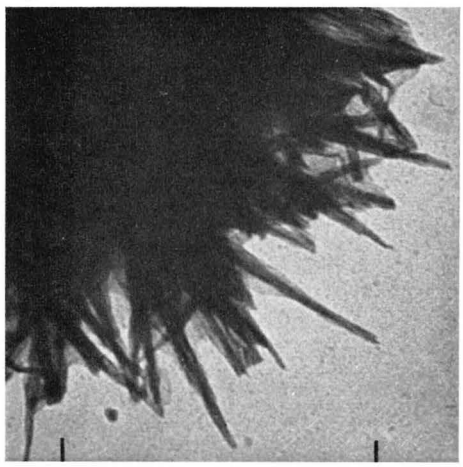

Fig. 352

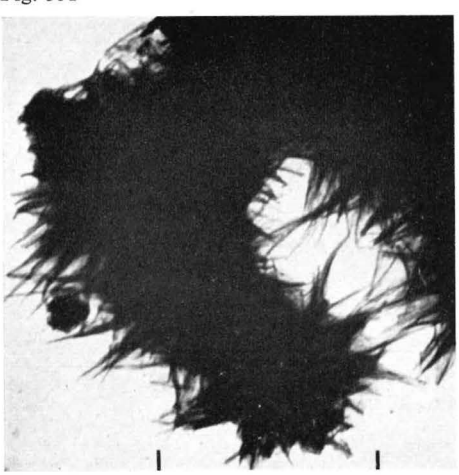

Fig. 353

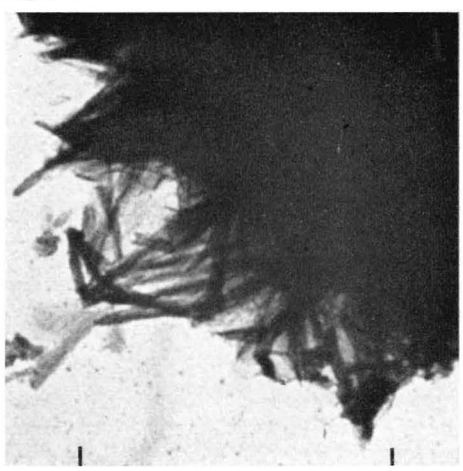

Fig. 354

91. **Hydrated cement**

Development of gel structures in alite paste with sulfate addition

Figs. 355—357. Sample Tp—3A.

An EM sample observed a few minutes after contact with water showed practically no signs of reaction, a sample observed after three hours showed surface structures in the beginning stage of growth.

EM (355): Sample after 24 hours, a large alite crystal with a coat of fibrous structures, and a plate phase of unknown identity.

EM (356): The edge structure at higher magnification, fibrous particles similar to those of previous sample (Tp-2).

EM (357): Dispersed fibrous structures, together with prismatic rods, radiating from a common origin. The ends of these rods show hexagonal contours, which indicates that the rods consist of hexagonal prisms of ettringite, formed from the reaction of gypsum with alumina and lime dissolved from the alite phase. Such well-formed ettringite rod structures are observed only rarely. As has been shown in earlier sections (cf. e.g. Figs. 109, 112), the ettringite-type structures are mostly dehydrated to such a degree that only the strands of the original structure remain.

No significant ED effects could be obtained from the fibrous surface structures. Certain isolated, large plates were identified as CH crystals by means of the single-crystal (*hk*) spot pattern. The X-ray diagram contained strong patterns of alite and CH, a weak pattern of gypsum, and the 9.8 Å reflexion of ettringite, together with some indications of other ettringite lines.

As observed in the original analysis by *Chatterji* (CBI internal report), the formation of ettringite in this sample indicates a "through-solution" mechanism of hydration of alite. At least part of the alumina initially fixed in the alite lattice is given off to the liquid phase, where its reaction with calcium and sulfate ions results in the formation of ettringite crystals.

Figs. 358—360. Sample Tp—3B.

EM (358): Sample after 14 days, survey micrograph showing larger aggregates with edge structures of various types, fibrous as well as irregular, and plates of CH crystals.

EMs (359, 360): The fibrous surface coat had developed further at 14 days of age. The separate particles seemed to be slightly thinner and more needle-like than those of the sulfate-free paste (Tp—2), in agreement with observations made by *Kurczyk* 1960.

The fibrous gel structures gave only very indistinct ED effects. The X-ray diagram contained a strong CH pattern, and weaker reflexions from residual alite and from ettringite (lines at 9.8, 5.6, 3.87, 2.78, 2.20 Å). The CH and ettringite patterns remained also at 3 months of age, but the alite reflexions had practically disappeared. Diffuse C-S-H gel reflexions at 3.04 and 1.815 Å were also detectable at this stage.

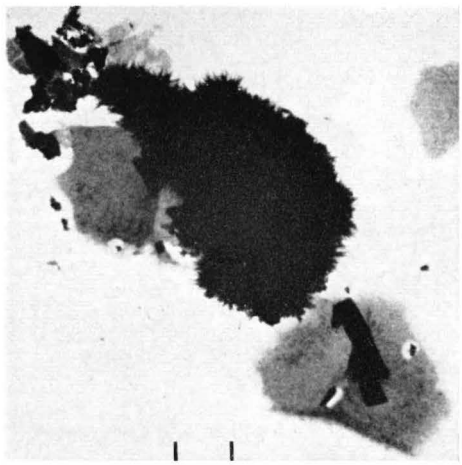

Fig. 355

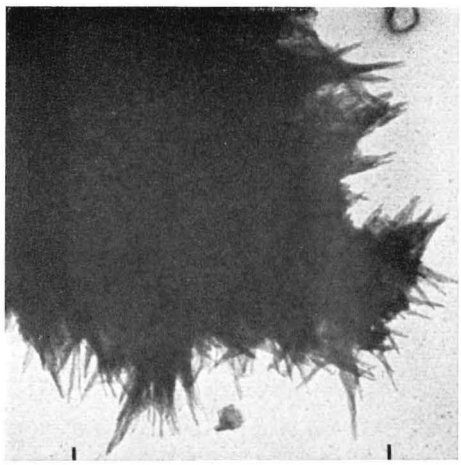

Fig. 356

Fig. 357

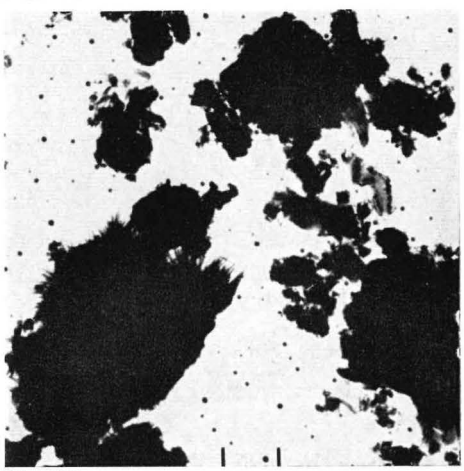

Fig. 358

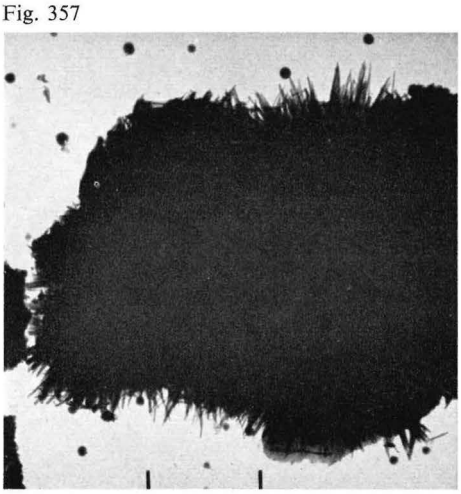

Fig. 359

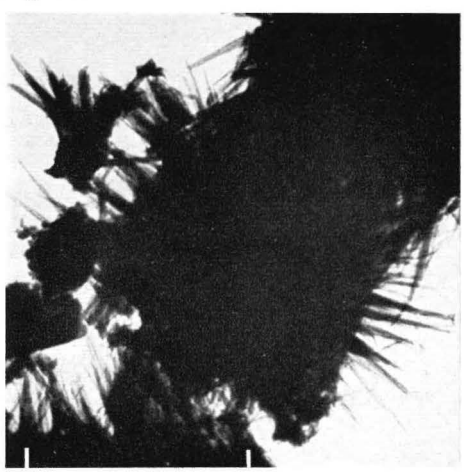

Fig. 360

92. Hydrated cement

Development of gel structures in alite-C_3A paste

Figs. 361 and 362. Sample TAp—1A.

A sample observed a few minutes after contact with water showed very little sign of reaction, but in a sample taken out after 3 hours the anhydrous crystals were covered with a very thin coat of hydrated structures. No products of hydration of C_3A could be identified with certainty.

EMs: After 24 hours, the cement particles were covered with fibrous structures similar to those observed in the alite and alite-sulfate pastes in preceding pages. A certain amount of a phase appearing as thin, irregular plates was also present, but its identity could not be established with certainty.

The X-ray diagram contained patterns of alite, C_3A, and CH, together with a very weak and diffuse reflexion at about 8.0 Å, indicating a the formation of traces of C_4AH_{13}. It was observed by *Chatterji* (CBI internal report) that the presence of alite (or rather, the saturated lime solution formed from it) tended to retard the C_3A reaction considerably.

Figs. 363—365. Sample TAp—1B.

EM (363): Sample after 14 days, survey micrograph showing representative structures, mainly gel particles with fibrous edge structures (not resolved at this magnification), and also plate particles identifiable as crystals of either CH or C_4A aq. (hex.).

EM (364): Most of the gel particles showed structures of fine fibers and also a large proportion of very irregular particle elements. The only ED effect given by these structures was the usual, weak ring at about 3.0 Å.

EM (365a): Large plate crystal.

ED (365b): Spot pattern of regularly-hexagonal symmetry, $a_H = 5.75$ Å, corresponding to the unit cell of the C-A-H(hex.) phases. The dimensions and the distribution of intensities in this patter are similar to those obtained for the patterns in e.g. Figs. 89, 94, 95, 98, and others.

The X-ray diagram of the 14-day sample showed a strong pattern of CH, further weak patterns of alite and C_3A, of which the alite reflexions at e.g. 2.78 and 2.73 Å had weakened more than the C_3A reflexion at 2.70 Å. The basal reflexion of C_4AH_{13} at 8.0 Å had become somewhat stronger and sharper.

The X-ray diagram of the sample at 3 months of age contained a CH pattern and a weak but sharp reflexion at 2.70 Å, indicating that the alite phase had disappeared but that some amount of unhydrated C_3A still remained. The C-S-H gel phase showed up with the usual, weak reflexions at 3.04, 2.78, and 1.82 Å. The C_4AH_{13} reflexion at 8.0 Å had almost disappeared, and instead, weak reflexions belonging to the C_3AH_6 pattern, of cubic symmetry, appeared at 5.12 (211), 3.34 (321), 2.28 (521), and 2.025 Å. (532) (611): The corresponding unit cell is $a_c = 12.50$ Å, or somewhat smaller than the value normally observed for C_3AH_6, $a_c = 12.58$ Å (cf. discussion of Fig. 54). This indicates that some replacement of water by silica (S for 2H) might have occurred in the hydrogarnet lattice.

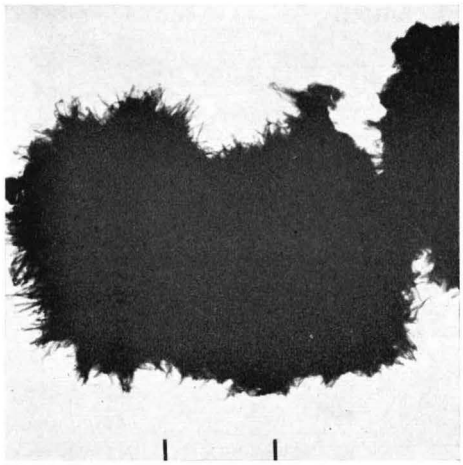

Fig. 361

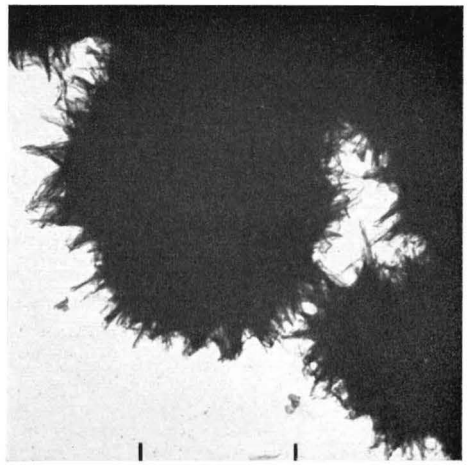

Fig. 362

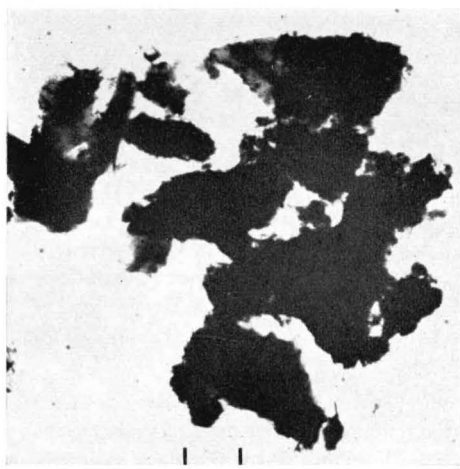

Fig. 363

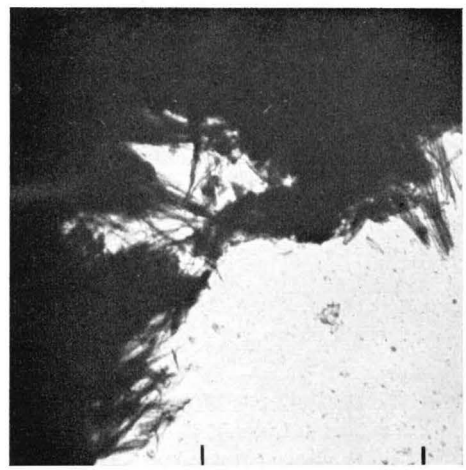

Fig. 364

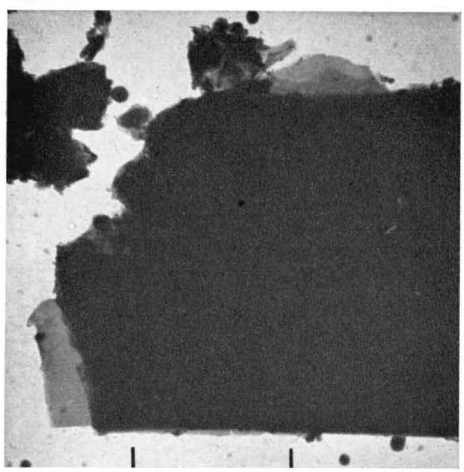

Fig. 365 a

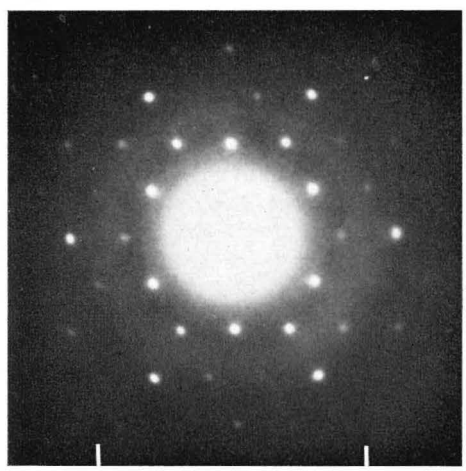

Fig. 365 b

93. Hydrated cement

Development of gel structures in alite-C_3A paste with sulfate addition

Figs. 366—368. Sample TAp—2A.

In the 3-hour sample, very little surface reaction could be detected, but some ettringite rods were observed.

EMs: After 24 hours, the cement particles were covered with fibrous structures of C-S-H gel, and numerous ettringite rods were also observed, as well as large CH crystal plates.

The X-ray diagram contained patterns of alite, C_3A, $C\bar{S}H_2$ (gypsum), and CH, and also a couple of weak ettringite reflexions at 9.8 and 5.6 Å.

Figs. 369—371. Sample TAp—2B.

EMs (369, 370): Sample after 14 days, the coat of fibrous or needle-like C-S-H gel particles on the surface of the aggregates had grown out further, similarly to preceding sample (TAp—1).

EM (371): Ettringite rods were also observed in several areas of the sample. The EM shows a whole stack of such rods.

The X-ray diagram of the 14-day sample contained a strong CH pattern, weakened alite and C_3A reflexions, and some ettringite lines, of which those at 9.8 and 5.65 Å. were most clearly resolved and did not interfere with lines from other substances present.

In the X-ray diagram of the 3-month sample, there are strong patterns of CH and $C_4A\bar{S}$ aq. (hex.) ("monosulfate"), the latter with reflexions at 8.95 (vs), 4.46, 4.00, 2.875, 2.74, 2.45, 2.415, 2.335, 2.26, 2.19, 2.07, 2.00, and 1.825 Å, in good agreement with values given by *Midgley* 1957. Some ettringite lines are also present, but they are weaker than in the 14-day sample. Rather weak and diffuse lines at 3.04, 2.78, and 1.815 Å indicate the presence of C-S-H gel phase. The alite pattern has disappeared, but the 2.695 and 1.908 Å reflexions of C_3A can still be discerned as weak but sharp lines.

The $C\bar{S}/C_3A$ ratio of this artificial cement sample is about 0.7. However, because of the low rate of solution of C_3A in the saturated lime solution formed by the alite reaction, the C-A-$\bar{S}$-H phase that develops first is of the trisulfate type. This starts to convert to monosulfate first when the ratio $C\bar{S}/C_3A$ (dissolved) has fallen below 3, and seems to persist even when this ratio approaches 1.

A similar paste mixture, although with a reduced sulfate content, corresponding to a $C\bar{S}/C_3A$ ratio of about 0.3, was also examined by *Chatterji* (CBI internal report). Also in this case, the X-ray reflexions of C_3A disappeared much more slowly than the reflexions of alite. At 24 hours, the X-ray diagram showed the $C_6A\bar{S}_3$ aq. lines at 9.8 and 5.6 Å. At 14 days, these lines had decreased in intensity and were just visible, and instead a couple of new low-angle lines had appeared at 8.95 and 8.3 Å. The first line is the stronger of the two, and most probably is the normal basal spacing of the monosulfate phase, $C_4A\bar{S}H_{10}$. The second line may correspond to a lower state of hydration, or may originate from a member of the $C_4A\bar{S}H_{10}$—C_4AH_{13} solid-solution series. These lines were the only ones remaining in the low-angle range after 1 month, whereas the ettringite lines had disappeared at this time.

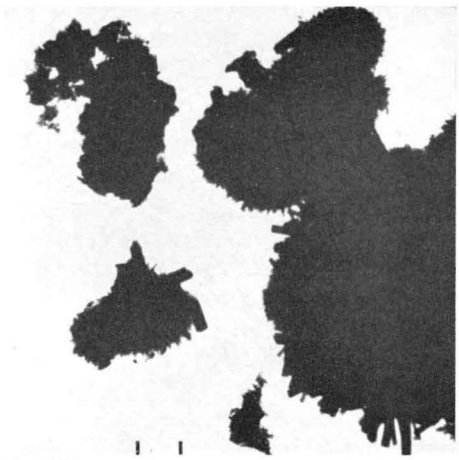

Fig. 366

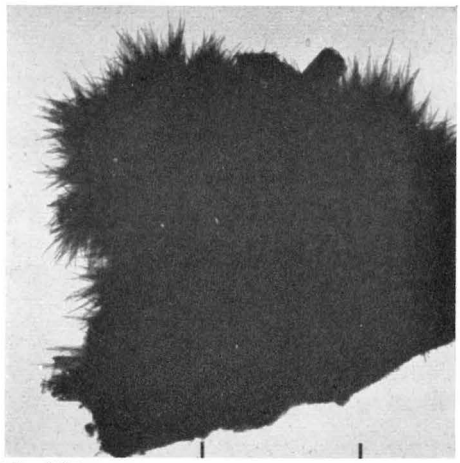

Fig. 367

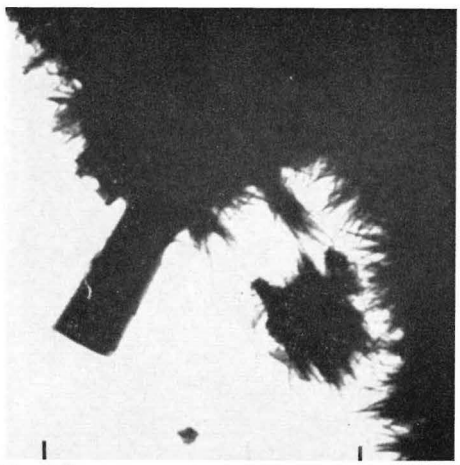

Fig. 368

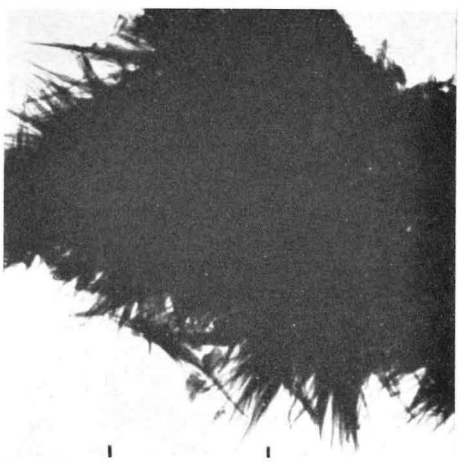

Fig. 369

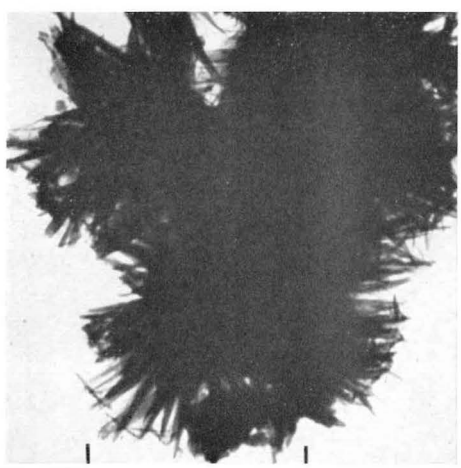

Fig. 370

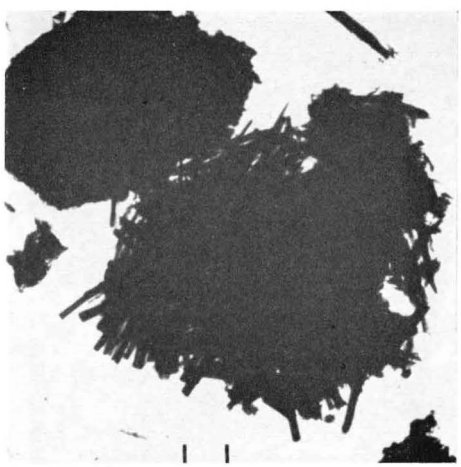

Fig. 371

94. **Hydrated cement**

Gel structures in steam-cured cement pastes

Figs. 372 and 373. Sample Ppq—1.

EMs: The microstructure of this paste, which was steam-cured for one day under very high pressure, was essentially similar to standard cement pastes cured at ordinary temperatures. The gel aggregates are seen to consist of small flakes or irregular fragments, with some elongated or rod-like particles, but no fibrous structures. C-A-H(hex.) structures could not be found, and instead small amounts of clay-type particles were observed (cf. Figs. 419 and 420).

Figs. 374—376. Sample Ppq—4.

EMs: The gel structures of this paste, which had been steam-cured for 3 days, consisted mainly of fine fibers or needles (Fig. 374), with some aggregates composed of irregular fragments of very fine texture (Fig. 375). Many CH crystal plates were also observed (Fig. 376 a).

ED (376b): CH single-crystal pattern, (*hk*.0) and associated (*hk*.1) spots.

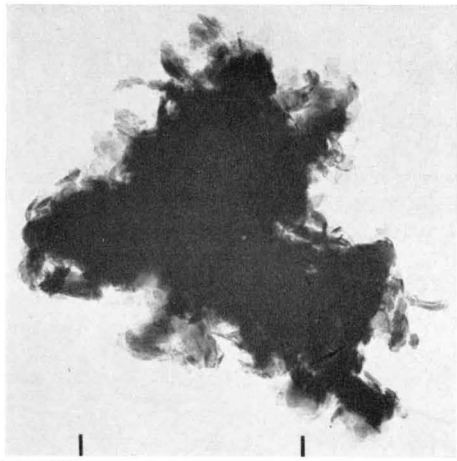

Fig. 372

Fig. 373

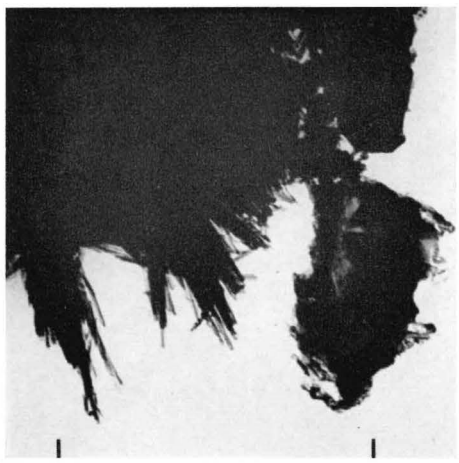

Fig. 374

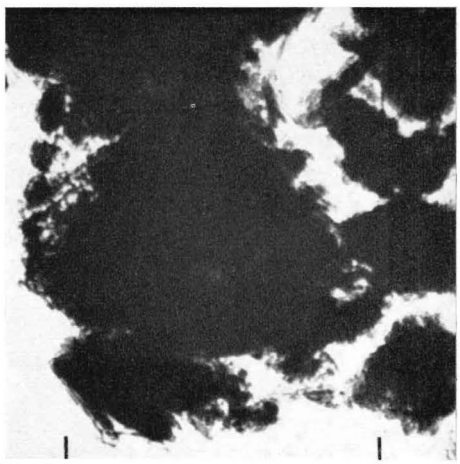

Fig. 375

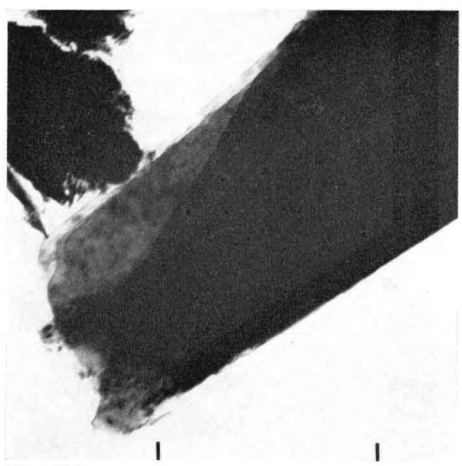

Fig. 376 a

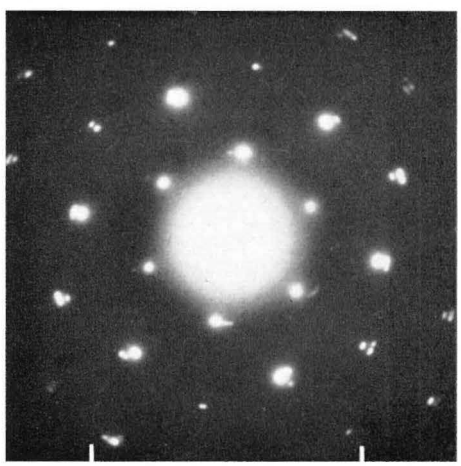

Fig. 376 b

95. **Hydrated cement**

Gel structures in steam-cured cement pastes (continued)

Figs. 377—380. Sample Ppq—5.

This paste, which was autoclaved at 200° C, contained only comparatively well crystallized material.

EM (377): Survey micrograph, showing various types of crystal chips or fragments.

EM (378): Similar crystal fragments at higher magnification.

EM (379): Acicular crystals, minor constituent of sample, probably $C_6S_2H_3$ crystals (cf. Figs. 216—218). (ED: Indistinct spot pattern, with certain features characteristic of a $C_6S_2H_3$ pattern).

EM (380): Rectangular, block-shaped crystal, probably α-C_2SH (cf. Figs. 219 and 220) (ED: Indistinct spot pattern).

In addition to these formations, several large, well-crystallized CH plates were also observed.

The X-ray diagrams indicate that the reaction is nearly complete at 7 hours, and there are only small differences between the diagrams after 7 and 72 hours. These contain strong patterns of CH and α-C_2SH, weak indication of $C_6S_2H_3$ reflexions, e.g. at 8.8 Å. and, remarkably enough, some lines which must be interpreted as originating from a residue of an unhydrated cement component.

Figs. 381 and 382. Sample PSpq—1.

EMs: Survey micrographs of representative parts of this sample, cement-silica paste autoclaved at 150° C, show that the large paste particles covered with a hydrated material of extremely fine subdivision, probably finely fibrous (cf. next page). The development of this substance is certainly conditioned by the addition of high-surface silica. Also visible in these EMs are a few particles with a habit of coarse, straight rods, resembling ettringite-type structures.

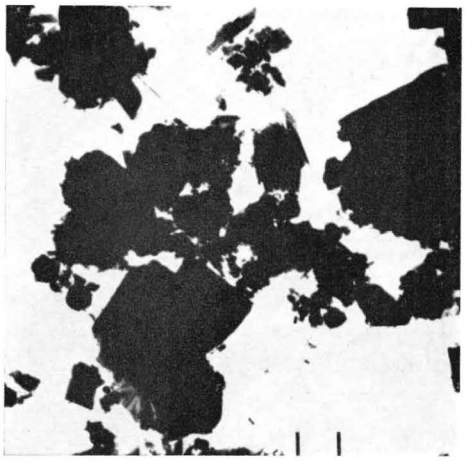

Fig. 377

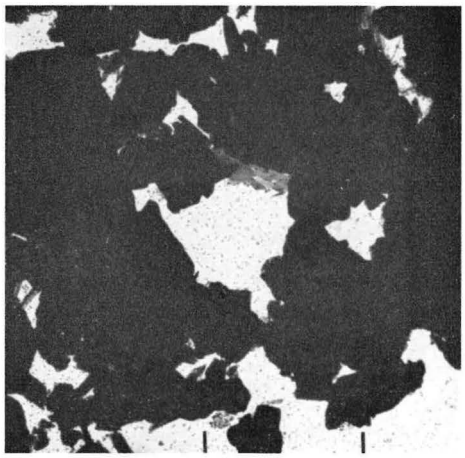

Fig. 378

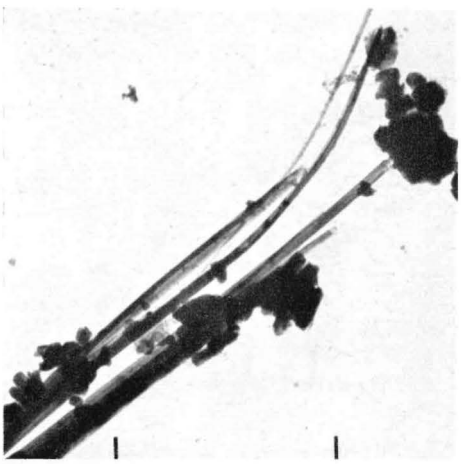

Fig. 379

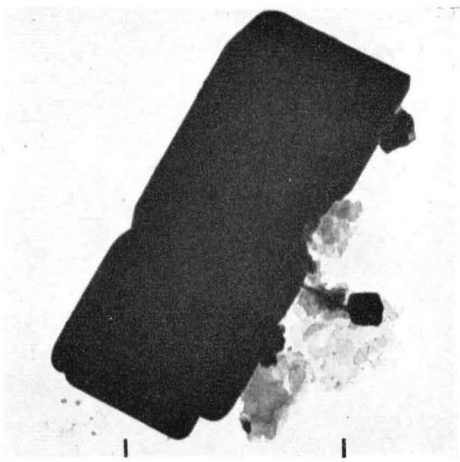

Fig. 380

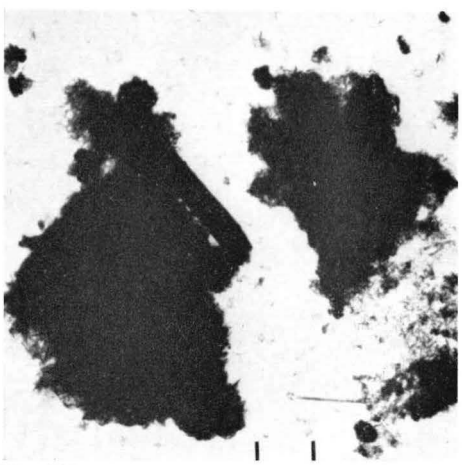

Fig. 381

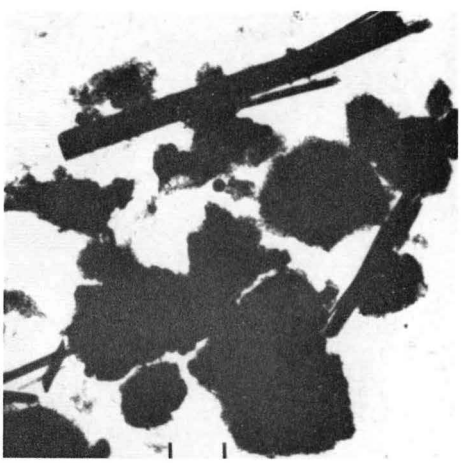

Fig. 382

96. **Hydrated cement**

Gel structures in steam-cured cement pastes (continued)

Fig. 383. Sample PSpq—1.

EM: Agglomerate of extremely small particles, fibers and more irregular specks of matter, of the order of 20—50 Å in diameter.

ED: Weak rings at 3.06 and 1.84 Å (more clearly visible in a few other diagrams), indicative of a C-S-H(I) or (II) gel phase.

The X-ray diagram of this sample consisted almost exclusively of a strong α-C_2SH pattern, with no sign of CH reflexions and only indistinct indications of the C-S-H(I) reflexions observed in ED diagrams. However, the crystal blocks ordinarily assumed to be representative of α-C_2SH phase are not very common in the EM film recorded.

The X-ray diagram also shows a couple of very weak reflexions at 9.8 and 5.65 Å, indicative of the presence of a small amount of ettringite-type phase. Ordinarily, ettringite is supposed to be unstable at elevated temperatures. However, as suggested by *Chatterji* (CBI internal report), ettringite is certainly formed in the initial period of curing at room temperature, and may then become stabilized by the incorporation of SiO_4 groups, probably replacing the AlO_4 tetrahedra of the thaumasite-like ettringite structure (see discussion under Fig. 116). Such a process may be facilitated by the availability of reactive silica in the reaction mixture.

Figs. 384—386. Sample PSpq—2.

EMs (384, 385): Cement-silica paste autoclaved at 200° C, survey micrographs of certain representative parts of the sample, consisting of a loosely flocculated mass of fibrous or acicular particles of cross-sectional dimensions ranging between very small (less than 50 Å) and rather large (about 2000 Å). Another part of the sample, which probably constitutes most of the mass, consists in large block-shaped crystals, sometimes wrapped in the finely-fibrous phase.

The X-ray diagram consisted mainly of a strong α-C_2SH pattern, with a few weak reflexions from other substances. A weak 9.8 Å line, possibly attributable to an ettringite-type phase, was present after 24 hours, but could not be detected in the 72-hour sample. Other reflexions outside the α-C_2SH pattern were noticed at 3.06 and 1.845 Å, and are probably identical with the strongest reflexions observed in ED patterns (cf. below).

EM (386a): The finely-fibrous phase at higher magnification.

ED (386b): Reflexions at *3.09*, 2.83, 2.07—1.96 (spotty region), *1.87*, 1.70, 1.57, 1.43 Å (the two strongest reflexions in italics). This pattern probably originates from a slightly expanded C-S-H(I) phase, and resembles the pattern shown e.g. in Fig. 160b.

The observations made on the last two samples indicate that the high-temperature steam-curing of cement paste with admixture of silica gel of high specific surface results in the formation of a two-phase mixture of hydrates. One of these, the α-C_2SH phase, constitutes the bulk of the material. The other one, a C-S-H(I)-type phase probably of high C/S ratio, seems to fill out the pore spaces and would therefore be responsible for the hydraulic properties of the composite material. It seems to be remarkably stable, judging from the fact that the X-ray patterns change very little in the period between 24 and 72 hours of autoclaving.

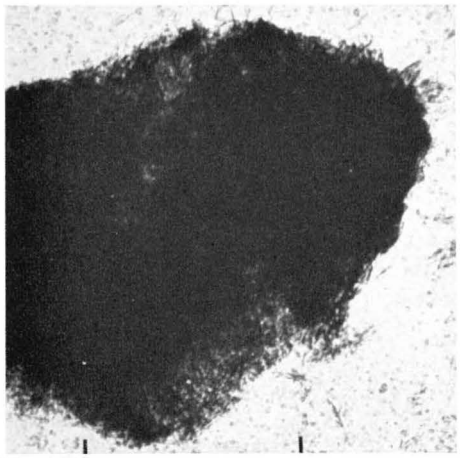

Fig. 383 a

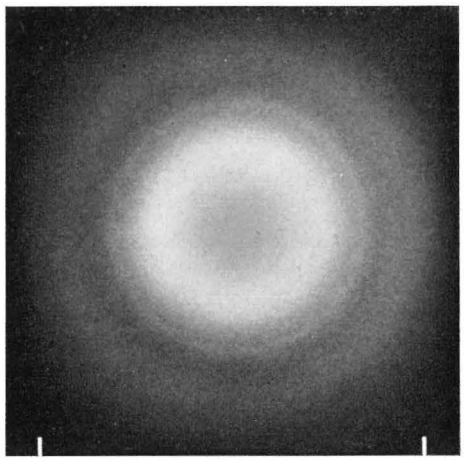

Fig. 383 b

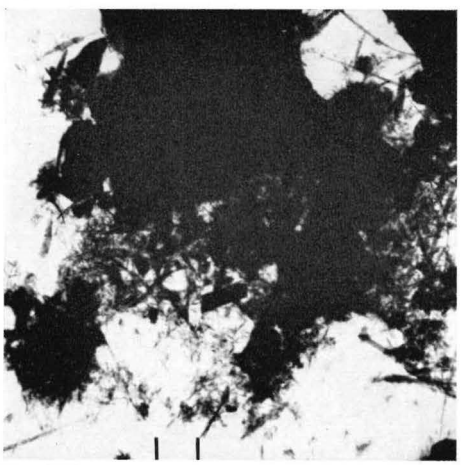

Fig. 384

Fig. 385

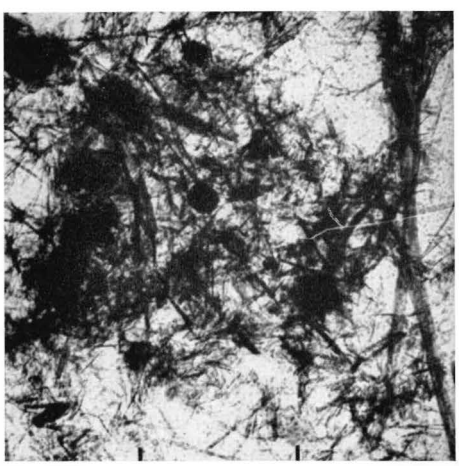

Fig. 386 a

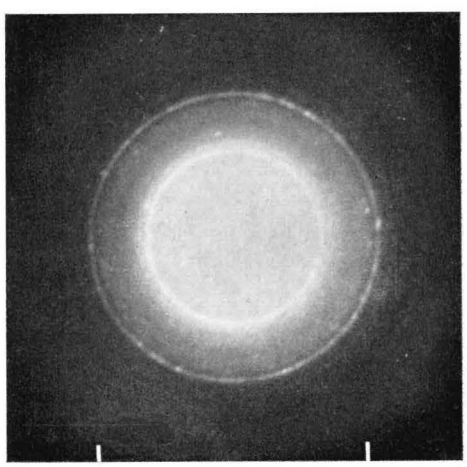

Fig. 386 b

97. **Hydrated cement**

Gel structures in steam-cured cement pastes (continued)

Fig. 387—390. Sample Ppq—2.

This paste can be taken to represent the products of autoclaving at high pressure and relatively high temperature.

EMs: The main gel structures are decidedly fibrous or acicular. The particle elements are often parallel-oriented and aggregated in bundles. Some aggregates have the appearance of puckered or corrugated sheets, resembling crepe paper, similar to the formations which develop in ordinary cement pastes observed by *Copeland* and *Schulz* 1962 a, b. Some plate crystals also visible can be identified either as CH or a clay-type phase (cf. Fig. 418). Occasional rod crystals are probably high-temperature C-S-H phases (cf. next page).

EDs: The fibrous C-S-H gel phase gives a diffuse ring with maximum intensity at 2.95—3.00 Å, and a sharp fiber reflexion at 1.82 Å. Thus it is not essentially better-crystallized than the fibrous phase developing in paste cured at ordinary temperature.

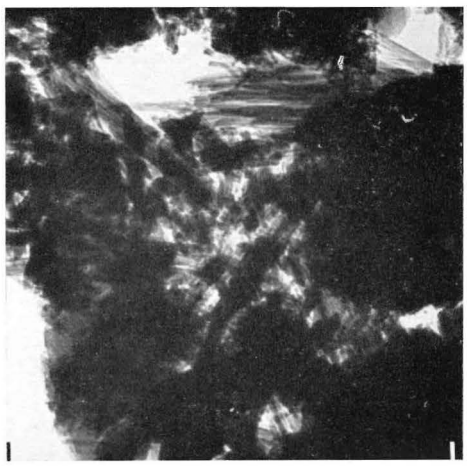

Fig. 387 a

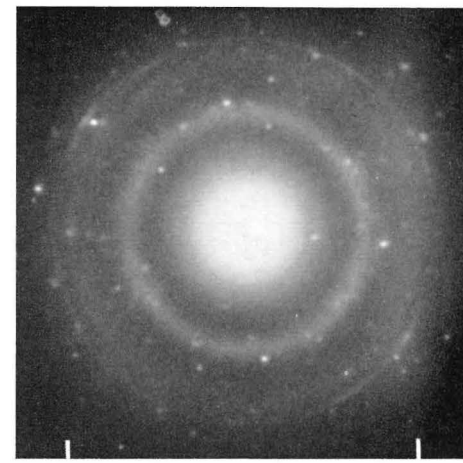

Fig. 387 b

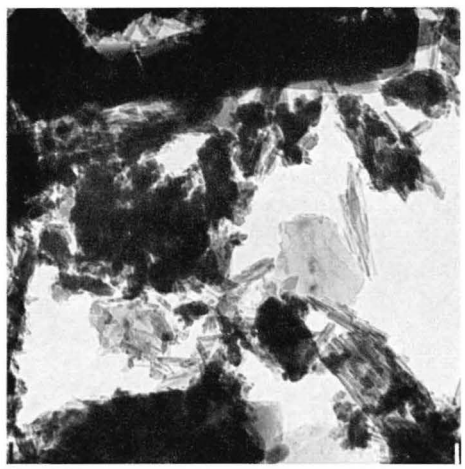

Fig. 388

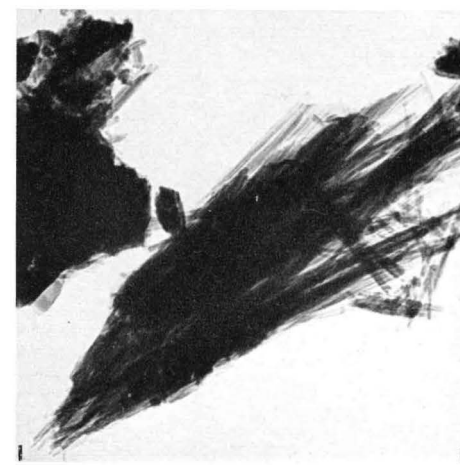

Fig. 389

Fig. 390 a

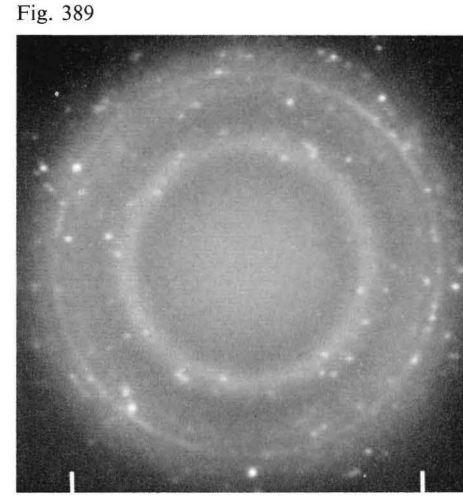

Fig. 390 b

98. **Hydrated cement**

Gel structures in steam-cured cement pastes (continued)

Figs. 391—394. Sample Ppq—2.

EMs: These are examples of rod-like or lath-like crystals found in minor amounts in this sample.

ED (391b): Irregular spot pattern. The pair of strong spots corresponds to 1.87 Å, probably the (00.4) reflexion of $C_6S_2H_3$ (cf. next two patterns).

EDs (392, 393): Parts of patterns given by rod-like crystals, 2—3μ long and 0.1—0.2μ wide (EMs not shown), spot reflexions in a simple, orthorhombic pattern, corresponding to a cell of dimensions 5.02×3.76 Å. The streaks halfway between the rows of spots in one direction show that the true unit cell is 2×3.76=7.52 Å. These data agree well with those of the unit cell of $C_6S_2H_3$, $a_H \times c_H = 10.0 \times 7.48$ Å, as given by *Buckle et al.* 1958 (cf. discussion of Fig. 218).

ED (394b): Two intersecting layer-line patterns. The angle of intersection is the same as the angle between the crystals in Fig. 394a. The unit cell of the ED patterns is $a \times b = 11.62 \times 7.26$ Å, with distinct spots for k even, streaks for k odd. This particular type of pattern is very similar to those given by the end product of autoclaving of lime-quartz mixtures at 195° C, described by *Grothe et al.* 1962, who observed a somewhat smaller spacing, 11.3 Å, which they interpreted as a basal spacing from a phase related to tobermorite. Alternatively, the pattern could be interpreted as originating from the $b \times c$ zone of hillebrandite, with which it agrees reasonably well with respect to both dimensions and general distribution of spots (cf. Fig. 215).

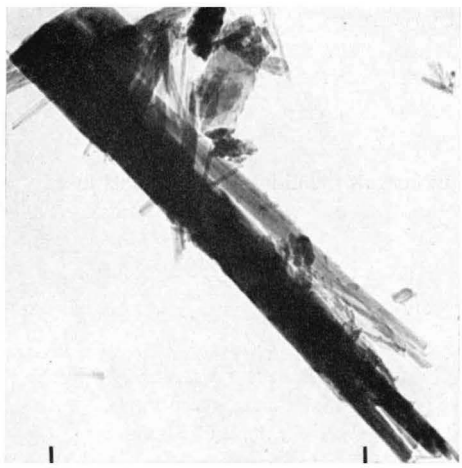

Fig. 391 a

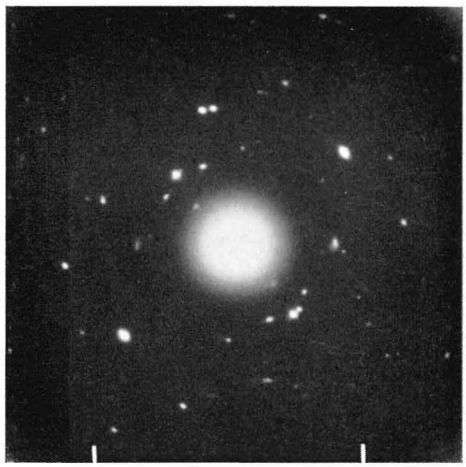

Fig. 391 b

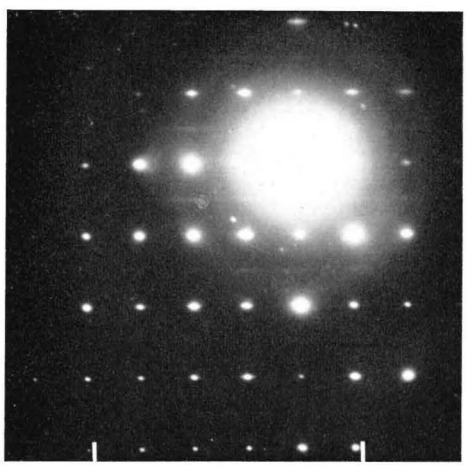

Fig. 392

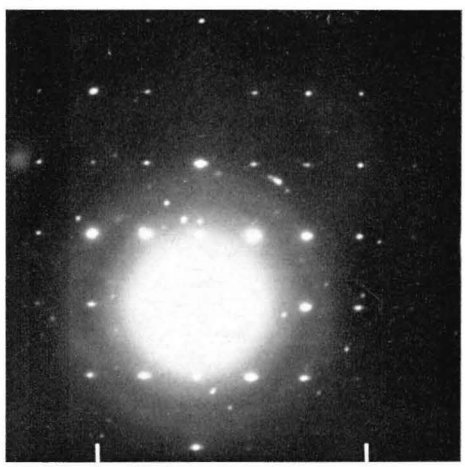

Fig. 393

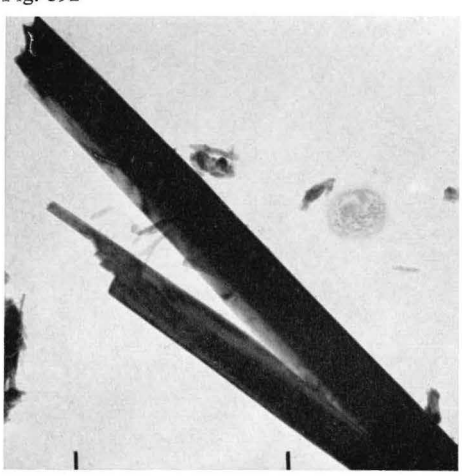

Fig. 394 a

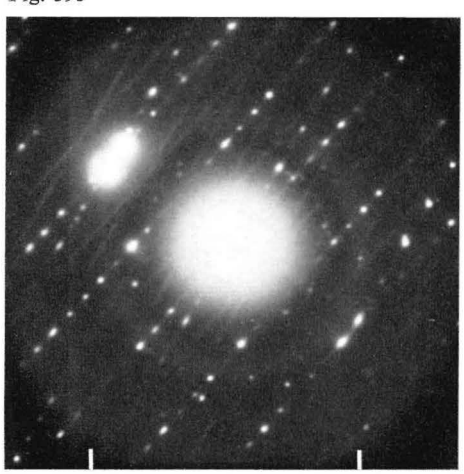

Fig. 394 b

99. **Hydrated cement**

Gel structures in steam-cured cement pastes (continued)

Figs. 395—397. Sample Ppq—3.

This paste can be taken as representing the products of autoclaving at high temperature (214° C) and saturation pressure. The sample contains no truly gelatinous components. only recrystallized material.

EMs: Various structures representative of this sample, such as block-shaped crystals of various dimensions (α-C_2SH), aggregates of thin plates (clay-mineral phase), and occasional needle-like particles ($C_6S_2H_3$).

EDs (395b, 396b): Large number of spot reflexions in irregular arrangement and without a pronounced tendency to ring formation. These patterns are believed to be representative of a collection of rather well crystallized particles of several phases, and cannot be interpreted.

ED (397b): Spot diagram containing a pattern of slightly distorted hexagonal symmetry, with a unit cell a_H of about 5.3 Å, a clay-mineral pattern given by the thin plate visible in Fig. 397a.

The X-ray diffractometer record of this paste contains strong patterns of CH and α-C_2SH, the latter with prominent peaks at e.g. 5.33, 4.225, 3.920, 3.545, *3.268*, 2.876, 2.662, 2.604, 2.530, *2.416* Å., and many others. Patterns from other phases are partly masked by the major-phase reflexions. There are low peaks at 8.75, 3.30, 2.50 and 2.47 Å, which probably originate from $C_6S_2H_3$, and certain other reflexion effects at 4.78, 3.00, 2.905, 2.745, and 2.235 Å indicate the presence of small amounts of hillebrandite, although in the latter case the intensity relations differ from those given by *Heller* and *Taylor* 1956.

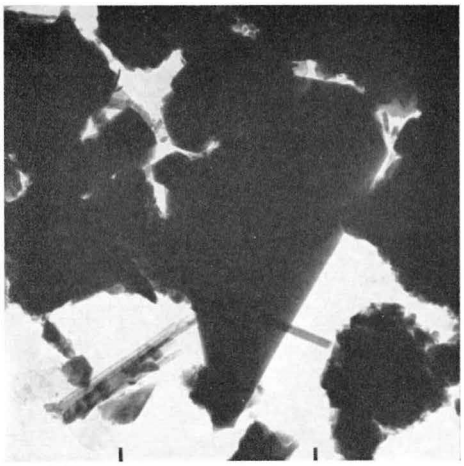

Fig. 395 a

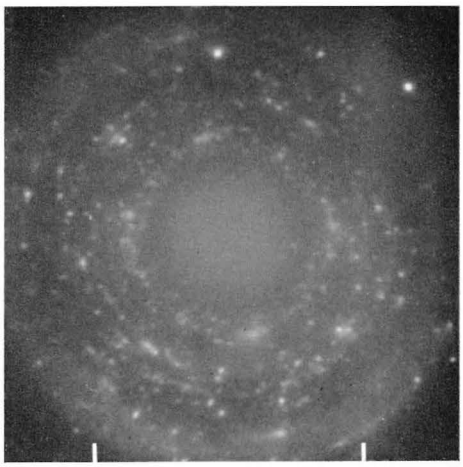

Fig. 395 b

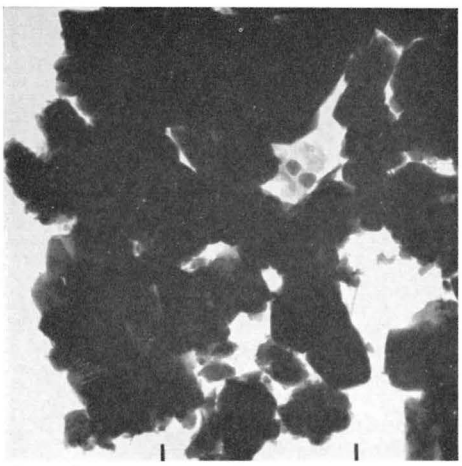

Fig. 396 a

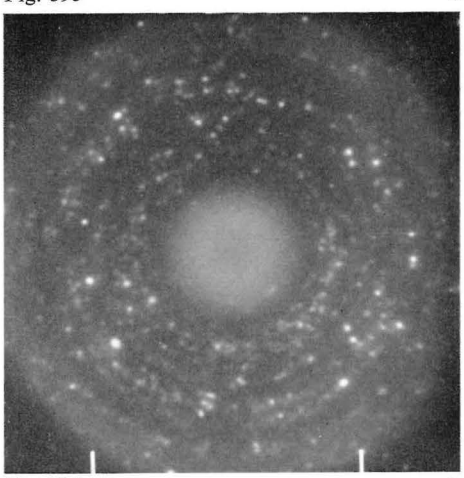

Fig. 396 b

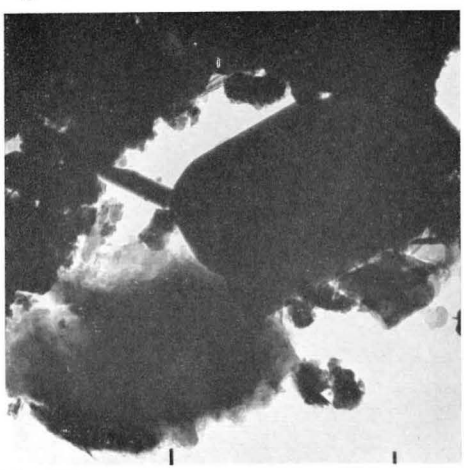

Fig. 397 a

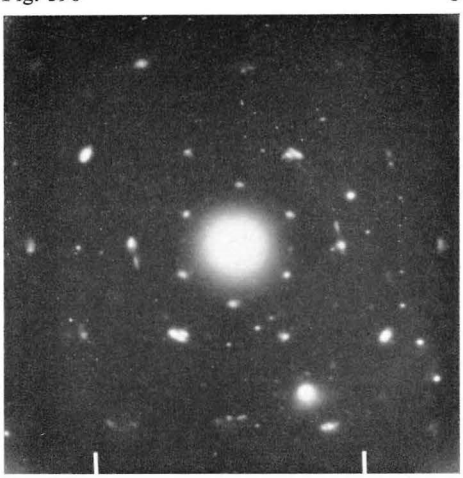

Fig. 397 b

100. **Hydrated cement**

Gel structures in steam-cured cement pastes (continued)

Figs. 398—400. Sample Ppq—3.

EM (398a): Network of crystals of the habit of thin rods or laths, about 100—200 Å wide.

ED (398b): Spot-ring diagram with scattered spots at 8.64, 4.96, 4.22, and 3.84 Å, and spot-rings at 3.29, *2.99*, *2.82*, 2.46, 2.08, *1.86*, 1.75, 1.62, 1.565 Å (prominent rings in italics), in fair agreement with the X-ray powder pattern of $C_6S_2H_3$ given by *Buckle et al.* 1958.

EM (399a): $C_6S_2H_3$ crystal rods, about 300—500 Å wide, with some other material.

ED (399b): Disordered spot diagrams given by the bundle of $C_6S_2H_3$ crystals, with the spots arranged in layer-lines. Especially prominent is the (00.4) reflexion streak at 1.88 Å.

EM (400a): Bundle of $C_6S_2H_3$ crystal rods, similar to the one in Fig. 399 a.

ED (400b): Spot pattern from single crystal rod, isolated by means of selected-area aperture, very similar to the patterns of Figs. 392 and 393, except that there are no polymorphic-disorder streaks for l odd in the present pattern. The pattern corresponds to the reflexions with k and l even from a cell $a_H \times c_H = 10.00 \times 7.46$ Å.

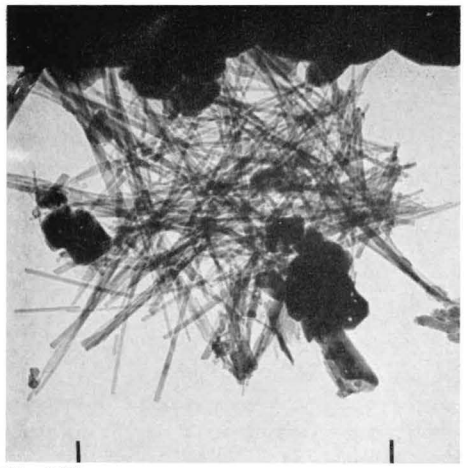

Fig. 398 a

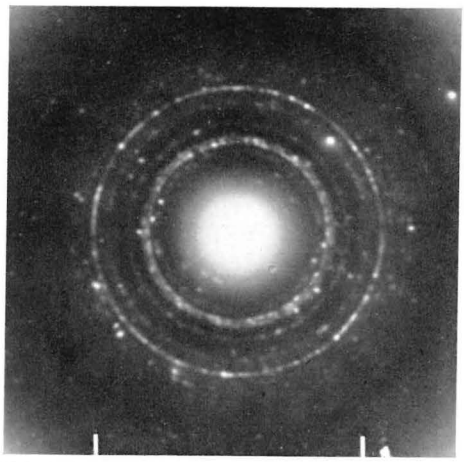

Fig. 398 b

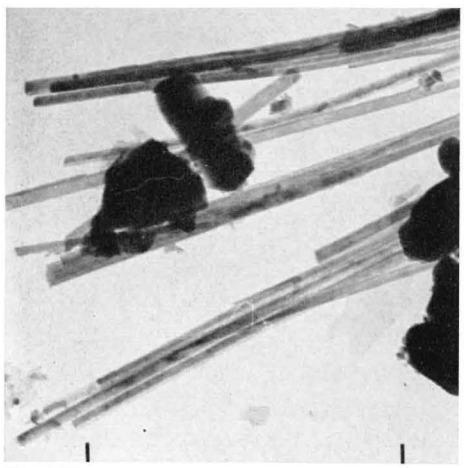

Fig. 399 a

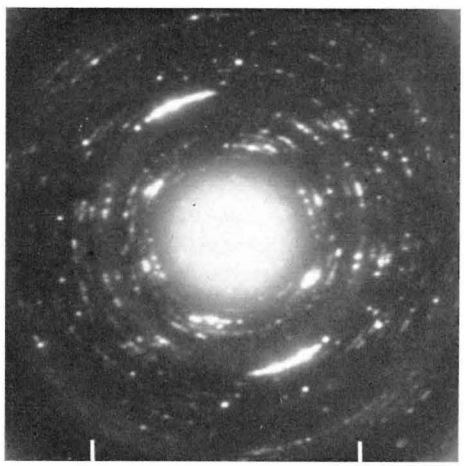

Fig. 399 b

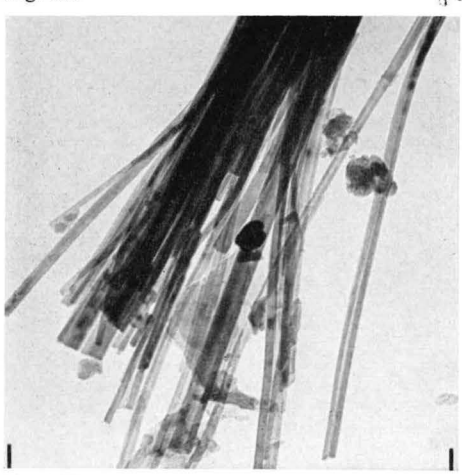

Fig. 400 a

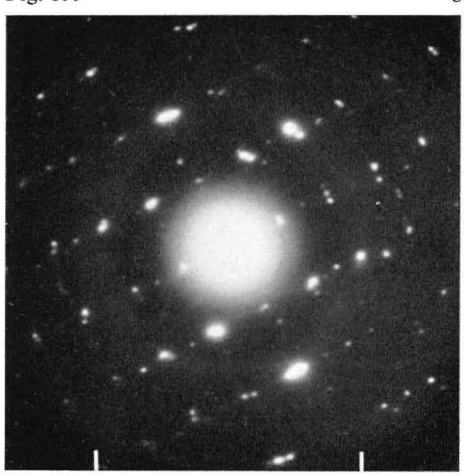

Fig. 400 b

101. **Hydrated cement**

Gel structures in steam-cured cement pastes (continued)

Figs. 401—403. Sample Ppq—3.

EMs: Examples of clay-mineral structures developing as aggregates of very thin plates together with other structures (see previous pages) in the paste steam-cured at high temperature. This type of formation is too common in the sample to be explained as a contaminant. According to the handbooks of clay mineralogy, hydrothermal treatment at 300° C or higher is mostly employed for the purpose of rapidly obtaining synthetic clay minerals from feldspars and similar starting materials. However, small amounts of clay mineral phase are likely to occur at much lower temperatures in autoclaved mixtures with the proper composition of cations in solution. The alkaline lime solution of a cement paste mix is likely to promote the formation of clay-type phases. These are probably composed chiefly of magnesium silicate hydrates, members of the M-S-H system, with certain substitutions of A or F for M in octahedral positions, A for S in tetrahedral positions of the oxide lattice.

It is difficult to estimate the actual degree of such substitutions. However, the C-S-H phases formed at higher temperatures of cement paste autoclaving, such as α-C_2SH and $C_6S_2H_3$, probably do not take up Al or Fe ions in their crystal structures quite as readily as do the badly-crystallized gel phases formed at lower temperatures. Consequently, there would be more Al and Fe ions available for accommodation in clay-mineral phases. Since in standard cement the content of M alone amounts to about 2.5 percent, it is realized that the content of clay-type phase in the steam-cured paste can easily be 10 percent or more.

ED (401b): Two (*hk*.0) hexagonal-symmetry spot patterns, mutually rotated about 30°. The measured hexagonal spacing is $a_H = 5.34$ Å, a unit cell dimension characteristic of M-S-H clay minerals, such as chlorite or vermiculite.

ED (402b): Spot-ring pattern, (*hk*.0) reflexions from a spacing $a_H = 5.34$ Å. There are some other, weak spot reflexions at 2.50 and 1.875 Å, probably the (00.3) and (00.4) reflexions of $C_6S_2H_3$ crystals also present in the EM, and occasional CH spots.

ED (403b): Composite diagram, containing two (*hk*.0) hexagonal-symmetry patterns, one with $a_H = 5.34$ Å. (clay-mineral phase), and one with $a_H = 3.59$ Å (CH). Other reflexions, at 2.50 and 1.87 Å, are probably the (00.3) and (00.4) reflexions of $C_6S_2H_3$ crystals.

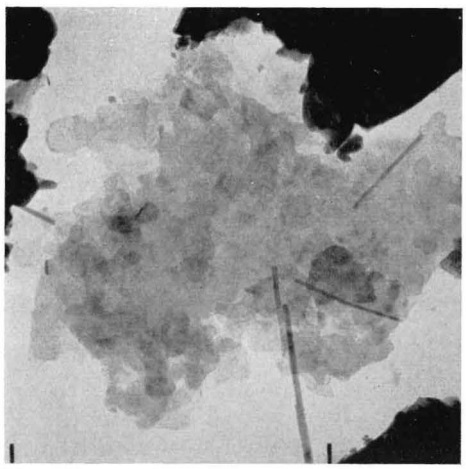

Fig. 401 a

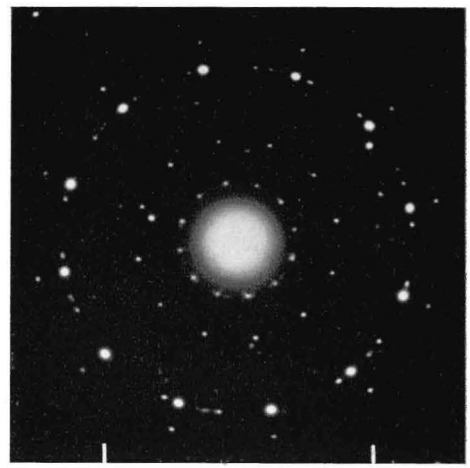

Fig. 401 b

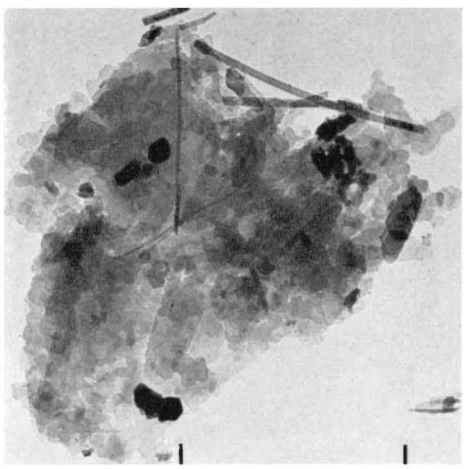

Fig. 402 a

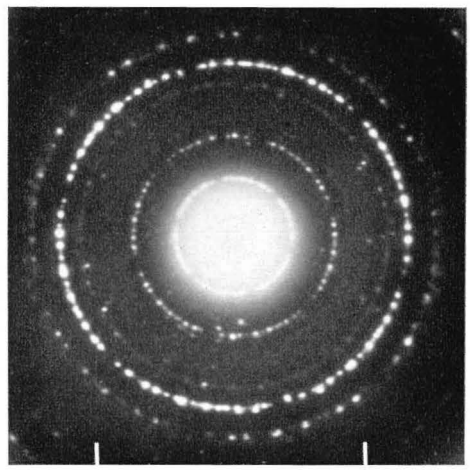

Fig. 402 b

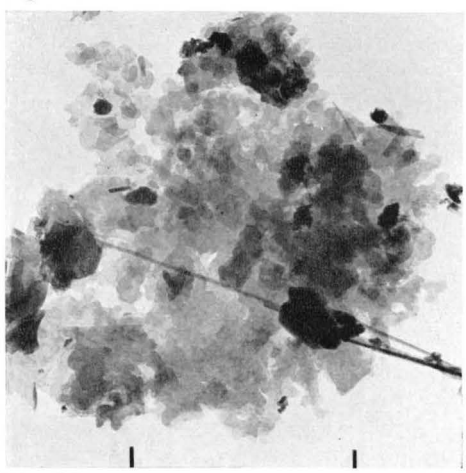

Fig. 403 a

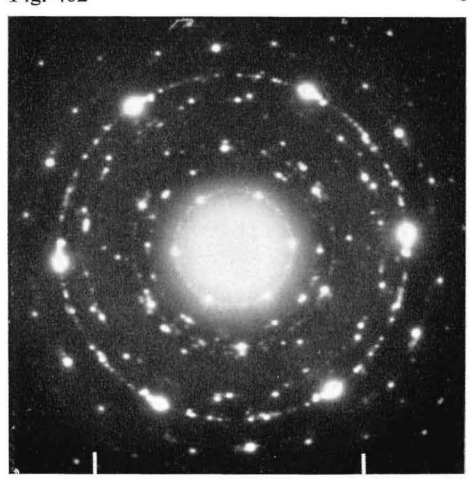

Fig. 403 b

102. **Hydrated C-A cement**

Gel structures in high-alumina cement pastes

Figs. 404 and 405. Sample Hp—1.

EMs: Large aggregates of gel particles, at many places dispersed into thin flakes or wavy foils with irregular edges.

EDs: Patterns of single-crystal spots in irregular distribution, more or less prominent reflexions at 3.54, 3.26, 2.70, 2.04, 1.84, 1.63, 1.32, and 1.27 Å. The identity of the corresponding compound is unknown. It is possible that the patterns originate from a secondary phase, formed from C-A-H(hex.) phases present in the paste, by the combined action of vacuum and irradiation in the EM column. However, there are hardly any indications of regularly hexagonal habits or angles of the thin plates, such as are observed as being retained in similar preparations of C_3A pastes or suspensions (cf. Figs. 66—74), in spite of the fact that the hydrated structures originally formed are transformed into amorphous material or anhydrous phases. Thus the EM observations seem to indicate that there are no hexagonal layer-lattice phases formed, as could be expected, but some other type of sheet-like structural elements.

The phase compositions of the anhydrous high-alumina cements used in the H samples are not known. According to *Lea* 1956, typical aluminous cements consist essentially of a mixture of CA, monocalcium aluminate, and C_2AS, gehlenite, the latter probably in an activated or reactive form, due to ionic substitutions of F for A in the lattice, together with variable amounts of ferrite-bearing phases, such as $C_6A_4F''S$ ($F''=FeO$) or C_6A_2F. The main products of hydration are, very schematically, CAH_{10} and C_2AS aq.(hex.) at low temperatures, C_2A aq.(hex.), C_2AS aq.(hex.) and AH_n at normal temperatures, and C_3AH_6(cub.) together with AH_n and probably C-S-H gel at somewhat elevated temperatures.

Figs. 406 and 407. Sample Hpq—1.

EMs: Structures very similar to those above.

EDs: Patterns equivalent to those above.

According to the EM data, the two samples, Hp—1 and Hpq—1, are identical, and thus the heat treatment seems to have had no effect. As stated in the list of samples, X-ray data indicated the presence of hexagonal phase in Hp—1, and cubic hydrogarnet phase in Hpq—1. However, neither of these phases can be detected in the EM specimens.

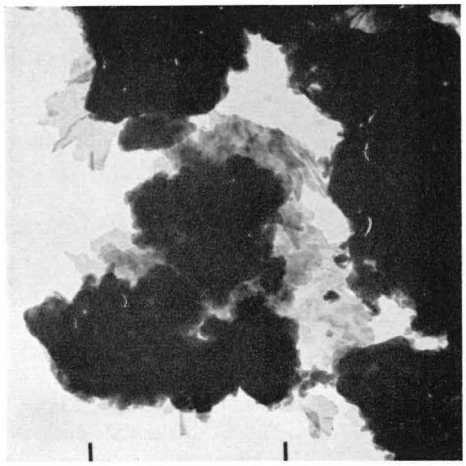

Fig. 404 a

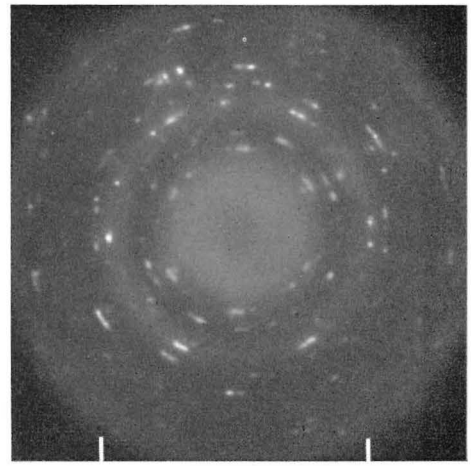

Fig. 404 b

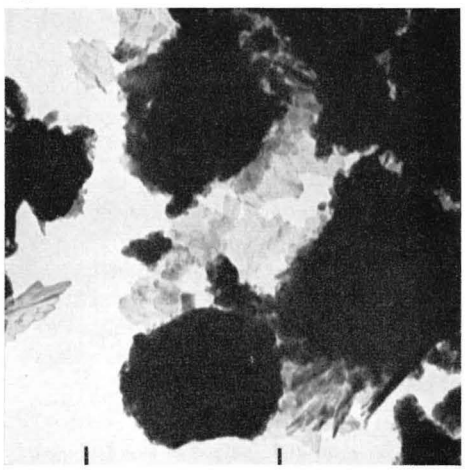

Fig. 405 a

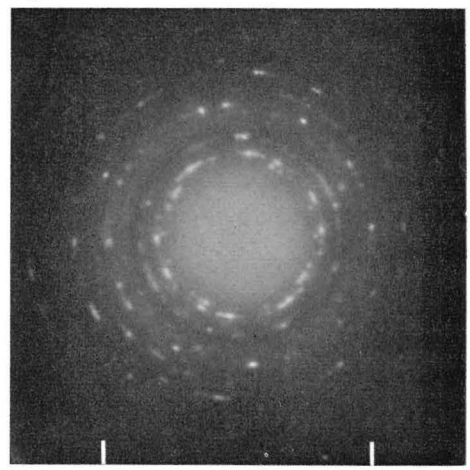

Fig. 405 b

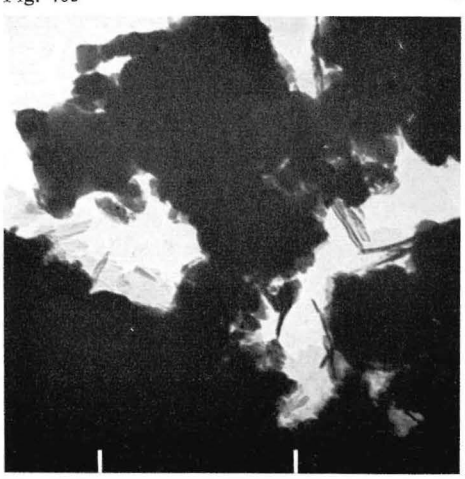

Fig. 406 a

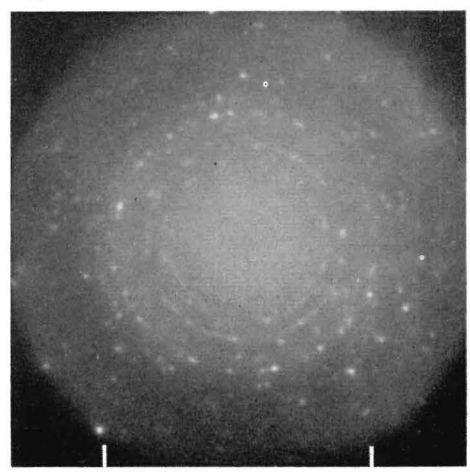

Fig. 406 b

103. Hydrated C-A cement

Gel structures in aluminous cement pastes

(Fig. 407, see preceding page)

Fig. 408. Sample Hp−2.

Fig. 409. Sample Hpq−2.

EMs: Both the unheated and the heated EM sample of this high-alumina cement paste contain aggregates of small flakes or foils. Most of these have rather irregular edges, but a few hexagonal plates were observed in the unheated sample. The ED patterns seemed very diffuse and indistinct, and no ED patterns were recorded photographically.

With regard to probable composition and X-ray data, the same observations apply as made for samples Hp−1 and Hpq−1 above.

Figs. 410 and 411. Sample Ap−1B.

EMs: C_4AH_{13} plates of more or less pronounced hexagonal symmetry, and C_3AH_6 (hydrogarnet) crystals of various cubic-symmetry habits (cf. e.g. Figs. 48−53). The hexagonal plates give ED patterns similar to those of e.g. Figs. 59b and 61b, with a unit cell $a_H = 5.80$ Å. The X-ray diagram of this 14-day sample contains a strong C_3AH_6(cub.) pattern, with $a_c = 12.56$ Å, and a C_4AH_{13} pattern, with a strong basal reflexion at 7.95 Å and certain other reflexions, e.g. at 2.875 Å (11.0) and 1.660 Å (30.0), both giving a hexagonal unit cell $a_H = 5.75$ Å. A weak C_3A pattern is also present, but has disappeared in the diagram recorded after 3 months, in which also the C_4AH_{13} pattern had become somewhat weaker.

Since the C/A ratio of this samples is 3, and since there are obviously no hydrated compounds present other than the hexagonal and the cubic phases, it seems natural to except that even the hexagonal phase should have an overall C/A ratio of 3, instead of 4 as assumed above. This brings up the much-debated question of the existence of a hexagonal C_3A aq. phase. According to *Turriziani* 1964, the C_3A aq.(hex.) phases reported by various authors have turned out to be either carboaluminate phases or equimolar mixtures of C_4A aq. (hex.) and C_2A aq.(hex.). Since the basal spacing of the latter phase is 10.7−10.4 Å corresponding to a unit with four oxygen layers, it cannot be present in appreciable quantities in sample Ap−1. However, the probable formation of C_3A aq.(hex.) in the C_4A aq.(hex.) structural unit, with three oxygen layers, can be explained in several alternative ways. In the C_4AH_{13} model proposed by *Buttler et al.* 1959, extra Al ions can be introduced, either in the octahedral layer, replacing Ca ions in excess of the normal proportion of one Al in every third octahedral site, or possibly in the water layer outside the base unit Ca_2AlO_6. In the C_4AH_{13} model suggested by *Grudemo* 1962, extra Al ions can easily be accommodated in empty octahedral or tetrahedral sites of the 1:1 clay-type unit, without much disturbance of the structure.

A substitution of Al for Ca ions would cause the hexagonal a_H unit cell to decrease, an introduction of Al ions into voids would lead to an increase in a_H. A comparison of the ED and X-ray data of the samples Ap−1B and Ap−3 shows no appreciable difference in the a_H dimensions, and the evidence available in these studies is thus inconclusive on this point.

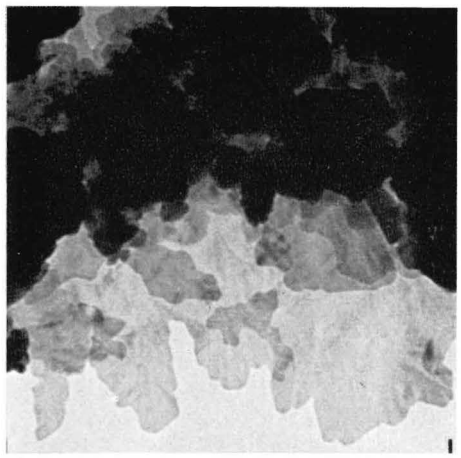

Fig. 407 a

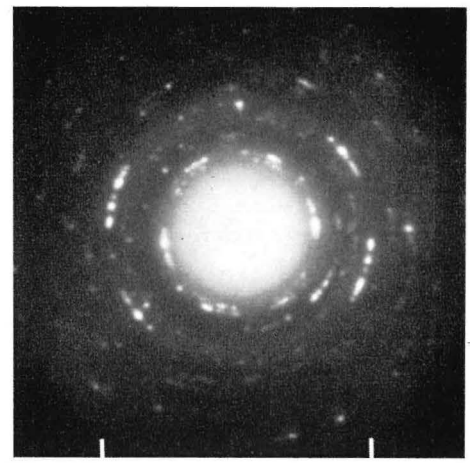

Fig. 407 b

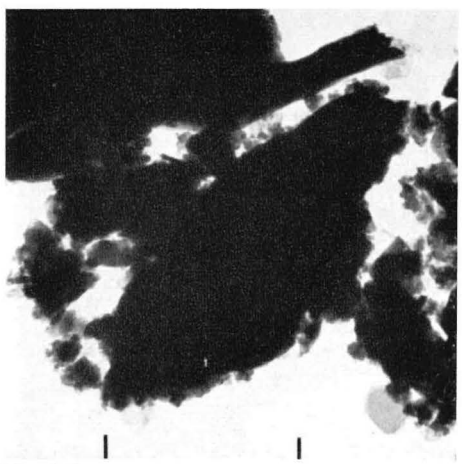

Fig. 408

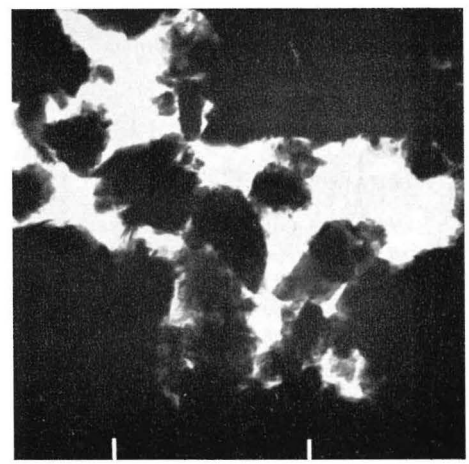

Fig. 409

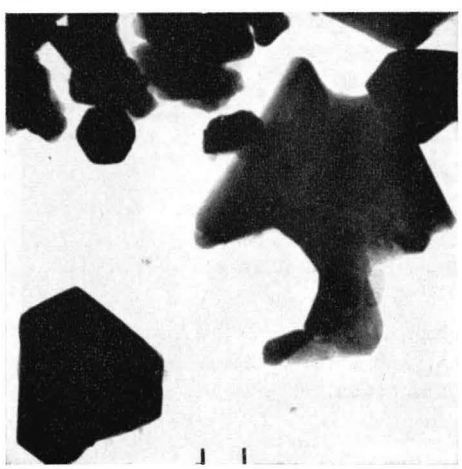

Fig. 410

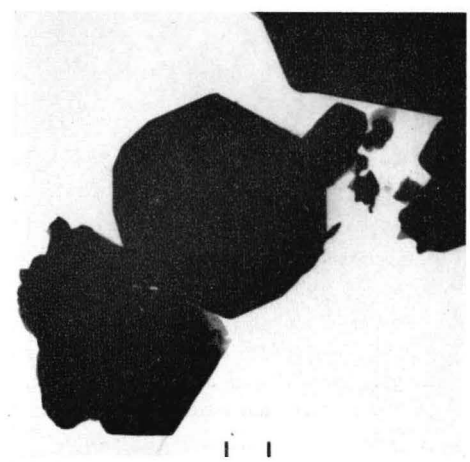

Fig. 411

104. **Hydrated C-A cement**

Gel structures in aluminous cement pastes (continued)

Figs. 412 and 413. Sample Ap−2C.

EMs: This sample has been described before in connection with Figs. 141−146, but representative structures are again shown here. They consist of plates sometimes of irregular angles and thicknesses, sometimes of regularly-hexagonal symmetry.

Further, it may be stated that several ED spot patterns show a slight deviation (of the order of 0.5 percent) from regularly-hexagonal symmetry, which is not evident in the samples without gypsum admixture. In some patterns, there is also a distinct tendency to two-fold symmetry in the distribution in intensities of the spot reflexions. These data are indicative of a transition from hexagonal to monoclinic symmetry of the plate phase, due to the introduction of $\bar{S}$ in the lattice. Only one ED pattern with superstructure spots, (similar to those discussed under Fig. 99) was recorded, other patterns were probably not exposed heavily enough for this effect to be noticeable.

The addition of sulfate also has the well-known effect of slowing down the hydration of C_3A considerably. In the present sample, the X-ray diffraction lines of C_3A were much more prominent than in sample Ap−1B, and were clearly visible even in the 3-month sample of Ap−2.

Figs. 414 and 415. Sample Ap−3.

EMs: This sample, of an overall composition approximating to C_4A aq., consists of a mixture of plates, mostly of a splintered appearance, and crystals of cubic habits. The ED patterns of the plates are regularly-hexagonal spot patterns with an average hexagonal unit cell $a_H = 5.80$ Å. The X-ray diagram contains patterns of C_4A aq.(hex.) (characteristic lines at 8.0 (00.1), 2.875 (11.0), and 1.660 (30.0) Å), C_3AH_6(cub.), CH, and C_3A (weak).

Figs. 416 and 417. Sample Ap−4.

EMs: This sample is essentially a superposition of the two preceding samples. Ettringite structures were observed in the 24-hour sample, but had disappeared after 14 days. The ED patterns from the plate particles are pseudohexagonal spot patterns from the $C_4A(\bar{S},H_3)$aq.(hex.) phase. The measured deviations from regularly-hexagonal symmetry are larger (1−2 percent) than the corresponding effect observed in sample Ap−2C (cf. above). The largest of the three a_H axes associated with a single pattern is between 5.72 and 5.80 Å, as measured in a few ED diagrams. Intensity distributions with two-fold or more irregular symmetry are also observed in the ED patterns.

The X-ray diagram contains patterns of monosulfate solid solution phase $C_4A(\bar{S},H_3)$aq. (hex.) (basal reflexion at 8.85 Å), and of C_4A aq.(hex.) (diffuse basal reflexion at 8.4−8.0 Å), together with a rather prominent C_3A pattern, a few weak CH reflexions, and faint indications of a C_3AH_6(cub.) pattern.

In the X-ray diagram taken after 3 months, the basal reflexions of the hexagonal-plate phases had developed into lines at 8.85 and 8.0 Å, with a zone of diffuse scattering in between. The C_3A and the CH patterns had become weaker, and instead a C_3AH_6 (cub.) pattern of moderate intensity had appeared.

Fig. 412

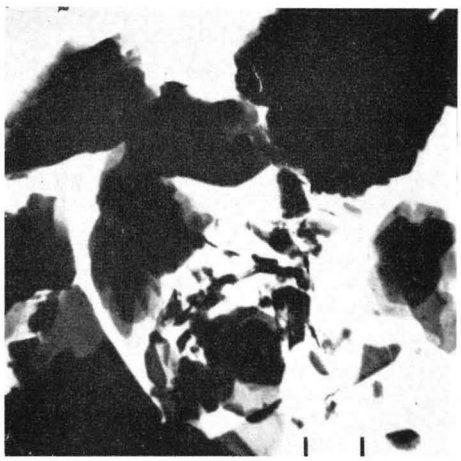

Fig. 413

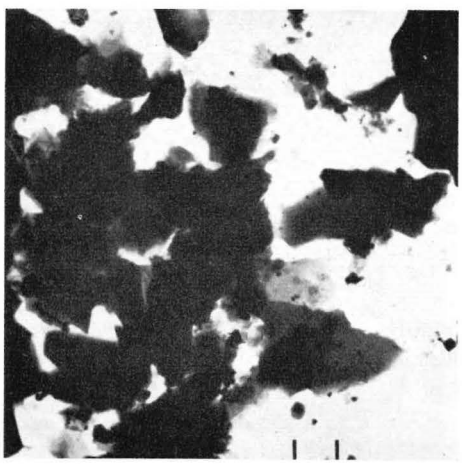

Fig. 414

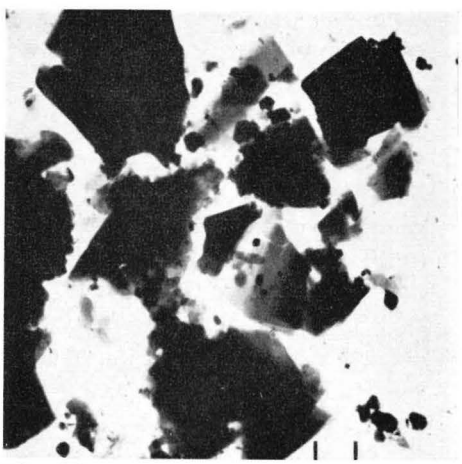

Fig. 415

Fig. 416

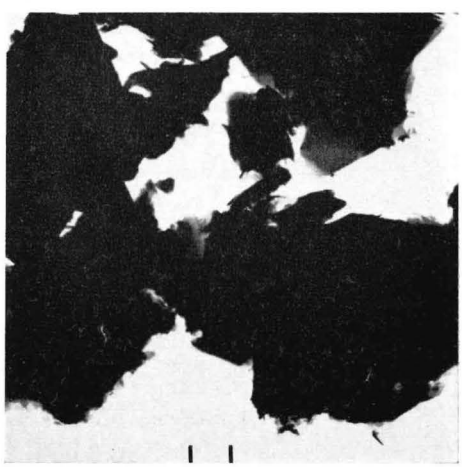

Fig. 417

105. (A, M)-S-H

Clay-mineral phases in steam-cured cement pastes

Plate crystals or crystal aggregates with properties characteristic of clay minerals are observed in small quantities in most cement pastes and similar materials.

Crystals of clay-type phases can either be present initially in the anhydrous cement or other starting material, or develop as a result of the process of hydration. The latter case is of course only possible in samples processed at higher temperatures. Some examples of this are given in Figs. 401—403. The formations shown below are possibly also developed in the hydrothermal curing at autoclaving temperatures of paste materials, in which the A and F constituents are incorporated in (A, F)-S-H phases, rather than in C-(A, F)-H compounds, which are unstable at the temperatures in question.

Fig. 418. Sample Ppq—2.

EM: Aggregate of plate crystals with hexagonal angles.

ED: Spot patterns of hexagonal symmetry, $a_H = 5.33$ Å, one strong pattern and a couple of patterns with slightly rotated spots.

Figs. 419 and 420. Sample Ppq—1.

EMs: Plate crystals with hexagonal angles, and with fibrous C-S-H gel material adsorbed on the surface.

EDs: Spot patterns of approximately hexagonal symmetry, with the strong spots corresponding to a pseudo cell a'_H of between 3.04 and 3.08 Å. Interstitial patterns of weak spots indicate a true unit cell $a'_H \sqrt{3} = a_H = 5.26—5.33$ Å. This is the largest a_H spacing measured along any diameter of the patterns.

Spacings measured in other directions of the patterns can be several percent smaller. As discussed above (e.g. under Fig. 99), this can either be a true effect, or caused by a tilting of the crystal.

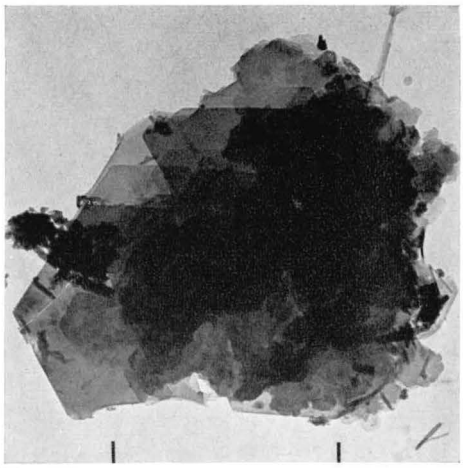

Fig. 418 a

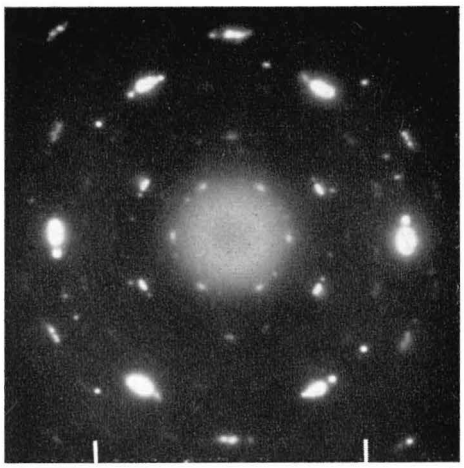

Fig. 418 b

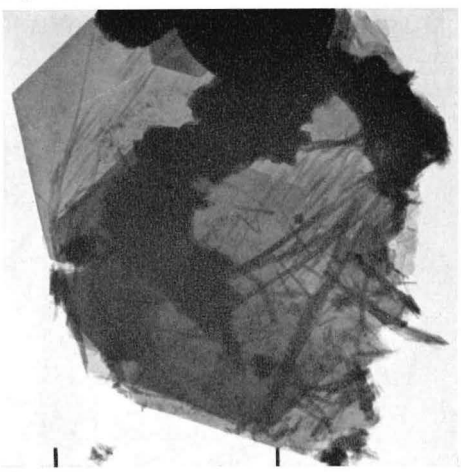

Fig. 419 a

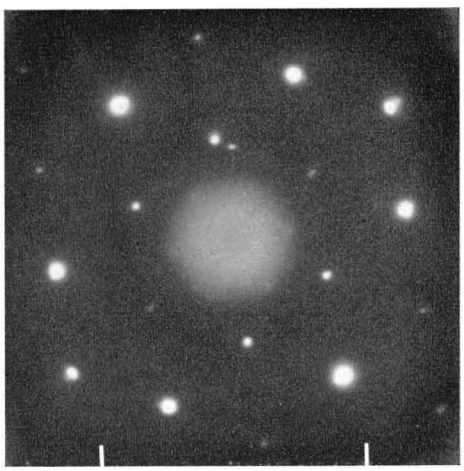

Fig. 419 b

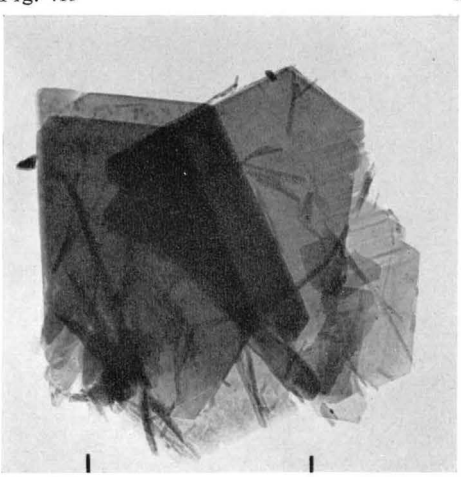

Fig. 420 a

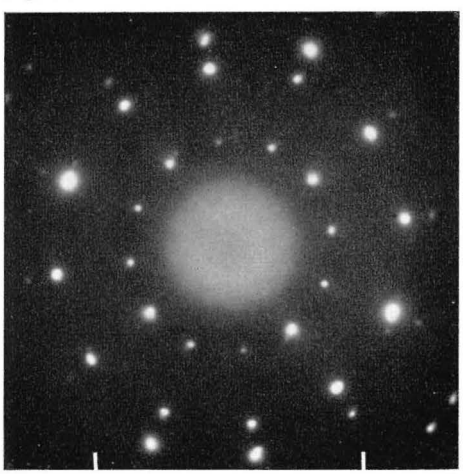

Fig. 420 b

106. (A, M)-S-H

Clay mineral phases in cement pastes

Fig. 421. Sample Pp—2.

Fig. 422. Sample Pp—3.

Fig. 423. Sample Pp—5.

EMs: These are examples of various forms of plate phases that can be found in ordinary cement pastes. The plate crystals are often associated with gel material, such as the irregular spherulites in Fig. 421a, and the network of fibers in Fig. 422a. Fig. 423a is an example of regularly-hexagonal shapes sometimes found in these crystals.

EDs: The spot patterns of these diagrams are of more or less regular, hexagonal symmetry, with an apparent unit cell a'_H of about 3.05 Å. This cell seems to be the true unit cell of the plates in Figs. 421 and 422, but the pattern in Fig. 423b contains interstitial weak spots, especially nearest to the primary beam ($(hk)=(10)$ and permutations), indicating a true unit cell of $a_H=a'_H\sqrt{3}=5.28$ Å.

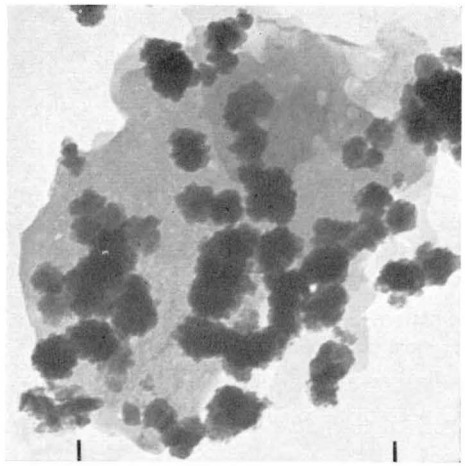

Fig. 421 a

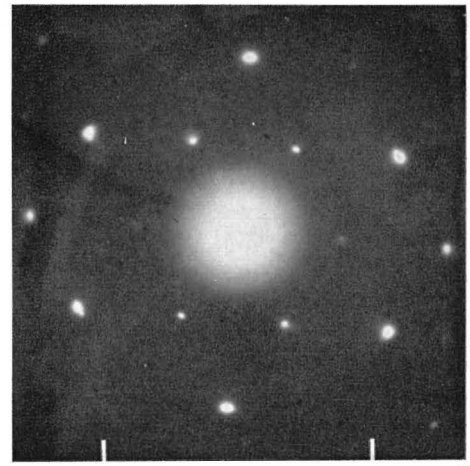

Fig. 421 b

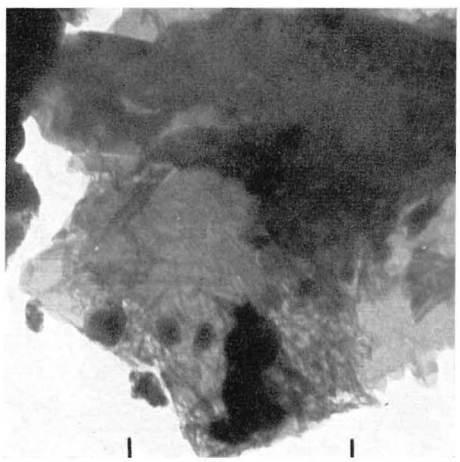

Fig. 422 a

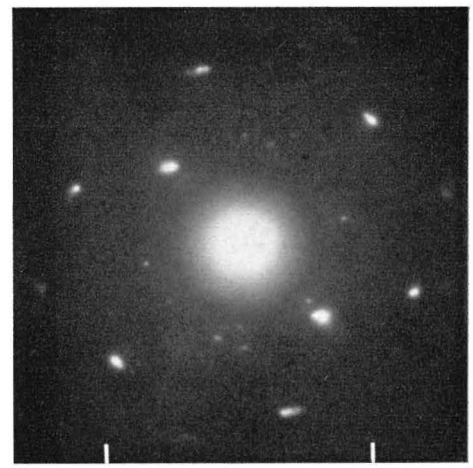

Fig. 422 b

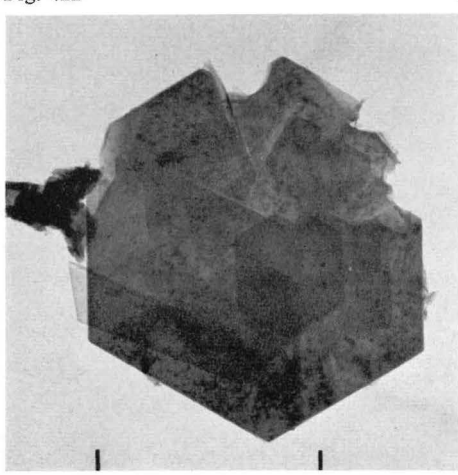

Fig. 423 a

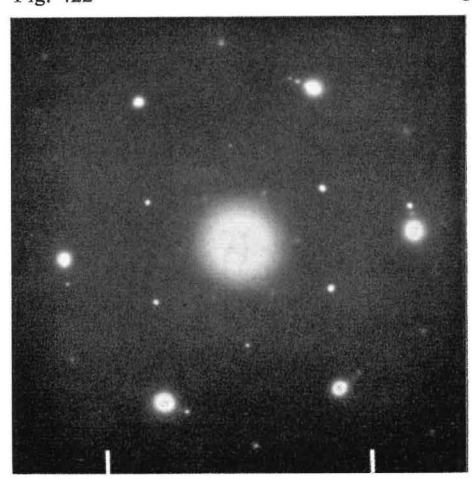

Fig. 423 b

107. (A, M)-S-H

Clay-mineral phases in cement pastes

Figs. 424 and 425. Sample Pp—6B.

Fig. 426. Sample Pp—1B.

EMs: These are further examples of clay-type crystal plates in cement pastes, showing regularly-hexagonal angles, and associated with fibrous structures of C-S-H gel and with rounded, spherulitic particles of other paste constituents.

ED (424b): The diagram contains a spot-ring pattern of hexagonal symmetry, given by the assembly of plates seen in the EM, with the most prominent reflexions corresponding to $(hk)=(10)$ and (11) from a cell $a'_H=3.05$ Å. Certain weak reflexions indicate a true unit cell $a'_H\sqrt{3}$. There are also rings at 3.02 and 1.82 Å, given by the fibrous C-S-H gel constituent (cf. Figs. 321—325).

ED (425b): Diagram similar to the previous one, with reflexions corresponding to a cell of slightly smaller size, $a'_H=3.01$ Å.

ED (426b): Although not evident in the reproduction, this pattern consists of spots which are doubled in a way that indicates the presence, in this particular crystal particle, of two a_H units of nearly equal size, about 5.16 and 5.28 Å. The effects of a sub-unit 3.0 Å. cell are strongly enhanced in this diagram also.

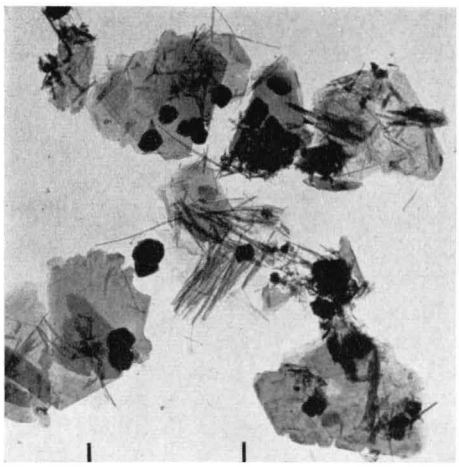

Fig. 424 a

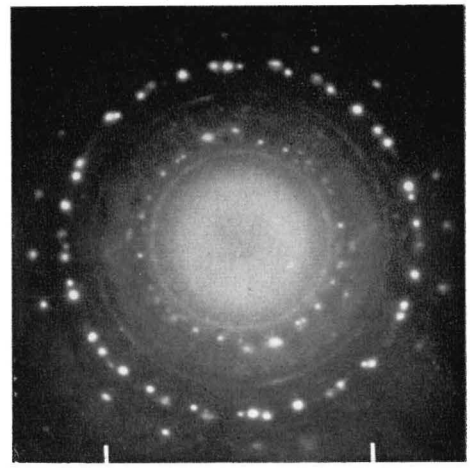

Fig. 424 b

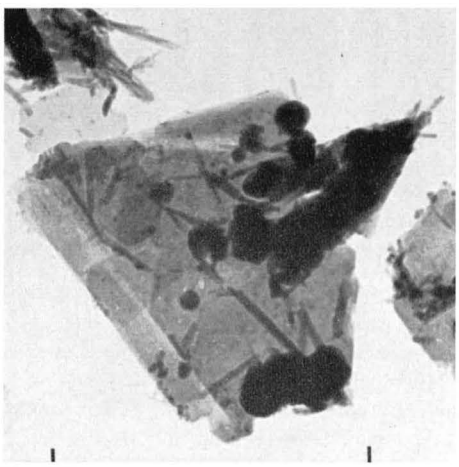

Fig. 425 a

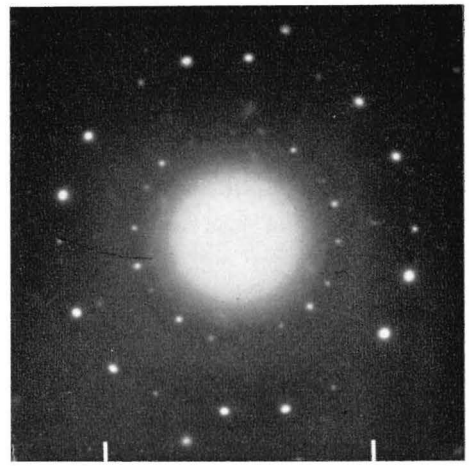

Fig. 425 b

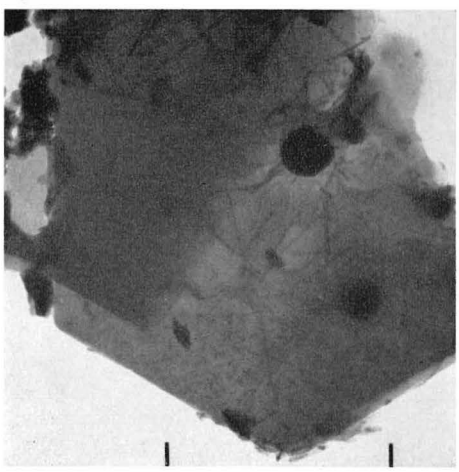

Fig. 426 a

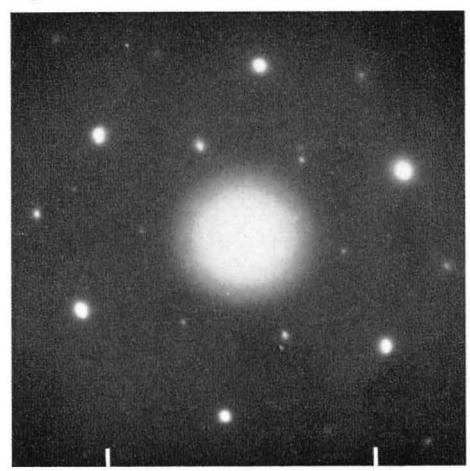

Fig. 426 b

108. (A, M)-S-H

Clay-mineral phases in cement pastes

Figs. 427 and 428. Sample Pp—10A.

Fig. 429. Sample Pp—10C.

These particles represent a clay-type phase, of which several examples were recorded in the Type IV (low-heat) cement paste. The ED patterns contain spot-rings at spacings of about 2.65, 1.53, and 0.885 Å, corresponding to reflexions with (*hk*) values of (10), (11), and (30), respectively, from a hexagonal cell $a'_H = 3.06$ Å (± 0.03 in various patterns). There are also other characteristic spot-rings outside these, generally showing spots that are slightly more indistinct or diffuse. The corresponding spacings for these reflexions are 2.42, 1.48, 1.30 Å., and some others which are less certain. These spacings might be referrable to some phase produced by partial dehydration of the original crystals, or they might be (10.*l*) and (11.*l*) spacings of a unit cell with a'_H as hexagonal base unit.

As mentioned in the discussion of Figs. 309—314, ordinary C-A-H (hex.) phases were not observed in the Type IV cement paste samples. It is suggested that part at least of the small amounts of Al, Fe, and Mg ions present in this cement are incorporated in the clay-type phase shown in the present figures.

The ED characteristics and in some measure also the habits of the clay-type particles appearing in cement pastes are rather different from those of various pure clay minerals (cf. *Forslind* 1948, *Grudemo* 1955, and the ED pattern of mica in Fig. 45). The hexagonal pseudo unit a'_H of about 3.06 Å is always strongly pronounced, the extra reflexions belonging to a true unit cell of $a_H = a'_H \sqrt{3}$ about 5.3 Å. are weak or absent.

The data indicate that the structure of these plate crystals is dominated by octahedral double-layers of hydroxyl ions, the structure element of various metal hydroxides, such as CH (portlandite), MH (brucite), and AH_3(gibbsite). The a_H distances of the two latter substances are 3.15 and 2.90 Å, respectively, the last value being an average of three slightly different pseudohexagonal axes. It is likely that the clay-type particles shown in the last four pages are essentially built up of MH-layers with Al ions partially replacing Mg ions in the octahedral sites, resulting in the observed intermediate value of a_H. These layers can be built together or interstratified with silica layers of composition (Si_2O_5) , with Al ions partially replacing Si ions in tetrahedral coordination. The (Si_2O_5) layers have a hexagonal (or pseudohexagonal) cell a_H of approximately $a'_H \sqrt{3}$, which facilitates the fit between the different layers, as in the ordinary clay minerals.

Many clay-mineral particles observed are probably present from the start. A certain exchange or leaching of cations is likely to take place between the clay lattice and the liquid phase formed in the cement reaction.

Similar particles were observed in various cement paste mixes by *Chatterji* and *Jeffery* 1963b. The crystals had a unit cell $a_H = 3.1$ Å and were interpreted as MH crystals.

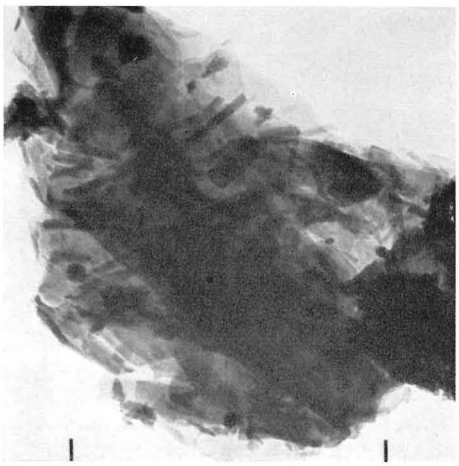

Fig. 427 a

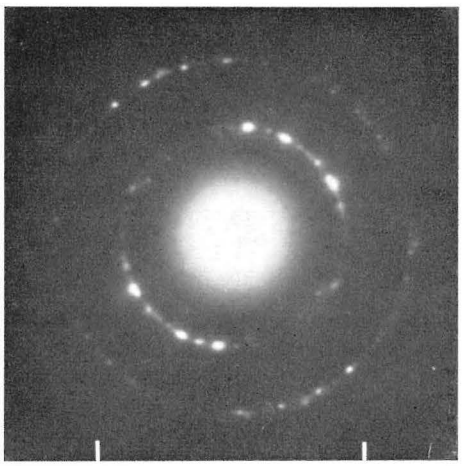

Fig. 427 b

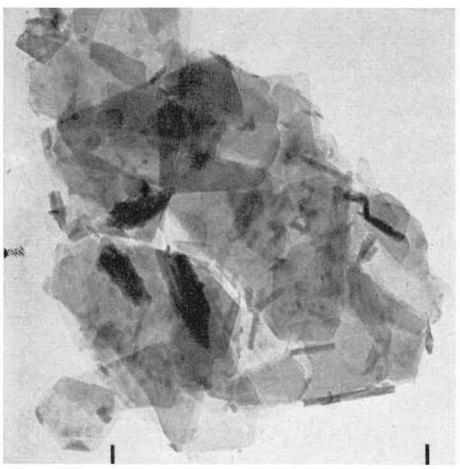

Fig. 428 a

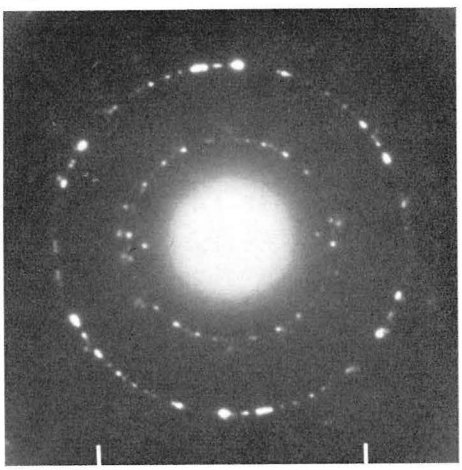

Fig. 428 b

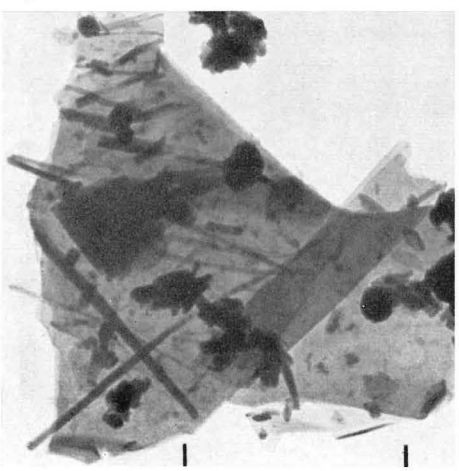

Fig. 429 a

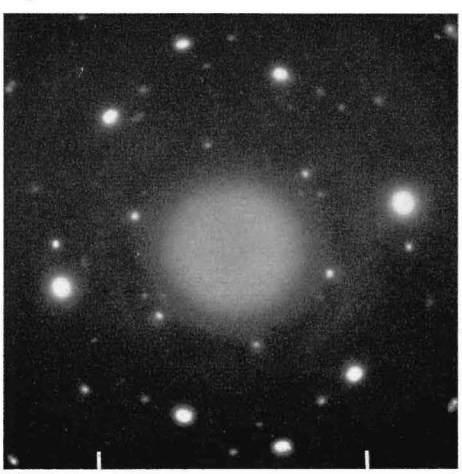

Fig. 429 b

109. **Graphite**

Graphite crystals in various preparations

The micrographs of the following four pages show the microstructural habits and ED diagrams of graphite crystals or crystal aggregates, observed in various preparations.

It seems that most cements and related raw materials, especially products that have been fired at high temperatures, contain minute amounts of graphite crystals. In a combined EM-ED examination, these crystals tend to attract some unjustified attention because of their ED patterns which are often brilliant and easily observed.

As is well known, graphite has a layer lattice with a unit consisting of a planar network of hexagonal rings of C atoms, and with $a_H = 2.461$ Å (*Bacon* 1950). The normal unit cell contains two layers stacked in hexagonal fashion (ABAB . . .), with $c_H = 6.708$ Å. Due to the occurrence of a small number of disoriented layers, the unit cell can alternatively contain three layers stacked in rhombohedral fashion (ABCABC . . .), with a corresponding increase in the equivalent c_H dimension. The average interlayer distance increases with an increasing number of such disoriented layers, and also with decreasing thickness of the crystal plates (*Bacon* 1951).

Fig. 430. Sample Dp—1.

Fig. 431. Sample Pp—1B.

Fig. 432. Sample Sl—1A.

Graphite crystals observed in various preparations. The EMs show aggregates of thin plates, often with a stepwise variation in thickness. The ED diagrams are mainly single-crystal patterns of hexagonal symmetry, with measured unit cells of about 2.46 Å.

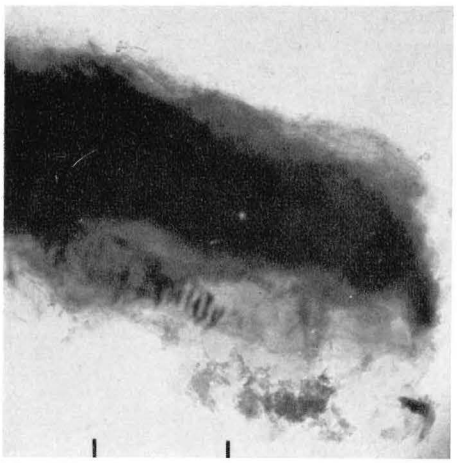

Fig. 430 a

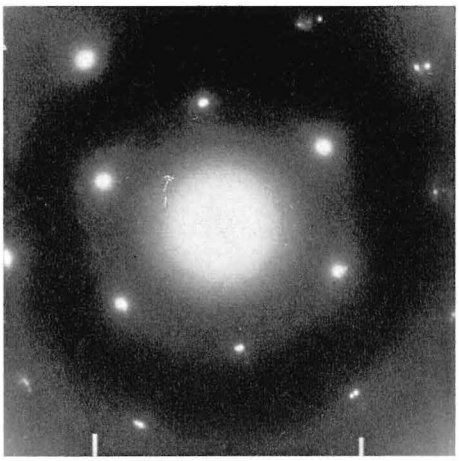

Fig. 430 b

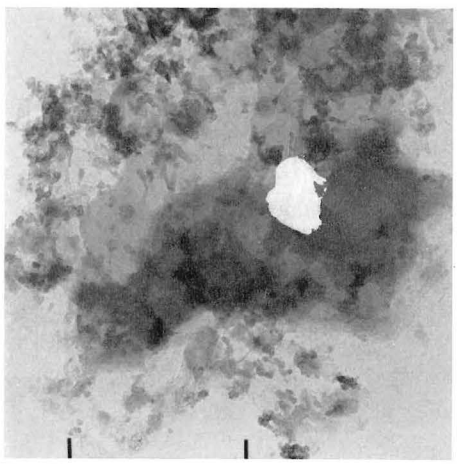

Fig. 431 a

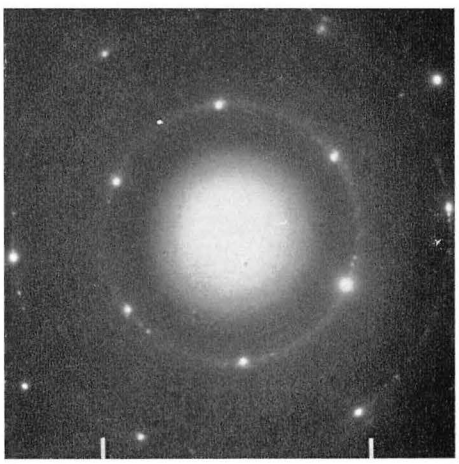

Fig. 431 b

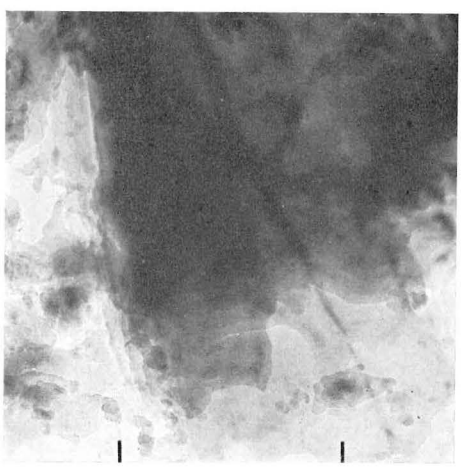

Fig. 432 a

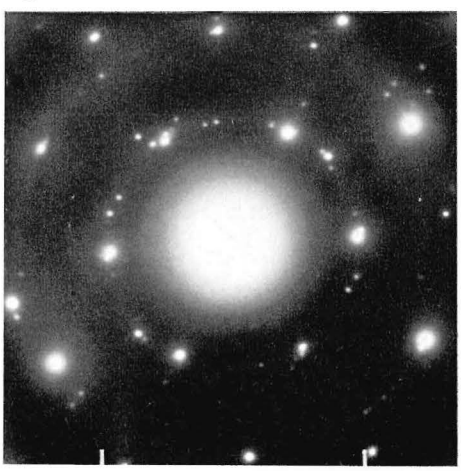

Fig. 432 b

110. **Graphite**

Graphite crystals in cement pastes

Fig. 433. Sample Pp—9.

Fig. 434. Sample Pp—10B.

Fig. 435. Sample Pp—6A.

Graphite crystal aggregates, similar in morphology to those of previous page. The ED patterns give a_H values very close to 2.46 Å, and show some additional features. In Fig. 434b, there is a very weak, continuous ring reflexion at 3.4—3.5 Å, corresponding to a somewhat expanded interlayer distance (00.2), probably originating from clusters of very small crystals attached to the larger plates. Fig. 435b contains similar spot reflexions at 3.39 Å, and shows additional (*hk*.1) reflexions (cf. next page).

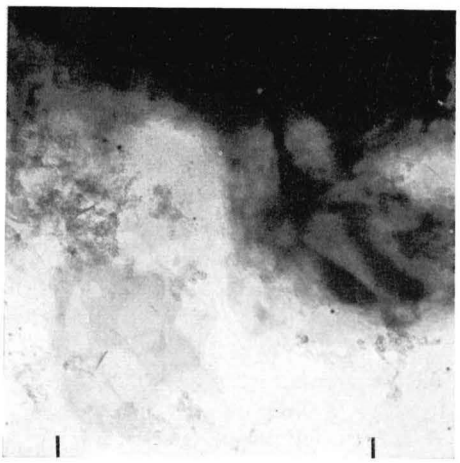

Fig. 433 a

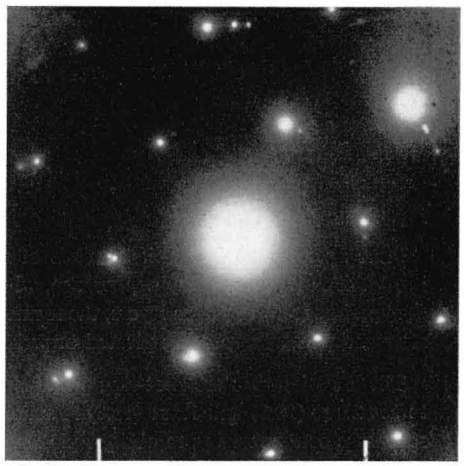

Fig. 433 b

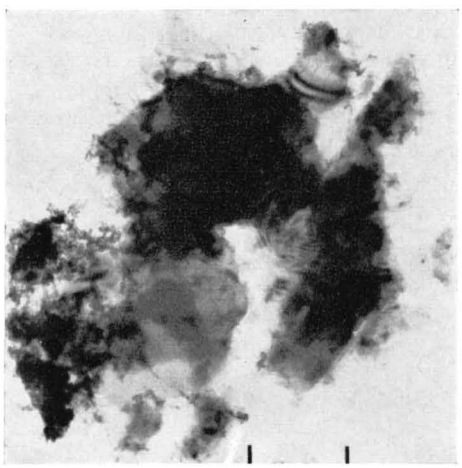

Fig. 434 a

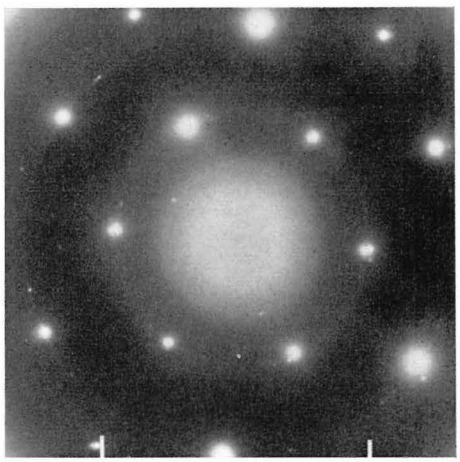

Fig. 434 b

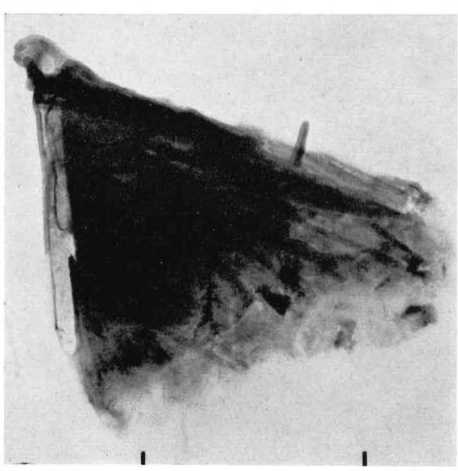

Fig. 435 a

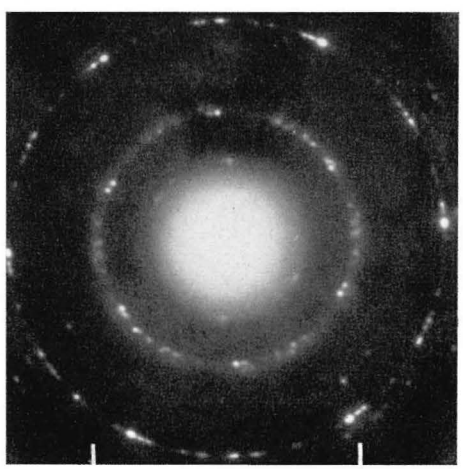

Fig. 435 b

111. **Graphite**

Graphite crystals in high-alumina cement pastes

Fig. 436. Sample Hp—1.

Fig. 437. Sample Hpq—1.

Fig. 438. Sample Hpq—2.

Plate aggregates of graphite crystals of slightly variable morphology. The particles seen in Fig. 436a have a cloudy appearance, whereas those of Figs. 437 and 438 seem to consist of superimposed, very thin layers, the former showing straight edges and regularly-hexagonal angles, the latter appearing pleated or wrinkled.

The ED diagrams are spot-ring patterns, with the two strongest reflexions corresponding to the 2.132 (10.0) and 1.231 (11.0) Å spacings of graphite. Outside these, there are certain reflexions corresponding to oblique planes, with $l=1$, 2, etc. for example (10.1) at 2.030 Å, (11.2) at 1.256 Å., and others for reflexions outside the area shown in the figures. As is most clearly seen for the (11.0) and (11.2) reflexions of Fig. 438b, the reflexions from oblique planes fall along the same diameter of the pattern as the corresponding (*hk*.0) crossgrating reflexions. A similar effect is observed for the (10.0) and (10.1) reflexions of the same diagram, but in this case the inner and outer spots in the same pair of reflexions are not well resolved, possibly indicating the presence of crystals with anomalously-high content of disordered, three-layer cells (cf. above).

All the patterns contain (00.2) reflexions, Fig. 437b several pairs of spots distributed between 3.35 and 3.55 Å, the others with reflexions at 3.45 and 3.5 Å.

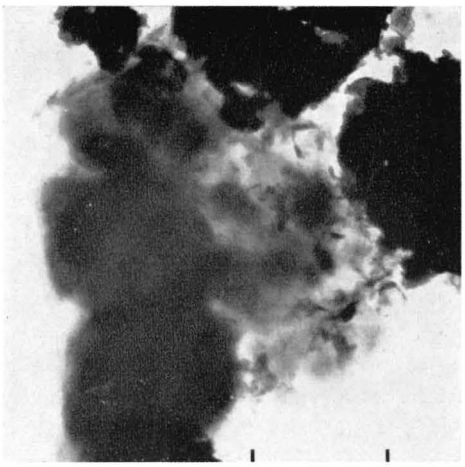

Fig. 436 a

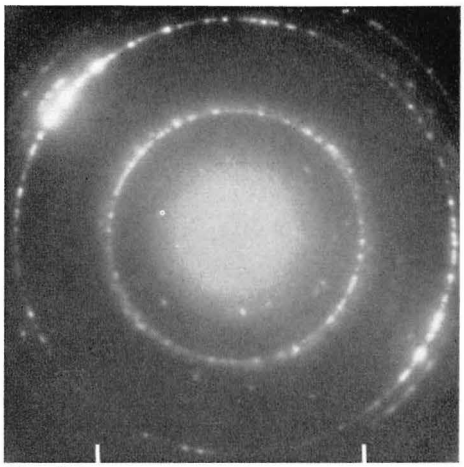

Fig. 436 b

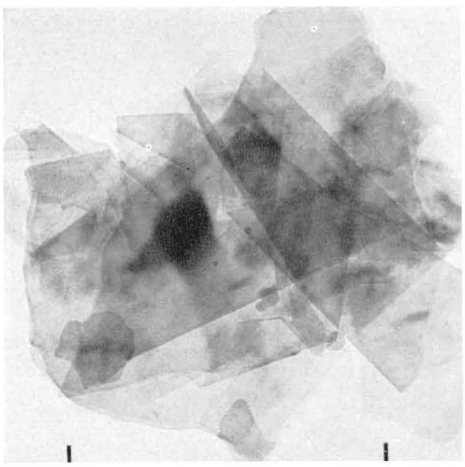

Fig. 437 a

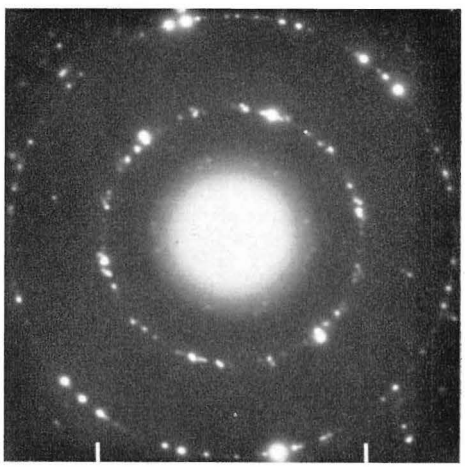

Fig. 437 b

Fig. 438 a

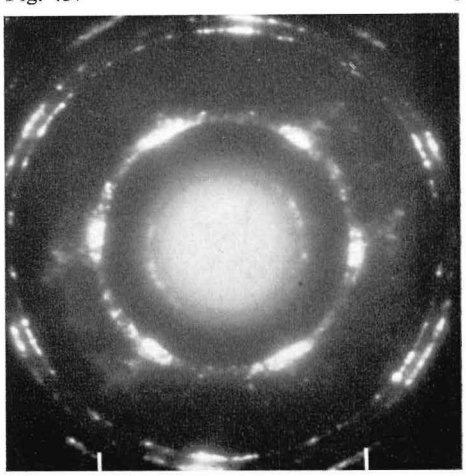

Fig. 438 b

112. **Graphite**

Graphite crystals in various steam-cured samples

Fig. 439. Sample CSwq—4.

Fig. 440. Sample TSwq—3.

Fig. 441. Sample DSpq—2.

Further examples of crystal aggregates of graphite, giving patterns of spots and spot-rings. The hexagonal patterns correspond to a cell a_H in the vicinity of 2.46 Å.

It can be noticed that these particular mixes of steam-cured samples were made with a special type of silica (Aerosil) of high surface area. It is likely, therefore, that this ingredient contains the very small amounts of graphite that are actually observed.

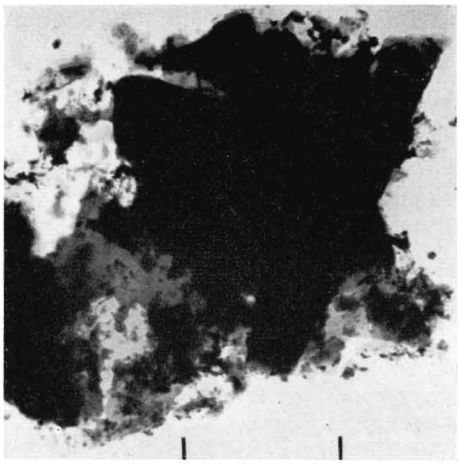

Fig. 439 a

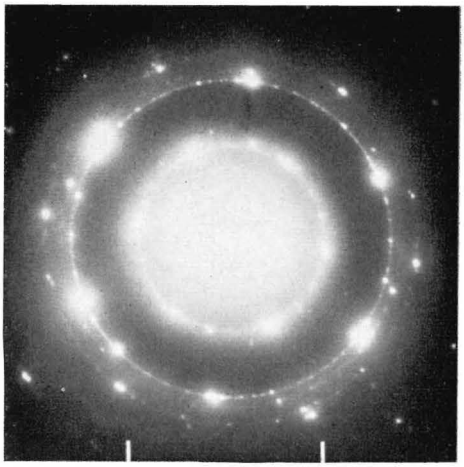

Fig. 439 b

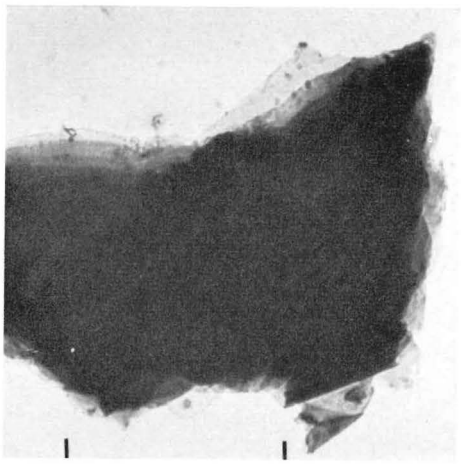

Fig. 440 a

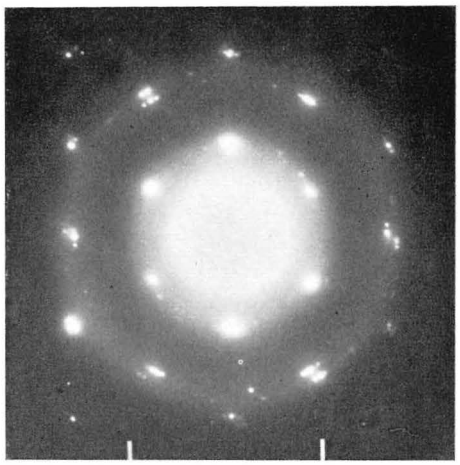

Fig. 440 b

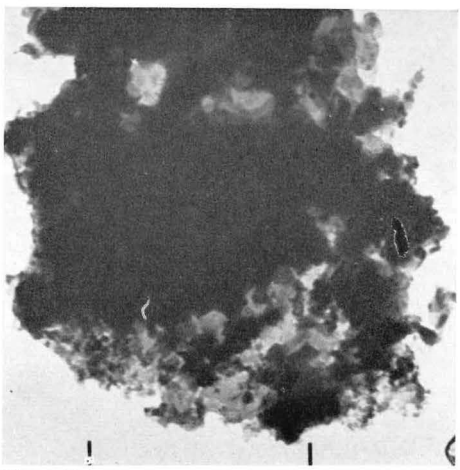

Fig. 441 a

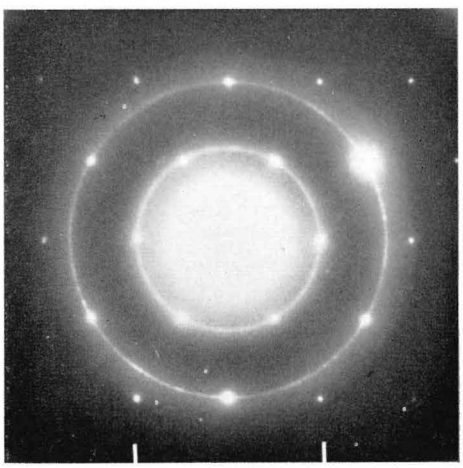

Fig. 441 b

113. **Graphite**

Graphite modification observed in certain pastes

Fig. 442. Sample Dp—1.

Fig. 443. Sample Pp—1B.

Fig. 444. Sample Pp—2.

The EMs show flocs or clusters of small plates or globules, often with a porous or burnt-out appearance.

The ED diagrams contain more or less diffuse reflexions at 3.55—3.45, 2.12—2.11, about 1.75, and 1.22—1.21 Å, probably the (00.2), (10.0), (00.4), and (11.0) reflexions of graphite. The (10.0) and (11.0) rings show an intensity profile with a sharp inner edge and a diffuse band outwards, which is characteristic of layer lattices with very small crystal units.

This special form of graphite-like material may be the result of graphitization of organic material.

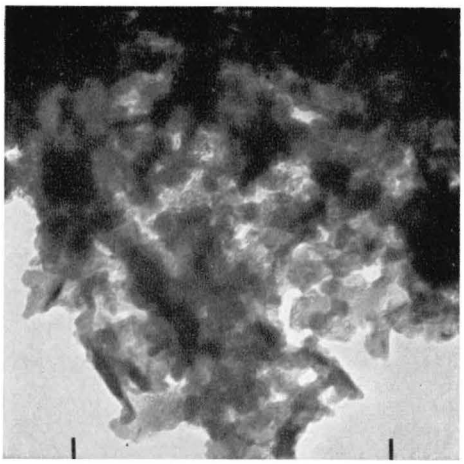

Fig. 442 a

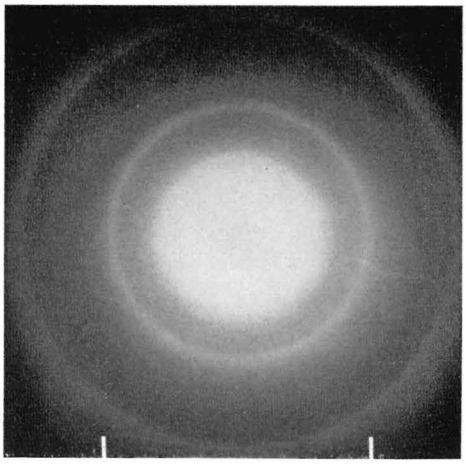

Fig. 442 b

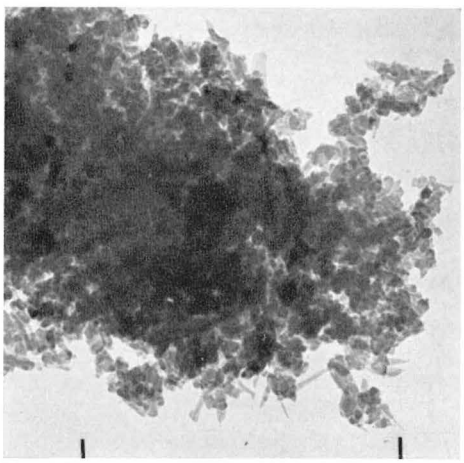

Fig. 443 a

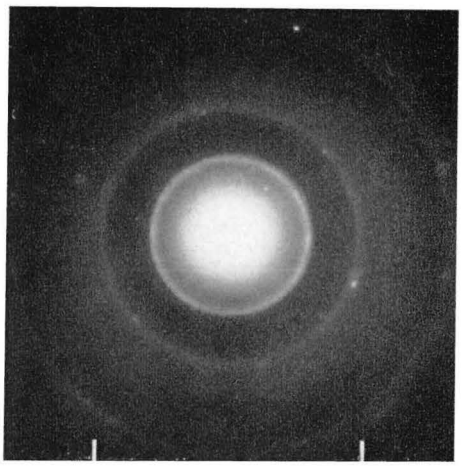

Fig. 443 b

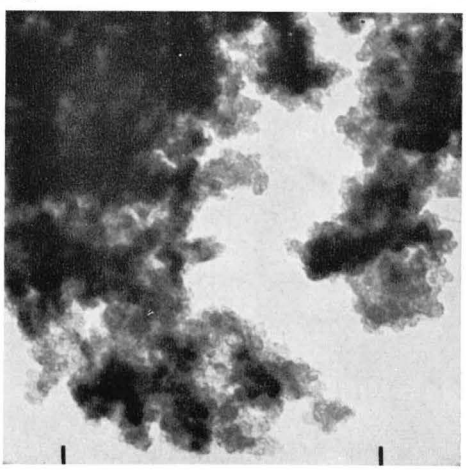

Fig. 444 a

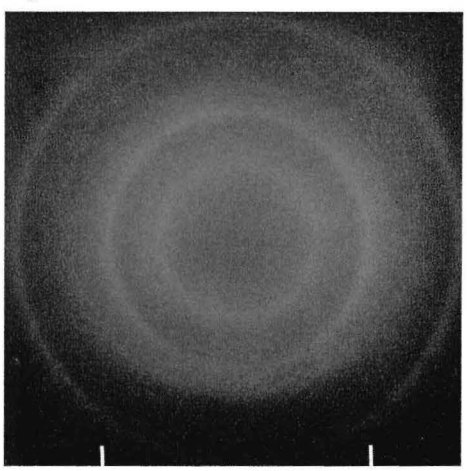

Fig. 444 b

114. S-H

Silica gels

Figs. 445 and 446. Sample Sw—1.

EMs: Loosely flocculated aggregates of larger (of the order of 1000 Å in Fig. 445a) and smaller (about 200 Å in Fig. 446a) particles, the only constituent observed in a single EM preparation of one type of silica (C. P.). Many of the larger particles, which were obviously single crystals, were of a more regular, oblong and slightly pointed shape.

EDs: Weak and somewhat spotty ring diagrams, with reflexions at 3.87, 3.54, 2.81, 2.65, 2.1 (diffuse), 1.935, 1.77, 1.55, and 1.48 Å. This silica sample seems to be crystallized, at least partly, but the crystalline compound that has given the ED patterns is still unidentified.

This type of silica was used in preparing sample Sl—5 (see Fig. 172), which consisted of apparently pure C-S-H(I) of a comparatively well crystallized type.

Fig. 447. Sample Sw—2.

EM: Agglomerate of extremely small silica gel particles, in sizes ranging from a few hundred Å down to about 20 Å, near the limit of resolution of the microscope.

ED: Diffuse rings at about 4.2, 2.1, and 1.2 Å. In the corresponding X-ray diagram of similar gels, a diffuse ring at about 4.5—4.0 Å is the most prominent feature. This spacing could possibly be explained as the distance between outer oxygen planes in the dimeric Si_2O_7 group.

This type of silica was used in the preparation of sample CSw—2 (see Figs. 181—183). A very similar brand was used in autoclaved cement-silica mixes, where it was active in producing an extremely fine-grained, hydrated material (see Figs. 381—386).

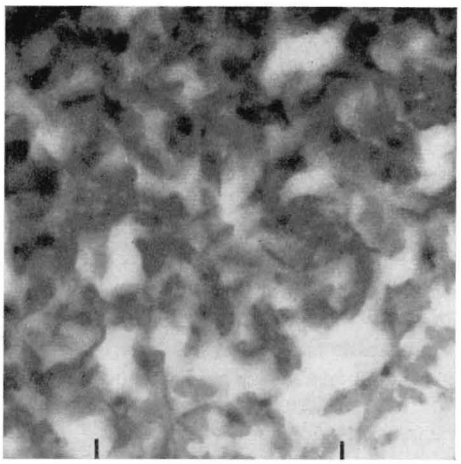

Fig. 445 a

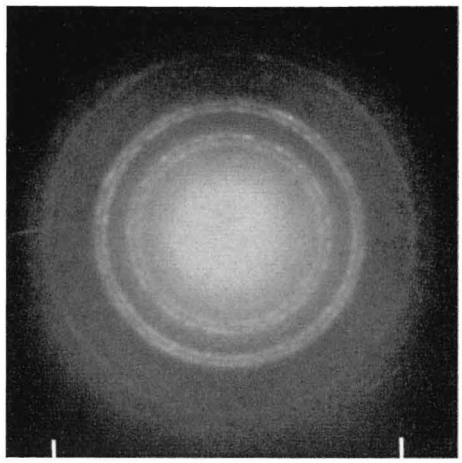

Fig. 445 b

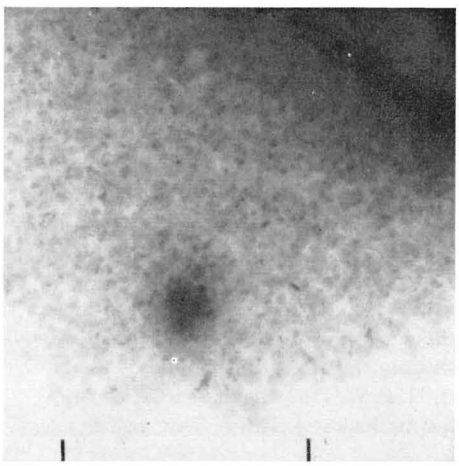

Fig. 446 a

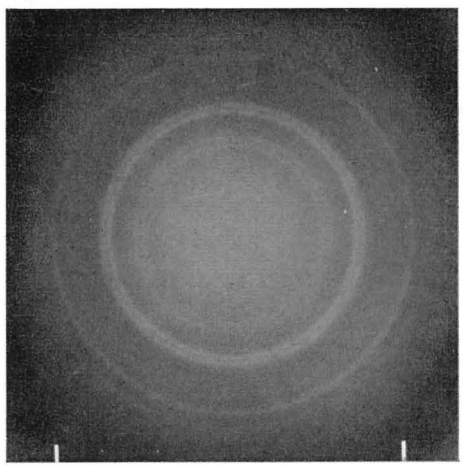

Fig. 446 b

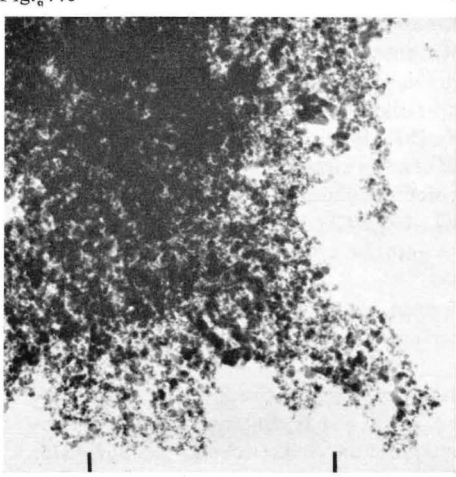

Fig. 447 a

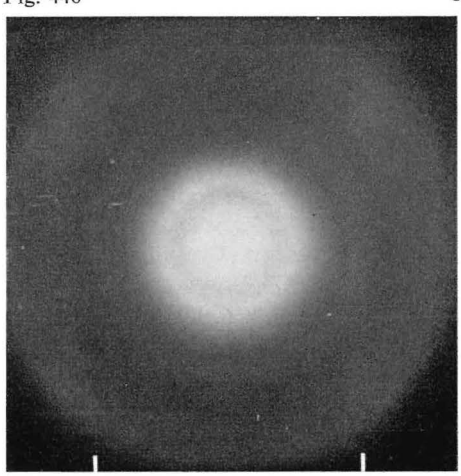

Fig. 447 b

References

AKAIWA S. and SUDOH G. 1956. Hydrothermal reaction products of the system CaO-SiO_2-H_2O, Semento Gijutsu Nenpo, *10*, 14—23 (in Japanese).

ASSARSSON G., 1936. Die Entstehungsbedingungen der hydratischen Verbindungen im System CaO-Al_2O_3-H_2O (flüssig) und die Hydratisierung der Anhydrokalziumaluminate, Sveriges Geologiska Undersökning, *30*, 1—202.

BACON G. E. 1950. Unit cell dimensions of graphite, Acta Cryst., *3*, 137—139.

BACON G. E., 1951. The interlayer spacing of graphite, Acta Cryst. *4*, 558—561.

BANNISTER F. A., 1936. Ettringite from Scawt Hill, Co. Antrim, Mineral. Mag., *24*, 324—329.

BERNAL J. D., 1954. The structures of cement hydration compounds, Proc. 3rd Intern. Symposium on the Chemistry of Cement, London 1952, 216—236.

BOGUE R. H., 1953. A note on the nomenclature of the calcium silicate hydrates, Mag. Concrete Research, *3*, 87—91.

BRUNAUER S. and GREENBERG S. A., 1962. The hydration of tricalcium silicate and β-dicalcium silicate at room temperature, Chemistry of Cement, Proc. 4th Intern. Symp., Washington D.C., 1960 (NBS Monograph 43, 1962), 429—468.

BUCKLE E. R., GARD J. A., and TAYLOR H. F. W., 1958. Tricalcium silicate hydrate, J. Chem. Soc. (London), *1958*, 1351—1355.

BUNN C. W., 1941. Some applications of X-ray diffraction methods in industrial chemistry. The setting of plaster of Paris, J. Sci. Instruments, *18*, 72—73.

BUTTLER F. G., DENT GLASSER L. S., and TAYLOR, H. F. W. 1959. Studies on $4\,CaO.Al_2O_3.13\,H_2O$ and the related natural mineral hydrocalumite, J. Amer. Ceramic Soc., *42*, 121—126.

CASPARI, W. A. 1936. Calcium sulphate hemihydrate and the anhydrites. I. Crystallography, Proc. Roy. Soc. London (A), *155*, 41—48.

CHATTERJI S. and JEFFERY J. W., 1962. Studies of early stages of paste hydration of cement compounds, I. J. Amer. Ceramic Soc., *45*, 536—543.

CHATTERJI S. and JEFFERY J. W., 1963 a. Studies of early stages of paste hydration of cement compounds, II, J. Amer. Ceramic Soc., *46*, 187—191.

CHATTERJI S. and JEFFERY J. W., 1963 b. Studies of early stages of paste hydration of different types of portland cement, J. Amer. Ceramic Soc., *46*, 268—272.

COPELAND L. E., KANTRO D. L., and VERBECK G., 1962. Chemistry of hydration of portland cement, Chemistry of Cement, Proc. 4th Intern. Symp., Washington D.C., 1960 (NBS Monograph 43, 1962), 429—468.

COPELAND L. E. and SCHULZ E. G., 1962a. Electron optical investigation of the hydration products of calcium silicates and portland cement, J. PCA Research and Development Labs., *4*, 2—12.

COPELAND L. E. and SCHULZ E. G., 1962b. Discussion of paper by *Grudemo* 1962, 648—655.

COPELAND L. E., SCHULZ E. G., and BRUNAUER S., 1960. Die Hydratation von Trikalziumsilikat und β-Dikalziumsilikat bei Raumtemperatur, Silikattechnik, *11*, 367—373.

DANIELSSON U., 1959. Über die Struktur der Hydratationsprodukte des Zements, Zement u. Beton, *16*, 22 (XIV—XVII).

DANIELSSON U., 1962. Heat of hydration of cement as affected by water-cement ratio, Chemistry of Cement, Proc. 4th Intern. Symp., Washington D.C., 1960 (NBS Monograph 43, 1962), 519—526.

FLINT E. P., MCMURDIE H. F., and WELLS L. S., 1938. Formation of hydrated calcium silicates at elevated temperatures and pressures, J. Research NBS, *21*, 617—638.

FLINT E. P. and WELLS L. S., 1944. Analogy of hydrated calcium silico aluminates and hexagonal calcium aluminates to hydrated calcium sulfoaluminates, J. Research NBS, *33*, 471—478.

FLÖRKE O. W., 1952. Kristallographische und röntgenometrische Untersuchungen im System $CaSO_4$-$CaSO_4 \cdot 2\,H_2O$, Neues Jb. Miner. Mh, *84*, 189—240.

FORSLIND E., 1948. The clay-water system. I. Crystal structure and water adsorption of clay minerals. Swed. Cement and Concrete Research Inst., Bull. No. *11*, 1—20.

FUNK H., 1960. Der Hydratationsverlauf von β-Dikalziumsilikat unter Bildung von nadelförmigem, tobermoritähnlichem Kalziumsilikathydrat, Silikattechnik, *11*, 373—375.

FUNK H., 1962. Two different ways of hydration in the reaction of β-Ca_2SiO_4 with water at 25 to 120° C, Chemistry of Cement, Proc. 4th Intern. Symp., Washington D.C., 1960 (NBS Monograph 43, 1962), 291—295.

GARD J. A., 1964. Electron microscopy and diffraction, Chapter 21 in The Chemistry of Cements, editor *H. F. W. Taylor* (Academic Press, London and New York).

GARD J. A., HOWISON J. W., and TAYLOR H. F. W., 1959. Synthetic compounds related to tobermorite: An electron-microscope, X-ray, and dehydration study, Mag. Concrete Research, *6*, 69—78.

GARD J. A., and TAYLOR H. F. W., 1957. A further investigation of tobermorite from Loch Eynort, Scotland, Mineral. Mag., *31*, 361—370.

GARD J. A. and TAYLOR H. F. W., 1959. Crystal structure of foshagite, Nature, *183*, 171—173.

GARD J. A. and TAYLOR H. F. W., 1960. The crystal structure of foshagite, Acta Cryst., *13*, 785—793.

GREENE K. T., 1962. Early hydration reactions of portland cement, Chemistry of Cement, Proc. 4th Intern. Symp., Washington D.C., 1960 (NBS Monograph 43, 1962), 359—385.

GROTHE H., SCHIMMEL G., and ZUR STRASSEN H., 1962. Discussion of paper by *Taylor* 1962, 194—196.

GRUDEMO Å., 1954. An X-ray examination of the structure of vermiculites, Swed. Cement and Concrete Research Inst., Proc. No. *22*, 1—56.

GRUDEMO Å., 1955. An electronographic study on the morphology of calcium silicate hydrates, Swed. Cement and Concrete Research Inst., Proc. No. *26*, 1—103.

GRUDEMO Å., 1956. The silicate-water system: Analogies between the montmorillonoids and the calcium silicate hydrates of the tobermorite group, Swed. Cement and Concrete Research Inst., Note on Research in Progress, No. *5*, 1—43.

GRUDEMO Å., 1959. Cementpastans mikrostruktur, Gullkornet, *9*, 16—28.

GRUDEMO Å., 1962. The microstructure of hardened cement paste, Chemistry of Cement, Proc. 4th Intern. Symp., Washington D.C., 1960 (NBS Monograph 43, 1962), 615—658.

GRUDEMO Å., 1964a. Electron microscopy of portland cement pastes, Chapter 9 in The Chemistry of Cements, editor *H. F. W. Taylor* (Academic Press, London and New York).

GRUDEMO Å., 1964b. A comparison of crystal structure elements in calcium aluminate hydrates and clay minerals. Swed. Cement and Concrete Research Inst. (unpublished report).

HANSEN W. C., 1962. False set in portland cement, Chemistry of Cement, Proc. 4th Intern. Symp., Washington D.C., 1960 (NBS Monograph 43, 1962), 359–385.

HELLER L., 1952. The structure of dicalcium silicate α-hydrate, Acta Cryst., *5*, 724–728.

HELLER L. and TAYLOR H. F. W., 1956. Crystallographic data for the calcium silicates, Her Majesty's Stationery Office, London.

JONES F. E., 1962. Hydration of calcium aluminates and ferrites, Chemistry of Cements, Proc. 4th Intern. Symp., Washington D.C., 1960 (NBS Monograph 43, 1962), 204–246.

JONES F. E., and ROBERTS M. H., 1962. The system $CaO\text{-}Al_2O_3\text{-}H_2O$ at 25° C, Building Research, Current Papers, Research Series 1.

KALOUSEK G. L. and PREBUS A. F., 1958. Crystal chemistry of hydrous calcium silicates. III. Morphology and other properties of tobermorite and related phases, J. Amer. Ceramic Soc., *41*, 124–132.

KANTRO D. L., BRUNAUER S., and WEISE C. H., 1959. The ball-mill hydration of tricalcium silicate at room temperature, J. Colloid Sci., *14*, 363–376, PCA Res. Dep. Bull. 107.

KANTRO D. L., COPELAND L. E., and BRUNAUER S., 1962. Quantitative analysis of portland cements by X-rays, Chemistry of Cements, Proc. 4th Intern. Symp., Washington D.C. 1960 (NBS Monograph 43, 1962), 75–80.

KHOL F., 1948. On the possibility of following the preparation of gypsum by X-rays, Zpavry Cekosl. Keram. a shlarskae spolecnosti, 115–123 (in Czechish).

KURCZYK H. G., 1960. Elektronenmikroskopische und thermochemische Untersuchungen über die Hydratation der Calciumsilikate $3CaO \cdot SiO_2$ und β-$2CaO \cdot SiO_2$ und der Einfluss von Calciumchlorid und Gips auf den Hydratationsvorgang, Dissertation D 82, T. H. Aachen, Tonindustrie-Zeitung, *24*, (1960).

KURCZYK H. G. and SCHWIETE H. E., 1962. Concerning the hydration products of C_3S and β-C_2S, Chemistry of Cement, Proc. 4th Intern. Symp., Washington D.C. 1960 (NBS Monograph 43, 1962), 349–358.

LEA F. M., 1956. The Chemistry of Cement and Concrete, 2nd ed. (Edward Arnold Ltd., London).

LIEBAU F., 1962. Die Systematik der Silikate, Die Naturwissenschaften, *49*, 481–491.

MAMEDOV K. S., KLEVTSOVA R. F., and BELOV N. V., 1959. The crystalline structure of tricalcium silicate hydrate, Doklady Akad. Nauk. SSSR, *126*, 151–154 (translated reprint in Crystal Chemistry of Large-Cation Silicates, by *N. V. Belov*, 79–81), (Consultants Bureau, New York, 1961).

MEGAW H. D., 1952. The structure of afwillite, $Ca_3(SiO_3OH)_2 \cdot 2H_2O$, Acta Cryst., *5*, 477–491.

MEGAW H. D. and KELSEY C. H., 1956. Crystal structure of tobermorite, Nature, *177*, 390–391.

MIDGLEY H. G., 1957. A compilation of X-ray powder diffraction data of cement minerals, Mag. Concrete Research, *9*, 17–24.

POWERS T. C., 1961. Some physical aspects of the hydration of portland cement, J. PCA Research and Development Labs., *3*, 47–56, PCA Res. Dep. Bull. 125.

POWERS T. C., 1962. Physical properties of cement paste, Chemistry of Cement, Proc. 4th Intern. Symp., Washington D.C. 1960 (NBS Monograph 43, 1962), 577–613.

POWERS T. C., 1964. The physical structure of portland cement paste, Chapter 10 in The Chemistry of Cements, editor *H. F. W. Taylor* (Academic Press, London and New York).

POWERS T. C. and BROWNYARD T. L., 1948. Studies of the physical properties of hardened portland cement paste, J. Amer. Concrete Inst. *41*, (1946–47), 101–132, 249–336, 469–504, 549–602, 669–712, 845–880, 933–992, PCA Res. Dep. Bull. 22 (1948).

SCHIMMEL G., 1957. Elektronenmikroskopische Untersuchungen an Calciumhydroxyd und Calciumcarbonat, Zement-Kalk-Gips, *10*, 134–138.

SWANSON H. E., FUYAT R. K., and UGRINIC G. M., 1955. Standard X-ray diffraction powder patterns, NBS Circular *539*, Vol. IV, 65–67.

TAMARU S. and SIOMI K., 1932. (Reaction $CH \rightleftarrows C+H$, p–T relationships), Zeitschrift f. physik. Chemie (A), *161*, 421–426.

TAYLOR H. F. W., 1950. Hydrated calcium silicates. I. Compound formation at ordinary temperatures, J. Chem. Soc. (London), *1950*, 3682–3690.

TAYLOR H. F. W., 1960. The chemistry of cement hydration, Progress in Ceramic Science, *Vol. 1*, 89–145.

TAYLOR H. F. W., 1962. Hydrothermal reactions in the system CaO-SiO_2-H_2O and the steam-curing of cement and cement-silica products, Chemistry of Cement, Proc. 4th Intern. Symp., Washington D.C. 1960 (NBS Monograph 43, 1962), 167–203.

TAYLOR H. F. W., 1964. The calcium silicate hydrates, Chapter 5 in The Chemistry of Cements, editor *H. F. W. Taylor* (Academic Press, London and New York).

TAYLOR H .F. W. and HOWISON J. W., 1956. Relationships between calcium silicates and clay minerals, Clay Minerals Bull., *3*, 98–111.

TURRIZIANI R., 1964. The calcium aluminate hydrates and related compounds, Chapter 6 in The Chemistry of Cements, editor *H. F. W. Taylor* (Academic Press, London and New York).

WELIN E., 1957. The crystal structure of thaumasite, $Ca_3H_2(CO_3/SO_4) \cdot 13H_2O$, Arkiv Mineral. Geol., *2*, 137–157.

WOOSTER W. A., 1936. On the crystal structure of gypsum, $CaSO_4 \cdot 2H_2O$, Z. Kristallogr. (A), *94*, 375–396.

Table of contents

Forts. fr. omsl. 2:dra sida

183. HALLÉN, ERIK, *Exact Solution of the Antenna Equation.* (Math. & Phys. 20) 22 s. 1961. Kr. 3: —.
184. ZETTERBERG, LARS-HENNING, *Data Transmission over a Noisy Gaussian Channel.* (El. Engng. 6) 87 s. 1961. Kr 9: 50.
185. LINDSTRÖM, OLLE, *Liquid Seed Treatment Studies.* (Chem. 16) 88 s. 1961. Kr. 9: 50.
186. *Supplement No. 3 to List of Publications of Members of the Staff of The Royal Institute of Technology, Stockholm.* 149. s. 1961. Kr. 13: —.
187. ROSÉN, ERIK, *Data and Calculations for the Gasification of Spent Cooking Liquors from the Pulp Industry. Part IV: The Behavior of the Elements Sulfur and Sodium.* (Chem. 17) 48 s. 1962. Kr. 6: —.
188. DYRSSEN, DAVID, *Extraction of Metal Ions with β-Isopropyltropolone (IPT) I.* (Chem. 18) 51 s. 1962. Kr. 6: —.
189. CARLSSON, JANNE, *Experimental Studies of Brittle Fracture Propagation.* (Mech. Engng. 6) 56 s. 1962. Kr. 6: 50.
190. PIECHNIK, STEFAN, *Steady-state Creep of Solid Bar under Combined Load.* (Mech. Engng. 7) 39 s. 1962. Kr 5: —.
191. EINARSSON, OLOV, *The Step Voltage Current Response of an Infinite Conducting Cylinder Functional Properties and Tables.* (El. Engng 7) 26 s. 1962. Kr. 3: 50.
192. PIECHNIK, STEFAN, *Stationary Creep of a Solid Circular Bar and Tube under Torsion and Tension.* (Mech. Engng. 8) 27 s. 1962 Kr. 3: 50.
193. STRÖMGREN, LARS, *Table of the Amplitude Functions of the Iterated Sine and Cosine Integrals of Two Variables.* (El. Engng. 8) 11 s. 1962. Kr 2: —
194. PIECHNIK, STEFAN, *Combined Tension-bending Creep for a Solid Bar.* (Mech. Engng. 9) 32 s. 1962. Kr. 4: —.
195. SCHLYTER, KURT, *Thermochemical Studies on the Hydrolysis of the Uranyl Ion.* (Chem. 19) 32 s. 1962. Kr. 4: —.
196. SCHLYTER, KURT, *Thermochemical Studies on the Hydrolysis of the Iron (III) Ion.* (Chem. 20) 38 s. 1962. Kr. 5: —.
197. ÅSTRÖM, KARL JOHAN, *Analysis and Synthesis of Inertial Platforms with Single Axis Gyroscopes.* (Aeron. Shipb. 2) 66 s. 1963. Kr. 7: 50.
198. KINNUNEN, S., *Punching of Concrete Slabs with Two-way Reinforcement with Special Reference to Dowel Effect and Deviation of Reinforcement from Polar Symmetry.* (Civil Engng. 6) 109 s. 1963. Kr. 11: —.
199. BJÖRKMAN, MONICA, and SILLÉN, LARS GUNNAR. *Thermochemical Studies on the Stepwise Formation of $Br^- - Hg^{2+}$ Complexes.* (Chem. 21) 19 s. 1963. Kr. 2: 50.
200. ANNELL, HANS, *The Alternating Current Impedance of a Solid Conductor of Circular Cross Section Placed in a Semi-Closed Circular Slot.* (El. Engng. 9) 34 s. 1962. Kr. 4: 50.
201. ANDERSSON, K. E. BERTIL, *Pressure Drop in Packed Beds.* (Chem. 22) 38 s. 1963. Kr. 5: —.
202. ANDERSSON, K. E. BERTIL, *Transition between Packed and Fluidized State.* (Chem. 23) 14 s. 1963. Kr. 2: —.
203. BLOMBERG, CLAS, *Statistical Analysis of Prognoses.* (Math. & Phys. 21) 23 s. 1963. Kr. 3: —.
204. LAMM, OLE, *Elements of a Macro-Dynamical Theory of Transport by Diffusion and Sedimentation, for Fluid Systems, Including a Weak Gel Character.* (Chem. 24) 19 s. 1963 Kr. 2: 50
205. CARLSSON, A. JANNE, *On the Mechanism of Brittle Fracture Propagation. Branching, Fracture Surface Appearance, and Influence of Stresswaves.* (Mech. Engng. 10) 39 s. 1963. Kr. 5: —.
206. BÄCK, A., *A New Test Bench for Measuring Optical Transfer Functions of Aerial Camera Lenses.* (Math. & Phys. 22) 24 s. 1963. Kr. 3: 50.
207. CARLSSON, A. JANNE, *Method for Continuous Measurement of Instantaneous Crack Propagation Velocities.* (Mech. Engng. 11) 27 s. 1963. Kr. 3: 50.
208. DAHLBERG, ERLING, *An Attempt at a One-dimensional Treatment of the Flow in a Hall-effect MHD-generator Channel.* (Math. & Phys. 23) 22 s. 1963. Kr. 3: —.
209. DAHLBERG, ERLING, *Quasi-one-dimensional Analyses of Magnetohydrodynamic Channel Flows* (Math. & Phys. 24) 18 s. 1963. Kr. 2: 50.
210. VAN BLADEL, J., *Boundary Excitation of Waveguides Containing Anisotropic Media.* (El. Engng. 10) 24 s. 1963. Kr. 3: 50
211. HELLSTRÖM, B., *Seiches and Wind Currents in Lakes.* (Civil Engng. 7) 32 s. 1963. Kr. 4:—.
212. ANDERSSON, JAN L., *Punching of Concrete Slabs with Shear Reinforcement.* (Civil Engng. 8) 59 s. 1963. Kr. 7:—.
213. BERONIUS, PER, *Electrochemical Methods in Kinetic Studies of Isotopic Exchange Reactions. Problems Concerning Reproducibility of Electro precipitation.* (Chem. 25) 60 s. 1963. Kr. 7:50.
214. HEDNER, GERT, *Total Strain Theory of Creep Including Recovery.* (Mech. Engng. 12) 33 s. 1963. Kr. 4: 50.
215. HELLSTRÖM, BO, and REINIUS, ERLING, *The Hydraulic Laboratory at the Royal Institute of Technology, Stockholm.* (Civil Engng. 9) 17 s. 1963. Kr. 2: 50
216. EINARSSON, OLOV, *The Current Distribution on Cylindrical Antennas of Arbitrary Length.* (El. Engng. 11) 26 s. 1963. Kr. 3: 50.
217. SANDHOLM, L., *Studies on the Synchronizing Process of Self-starting Synchronous Motors.* (El. Engng. 12) 47 s. 1963. Kr. 6: —.
218. WALÖEN, ÅGE, *Asymmetrical Loading of Conical Shells.* (Mech. Engng. 13) 34 s. 1964. Kr. 4: 50.
219. HALLERT, B., *The Geometrical Quality of Rays. Reconstructed from Photographs.* (Math. and Phys. 25) 23 s. 1964. Kr. 3: 50.
220. DYRSSEN, DAVID, *Stability Constants and Solubilities of the Metal Dioximes.* (Chem. 26) 15 s. 1964. Kr. 2: —.

Forts. å omsl. 4:de sida

Forts. fr. omsl. 3:dje sida

221. KÖSZEGI, LASZLO, and ROSÉN, ERIK, *Data and Calculations for the Gasification of Spent Cooking Liquors from the Pulp Industry. Part V. Experimental Studies of the Equilibria* $Na_2S(s) + CO_2 + H_2O \rightleftharpoons Na_2CO_3(s) + H_2S$ *and* $K_2S(s) + CO_2 + H_2O \rightleftharpoons K_2CO_3(s) + H_2S$. (Chem. 27) 22 s. 1964. Kr. 3:—.
222. ANDERSSON, B., HATCHER, M., and STELLING, O., *Mass Transfer in Multiparticle Systems.* (Chem. 28) 63 s. 1964. Kr. 7:50.
223. ROSÉN, ERIK, *Data and Calculations for the Gasification of Spent Cooking Liquors from the Pulp Industry. Part VI. Treatment of Sulfite Spent Liquors Containing Sodium or Potassium as the Metal Constituent.* (Chem. 29) 28 s. 1964. Kr. 4:—.
224. HÖGFELDT, E., and BOLANDER, B., *On Extraction with Long-chain Tertiary Amines. I. Extraction of Water and Nitric Acid by Mixtures of Trilaurylamine (TLA) and n-Octanol Dissolved in n-Octane or n-Dodecane.* (Chem. 30) 32 s. 1964. Kr. 4: —.
225. HÖGFELDT, E., BOLANDER, B., and FREDLUND, F., *On Extraction with Long-chain Tertiary Amines. II. Extraction of Water and Nitric Acid by Mixtures of n-Octanol with Tri-isooctylamine, Tri-n-octylamine, Tri-n-decylamine and Tri-n-dodecylamine Dissolved in n-Octane, n-Dodecane or Xylene.* (Chem. 31) 28 s. 1964. Kr. 4: —.
226. HÖGFELDT, E., and FREDLUND, F., *On Extraction with Long-chain Tertiary Amines. III. Aggregation in the System Trilaurylamine-m-xylene-nitric Acid-water Studied by Two-phase emf-titrations.* (Chem. 32) 28 s. 1964. Kr. 4: —.
227. HÖGFELDT, E., and FREDLUND, F., *On Extraction with Long-chain Tertiary Amines. IV. Aggregation in the System Trilaurylamine-o-xylene-nitric Acid-water Studied by Two-phase emf-titrations.* (Chem. 33) 16 s. 1964. Kr. 2: —.
228. HÖGFELDT, E., and MARIA DE JESUS TAVARES, *On Extraction with Long-chain Tertiary Amines. V. Extraction of Hydrochloric Acid and Water by Trilaurylamine Dissolved in o-Xylene and the Aggregation of the Amine-acid Complex.* (Chem. 34) 28 s. 1964. Kr. 4: —.
229. HÖGFELDT, E., FREDLUND, F., and RASMUSSON, K., *On Extraction with Long-chain Tertiary Amines. VI. Aggregation of the Trilaurylamine-nitric Acid Complex in n-Octane and n-Dodecane Studied by Two-phase emf-titrations.* (Chem. 35) 16 s. 1964. Kr. 2: —.
230. HALLERT, B., *Tolerances of Photogramm... Instruments and Methods.* (Math. & Phys. 26) 2... s. 1964. Kr. 3:50.
231. JANSON, LARS-ERIC, *Frost Penetration in Sa... Soil.* (Civil Engng. 10) 167 s. 1964. Kr. 14:
232. PETERSONS, NILS, *Strength of Concrete in Fi... ished Structures.* (Civil Engng. 11) 189 s. 196... Kr. 16: —.
233. ALFREDSSON, LENNART, *Investigation of Bac... ward-Wave Modes in Plasma Waveguides* (El. Engng. 13) 21 s. 1964. Kr. 3: —.
234. BERONIUS, PER, *An Interpretation of the Plateau Limits of the Current Efficiency Against Curren... Density Curve for Deposition of Iodide on Silve... Electrodes.* (Chem. 36) 10 s. 1964. Kr. 1:5...
235. BONNEVIER, BJÖRN, *Tables of the Magnetic Field from a Circular Current Loop.* (El. Engng. 14) 29 s. 1964. Kr. 9: —.
236. ÅSLANDER, ALFRED, and ARMOLIK, NEEME, *The Influence of Organic Materials on the Potassium Fixation in the Soil.* (Arch., Build., Surv. 3) 45 s. 1964. Kr. 11: —.
237. HÖGLUND, TORSTEN, *Thin Plate I Girders Subjected to Eccentric Compressive Loads.* (Civil Engng. 12) 30 s. 1964. Kr. 10:—.
238. BERONIUS, PER, *Isotopic Exchange between Iodoacetic Acid and Iodide Ions. The Use of Electrochemical Separation to Avoid Separation Induced Exchange.* (Chem. 37) 8 s. 1964. Kr. 8:—.
239. BERONIUS, PER, *Kinetic Studies of Moderately Rapid Isotopic Exchange Reactions.* (Chem. 38) 28 s. 1964. Kr. 10:—.
240. PETERSSON, GUNNAR, *On Oseen's Extinction Theorem.* (El. Engng. 15) 15 s. 1964. Kr. 8:—.
241. PETERSSON, GUNNAR, *The Current Distribution on Infinite Antennas with and without a Dielectric coating.* (El. Engng. 16) 76 s. 1965. Kr. 18:—.
242. GRUDEMO, ÅKE, *The Microstructures of Cement Gel Phases.* (Civil Engng. 13) 288 s. 1965. Kr. 45:—.

Pris Kronor 45:—.

ELANDERS BOKTRYCKERI AKTIEBOLAG - GÖTEBORG 1965